16 February 2007 | $10

Science

AAAS

Volume 315, Issue 5814

COVER

Tectonic fractures within the Candor Chasma region of Valles Marineris, Mars, retain a ridgelike morphology as the surrounding bedrock erodes away. Such findings offer clues about past fluid flow and geochemical conditions within the subsurface. The image is about 1 kilometer across; illumination is from the upper left. See page 983.

Image: Lunar and Planetary Laboratory, University of Arizona/JPL/NASA

DEPARTMENTS

EDITORIAL

NEWS OF THE WEEK

NEWS FOCUS

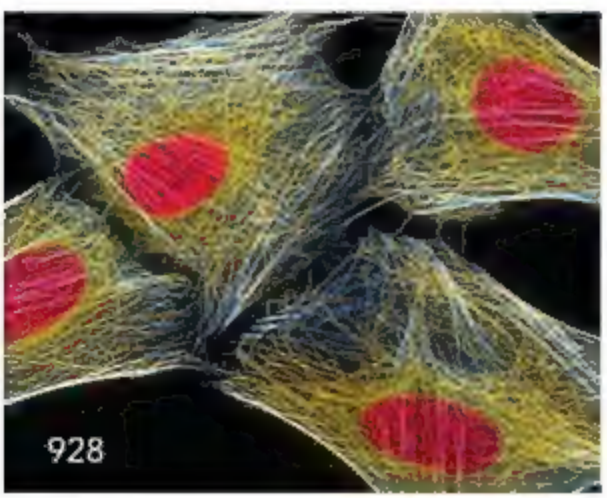
928

LETTERS

BOOKS *ET AL.*


941

POLICY FORUM

PERSPECTIVES

CONTENTS continued >>

Science

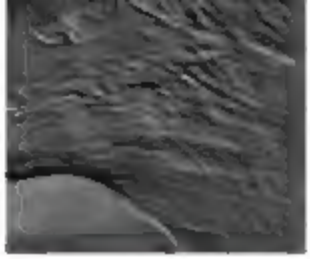

SCIENCE EXPRESS

www.sciencexpress.org

PHYSICS

BREVIA: Room Temperature Quantum Hall Effect in Graphene
K. S. Novoselov et al.
The quantum Hall effect, usually seen near 0 degrees kelvin, occurs at room temperature within single graphene sheets, in which the charge carriers behave as massive relativistic particles.
10.1126/science.1137201

CHEMISTRY

Thermoelectricity in Molecular Junctions
P. Reddy, S.-Y. Jang, R. Segalman, A. Majumdar
Measuring the induced voltage of organic molecules held between gold contacts at different temperatures reveals whether holes or electrons carry the current.
10.1126/science.1137149

CLIMATE CHANGE

An Active Subglacial Water System in West Antarctica Mapped from Space
H. A. Fricker, T. Scambos, R. Bindschadler, L. Padman
Satellite measurements reveal that water is flowing rapidly under the Antarctic Ice Sheet, forming and draining subglacial lakes and impacting assessments of its stability.
10.1126/science.1136897

NEUROSCIENCE

Human Neuroblasts Migrate to the Olfactory Bulb via a Lateral Ventricular Extension
M. A. Curtis et al.
As in rodents, adult human neurons born along the fluid-filled ventricles in the brain migrate to the olfactory bulb along a tubelike extension of the ventricle.
10.1126/science.1136281

REVIEW

BREVIA

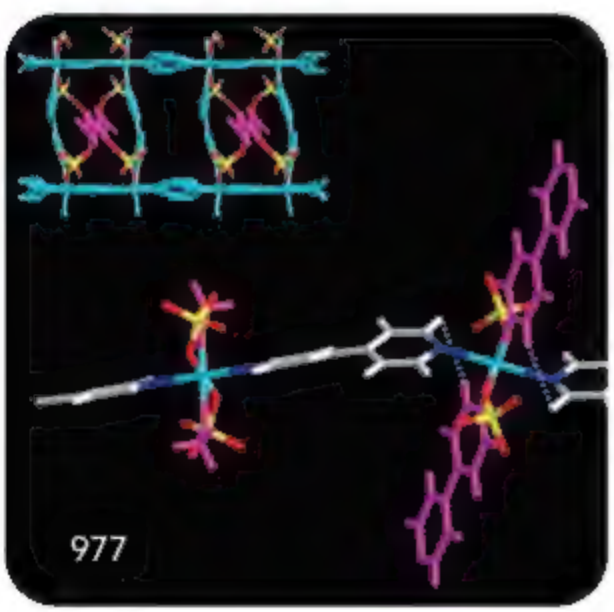

RESEARCH ARTICLE

REPORTS

CONTENTS continued >>

Science

CONTENTS

REPORTS *CONTINUED...*

952 & 1006

AAAS
ADVANCING SCIENCE, SERVING SOCIETY

SCIENCE (ISSN 0036-8075) is published weekly on Friday, except the last week in December, by the American Association for the Advancement of Science, 1200 New York Avenue, NW, Washington, DC 20005. Periodicals Mail postage (publication No. 484460) paid at Washington, DC, and additional mailing offices.

Domestic individual membership and subscription ($1 issue): $142 ($74 allocated to subscription). Domestic institutional subscription ($1 issue): $750. Foreign postage extra: Mexico, Caribbean (surface mail) $55; other countries (air assist delivery) $85. First class, airmail, student, and retired rates on request. Canadian rates with GST available upon request, GST #125439 8572. Publications Mail Agreement Number 1069624. **Printed in the U.S.A.**

Change of address: Allow 4 weeks, giving old and new addresses and 8-digit account number. **Postmaster:** Send change of address to AAAS, P.O. Box 96178, Washington, DC 20090–6178. **Single-copy sales:** $10.00 current issue, $15.00 back issue prepaid. Includes surface postage; bulk rates on request. **Authorization to photocopy** material for internal or personal use under circumstances not falling within the fair use provisions of the Copyright Act is granted by AAAS to libraries and other users registered with the Copyright Clearance Center (CCC) Transactional Reporting Service, provided that $30.00 per article is paid directly to CCC, 222 Rosewood Drive, Danvers, MA 01923. The identification code for Science is 0036-8075. *Science* is indexed in the *Reader's Guide to Periodical Literature* and in several specialized indexes.

CONTENTS continued >>

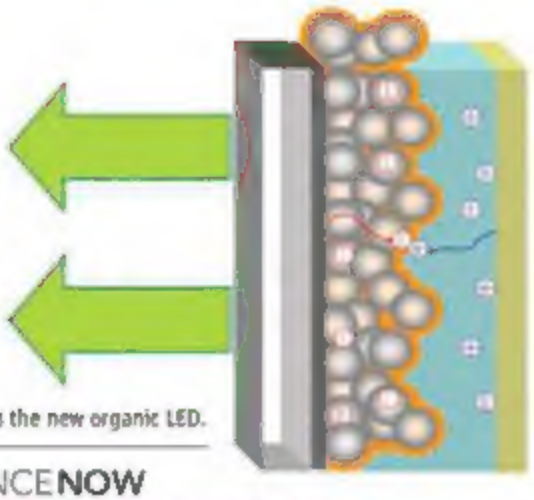

Light exits the new organic LED.

SCIENCENOW

www.sciencenow.org DAILY NEWS COVERAGE

The Chimpanzee Stone Age
New find suggests chimps have used stone tools for thousands of years.

Taking Stock of Trees
Bank grant makes possible worldwide comparison of forest dynamics.

Truly Tubular TV
Improved organic LEDs might lead to roll-up video screens.

The blossoming of kinase inhibitor research.

SCIENCE'S STKE

www.stke.org SIGNAL TRANSDUCTION KNOWLEDGE ENVIRONMENT

PERSPECTIVE: Meeting Report—Targeting the Kinome, 20 Years of Tyrosine Kinase Inhibitor Research in Basel
L. Bozulic, P. J. Morin, T. Hunter, B. A. Hemmings
Scientists explore the past, present, and future of protein kinase research in light of cancer therapy development.

EVENTS
Search or browse this updated list of signaling-related meetings and conferences.

Do your homework before accepting an offer.

SCIENCE CAREERS

www.sciencecareers.org CAREER RESOURCES FOR SCIENTISTS

US: Tooling Up—Employment Due Diligence
D. Jensen
Anyone who accepts a job offer without doing a background investigation is taking a serious risk.

US: Opportunities—A Day in the Life
P. Fiske
An unlikely entrepreneur sniffs out a new opportunity.

GLOBAL: Mastering Your Ph.D.—Dealing With Setbacks
P. Gosling and B. Noordam
Get tips on how to pick yourself up, brush yourself off, and move on.

CREDITS: (SCIENCE NOW) SAM MAGUIRE; (SCIENCE CAREERS) CREATIVE COMMONS LICENSE AMY JAZZAR

Separate individual or institutional subscriptions to these products may be required for full-text access.

CREDITS (TOP TO BOTTOM): PHOTOS.COM; FREY AND DUECK

<< Routes of Chili Pepper Domestication

A wide variety of chili peppers were cultivated and used in cooking throughout the New World. **Perry *et al.*** (p. 986; see the Perspective by **Knapp**) identified a starch from chili peppers on ancient pottery and stone tools that is diagnostic of groups of chili species. The starches were found at various archaeological sites, including from about 6500 years ago in Ecuador, and suggest multiple domesticated chili species by about 4000 years ago.

Delayed Choice for Quantum Mechanics

Wave-particle duality is at the heart of quantum mechanics. Particles and photons can display both properties, and which property is measured depends on the type of measurement made. What if the experimental setup changes when the photon or particle is "in flight" and has already entered the experimental apparatus? **Jacques *et al.*** (p. 966) report an almost ideal realization of such a "delayed choice" experiment as formulated by Wheeler. A triggered single-photon source provides a mechanism for precise timing of the experiment within laboratory conditions. The behavior of the photon in the interferometer depends on the choice of the observable that is measured, even if that choice is made when the photon is already in the system.

Water Marks

Water may have once flowed on the surface of Mars when it was warm and wet. Today, however, all that remain are mineral deposits, including sulfates and clays. **Okubo and McEwen** (p. 983; see the cover) show in very detailed images from the Mars Reconnaissance Orbiter that water once flowed along fractures that crossed the layered deposits in western Candor Chasma. Geochemical bleaching and cementation are seen in the fracture zones that are similar to water-related processes on Earth.

Finding a Good Example

Complex data sets can be more readily analyzed if representative examples can be identified. Such "exemplars" might be points around which data will cluster, archetypal faces among a gallery of actual photos, or possible exons in a gene sequence. Unfortunately, extracting exemplars is computationally intensive, and conventional techniques only work well with numerical measures of data-point similarity and if the initial guess is close. **Frey and Dueck** (p. 972, published online 11 January; see the Perspective by **Mézard**) now report a method that enables much faster exemplar detection. The algorithm works by having the data points exchange "messages" that communicate whether a particular point could be an exemplar; iteration of the message-passing process allows dramatically faster processing as certain data points emerge as truly representative.

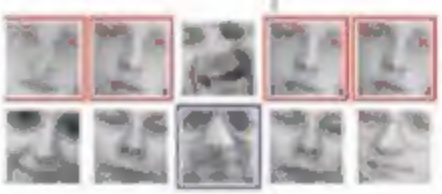

Guests Move in When It's Hot

Microporous metal-organic extended arrays can absorb guest molecules at specific sites, and **Bradshaw *et al.*** (p. 977) show that water molecules in a Co extended array, $[Co_2(bipy)_3(SO_4)_2(H_2O)_2]$, can undergo substitution reactions with sorbed methanol and bipyridine molecules upon heating in a dry inert atmosphere. Hydrogen-bonding interactions place two bipyridines or two methanols near alternating Co atoms along linear chains within the solid. When these molecules displace the water ligands, the chains adopt a zigzag geometry. Other Co sites are spectators that help maintain the framework while this reaction proceeds. The reaction can be reversed by rehydrating the crystal at room temperature.

Unpeeling Granite's History

Large granite bodies may have formed within Earth's crust by intrusion of new magma or by remelting of igneous varieties of crustal rocks. The evolutionary history of granites can be revealed by examining the chemistry of successive layers of its large constituent crystals, notably zircon. **Kemp *et al.*** (p. 980; see the Perspective by **Eiler**) have measured hafnium and oxygen isotopes in zoned zircon crystals from the classic granites of eastern Australia. They found that these granites formed by the recycling of deep crustal rocks as mantle magma rose through them, rather than by remelting ancient, shallower crust, as was widely believed.

Hippocampal Dualism

The formation of discrete representations in memory has been hypothesized to reflect neuronal pattern separation at the early stages of the hippocampal formation, but both location and mechanisms of the process have remained elusive. **Leutgeb *et al.*** (p. 961; see the Perspective by **Fenton**) show that the hippocampus has at least two mechanisms for pattern separation associated with different parts of the hippocampal circuit. In the dentate gyrus, signals are separated by high-fidelity decorrelation of coactivity patterns within a subset of active cells. In CA3, further separation is achieved by activation of nonoverlapping neuronal subpopulations. The two mechanisms of pattern separation, associated with different parts of the circuitry, support distinct forms of ensemble representation in the hippocampus.

Continued on page 911

Continued from page 909

And Then There Were Three

During development, stem cells usually generate two daughter cells that go on to differentiate as well as another stem cell. **Ohlstein and Spradling** (p. 988) now describe one type of stem cell in the *Drosophila* intestine that produces three offspring fates—a stem cell, an enterocyte, and an enteroendocrine cell. The choice in fate seems to depend on the amount of the protein Delta (a membrane-bound signaling ligand that can activate the signaling receptor Notch) that is expressed in the stem cell at the time of cell division. Daughter cells with high amounts of Delta-Notch signaling become enterocytes, those with lower amounts become enteroendocrine cells, and those with the least amount retain the stem cell fate.

Sticky Fingers

As animal cells migrate across a surface, they send out processes known as filopodia that explore the substratum. **Galbraith *et al.*** (p. 992) now find that the intracellular actin network directs very local protrusions that contain clusters of cell surface-adhesion molecules at their tips that are primed to interact with molecules of the extracellular matrix. These "sticky fingers" at the leading edge of motile cells appear to search for suitable sites of adhesion that can then be used to help move the rest of the cell.

Locust Navigation

The plane of polarization of sunlight depends on the Sun's position, and a variety of insects use polarization patterns to guide spatial orientation. **Heinze and Homberg** (p. 995) show that the orientations of electric field vectors of linearly polarized light (*E*-vectors), presented from above the animal, are represented as a topographical map in the columns of the central complex in the locust brain. The central complex acts as an internal compass that uses the polarization pattern of the blue sky to code spatial directions relevant to animal orientation.

Lethal Injection

Pathogenic bacteria can inject into host cells virulence factors via the so-called type III machinery. **Li *et al.*** (p. 1000) describe a family of bacterial virulence factors that have a previously unknown phosphothreonine lyase activity that can remove the phosphate from signaling mitogen-activated protein kinase family members involved in innate immunity. This family of effectors is important in the virulence of a variety of animal and plant bacterial pathogens, including *Shigella*, *Salmonella*, and *Pseudomonas syringae*.

A RuBisCo with No Taste for CO_2

In photosynthetic organisms, RuBisCo (ribulose-1,5-bisphosphate carboxylase-oxygenase) fixes CO_2 through the "dark reaction" to make organic compounds such as sucrose, but one type of RuBisCo, found in nonphotosynthetic anaerobic archaeon, does not. **Sato *et al.*** (p. 1003) found that type III RuBisCo, acting solely as a carboxylase, in combination with newly revealed archaeal nucleoside phosphorylase and ribose-1,5-bisphosphate isomerase functions, converts CO_2, water, and adenosine 5′-monophosphate into 3-phosphoglycerate, which feeds ribose into carbon metabolism, salvages adenine, and generates ATP.

Joint Effort

Rheumatoid arthritis (RA) is an autoimmune condition that leads to joint inflammation. **Lee *et al.*** (p. 1006, published online 25 January; see the Perspective by **Firestein**) identify a new regulator of the cellular organization of the synovium that might also provide a potential therapeutic target for inflammatory arthritis. Mice lacking the cell adhesion molecule cadherin 11 showed significantly reduced growth of the synovium and were resistant to the development of an experimentally induced RA-like condition. Joint inflammation in mice could be inhibited with a monoclonal antibody to cadherin-11.

CREDIT: CATHERINE G. GALBRAITH AND JAMES A. GALBRAITH/NINDS, NIH

R. K. Pachauri is director general of The Energy and Resources Institute in New Delhi, India, and chairman of the Intergovernmental Panel on Climate Change.

Sustainable Well-Being

ECONOMIC PROGRESS ACHIEVED SINCE THE ADVENT OF INDUSTRIALIZATION HAS RESULTED largely from advances in science and technology (S&T). Yet even as society benefits from S&T through choices that we have come to take for granted, decisions on its future are increasingly being questioned and scrutinized. The current path of economic growth deviates from the objectives of sustainable development. It is not only society at large, spearheaded by leaders of public opinion, that is expressing concerns, but also the scientific community itself, which is looking for ways to promote the sustainable well-being of all humanity.

This microscopic analysis of science and its applications emanates from several valid concerns: the role of science in the development and extensive use of lethal weapons; the continuing existence of widespread poverty, with over a billion people in the world remaining virtually untouched by the benefits of modern S&T; and the threat of serious environmental externalities from unprecedented levels of production and consumption of goods and services.

A meaningful discussion of S&T solutions to contain war, terrorism, and heinous crime cannot be included in this limited space, but the other two issues deserve elaboration. The distinguished economist Kenneth Boulding, a rare intellectual far ahead of his time, pointed out that two centuries earlier, the difference in average income between the poorest country in the world and the most prosperous was no more than 1:5. When he expressed this concern 30 years ago, he estimated it as being 1:50. Income and wealth disparities are even sharper today. Despite astounding progress globally, the S&T gap between rich and poor nations is ironically wider now. If this growing chasm is not bridged, fissiparous tendencies will inhibit and even reverse prospects for enhancing human welfare. Unfortunately, the global community has failed to bring technological opportunities and skills to underprivileged and impoverished communities across the globe.

The challenge of widespread worldwide poverty has typically been addressed through doles and handouts as convenient but largely ineffective palliatives. Seldom have programs in this area created avenues for applying modern S&T to develop local skills and capacity, which alone can generate income and employment on a sustainable basis. A program being spearheaded by The Energy and Resources Institute embodies technological innovation in the allied fields of agriculture, energy, natural resource management, and information technology in partnership with local entrepreneurs for the sustainable well-being of rural communities in Asia and Africa. This approach, called Integrating New and Sustainable Technologies for Elimination of Poverty, meets a challenge that could become insurmountable if ignored any longer. Creating opportunities for the productive application of S&T by the most dispossessed communities of the world is a task that scientists and policymakers must embrace with urgency.

Among the negative externalities created by human activities, the cumulative emissions of greenhouse gases have had by far the most serious consequence in the form of global climate change. Cuts in emissions of these gases require technological initiatives to stabilize the concentration of greenhouse gases. Because the impacts of climate change will continue for centuries, adaptation measures will also require the timely application of S&T. However, these will not take place in a policy vacuum. Regulatory and fiscal measures will have to be put in place by governments, facilitated if necessary by multilateral agreements to trigger the development and application of appropriate technological solutions.

The agenda for the global scientific community is very clear. We must recognize and evaluate the most critical impediments to the sustainable welfare of human society, including various threats to human life and global peace, disruptions in the delicate balance of Earth's natural systems, and the growing gap between rich and poor. These three sets of conditions are intimately interlinked, requiring a coordinatped approach to solve them. Scientists must work with decision-makers to devise rational policy measures that mobilize desirable responses in the form of development and deployment of suitable S&T solutions in these areas.

– R. K. Pachauri

10.1126/science.1140975

EDITED BY GILBERT CHIN AND JAKE YESTON

BIOCHEMISTRY

Squaring a Cube

The detection of environmental changes is of paramount importance for microbes, and a host of mechanisms have evolved in which signal detection is coupled to an amplification step in order to increase sensitivity and to reduce response time. The bacterial regulator of fumarate and nitrate reduction (FNR) regulates the transcription of more than 100 genes in response to the transition from anaerobic to aerobic growth; molecular oxygen triggers a conversion of its $[4Fe\text{-}4S]^{2+}$ cluster into a $[2Fe\text{-}2S]^{2+}$ cluster, leading to conformational changes in FNR and dissociation from DNA.

Crack *et al.* report that this reaction not only detects dioxygen, but actually uses it to amplify the signal, consuming some in doing so. The first step in signal detection is a one-electron oxidation of the $[4Fe\text{-}4S]^{2+}$ cluster that transforms it into a $[3Fe\text{-}4S]^{1+}$ cluster, and a kinetic analysis confirmed the oxygen-dependent coincident loss of the [4Fe-4S] cluster and the appearance of the ejected Fe^{2+} and the superoxide anion ($O_2^{-\bullet}$). The second step is about 10 times slower, and a second Fe departs (as Fe^{3+}) in the conversion of the $[3Fe\text{-}4S]^{1+}$ cluster into a $[2Fe\text{-}2S]^{2+}$ cluster. Superoxide is known to undergo dismutation into oxygen and hydrogen peroxide, which can itself dismutate into oxygen and water. In sum, one O_2 molecule can trigger the disassembly of four [4Fe-4S] clusters. — GJC

Proc. Natl. Acad. Sci. U.S.A. **104**, 2092 (2007).

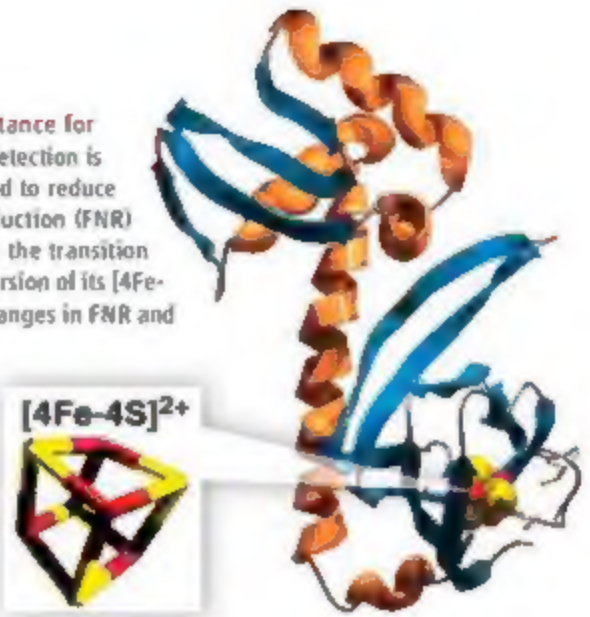

A model of FNR, with its DNA binding domain at the top and the iron (red)–sulfur (yellow) cluster at the bottom.

GENETICS

Recognizing Oneself

Self-incompatibility, a plant's rejection of pollen from itself or a closely related individual, prevents inbreeding, which can lead to a loss of heterozygosity and deleterious combinations of recessive alleles. *Arabidopsis* has become self-compatible, whereas several closely related species, including *Brassica*, remain self-incompatible. Both the *S*-locus receptor kinase (SRK) and the *S*-locus protein 11 (SP11/SCR) are implicated in the phenomenon.

Shimosato *et al.* have investigated the interaction between SP11 and SRK in *Brassica*. Two proteins of 60 and 100 kD were previously shown to bind to SP11; both are forms of SRK, with the smaller one being a truncated, though still membrane-bound, form of the full-length protein. The latter binds to SP11 with high affinity whereas the former does not, suggesting that they may function differently. Sherman-Broyles *et al.* have investigated the maintenance and degradation of the *SRK* and *SCR* genes. They found that in comparison to the fully sequenced *Arabidopsis* Columbia-0 accession, both genes in the C24 accession have undergone extensive rearrangement and significant parts of the *SCR* gene have been deleted, possibly through the insertion and deletion of transposable elements. These differences in the *S* locus region suggest that these genes have followed different trajectories after the loss of self-incompatibility. — LMZ

Plant Cell **19**, 10.1105/tpc.105.038869; 10.1105/tpc.106.048199 (2007).

CELL BIOLOGY

Life Without Amyloid

The amyloid precursor protein (APP) is a transmembrane protein that has been linked to some forms of familial Alzheimer's disease, but the normal function of the protein is a mystery. The nematode worm *Caenorhabditis elegans* possesses a single APP-related gene, termed *apl-1*. Hornsten *et al.* have examined the role of *apl-1*, which is expressed in a variety of tissues, including neurons. Worms with a disrupted *apl-1* gene died as larvae, exhibiting defects in molting, locomotion, and morphogenesis. These mutants could be rescued by the expression of the soluble extracellular domain of APL-1 protein in neurons. In addition, overexpressing the APL-1 protein in a wild-type background was detrimental; this effect could be mitigated by reducing the levels of SEL-12, which is a *C. elegans* homolog of presenilin, an enzyme that cleaves APP in humans. Thus, it appears that APL-1 performs an essential function during development in the nervous system. Interfering with APP expression or modifications in patients may therefore have unintended and unexpected consequences. — SMH

Proc. Natl. Acad. Sci. U.S.A. **104**, 1971 (2007).

***apl-1* is expressed in a variety of tissues (green).**

ATMOSPHERIC SCIENCE

Wind, Rain, and Aerosols

Theory suggests that a rising concentration of aerosols should reduce wind speeds below, due mainly to the increase in atmospheric stability that such loading would cause. Consequences range from decreased evaporation and rainfall to a multitude of secondary impacts, such as reduced availability of wind energy for the generation of electricity and decreased hydroelectric potential. Jacobson and Kaufman use a three-dimensional computer model and satellite data to examine the potential effects of aerosol particles on the distribution of wind speeds and the resulting feedbacks to precipitation, water supply, and wind energy

CREDITS (TOP TO BOTTOM): CRACK *ET AL.*, *PROC. NATL. ACAD. SCI. U.S.A.* **104**, 2092 (2007); HORNSTEN *ET AL.*, *PROC. NATL. ACAD. SCI. U.S.A.* **104**, 1971 (2007)

across California. They find that pollution by aerosols may be decreasing local winds by up to –8% and, together with the second indirect aerosol effect, may be reducing precipitation by 2 to 5%. These effects have obvious and unwelcome practical consequences, but they also raise the hopeful possibility that by limiting or reducing aerosol pollution, California can lessen future strains on its water supply and wind/hydroelectric power-generation systems. — HJS

Geophys. Res. Lett. **33**, L24814 (2006).

MATERIALS SCIENCE

Inserted in Isolation

Microcontact printing (μCP) with elastomeric stamps can be used to pattern self-assembled monolayers (SAMs) on surfaces, but it can also be useful to create mixed SAMs in which one of the molecules is diluted within the other layer. Mullen *et al.* show that more diffusive molecules, which are often difficult to pattern with μCP, can be inserted into more stable SAMs by a method they term microcontact insertion printing (μCIP). An existing SAM (in this case, 1-octanethiolate assembled on gold) is contacted in a subsequent μCP step with a second molecule, either 11-mercaptoundecanoic acid (MUDA) or 1-dodecanethiolate.

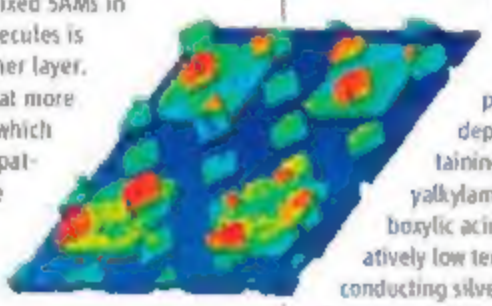

Large and small MUDA blocks patterned sequentially on gold.

The extent of insertion, which occurs preferentially at defect sites, can be controlled by changing the contact time and concentration of molecules on the stamp, and more complex patterns can be created with additional rounds of μCIP. — PDS

Appl. Phys. Lett. **90**, 10.1063/1.2457525 (2007).

CHEMISTRY

A Silver Solution

Despite widespread efforts toward development of printable semiconductors for large-area, flexible electronics media, far less attention has been given to the printable conducting material required for the wiring and connections within such devices. Both gold and silver possess high conductivity and operational stability, but precise patterning with these metals typically requires vacuum deposition. Wu *et al.* have devised a simple solution-based process for patterning conductive silver features on a substrate. Using coating, stamping, or printing techniques, they deposit an alcohol solution containing a silver(I) salt, a hydroxyalkylamine, and a long-chain carboxylic acid. Subsequent heating at relatively low temperature (150°C) forms the conducting silver elements. The amine functions as a gentle reducing agent, with sufficient volatility to evaporate easily afterward. Achieving high conductivity requires acid additives with decyl or longer alkyl tails, which foster the growth of films without discernible grain boundaries. The method was applied to fabrication of a layered thin-film transistor device, in which the silver showed conductivity comparable to that of more costly vacuum-processed gold. — MSL

J. Am. Chem. Soc. **129**, 10.1021/ja067596w (2007).

www.sciencemag.org

Science

1200 New York Avenue, NW
Washington, DC 20005
Editorial: 202-326-6550, FAX 202-289-7562
News: 202-326-6500, FAX 202-371-9227

Bateman House, 82-88 Hills Road
Cambridge, UK CB2 1LQ
+44 (0) 1223 326500, FAX +44 (0) 1223 326501

Subscription Services For change of address, missing issues, new orders and renewals, and payment questions: 866-434-AAAS (2227) or 202-326-6417, FAX 202-842-1065. Mailing addresses: AAAS, P.O. Box 96178, Washington, DC 20090-6178 or AAAS Member Services, 1200 New York Avenue, NW, Washington, DC 20005

Institutional Site Licenses please call 202-326-6755 for any questions or information

Reprints: Author Inquiries 800-635-7181
Commercial Inquiries 803-359-4578

Permissions 202-326-7074, FAX 202-682-0816

Member Benefits Bookstore: AAAS/BarnesandNoble.com bookstore www.aaas.org/bn; Car purchase discount: Subaru VIP Program 202-326-6417; Credit Card: MBNA 800-847-7378; Car Rentals: Hertz 800-654-2200 CDP#343457, Dollar 800-800-4000 #AA1115; AAAS Travels: Betchart Expeditions 800-252-4910; Life Insurance: Seabury & Smith 800-424-9883; Other Benefits: AAAS Member Services 202-326-64[illegible] or www.aaasmember.org.

science_editors@aaas.org (for general editorial queries)
science_letters@aaas.org (for queries about letters)
science_reviews@aaas.org (for returning manuscript reviews)
science_bookrevs@aaas.org (for book review queries)

Published by the American Association for the Advancement of Science (AAAS), Science serves its readers as a forum for the presentation and discussion of important issues related to the advancement of science, including the presentation of minority or conflicting points of view, rather than by publishing only material on which a consensus has been reached. Accordingly, all articles published in Science—including editorials, news and comment, and book reviews—are signed and reflect the individual views of the authors and not official points of view adopted by the AAAS or the institutions with which the authors are affiliated.

AAAS was founded in 1848 and incorporated in 1874. Its mission is to [illegible] and technology for everyone, enhance the science and technology workforce and infrastructure, increase public understanding and appreciation of science and technology, and strengthen support for the science and technology enterprise.

Information for Authors

See pages 120 and 121 of the 5 January 2007 issue or access www.sciencemag.org/feature/contribinfo/home.shtml

EDITOR-IN-CHIEF **Donald Kennedy**
[illegible] **Monica M. Bradford**
[illegible]
R. Brooks Hanson, Barbara R. Jasny, Katrina L. Kelner [illegible] **Colin Norman**

[illegible] **Philip D. Szuromi** [illegible]

EXECUTIVE PUBLISHER **Alan I. Leshner**
PUBLISHER **Beth Rosner**

Fulfillment & Membership Services (membership@aaas.org) [illegible] manager Waylon Butler [illegible] Andrew [illegible] Pat Butler [illegible] Baker [illegible] Cynthia Johnson [illegible] Tomeka Diggs, Tarrika Hill, Erin Layne

Business Operations and Administration director Deborah Rivera-Wienhold; business manager Randy Yi; senior business analyst Lisa Donovan; business analyst Jessica Tierney; financial analyst Michael LoBue, Farida Yeasmin; rights and permissions: administrator Emilie David; associate Elizabeth Sandler; marketing: director John Meyers; marketing managers Darryl Walter, Allison Pritchard; marketing associates Julianne Wielga, Mary Ellen Crowley, Catherine Featherston, Alison Chandler, Lauren Lamoureux; international marketing manager Wendy Sturley; marketing executive Jennifer Reeves; [illegible] services director Linda Rusk; site license sales Jason Hannaford; [illegible] sales director Tom Ryan; sales and customer service Mehan Dossani, Kiki Forsythe, Catherine Holland, Wendy Wise; electronic media: manager Lizabeth Harman; project manager Trista Snyder; assistant manager Lisa Stanford; production associates Nichele Johnston, Kimberly Oster

Advertising director worldwide ad sales Bill Moran

Product (science_advertising@aaas.org); midwest Rick Bongiovanni [illegible]; west coast/w. canada Teola Young 650-964-2266; east coast/e. canada Christopher Breslin: 443-512-0330, FAX 443-512-0331; uk/europe/asia Julie Skeet: +44 (0) 1223-326-524, FAX +44 (0) 1223-325-532; japan Mashy Yoshikawa: +81 (0) 33235 5961, FAX +81 (0) 33235 5852; traffic manager Carol Maddox; sales coordinator Dejandra Simms

Commercial Editor Sean Sanders: 202-326-6430

Classified (advertise@sciencecareers.org); u.s.: [illegible] Ian King: 202-326-6528, FAX 202-289-6742; [illegible] Darrell Bryant: 202-326-6533; [illegible] Daryl Anderson: 202-326-6543; [illegible] Allison Millar: 202-326-6572; [illegible] Fernando Junco: 202-326-6740; [illegible] Kane Putney: 202-326-6577; sales coordinators Erika Bryant, Rohan Edmonson, Shirley Young; international: sales manager Tracy Holmes: +44 (0) 1223-326525, FAX +44 (0) 1223-326532; sales Christina Harrison, Svitlana Barnes; sales assistant Louise Moore; japan: Jason Hannaford: +81 (0) 52-757-5360, FAX +81 (0) 52-757-5361; advertising production operations manager Deborah Tompkins; associates Christine Hall, Amy Hardcastle; marketing assistants Robert Buck, Mary Lagnaoui

AAAS Board of Directors retiring president, chair Gilbert S. Omenn; president John P. Holdren; president-elect David Baltimore; treasurer David E. Shaw; chief executive officer Alan I. Leshner; board Rosina M. Bierbaum, John E. Dowling, Lynn W. Enquist, Susan M. Fitzpatrick, Alice Gast, Thomas Pollard, Peter J. Stang, Kathryn D. Sullivan

ADVANCING SCIENCE, SERVING SOCIETY

Science International

[illegible] Caroline Ash (General: +44 (0) 1223 326500) [illegible] Stella M. Hurtley, Ian S. Osborne, Stephen J. Simpson, Peter Stern; associate editor Joanne Baker; [illegible] Alice Whaley; Deborah Dennison; [illegible] Janet Clements, Phil Marlow, Nil White; [illegible] Daniel Clery; [illegible] Gretchen Vogel (Berlin: +49 (0) 30 2809 3902, FAX +49 (0) 30 2809 8365); [illegible] Michael Balter (Paris), Martin Enserink (Amsterdam and Paris), John Bohannon (Vienna)

Asia Japan Office: Asca Corporation, Eiko Ishioka, Fusako Tamura, 1-8-13, Hirano-cho, Chuo-ku, Osaka-shi, Osaka, 541-0046 Japan; +81 (0) 6 6202 6272, FAX +81 (0) 6 6202 6271; asca@os.gulf.or.jp; [illegible] Richard Stone +66 2 662 5818 (rstone@aaas.org); [illegible] Hao Xin, + 86 (0) 10 6307 4439 or 6307 3676, FAX +86 (0) 10 6307 4358; cindyhao@gmail.com; [illegible]

Africa Robert Koenig [illegible]

EDITED BY CONSTANCE HOLDEN

SOCCER MAN ON DISPLAY

The Musée de l'Homme in Paris has recruited a superstar. A new exhibition on the history of humankind opening this week will feature a cast of the skull of world-famous soccer player Lilian Thuram. His skull will be reproduced using a magnetic resonance imaging scanner. It already will be in the company of two other Frenchmen: a 17th-century philosopher, René Descartes, and a well-preserved 30,000-year-old male Cro-Magnon fossil on display for the first time.

The museum wanted a living person's skull in the exhibit. It picked Thuram, a campaigner against racism and social injustice and a symbol of the unity of mankind. That message comes through in the February issue of *Sciences et Avenir*, which says the exhibit "shows we are all from the same family."

The museum's goal is a comment on the modern world's own history, says archaeologist Nathan Schlanger of the National Institute for Research in Preventive Archaeology in Paris. The Musée de l'Homme originally had buried the remains of Saartjie Baartman, an early 19th-century Khoisan woman from South Africa known as the "the Hottentot Venus" who was taken around Europe as a curiosity and whose skeleton, genitals, and brain were on display in the museum after she died. She was returned to South Africa in 2002. "Sometimes in the past, a desire to control context as a [illegible] says Schlanger. "There was a mindset that brains were supposed to be black and white athletes whose bodies are special."

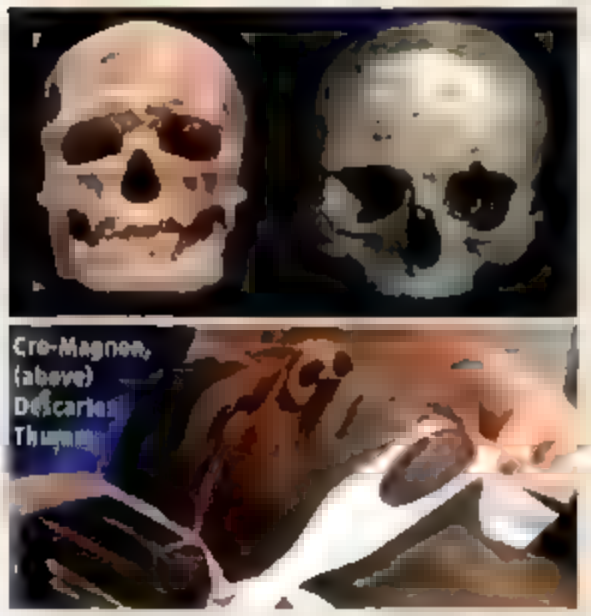

CREDITS, CLOCKWISE FROM UPPER LEFT: DANIEL PORS AND MUSÉE DE L'HOMME; RAMEN LAMBEOUP'S; NATIONAL WEATHER SERVICE; SOURCE: GLOBAL CROP DIVERSITY TRUST

Watch That Passwd

What should be your score as a computer password? Engineer Michael Cukier and colleagues at the University of Maryland, College Park, sought to find out by analyzing attacker behavior on networks of four Linux computers connected to the Internet. Over 24 days, there were 269,262 hacker attempts.

Root was by far the most commonly attempted username, tried on more than 12% of the attempts. Next came a string of test, guest, info, adm, mysql, user, administrator, and oracle. Attempted passwords were even more banal. In addition to trying the username, most went with such digits as "1234" or with "password," "passwd," or "test."

Cukier says the work should help security administrators combat mass automated assaults, the most common type of hacking.

NET WATCH

Way Back Weather

Three funnels sample from a roiling storm cloud in the earliest known storm photograph (below). Snapped in 1884 near Howard, South Dakota, it is one of several dozen vintage images on display at this gallery from the U.S. National Weather Service.

The illustrations and photos, from the early 1800s to the 1990s, explore the effects of floods, hurricanes, tornadoes, and other types of extreme weather. Visitors can relive the dust storms that swept the Great Plains in the 1930s and view some of the data and film that came across when warnings for Gulf Coast 36 years before Katrina failed. The gallery also records advances in weather observation technology and tells what it might be like to be the object of a photographic image of a weather event, which shows a cone funnel lowering toward Bassett, Nebraska, in 1948.

Seed Bank Blueprints Unveiled

A "Doomsday" seed vault, designed to preserve the world's agricultural diversity, will be built to survive the worst scenarios of global warming for at least 2 centuries, according to architectural plans released last week. The $4.8 million Svalbard Global Seed Vault will be located on a Norwegian island just 1000 kilometers from the North Pole (*Science*, 23 June 2006, p. 1730). The plans call for two chambers dug deep into a mountainside 130 meters above sea level—more than high enough to stay dry even if all the ice in Greenland and Antarctica melts. The chambers will be connected to the outside via a 120-meter-long tunnel.

"This design takes us one step closer to guaranteeing the safety of the world's most important natural resource," says Cary Fowler of the Global Crop Diversity Trust, which will help fund the operation and coordinate the acquisition of seeds. Construction should begin next month and be finished by September. The architects designed an entrance with lighting so that it will "gleam like a gem in the midnight sun."

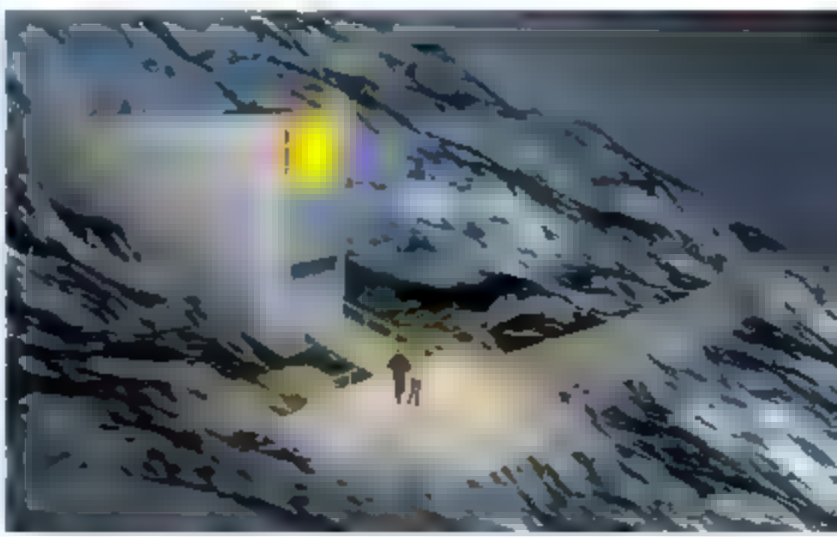

EDITED BY YUDHIJIT BHATTACHARJEE

<< In the Courts

SENTENCED. Scores of letters pleading for leniency did not stop a Los Angeles judge this month from sentencing the pioneering gene-therapy researcher W. French Anderson to 14 years in prison. Anderson was convicted last summer of molesting a young girl (*Science*, 28 July 2006, p. 437). "It is a tragedy for everyone," says Laurence Kedes, director of the Institute for Genetic Medicine at the University of Southern California in Los Angeles, where Anderson worked until he resigned last September. Anderson's lawyer told the court the 70-year-old will need to be kept apart from other prisoners, making this, as Kedes says, the equivalent of a "life sentence" in solitary confinement.

AWARDS

MAHIDOL PRIZE. Sometimes the simplest solution is also the most effective. Four decades ago, researchers discovered that oral rehydration therapy (ORT), a mixture of glucose, salts, and water, could prevent patients from succumbing to cholera and other diarrheal diseases. The low-tech breakthrough saves more than 1 million lives each year, primarily in developing countries. At a ceremony in Bangkok's Royal Palace on 31 January, King Bhumibol Adulyadej of Thailand bestowed the Prince Mahidol Award on four physician-scientists who played key roles in ORT's development: Stanley Schultz, David Nalin, and Richard Cash of the United States and Dilip Mahalanabis of India.

The award is named after King Bhumibol's father, Prince Mahidol of Songkla, a Harvard-trained physician who is known as the "Father of Public Health" in Thailand. Schultz took home $50,000 for the medicine prize; the others shared $50,000 for the public health prize. During a private audience, King Bhumibol quizzed the awardees on topics such as stemming soil erosion to reduce the severity of seasonal flooding. "His Majesty knows his science," Cash says.

FAISAL PRIZES. A British chemist, a Canadian endocrinologist, and a U.S. urologist are among the winners of this year's $200,000 King Faisal International Prizes awarded by the King Faisal Foundation of Saudi Arabia. U.K.–born James Stoddart of the University of California, Los Angeles, receives the science prize for his work on the self-assembly of molecular structures, a cornerstone of nanoscience. The medicine prize is shared by Fernand Labrie of Laval University in Quebec City, Canada, and Patrick Walsh of Johns Hopkins University School of Medicine in Baltimore, Maryland, for improving the management of prostate cancer using therapeutic and surgical approaches. Islamic scholar Roshdi Rashed, a former researcher at France's National Center for Scientific Research, is being honored for studies on Muslims' contributions to basic science, particularly mathematics and optics.

MOVERS

CRISIS MANAGEMENT. The Global Fund to Fight AIDS, Tuberculosis, and Malaria has a new guardian. Michel Kazatchkine, an HIV/AIDS immunologist who is currently France's ambassador for HIV/AIDS and communicable diseases, will become director of the $7 billion organization based in Geneva, Switzerland, on 31 March.

The fund's outgoing director, British public health expert Richard Feachem, has been dealing with allegations that money was misspent on luxuries. But observers are optimistic that Kazatchkine can steer the organization into smoother waters. "Kazatchkine is not only an extremely accomplished AIDS physician with 20 years of experience, but he successfully ran [the French national agency for AIDS research], one of the largest AIDS organizations in the world," says Iain Simpson, spokesperson for the World Health Organization.

CREDITS: (TOP TO BOTTOM) KINGDOM OF THAILAND/POOLIAFP/PHOTO; ANDREW SAMUEL BOLLENDORF/FAL DE PUEUR; HAND CARVED/SHUTTERSTOCK

Money Matters

TO HIS CREDIT. T. Denny Sanford, a South Dakota businessman who made a fortune in the credit card industry, is donating $400 million to create a world-class health care system and research center in Sioux Falls, South Dakota. And he wants researchers to choose a single area that will receive a significant chunk of the cash. The project is expected to employ more than 100 researchers, and Sanford hopes it will "come up with a cure" in the chosen area.

This isn't Sanford's first foray into scientific philanthropy. Last year, he promised to give South Dakota $70 million toward an underground lab if the National Science Foundation chose its site in an upcoming competition. Hospital officials hope his latest act of generosity, which prompted the Sioux Valley Hospitals and Health System to change its name to Sanford Health, will transform the center into a national hub of medical research and patient care.

Got a tip for this page? E-mail people@aaas.org

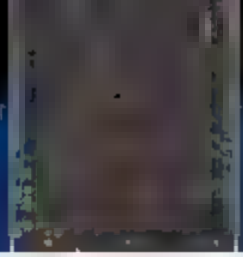

Cancer risk sparks debate 924

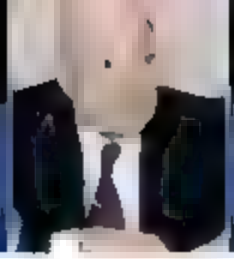

Manager of the budget 927

U S ACADEM A

MIT Hunger Strike: Sour Grapes, Or the Bitter Taste of Racism?

James Sherley an African-American stem cell researcher at the Massachusetts Institute of Technology (MIT) in Cambridge began a hunger strike last week to protest the school's denial of his bid for tenure. Claiming that racism played a part in his rejection, Sherley vows to maintain a daily presence outside the provost's office until MIT admits" its bias and grants him tenure. His protest has divided the faculty and shined a spotlight on the dearth of tenured African-American scientists at the nation's elite research institutions.

Sherley, an associate professor, would have been the first tenured African American in the 41-person biological engineering department on a campus where 4 out of all the tenured faculty are underrepresented ethnic minorities. Despite winning a $2.5 million Director's Pioneer Award from the National Institutes of Health for work on expanding lines of human adult stem cells, Sherley's request for tenure was denied in January 2005. Two external reviews didn't change the decision. Sherley's list of complaints includes the allegation that he was given less laboratory space than other colleagues and that the department chair asked his wife—a departmental colleague who often clashed with Sherley—to weigh in on the tenure decision. He also believes that some of the hostility from his colleagues is fueled by his opposition to human embryonic stem cell research.

"This is about ending the injustice that many African-American scientists before me have endured in silence," says Sherley, who has vowed to drink only water and take vitamins and electrolyte supplements. "We're destroying careers, throwing talent away. It's not right, it's not smart, and I've decided to do something about it." A day after Sherley began his strike, 11 professors including linguist Noam Chomsky circulated a letter demanding a review of the grievance process by a committee "composed of members from inside and outside MIT."

At the same time, some 20 department members have signed a statement contesting Sherley's allegations. "Was this absolutely the most perfect tenure review? I don't think there is such a thing," says associate provost Claude Canizares, whose office asked a three-person committee to reexamine the tenure review. "But there was every attempt made to conduct the review with absolute fairness and integrity."

Public protest. James Sherley begins each morning outside the MIT provost's office before returning to his lab in the afternoons.

Sherley says he hopes his protest will hit the school "like a nuclear explosion" and force it to examine the question of institutional racism. Three days before he began his strike, MIT President Susan Hockfield announced "a comprehensive, rigorous, and systematic study of the impact of race on the hiring, advancement, and experience of minority faculty at the Institute." Canizares says the study "take[s] advantage in an ironic way, of the opportunity for discussion" created by Sherley's dramatic step. "It has energized people on campus to talk about the issue."

Sherley's hunger strike has also elicited support from two former MIT researchers, both African Americans who say they encountered an adverse climate at the school. "Some of my experiences during that time undercut my status and represent the kind of racism that Sherley is opposing," wrote Sylvia Sanders, an assistant professor of biology between 1997 and 2001, in a 7 February letter circulating among MIT faculty. In one case, she says, a senior white professor told her that she had violated rules by bringing students into the faculty lunchroom. (There is no such rule.)

Sanders's letter also cited the reaction of a white colleague after returning from a neuroscience meeting. "There were 10,000 neuroscientists there, and the only black people I saw were the waiters. Why is that?" he asked her during an elevator ride. When she responded by asking him, "Why are there so few African Americans at MIT?," he replied, "Anyone can be a neuroscientist, but this is MIT!" Sanders now teaches third grade at a public school in Palo Alto, California.

A second scientist, now a tenured professor of chemistry at the University of Illinois, Urbana-Champaign, believes that his failure to win tenure at MIT wasn't based entirely on an assessment of his contributions to science and the profession. "Judgments are constantly being made whether you are aware of them or not, and your idiosyncrasies stand out much more if you are black than if you are white," says Philip Phillips, an African American who spent 10 years at MIT's chemistry department. Phillips says he doesn't know "what happened behind closed doors" during his tenure review in 1991. "But I was told later that, for at least one faculty member involved in the decision, the fact that I wore baggy pants was an issue."

Sherley, whose appointment ends 30 June, hopes that his protest, begun 5 February, will force the university to confront such attitudes. Sherley says he's lost 14 pounds since beginning his regimen of spending every morning outside the provost's office before returning to his lab in the afternoon. He promises to continue the routine indefinitely. "Something has got to change at MIT," he says.

–YUDHIJIT BHATTACHARJEE

CREDIT: DAVID L. RYAN/GLOBE STAFF

RESEARCH INTEGRITY

Bubble Fusion Researcher Cleared of Misconduct Charges, but Doubts Linger

Purdue University officials last week declared that an internal inquiry has cleared bubble-fusion researcher Rusi Taleyarkhan of allegations of research misconduct. The announcement appears to bring to an end a nearly yearlong row that has split the university. But with scientific claims and counterclaims still reverberating around the community, the battle over tabletop bubble fusion shows no sign of dying down.

"I feel vindicated and exonerated," Taleyarkhan says. "It's been a pressure cooker for about a year." Taleyarkhan is the chief proponent of sonofusion, the controversial idea that sound waves can collapse bubbles in a way that yields energy through nuclear fusion. If true, the research holds out the promise of a clean, limitless energy source. Taleyarkhan's purported evidence for sonofusion drew scientific skepticism from the start (*Science*, 8 March 2002, p. 1808), and early independent efforts failed to reproduce his results, including one in 2002 by his former colleagues at Oak Ridge National Laboratory in Tennessee.

Last year, an article in *Nature* stoked the controversy when it reported that several of Taleyarkhan's colleagues at Purdue in West Lafayette, Indiana, where he moved full-time in 2004, had complained that he obstructed their work and tried to stop them from publishing results that contradicted his own. Other researchers continued to challenge Taleyarkhan on scientific grounds. Last year, one critic, sonochemist Kenneth Suslick of the University of Illinois, Urbana-Champaign, even raised the issue of possible scientific fraud in an e-mail to a Purdue research official.

Purdue appointed a committee to review the matter, although just what allegations were investigated has never been made clear. In June, the university reported that it had completed an initial inquiry and it launched a second one. Now, university officials say the inquiries have cleared Taleyarkhan of misconduct, but details of the findings, the charges, and even the makeup of the committees will be kept confidential, in keeping with the university's policies. "We respond with it," says Purdue spokesperson Jeanne Norberg.

Other experts both inside and outside the university say the process was shrouded in so much secrecy that it's impossible to know what the reviews entailed. "It's outrageous. I don't know what Purdue is doing," says Dieter Tsoukalas, a nuclear engineer at Purdue who initiated some of the allegations against Taleyarkhan. Tsoukalas says he spoke to the initial review committee last spring and was asked to resubmit written allegations in September, which he says he did. Yet Tsoukalas says, neither he nor anyone else he knows was ever interviewed by the second panel. Suslick and Seth Putterman, a physicist at the University of California, Los Angeles, who headed a Defense Advanced Research Projects Agency–funded effort to replicate Taleyarkhan's work, say that they too were never contacted by the panel and are frustrated by its secrecy.

Efforts to understand just what is going on inside Taleyarkhan's tabletop fusion devices remain equally controversial. Last spring, Taleyarkhan invited two separate teams to use his experimental setup at Purdue to see whether they could spot the telltale signs of fusion. The experiment is deceptively simple: ultrasound to collapse bubbles in an organic solvent and force deuterium atoms in the bubbles to fuse, liberating either tritium and a proton or helium-3 and an exact neutron, pulses of energy. In May, Ted Forringer, a physicist at LeTourneau University in Longview, Texas, ran the experiment with two undergraduate students using two different types of neutron detectors, both of which he says recorded significantly higher levels of neutrons than did controls. In June, William Bugg, a physicist emeritus at the University of Tennessee, Knoxville, also ran the experiment and says he too found evidence for excess neutrons.

Neither of these experiments has been published in full, however. Stanley Milora, a physicist at Oak Ridge, says that in a write-up of the Forringer experiment that he's seen, electronic neutron counters called scintillation detectors only collected data for 60 seconds. In addition to longer data collection, Milora says he'd like to see evidence of where any proposed neutrons are coming from. If deuterium atoms are fusing in the collapsing bubbles, neutrons should hit the detectors just a few nanoseconds after the bubbles collapse and give off a burst of light. But Milora says there was no effort to track such correlations.

Putterman, Suslick, and their colleagues did attempt to register such correlations using Taleyarkhan's own engineering diagrams to construct their sonofusion apparatus. In a paper they published last week in *Physical Review Letters*, the researchers report that they detected no neutrons above background and saw no correlations between light flashes and neutrons.

The bottom line, Milora says, is that most people won't believe bubble fusion is real until the work is verified outside Taleyarkhan's lab. "I think a fully independent reproduction of these results would turn a lot of people around," he says. Until that happens, the chief form of energy produced by bubble fusion is likely to be heated arguments. —ROBERT F. SERVICE

CREDIT: LYNN FREENY/DOE

DATA SHARING

New Swiss Influenza Database to Test Promises of Access

The world will soon know whether dozens of scientists and health experts meant business when they pledged to share crucial data on bird flu 6 months ago. Behind the scenes, a small group of experts has arranged for a brand-new influenza database housed at the Swiss Institute of Bioinformatics (SIB) in Geneva, that plans to open the first week of March to turn their promise into reality.

If all goes according to plan, researchers and H5N1-affected countries will use the database to reveal information about the virus to the world immediately, with the assurance that nobody can use their data to produce papers, drugs, or vaccines without their permission.

About 15 flu labs currently share key genetic data about H5N1 in a password-protected compartment at the Influenza Sequence Database (ISD) at Los Alamos National Laboratory in New Mexico. That deal, under the auspices of the World Health Organization (WHO), came under fire last year from researchers, led by Italian veterinary virologist Ilaria Capua, who believes that everyone—not just a select group—should have access. Their criticism sparked the creation of the Global Initiative on Sharing Avian Influenza Data (GISAID), announced in a letter in *Nature*, in August 2006 that was signed by more than 70 experts. The plan was spearheaded by media consultant Peter Bogner and, then unknown in the influenza world (*Science*, 25 August 2006, p. 1026).

A small group including Bogner, Capua, and Nancy Cox, head of the influenza division at the U.S. Centers for Disease Control and Prevention in Atlanta, Georgia, has now hammered out details of the plan. They reviewed final arrangements at a meeting in Munich last week. Anyone can get access to the new database, provided they register, log in, and accept an agreement limiting their use of the data, Bogner says. Those who provide data have 6 months to take care of patents and scientific publications; after that, the information will be entered into three large public databases.

Bogner declined to provide details of the user agreement, which will be made public shortly. But these rules—and whether they're followed—will be crucial to GISAID's success, says Albert Osterhaus of Erasmus University Medical Center in Rotterdam, the Netherlands. As a signatory to the *Nature* letter, Osterhaus says he's "committed in principle" to depositing information in the database, "but I want to see the exact terms first." WHO has not been involved in the plan but welcomes it, says David Heymann, head of the agency's flu efforts.

SIB Director Amos Bairoch says that when GISAID's database kicks off, it will be filled with decades' worth of influenza data from humans, birds, and other species. Bairoch believes Switzerland's famed neutrality will help win over countries reluctant to contribute to a U.S.-sponsored database.

Sharing. Peter Bogner has financed GISAID's efforts himself.

CREDIT: COURTESY OF P. BOGNER

ISD head Catherine Macken says researchers may prefer GISAID because it's free of charge—but she's okay with that. The bad press ISD has received because of the H5N1 compartment has been "a nightmare," she says. "If someone else wants it, they're welcome." "A sense of civic duty" led Bogner to bankroll the entire operation so far with his own money. But corporate backers, which he declined to name, are interested in helping out, he says.

The issue of influenza sharing made fresh headlines last week when Indonesia announced it would no longer share viral samples of H5N1 with WHO without a so-called Material Transfer Agreement that limits commercial use of the virus. But even if Indonesia no longer shares viruses, Bogner says he has guarantees that it will keep sharing its H5N1 sequence data with GISAID.

—MARTIN ENSERINK

FAIR Deal for India

Three accords have opened a new era in scientific collaboration between Europe and India, bolstered last week at a meeting in New Delhi between India's science minister and his counterparts from the European Union (E.U.).

The first such gathering outside Europe, the parley featured India committing to a $250 million contribution for the $1.5 billion Facility for Antiproton and Ion Research (FAIR) at the GSI heavy-ion research lab in Darmstadt, Germany. Indian scientists will collaborate on the project, which once completed in 2014 will produce beams for research into nuclear physics, plasmas, and nuclear astrophysics. "It's good to have India on board," says John Wood, head of the U.K.'s Central Laboratory of the Research Councils.

In addition, India and the E.U. will each contribute $7.5 million annually to a joint research fund for projects in health, climate, and energy. Indian scientists will also be able to compete for grants under the E.U.'s 7-year, $75 billion Seventh Framework Programme, which began earlier this year. "India will be the most important and first partner in the Seventh Framework Programme," said Annette Schavan, Germany's minister for education and research, who led the E.U. delegation. Indian science minister Kapil Sibal called the agreement "historic."

—PALLAVA BAGLA

Korea Targets Lab Mischief

SEOUL—The South Korean government last week set new penalties for scientific misconduct and mandated a new system for investigating alleged misconduct in state-funded science. Drafted in response to the Woo Suk Hwang cloning scandal, the rules require government labs, universities, and research centers that receive state funds to tighten oversight to thwart scientific misconduct including plagiarism, data tampering, and intimidation of whistleblowers. The guidelines, which contain new wording on training, call on institutions to form investigative committees comprised of at least five persons including experts and outsiders to probe allegations.

Under the guidelines, penalties for misconduct include the government ending state-run projects and barring institutions from receiving state funding for up to 3 years. In-il Lee, a ministry official, said that the government hopes that setting up this system will force scientists to take more responsibility in their research.

—D. YVETTE WOHN

DIAGNOSTICS

Amid Debate, Gene-Based Cancer Test Approved

In the chaotic and rapidly expanding field of "personalized medicine," dozens of companies aim to create tests that read a disease's biochemical tea leaves and anticipate the course it will take. The predictions, which often rely on gene expression patterns, can have a momentous effect, for example prompting doctors and patients to eschew chemotherapy when a test suggests that a breast cancer has a low risk of recurring.

But as these largely unregulated tests move into clinical use, researchers are asking some fundamental questions: Are they based on sound science? And can physicians readily interpret the results?

Last week, the U.S. Food and Drug Administration (FDA) stepped full force into this debate, issuing its first-ever approval of a multigene prognostic test and 2 days later holding a contentious meeting to discuss more stringent oversight of this area. Called MammaPrint, the test approved by FDA was developed by Amsterdam-based Agendia and aims to predict a breast cancer's risk of recurrence. MammaPrint is currently available in Europe, South America, and elsewhere. Agendia says it has performed more than 5000 tests so far.

In the United States and Europe, diagnostics such as MammaPrint and another breast cancer prognosticator called Oncotype DX are not generally approved the way drugs and devices are. Instead, in the U.S., they're considered laboratory tests and are allowed on the market with little scrutiny of their science when performed under the auspices of a single lab. Agendia sought FDA approval of MammaPrint in part on the agency's request and in part to reassure physicians that the test is sound, says the company's co-founder and chief scientific officer Rene Bernards. Based largely on results from 302 European breast cancer patients, FDA expressed confidence in MammaPrint's quality.

But now FDA wants to extend its oversight to many more gene-based tests. In September, the agency released a draft document suggesting that many prognostic tests should be regulated as medical devices, which would vastly expand the agency's oversight of them. This policy would cover many candidate tests, including, possibly, a method for identifying the primary source of metastatic cancer and a blood test to determine whether a transplanted heart is being rejected. "We had concerns" about this class of products, said Steven Gutman, FDA's director of the Office of In Vitro Diagnostic Device Evaluation and Safety, at last week's meeting in Gaithersburg, Maryland. Accuracy is one concern, he says, as is a "lack of transparency" about how the tests are performed. FDA is accepting comments until 5 March.

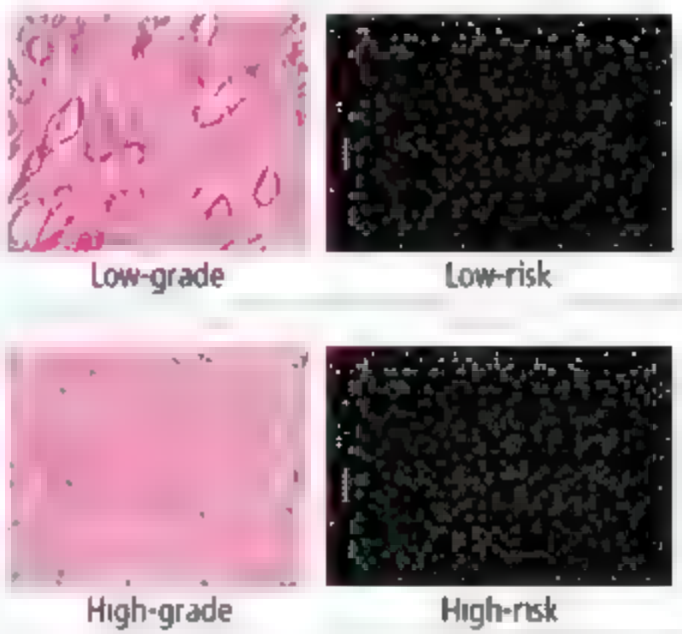

Next generation. Cancers have long been evaluated by direct observation (*left column*); a new test uses gene expression to judge the risk of recurrence (*right column*).

At FDA's meeting, many companies and some patient advocacy groups argued against FDA's proposed policy. They suggested that requiring more extensive clinical trials would impose a financial burden that diagnostics outfits can't afford and possibly add a decade's delay. "We can't wait that long," says Charles Perou, a geneticist at the University of North Carolina, Chapel Hill, who is trying to commercialize a breast cancer prognostic test but did not attend the meeting.

Two of the breast cancer tests that are farthest along, MammaPrint and Oncotype DX, have settled on a middle ground: The companies are marketing their tests to doctors on the basis of retrospective studies of stored tissue while long-term clinical trials of breast cancer patients run simultaneously. MammaPrint assesses 70 genes' significance in certain women with breast cancer that hasn't spread, typically one of the groups that may avoid chemotherapy, into "low-risk" or "high-risk" categories. Oncotype DX relies on a 21-gene analysis to help inform clinicians whether patients with localized, estrogen-receptor-positive cancer are at risk of relapse. And although CEO Randy Scott of Genomic Health, the Redwood City, California, company that makes Oncotype DX, believes that these tests should be developed as "you would develop a drug," he does not think they should be regulated as such. "We're not injecting anything into the body," he says.

But some physicians see significant risks. "If I withhold life-saving therapy from a patient because of a bad test, that's every bit as bad as if I gave her a bad drug," says Daniel Hayes, a breast cancer specialist at the University of Michigan, Ann Arbor, who helps run an Oncotype DX trial.

Physicians such as Hayes, meanwhile, continue to puzzle over what some prognostic tests are really telling them. In cancer, it may be that at 5 years, one group has a 20% relapse rate, the other has a 75% relapse rate, but what's going to happen at 10 years? Are we measuring the chance of metastases, or the rate?" asks Larry Norton, deputy physician-in-chief for breast cancer programs at Memorial Sloan-Kettering Cancer Center in New York City. He also notes that many of the genes used by these tests are linked to tumor growth, despite emerging data that other genes, such as those that affect inflammation, could also be critical.

Another concern, says Hayes, is that because many studies were designed to answer a simple question—did the patient live or die?—some of the data could be misleading. A participant whose tumor responds unusually well to chemotherapy, for example, may be misclassified as one with a positive prognosis from the outset. In such a case, says Hayes, a test result could lead to "withholding the very agent that made their prognosis good."

–JENNIFER COUZIN

FAITH AND SCIENCE

In Europe's Mailbag: A Glossy Attack on Evolution

PARIS—It's the most gorgeous-looking attack on evolution seen in a long time. That's the consensus among European scientists who in recent weeks have received unsolicited free copies of the *Atlas of Creation*. The 768-page, lavishly produced tome was written by Harun Yahya, a Turkish author who denounces Darwinism as the source of many evils, including 9/11. Its publisher has sent hundreds if not thousands of copies of the book to researchers in at least four countries in Western Europe.

Mass mailing. Schools in France have received a slick volume that purports to disprove evolution science.

A source of amusement to some, the book has troubled and outraged others, especially in France, where a French translation landed in the mailboxes of hundreds of high school directors and librarians. "This is a nasty attack on our education system," says evolutionary biologist Armand de Ricqles of the College de France, who worries that the book might touch off a battle over the teaching of evolution in Europe. French Education Minister Gilles de Robien swiftly warned schools to keep the book out of pupils' hands.

Harun Yahya is the pen name of Adnan Oktar, the head of the Foundation for Scientific Research (BAV) in Ankara, which has promoted Islamic creationism since 1997 (*Science*, 18 May 2001, p. 1286). Yahya is credited with hundreds of books; he is "more like a brand name" for a group of writers he leads, says Taner Edis, a Turkish-born physicist at Truman State University in Kirksville, Missouri, who has studied Islamic creationism.

Yahya accepts that the world is billions of years old but rejects the concept of evolutionary change. More than 500 pages in the *Atlas of Creation*, the first in a series of seven volumes, are filled with pictures of fossils accompanied by modern-day organisms that look strikingly similar—proof, Yahya says, that evolution theory is false. It's an "absurdly ridiculous" logic, says Gerdien de Jong, one of five biologists at Utrecht University in the Netherlands who received a copy.

Within Turkey, BAV has been "quite successful" in promoting creationism, says biologist Aykut Kence of the Middle East Technical University in Ankara. One recent survey found that more than 50% of biology teachers in secondary education "are not sure about the validity of evolution," says Kence. Yahya's books have also been translated into Arabic, Urdu, and other languages of the Islamic world.

How BAV can afford mass distribution of books, as well as a plethora of DVDs and Web sites in several languages, is unclear. Rumors abound—for instance, about Saudi or U.S. backers—but Turkish law makes finding out the facts very difficult, Edis says. In an e-mailed response to questions, a spokesperson for Yahya declined to address finances. He added that France "can gather up and burn all the books, just like in the days of the Nazis, ... yet the collapse of Darwinism cannot be prevented by prohibitions and bans."

French scientists say they need to operate carefully so as not to inflame tensions with France's sizable Muslim minority. But a response is needed, says de Ricqles, if only to arm teachers with counterarguments. Kence says he and others have tried to promote evolution, but he says he never engages in direct debates with creationists, because that would enhance their credibility.

Meanwhile, some readers were trying to find new uses for Yahya's book last week. Ecologist Michael Hassell of Imperial College London says he's using the 5-kilogram opus as a lamp stand. His colleague Peter Knight, another recipient, says he donated his copy to his ecology group. "I hope they found it was biodegradable and recyclable," he says.

–MARTIN ENSERINK

CREDIT: BERTRAND GUAY/AFP/GETTY IMAGES

SCIENCESCOPE

$25 Million Prize for Greenhouse Whizzes

Mega-entrepreneur and adventurer Richard Branson is offering what he calls "the largest ever science and technology prize" to entice development of a solution to global warming. Modeled after the $10 million Ansari X Prize that led to the development of a reusable crewed rocket in 2004, the $25 million Virgin Earth Challenge will be awarded to whoever can develop a commercially viable technology capable of removing at least a billion tons of carbon dioxide, a major greenhouse gas, from the air every year. Current air capture techniques cost three to four times more than the market will bear. "I think it's great," says physicist Martin Hoffert of New York University, who nonetheless warned that it's going to be a tougher nut to crack than building a better spaceship. Current technology to grab CO_2, he notes, is "very energy-intensive."

–RICHARD A. KERR

Greening the Forest

The Smithsonian Tropical Research Institute (STRI) in Panama has received an $8 million grant from the London-based banking giant HSBC to expand its century-long studies of rain forests to better understand the effects of climate change. Working with Harvard University, STRI's Center for Tropical Forest Science will conduct an annual census across a network of 20 study plots in 15 countries, as well as study the carbon cycle in these tropical forests. The gift is STRI's biggest ever private donation and lets it tackle "important scientific questions that single-site [studies] can't address," says center director Stuart Davies.

–ELIZABETH PENNISI

A Bounty on a Killer

Five nations and the Bill and Melinda Gates Foundation are dangling a $1.5 billion carrot in hopes that the pharmaceutical industry will produce a vaccine for the developing world against *Streptococcus pneumoniae*, which causes pneumonia and meningitis. Last week the consortium pledged to purchase future vaccines at a guaranteed price once the product is proven safe and effective. Pneumococcal infections kill as many as 1.6 million people annually, most of them children. "Now companies know that if they have the technology and they build a plant, they can sell the vaccine," says Robert Black of the Johns Hopkins Bloomberg School of Public Health in Baltimore, Maryland. Black says the arrangement can also be a tool against other diseases plaguing poor nations.

–MARTIN ENSERINK

U.S. NANOTECHNOLOGY

Health and Safety Research Slated for Sizable Gains

Heeding calls for increased basic research on the health and environmental implications of nanotechnology, the Bush Administration has proposed a $3-million-a-year network of academic centers to pursue the topic and disseminate the findings. But that network, part of President George W. Bush's 2008 budget request sent last week to Congress, doesn't address what many consider a bigger problem for the field: the lack of research tied more tightly to the development of new U.S. regulations.

In 2006, the federal government funded $38 million in research on nanotechnology's environmental health and safety. That is likely to grow to $46 million this year (Congress was expected to take final action on the federal budget this week), and the president's budget would boost it to $59 million. At the cornerstone of this new push is a network of centers, funded by the National Science Foundation and modeled after existing NSF networks.

Vicki Colvin, a chemist at Rice University in Houston, Texas, who directs Rice's Center for Biological and Environmental Nanotechnology, says that she believes spending more money on basic research and a network of centers is the right way to go. "It's great news," Colvin says. She notes that nanotechnology remains in its early development despite some 380 products containing nanomaterials that are already on the market. At this stage, she says, it's important to learn more about how nanomaterials interact with biological systems.

The NSF network proposes to do just that, she says, by investigating how the structure of a wide array of different nanomaterials affects their environmental behavior. "Forming a network that permits everyone to exchange supplies and methodology will really fast-forward this field by a couple of years," she says.

But not everyone agrees that basic research is the best investment the government could be making to understand the environmental health and safety aspects of nanoproducts. Nanotechnology "has stopped being a pure science project," says David Rejeski, who directs the Project on Emerging Nanotechnologies at the Woodrow Wilson International Center for Scholars in Washington, D.C. "Nanotechnology is being commercialized at a very fast pace right now. You've got to position the science ahead of that."

Rejeski argues that U.S. regulatory agencies, such as the Environmental Protection Agency (EPA) and the National Institute for Occupational Safety and Health, are struggling to keep up with the questions being raised about how best to regulate nanotech products entering the market. And although EPA would receive $9.6 million in 2008, up from $3.7 million in 2006, Rejeski argues that considerably more is needed.

Last September, both Republican and Democratic leaders of the House Science Committee called for expanding the research needed for regulatory agencies to ensure the safety of nanomaterials in the environment. And supporters have reason to believe legislators will heed that plea. In every year since the U.S. National Nanotechnology Initiative began in 2001, Congress has topped the president's request.

—ROBERT F. SERVICE

U.S. ACADEMIA

Radcliffe Historian Named Harvard President

Harvard University's search for a new president to succeed the controversial Lawrence Summers ended this week with the appointment of a Radcliffe historian and Civil War historian. Drew Faust, 59, will become the first woman to lead the oldest and wealthiest university in the United States. She emerged as the top candidate in the yearlong search after Thomas Cech, biochemist and president of Howard Hughes Medical Institute, withdrew his name from consideration earlier this month.

After her selection was announced on 11 February, Faust spoke out strongly in favor of a new initiative to increase interdisciplinary work in Harvard's extensive science program (*Science*, 26 January, p. 449) and added that she wants to break down the barriers between the sciences and the humanities. She takes over 1 July from interim president Derek Bok.

Some search committee members wanted a physical or biological scientist for the post, but friends and colleagues of Faust insist she has a good track record in supporting research in her current job as dean of the Radcliffe Institute for Advanced Study, a school with a

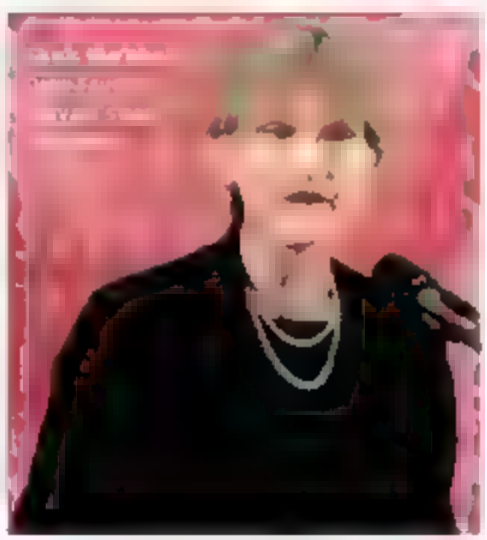

ADAM HUNGER/REUTERS

Harvard. "She is not a scientist, but I am certain she has the ability to ably lead the university's expansion of its science efforts," says Barbara Grosz, a computer scientist and Radcliffe science dean who has worked closely with Faust.

Right from the start, I had many people say to me, 'You should give up on having science at Radcliffe,'" Faust says in an article appearing in the most recent issue of the *Radcliffe Quarterly*. "It was clear to me from the outset that science needed to be an important commitment for the new institute." It also runs in the family. Her husband, Charles Rosenberg, is a historian of medicine and science at Harvard.

Female faculty members at Harvard said they were delighted with the appointment of Faust, a successor to Summers, whose controversial comments about women's ability to succeed in the sciences contributed to his resignation last February. "This is an inspired choice," says Evelyn Hammond, senior vice provost for faculty development and diversity and a historian of science, who has known Faust for years. "She has extraordinary leadership qualities and enormous integrity."

In a press conference after she was named, Faust praised Summers, an economist and former treasury secretary in the Clinton Administration, for his analytical skills. But then she added, "I think women have the aptitude to do anything, and that includes being president of Harvard."

—ANDREW LAWLER

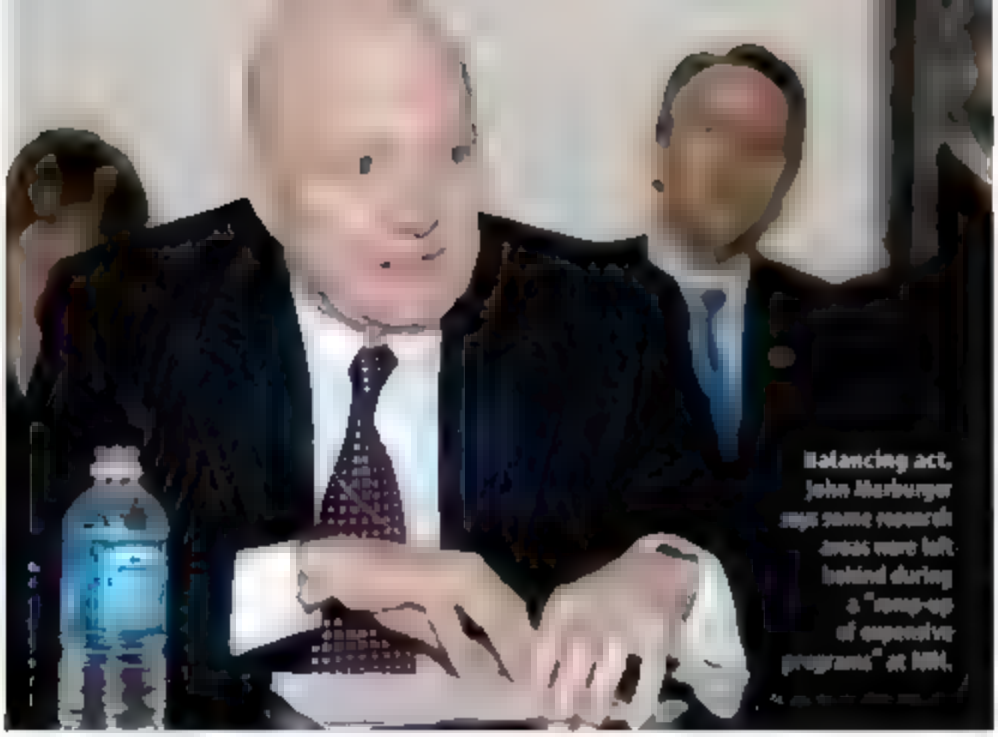

Balancing act. John Marburger says some research areas were left behind during a "ramp-up of expensive programs" at NIH.

U.S. RESEARCH FUNDING

Science Adviser Says That Pruning Is the Key to a Healthy Budget

The U.S. science community needs to figure out how to live with it its means, says John Marburger, science adviser to President George W. Bush. In particular, he believes biomedical scientists need to curb their appetite for federal funding and space scientists must learn to turn off a mission before building and launching a new one.

Speaking last week at *Science* about the president's 2008 budget request to Congress, Marburger defended the Administration's plans to give a sizable boost to a few agencies while starving most of the rest of the science establishment (*Science*, 9 February, p. 750). He says that "no president has been a stronger supporter of science and technology as a way to benefit society," and he rejects complaints from science lobbyists that the budget request threatens the health of the U.S. scientific enterprise.

"I think the overall federal scientific enterprise is well-funded," Marburger says. "But there's been a ramp-up of expensive programs in some areas, while important programs in other areas are underfunded." He notes that the American Competitiveness Initiative, first proposed last year, attempts to correct that imbalance in the physical sciences by boosting the budgets of the National Science Foundation (NSF), the Department of Energy's (DOE's) Office of Science, and the core labs at the National Institute of Standards and Technology. And he says that other agencies can thrive with their current budgets by setting priorities and sticking to them.

Marburger was scheduled to testify this week before the House Committee on Science and Technology, kicking off the year-long budget cycle. And although the Democratic Congress will surely revise the president's request for science and every other sector of federal spending, Marburger's comments, edited for space, shed light on the nature of the government's $55 bid on commitment to basic and applied research.

–JEFFREY MERVIS

On the National Institutes of Health (NIH) budget:

I think they have a structural problem, and I don't have a quick answer. ... There is no way the federal government can ever satisfy the demands created by the doubling of the NIH budget between 1998 and 2003. It's led to what I call an unregulated research market, with booms and busts that are beyond the ability of the government to control.

[At the same time,] NIH funding got way out of step with funding for the physical sciences. Biomedical research is funded much closer to the level of its needs than are the physical sciences. And there are imbalances within the biomedical research enterprise in which it's not clear that the pattern of expenditures matches the importance of the research. A lot of its $28 billion budget is aimed at treatments and therapies for specific diseases rather than basic cell biology and molecular biology, which raises the question of whether we're spending enough on basic research. The leadership understands these issues, and the director's Roadmap addresses these challenges.

On NASA's budget crunch:

Large space science programs face two fundamental problems. The first is the inability to make accurate cost estimates early in the life of the program. Once the price starts to go up, the agency has to either cancel the program or come up with more money. And the money is very hard to find; most of the time, you can't do it without digging into other programs.

Second, the programs are sustained for longer than expected. So if you meet your goal of a certain number of launches per year, and those missions are sustained for a longer period of time, eventually something has to give. Do you know how many space science platforms are active right now? You might guess one or two dozen. The actual number is 55, which is a lot. We are spending a lot of money on space science—far ahead of everybody else in the world. But there needs a better appreciation of the need for strategic management of those assets.

On better project management:

We need new financial models for addressing the transition from construction to operation of a major scientific facility and for deliberately phasing out programs that are expensive once they have accomplished their mission. We can't expect them to last forever, because we can't afford them. We need to continually renew our infrastructure to keep up with what's happening in the rest of the world.

Industry faces a similar challenge. It's a hard decision to shut down an operation that's profitable and productive and invest in new facilities that will be more productive. But it has to be done. ... Look at the Hubble [Space Telescope]. We probably made the wrong decision decades ago to have it maintained by the space shuttle, because it turned out to be much more expensive than anybody realized. We could have launched many other science platforms for the price of maintaining one Hubble.

And the problems associated with life-cycle planning estimates are not an issue to NASA. NSF has experience with this, too, but as its projects become larger and more complicated, the management problems become harder. DOE may do the best job. It has phased out aging facilities before it builds new ones.

We are America. We should be able to manage these projects.

Cases of Mistaken Identity

For decades, biologists working with contaminated or misidentified cell lines have wasted time and money and produced spurious results; journals and funding agencies say it's not their job to solve this problem

IN THE 1980S, WHEN HE WAS A postdoctoral fellow at the Scripps Research Institute in San Diego, California, Reinhard Kofler received what was supposed to be a human cancer cell line from a colleague. "We cultured it, we created clones out of it," he recalls, then "[we] genotyped and realized it was 100% mouse."

After scores of similar experiences with misidentified cells, Kofler and his colleagues at the Tyrolean Cancer Research Institute in Innsbruck, Austria, now authenticate every line as soon as it arrives at the institute. And periodically afterward, they use a simple, cheap, quick, and reliable DNA fingerprinting technique to verify that each cell line continues to be what it should be. "It's an absolute must now," says Kofler. He has also repeatedly encountered problems with cell line contamination and without this checks and vigilance, Kofler says, "I wouldn't be confident about our work."

Not every biologist is so wary. A 2004 survey of nearly 500 biologists by Gertrude Buehring of the University of California, Berkeley, and her colleagues showed that less than 50% of researchers regularly verify the identities of their cell lines using any of the standard techniques such as DNA fingerprinting. "Everybody's concerned about the widespread problem of cell line cross contamination," says Charles Patrick Reynolds of the University of Southern California and the Children's Hospital Los Angeles Institute for Pediatric Cancer Research, who established new pediatric cancer cell lines and tests potential cancer drugs on existing lines.

Indeed, many studies have shown that a surprisingly large number of cell lines have become contaminated, often by older, more well established cancer cells. For example, according to a 1999 paper by Roderick MacLeod and his colleagues at the German Cell Bank (DSMZ) in Braunschweig, 18% of 252 lines donated to the bank were misidentified or contaminated. The extent of the problem "always seems to come as a surprise for people," says John Masters of University College London, president of the European Tissue Culture Society.

And even though biologists read and hear about cross contamination, people "just think that this is not a problem in my lab," says Reynolds. If contaminated cell lines are used merely as "test tubes" to express proteins, a lab's work may not be affected. But, says Masters and others, research with contaminated lines can lead to obscure potential drug leads and

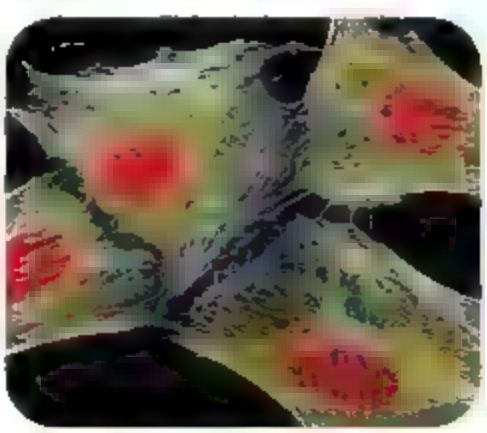

Early warning. HeLa cells have contaminated scores of cell lines for more than 4 decades.

CREDITS: (TOP TO BOTTOM) DSMZ; TORSTEN WITTMANN/PHOTO RESEARCHERS INC.

generate a large amount of artifacts in the scientific literature.

Troubled by this ongoing problem, Roland Nardone, a cell biologist and professor emeritus at the Catholic University of America in Washington, D.C., has taken it upon himself to become the Paul Revere of cell contamination. In a recent white paper chastising the scientific community, Nardone calls for stricter policing of cell identities. He argues that journals and funding agencies such as the U.S. National Institutes of Health (NIH) should mandate authentication of cell lines.

Several professional groups—including the Society for In Vitro Biology, the European Tissue Culture Society, and the American Society for Cell Biology—have endorsed the white paper, as have several cell repositories. But journals and NIH are wary of taking on the role of cell cops, and Reynolds is skeptical that Nardone will succeed where he and others have failed. "No amount of passioned discussion by myself or Dr. Nardone will fix what has been and continues to be a widespread problem," he says. Merely suggesting what needs to be done, Reynolds adds, "is a long way from people actually doing it." Koffler cites his own record as a cautionary tale. "We have started doing this [regularly fingerprinting lines] only 5, 6, or 7 years ago. Before that, even we were lazy."

Murphy's law

How do cell lines assume secret identities, and why does it happen so often? "It's like Murphy's law," says Koffler. "Everything that can go wrong will go wrong. It's just a matter of time." Although most researchers are aware of the possibility of contamination and cautious when handling cells, accidents happen. Cell lines get mislabeled or contaminated with fast-growing cells that can in no time take over the original lines.

The only way to prevent cross contamination is to spot it before it spreads. In 2001, Masters, who has been advocating for increased awareness of the problem for decades, published a description of a DNA fingerprinting technique that has become the standard tool for authenticating cell lines. When a line is established, it is crucial to record the donor's genetic profile and then do the same for the new line, says Masters. If this is done and the fingerprints made available publicly, it would provide other scientists with an authentic signature to verify the identity of the lines. Reynolds and his colleagues recently estimated the cost for a single DNA fingerprinting experiment to be $30. "It's so cheap, so obvious, so trivial, and yet it's not being done," says Masters.

Ignoring history

The roots of the contamination problem go back to the beginning of studies with cell lines. Between the mid-1960s and the early 1980s, Walter Nelson-Rees of the Cell Culture Laboratory of the University of California, Berkeley, at Oakland found more than 40 different cell lines—both human and animal—cross-contaminated by the HeLa line, the first human cell line to be grown successfully in a laboratory. By the time he published his findings, there were already hundreds of papers describing research using the contaminated lines.

Nelson-Rees made it his personal mission to warn others about the dangers of

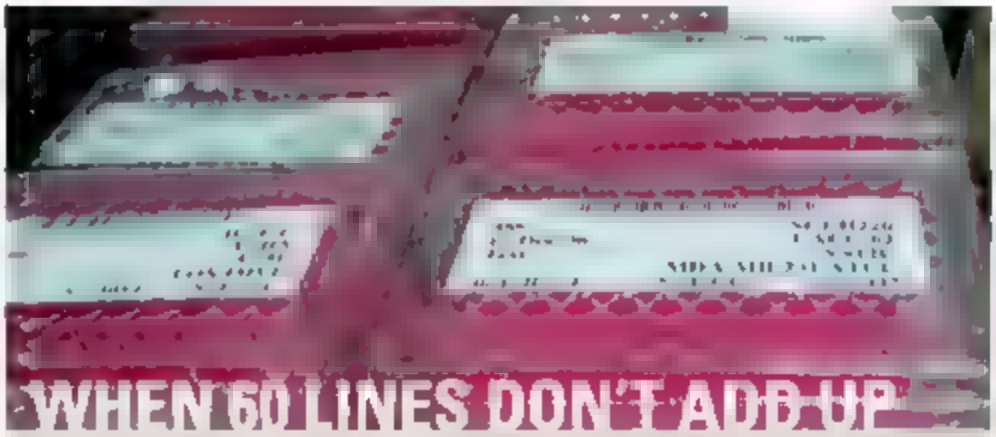

WHEN 60 LINES DON'T ADD UP

Even the bedrock of present-day cancer research, the NCI 60 panel—a group of 60 cancer cell lines maintained by the U.S. National Cancer Institute (NCI) and used widely for both basic research and drug discovery—has not escaped the scourge of cross contamination. In the late 1990s, Moidechai Liscovitch of the Weizmann Institute of Science in Rehovot, Israel, had obtained from the institute the breast cancer line MCF-7 and its drug resistant daughter line, once known as MCF-7/AdrR (for Adriamycin resistance)—both part of the NCI 60 panel. A few years ago, a comparison of the lines in his lab revealed certain biochemical differences that illustrated how [illegible] to drugs. "I knew right away that I had detected a nice story," says Liscovitch.

Early in 2001, he submitted a manuscript on the work to *Oncogene* and was awaiting its publication. Then one of his students stumbled upon a 2000 letter in the *Journal of the National Cancer* [illegible] saying that DNA fingerprinting had revealed that MCF-7 and MCF-7/AdrR were in fact identical. Liscovitch and his colleagues quickly [illegible] their paper [illegible] before it went to print. "It was a big blow for us," Liscovitch says.

Not only was MCF-7/AdrR unrelated to MCF-7, but it also turned out to be identical to an ovarian cancer cell line in the NCI 60 panel. That is not the only case of mistaken identity within the NCI-60 panel. The SNB19 and U251 lines, once thought to be distinct central nervous system lines, are identical to each other and came from the same individual. And MDA-MB-435, a prevalent model for metastatic breast cancer research at the panel's [illegible] M14. NCI has yet to trace the history of MDA-MB-435, which was originally established in 1976 at M. D. Anderson Cancer Center in Houston, Texas. NCI found that the NCI 60 panel's version is the same as a sample of the line originally deposited at a cell bank by M. D. Anderson and as a sample given to an NCI researcher by the cancer center. The [illegible] of the M14 likely happened early in the history of the cell line," NCI says on its Web site.

Although the NCI 60 panel Web site now details the history behind its "misidentified" cell lines, Daniel Zaharevitz, chief of the information technology branch at NCI Developmental Therapeutics Program, considers that a [illegible] more accurate term. Contamination of misidentified the [illegible] done a good way. Contaminated researchers who obtained new lines in the past trust the lines are now suspect. Zaharevitz says the agency is wary of creating undue concern, because much of the work with such lines, such as drug testing, is unlikely to have been compromised.

Liscovitch feels that greater exposure of the problem is needed. He publicized the story of MCF-7/AdrR, now known as NCI ADR/RES, in the 8 January *Cancer Letters*. There may be more such stories in the future. There is some evidence that the NCI-60 panel's version of the colon cancer cell line HCT 15 is not the same as the original line. **–R.C.**

CREDIT: B. CHAPPELL/SCIENCE

HeLa contamination. But the scientific community mostly reacted with hostility and Nelson-Rees eventually gave up (see sidebar, below). No one was willing to withdraw their papers or lose their credibility.

And now researchers continue using the contaminated lines. Nardone, Reynolds, Koffler, and other researchers are worried that history is being repeated, especially because the number of new cell lines has proliferated dramatically.

In 2003, MacLeod and Hans Drexler of DSMZ and their colleague, Yoshinobu Matsuo, then at Fujisaki Cell Center in Okayama, Japan, checked the identity of 550 lymphoma-leukemia lines collected from researchers around the world and found 15% of them to be contaminated, mostly with faster-growing, well-established cell lines. In a letter in the 23 February 2006 issue of *Nature*, they estimated that 20% of all human tumor cell line submissions to the DSMZ include cross contaminations. Because of the small sample sizes, these figures are, at best, "a significant underestimate," says MacLeod.

Estimating the real extent of the problem is difficult: there are far too many cell lines being established every year, and very few of them ever get their identities profiled. Repositories such as the German Cell Bank and the American Type Culture Collection (ATCC) profile every line in their labs. But most new lines are established in individual labs and from thereon are freely exchanged between labs, rarely having their identities checked. "These cell lines never pass through our doors, so they are never subject to accurate authentication," says MacLeod. He and his colleagues have found that about 90% of scientists ignore or refuse a cell bank's request to send in new lines, and MacLeod argues that depositing lines should be required so that DNA fingerprints can be established and stored for

A LONELY CRUSADE

In 1951, a 31-year-old African-American woman was admitted to Johns Hopkins Hospital in Baltimore, Maryland, for treatment for cervical cancer. The hospital sent a sample of her cancerous tissue to Hopkins tissue culture expert George Gey, who successfully cultured it in his lab. Henrietta Lacks's ferocious cancer cells spread throughout her body and eventually killed her. And her immortalized cells, named HeLa cells after her, quickly spread through labs across the world—and not always because researchers had requested a sample for study.

In 1966, Stanley Gartler of the American Type Culture Collection found that 18 of the first 20 human cell lines established were chromosomally and biochemically identical to HeLa cells. All 18 lines were known to have come from Caucasian individuals. Yet Gartler found that each had a genetic variant of an enzyme found only in the small percentage of African American population that Lacks had belonged to. Gartler published his findings in *Nature* in 1968, marking the first reported case of HeLa contamination. It was only the beginning.

A few years later, Walter Nelson-Rees began discovering contaminations in lines from laboratories across the world. At the time, he was at the Cell Culture Laboratory of the University of California, Berkeley, at Oakland, characterizing, storing, and distributing cell lines for the U.S. National Cancer Institute (NCI). Over more than 10 years, he counted 279 contaminated lines from 45 different laboratories. Many were contaminated with cells from other species, but the bulk—more than 40 individual lines—had been overcome by HeLa cells. "This sort of scenario happened many, many times, people who thought they were working with one type of cells [were later found to be] working with HeLa cells," he says.

Nelson-Rees published his results in a series of papers in *Science* in the 1970s, urging scientists to stop using contaminated cell lines, re-evaluate their previous research, and employ simple quality-control practices such as regularly verifying their lines' authenticity.

Nelson-Rees's revelations threw the community into a frenzy. Many studies were called into question, and Nelson-Rees was naming names. Some biologists reacted with hostility, and *Nature* in an editorial called Nelson-Rees a "self-appointed vigilante." In a 2001 commentary on cell line authentication, Stephen O'Brien of NCI in Bethesda, Maryland, who had worked with Nelson-Rees, recalled the tension: "Human emotions were on edge, red faces were appearing in the most prestigious laboratories, and discussions of the problem lost any semblance of civility." Nelson-Rees even remembers an anonymous telegram offering to send him a one-way ticket to South Africa. "My aim was to clear up a morass of contamination, and it wasn't easy," he says.

The attacks ultimately took their toll. In 1981, Nelson-Rees quit science and opened an art gallery in San Francisco.

HeLa continues to spread today. In 2004, Gertrude Buehring of the University of California, Berkeley, and her colleagues surveyed 485 researchers from 48 countries who were working with specific cell lines and found that 49 were using seven lines that others had shown to be contaminated by HeLa. When Buehring conducted a PubMed search to identify the number of publications from researchers wrongly using HeLa-contaminated lines as though they still had cells of the original line, she found a total of 220 papers between 1969 and April 2004. And the number of publications on research using cell lines shown to have become contaminated by HeLa had increased by a factor of 10 between 1969 and 2004, whereas the total number of publications had increased by only a factor of 2.7.

But perhaps Nelson-Rees will finally get his due. Other scientists are now taking up his fight against cell line contamination (see main text). And in 2004, the Society for In Vitro Biology publicly recognized his contribution to science with a lifetime achievement award.

–R.C.

Eponymous. HeLa cells came from Henrietta Lacks's cervical cancer.

CREDITS: (TOP TO BOTTOM) PUBLISHED WITH PERMISSION OF THE SOCIETY FOR IN VITRO BIOLOGY 2004; OBSTETRICS & GYNECOLOGY/PHOTO RESEARCHERS INC.

future verification attempts.

Researchers sometimes publish papers on individual mix-ups, hoping to warn the rest of the community about a particular cell line. But these warnings are typically restricted to specialized journals and fail to grab the attention of the larger scientific community. For example, Mordechai Liscovitch, a cancer researcher at the Weizmann Institute of Science in Rehovot, Israel, says he and his lab wasted 3 years because they hadn't noticed a publication revealing that the two breast cancer lines they were studying were not actually related—a fact the U.S. National Cancer Institute knew and attempted to publicize although it continues to use and distribute the contaminated lines for drug testing (see sidebar, p. 929).

A birthday resolution

Nelson-Rees may have failed to stop the spread of HeLa cells, but Nardone is taking up his battle. The retired director of R. M. Nardone Associates, a biotechnology training company, Nardone has for more than 2 decades educated graduate students and postdocs at NIH about cell culture techniques. "Each year, I give a lecture on cross contamination," he says. "And each year, I get the same blank stares that tell me they aren't adopting the techniques."

In 2005, he happened to give this lecture on his 77th birthday. After the class, when his son asked him whether he had a birthday resolution, Nardone realized that he was "so damn mad" about the reluctance of scientists to acknowledge the seriousness of the problem that he decided to do more than give an annual talk to a few biologists.

Several weeks later, Nardone put together a white paper titled *Eradication of Cross-Contaminated Cell Lines: A Call to Action*. "Clearly, the current situation is intolerable and requires a broad, coordinated effort involving those who do research, fund research, publish findings of research, and educate researchers," he writes.

Nardone's "call for action" seeks two broad changes: more regulations and increased education efforts. Nardone argues that journals and funding agencies should impose strict rules on researchers, forcing them to submit proof of cell line identity along with their manuscripts and grant proposals, respectively. This, he says, has to be supplemented by renewed education efforts to increase awareness of the cross-contamination problem, especially among younger researchers who are unfamiliar with its history.

The journals and agencies targeted by Nardone seem to embrace his warnings but not his solutions. In an e-mail, Sally Rockey, deputy director of NIH's Office of Extramural Research, told *Science* that NIH is aware that contamination of cell lines is a serious issue that can result in loss of biological products and render research worthless. "... The career and reputation of scientists can be affected if research is conducted using contaminated cell lines." Yet, Rockey argues, "It would be impractical to require authentication as a condition of award as cell lines are used routinely in thousands of basic science studies that NIH funds. ... NIH believes that professional societies and scientists themselves should be driving the profession toward best practices in avoiding cell culture contamination instead of placing the responsibility on the funding agencies."

Journals also hesitate to assert authority. This is a requirement that would be imposed by the field, not by the journal, says *Science* Deputy Editor for Biology Katrina Kelner. "We do not have an explicit policy but will certainly keep our eye on this if it is something that becomes a standard." *Nature* did recently mandate DNA fingerprint data for papers reporting new human embryonic stem cell lines, but this policy doesn't extend to all cells. "I think, we would agree with the sentiment" in the white paper, says Natalie DeWitt, a biology editor at *Nature*. But "you can't just suddenly say we need to verify cell lines, we don't have labs in our offices, and we can't check the lines ourselves and say it's from hamster and not from mouse."

Rebecca Chasan, executive editor of the *Journal of the National Cancer Institute* (*JNCI*), says reviewers sometimes raise questions about cell line identity, but after reviewing Nardone's white paper, *JNCI* may take a firmer line. The journal is planning to begin asking authors to confirm that they have authenticated their lines. Some issues need to be worked out, however. For example, should that request come before or after a paper undergoes review? "If a paper has gone through the peer-review process and the authors aren't able to confirm the identity of the cell line, it's not yet clear what we would do," says Chasan. If the genetic signatures of all established cell lines were available in a public database, then it would be easier for journals to step in, notes DeWitt.

As journals wrestle with the problems posed by cell line mix-ups, Reynolds goes so far as to estimate that journals would have to retract 35% to 40% of their previously published cell biology papers to weed out invalid data. Some organizations are trying to help in different ways. The Society for In Vitro Biology will hold a symposium at its 2007 annual meeting in which Yvonne Reid of ATCC will talk about how contamination can be prevented. Nardone, Masters, and Joseph Perrone of ATCC are also organizing a conference to discuss standards and guidelines that could lead to profession-wide compliance for authentication. And ATCC, which has for decades sold lines overtaken by HeLa, recently decided to stop routinely distributing the lines, except for special requests from researchers. But these efforts will have limited effect, says Nardone, if journals and grant-awarding agencies won't mandate cell line authentication. What biologists need, he concludes, is a "stick saying that if you don't do this, there will be a consequence."

—RHITU CHATTERJEE

Rhitu Chatterjee is a science writer in Washington, D.C.

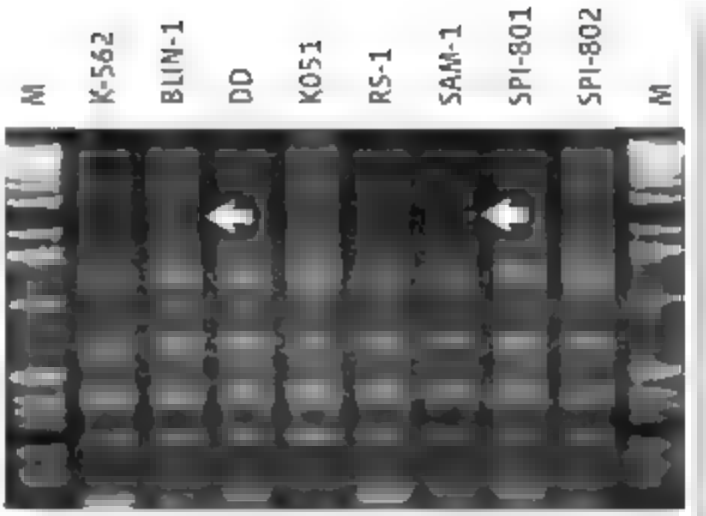

Identity theft. DNA fingerprinting of these cancer cell lines shows that most, if not all, are identical to the chronic myelogenous leukemia line K-562. RS-1, for example, had been thought to be an acute myelogenous leukemia line.

CREDIT: DREXLER ET AL., LEUKEMIA 17, 416 (2003)

Long time coming. This 5-meter-radius FFAG built at the KEK laboratory in Japan outperforms traditional synchrotrons

PHYSICS

A Half-Century Late, Alternative Accelerator Takes Off

It's not quite a cyclotron and not really a synchrotron, but the fixed-field alternating-gradient synchrotron could create a whole new role for particle beams

When physicists started developing particle accelerators known as fixed-field alternating-gradient synchrotrons (FFAGs), Dwight Eisenhower was president of the United States, and Elvis Presley was a promising unknown. Now, 50 years later, researchers are starting to build FFAGs that really work. Proponents say these accelerators may bring particle beams to bear on new fields and applications, destroying tumors with pinpoint precision, slashing the half-life of radioactive waste, and teasing out the properties of the most fundamental particles of nature. "FFAGs could revolutionize accelerator-driven science in general," says Robert Cywinski, an experimental physicist at Leeds University in the U.K. "Every university should have one."

Like the synchrotrons and cyclotrons familiar to today's scientists, FFAGs use electric fields to accelerate bunches of charged particles, such as protons or electrons, around a ring at close to the speed of light. But they differ in the way they guide the particles around the circle. In cyclotrons, a fixed magnetic field forces a beam of charged particles to move in a circle, but regular voltage "kicks" boost the particles' speed and make them spiral outward. The size of the huge magnets needed to keep the particles inside the machine limits the energy of the beam.

Synchrotrons overcome that problem by using variable magnetic fields that ramp up as the particles increase in energy. But once the field is geared up for high-energy particles, you cannot inject more, low-energy particles into the accelerator. That cutoff puts a ceiling on the beam's intensity.

FFAGs solve those problems by using a magnetic field that stays fixed in time but that grows stronger toward the outside of the ring. As particles gain energy and drift outward, the strong field keeps them on track. As a result, particles with a range of energies can all orbit at the same time, enabling FFAGs to produce particle beams more energetic than a cyclotron's and more intense than a synchrotron's.

The idea was originally put forward by Japanese physicist Chihiro Ohkawa in 1953. Researchers in the United States built three small FFAGs in the late 1950s and early 1960s. But the difficulty of creating the carefully shaped magnetic fields made larger devices impractical.

However, better magnets and computer simulations of three-dimensional magnetic fields have renewed interest in FFAGs. The spur came in the late 1990s from plans to build a neutrino factory, a multibillion-dollar facility that would produce extremely intense and high-energy beams of neutrinos. Yoshiharu Mori and colleagues at the KEK particle physics lab near Tokyo thought that an FFAG would be ideal for accelerating particles needed to create the neutrinos. In 2000, they built a small "proof of principle" device and have since constructed a larger machine with a radius of about 5 meters. Last year, this machine accelerated protons up to 100 million electron volts at a rate of 100 bunches a second—twice the maximum rate attained with a synchrotron.

This prototype machine was designed to test applications such as hadron therapy, which uses protons and other charged particles to destroy tumors. Mori has also joined Kaichiro Mishima and colleagues at Kyoto University to test whether an FFAG proton beam can slash the half-life—and therefore the threat to future generations—of some long-lived radioactive waste. Other attempts at "transmutation" of nuclear waste involve using linear accelerators, but Mishima thinks FFAGs have the edge because they are cheaper, smaller, and more efficient. "Whereas a linear accelerator would need to be up to a kilometer long, an FFAG would probably be just a few tens of meters in diameter," he says.

First, however, FFAGs must clear some major technical hurdles. KEK has so far concentrated on "scaling" FFAGs, in which the orbits of the particles remain a constant shape as the size of these orbits increases, or "scales," with momentum. But these require large magnets and are extremely complex. Much simpler and more compact, theorists say, would be a "nonscaling" FFAG, in which particle orbits change shape with increasing energy. No one has built one yet, because it has been assumed that the shape-shifting orbits make the beam almost impossible to confine. But a new U.K.–led consortium of universities and radiation oncology centers believes it can solve that problem. "We're kicking particles so quickly that the beam will not have time to spread significantly."

The consortium recently received $16 million to build a small demonstration nonscaling electron FFAG, known as EMMA, at the U.K. government's Daresbury Laboratory and design a proton device for hadron therapy. "There's an element of risk involved," says Roger Barlow of the University of Manchester, who leads the U.K. project. "But I'm confident it will work. It's a question of how hard it will be to get EMMA up and running." Meanwhile, physicists at Brookhaven National Laboratory in Upton, New York, working with researchers from industry, hope to get funding to build their own nonscaling device.

If all goes as planned, a nonscaling FFAG could be treating patients at a British hospital within 6 or 7 years, says consortium member Bleddyn Jones, a cancer specialist at University Hospital Birmingham.

–EDWIN CARTLIDGE

Edwin Cartlidge is news editor of *Physics World* magazine in Bristol, U.K.

ARCHAEOLOGY

Saving a Lost Culture's Megalithic Jars

Iconic and baffling, massive stone urns scattered across Laos may hold clues to the rise of Southeast Asia's first cities

XIENG KHOUANG, LAOS—You could easily insert a full-grown adult into any of the dozens of huge gray jars strewn across a windswept promontory in central Laos. Or a husband and wife, for that matter, or several small children. The hallowed corpse of a king, or shrieking prisoners captured in battle. The gruesome possibilities are endless. Although the origins of the prehistoric sandstone vessels are hazy, divining their purpose requires minimal, albeit morbid, imagination. "All around these jars are graves," says Julie Van Den Bergh, UNESCO archaeologist for the Plain of Jars. She and other experts speculate that bodies were put in the jars to decompose, and then the remains were scooped out for burial.

The world's biggest mortuary vessels, some upright and some tipped over in scraggly grass parched brown in the winter dry season, "are a spectacular enigma," says Peter Bellwood, an archaeologist at Australian National University in Canberra. For starters, no one knows which culture they belong to. Their utter lack of adornment has cloaked them in mystery. The urns presumably were hewn from nearby quarries, but radiocarbon dating has left the

map. So is their location. There are nearly 2500 jars, lids, and stone disks at 52 known sites on the Plain of Jars, defined as the diamond-shaped, 15 000-square-kilometer Xieng Khouang Province.

A concerted effort is now under way to save one of Asia's enduring archaeological riddles. UNESCO and the Laos government have just launched a new phase of a program to safeguard the Plain of Jars before it is nominated, anticipated in 2008, for the U.N. agency's World Heritage List. One task is to protect the Xieng Khouang Plateau from an expected influx of tourists. Another is to protect the tourists themselves from unexploded ordnance (UXO) that claims dozens of victims in the countryside each year, a legacy of the U.S. "Secret War" waged here in the 1960s and early '70s.

Deciphering the meaning of the jars "could shed light on the relationship between increasing social complexity and megalith construction," says paleoanthropologist Russell L. Ciochon, a Southeast Asia specialist at the University of Iowa, Iowa City, who compares the jars to other enchanting and better known megaliths: Britain's Stonehenge and the *Moai* faces of Rapa Nui (Easter Island). Tracing the jars' provenance, Ciochon adds, "would offer valuable insight into social organization in prehistoric Southeast Asia" during its transformation from a loose collection of subsistence farming communities to a web of urban centers that traded with China and India and also imported their religions, Buddhism and Hinduism.

Drained of lifeblood

According to local lore, the jars were made to store *lao lao*, or rice whiskey, for a feast 1500 years ago to celebrate the military victory of King Khun Chuang over an unruly chieftain, Chao Angka. In the 1930s, Madeleine Colani, a French archaeologist, pieced together a more macabre story. Near the town of Phonsavan in Xieng Khouang, at Thong Hai Hin (also called Ban Ang or Site One), one of the bigger fields with more than 250 urns, Colani unearthed grave goods including glass and carnelian beads, ceramic potsherds, bronze bracelets, and spearheads. The artifacts resemble those from Iron Age sites in northeastern Thailand, says Charles Higham, an archaeologist at the University of Otago in Dunedin, New Zealand, who is excavating a Thai site from that period. Higham pegs the Laos grave goods to the 2nd to 5th centuries C.E.

Colani also found charred bone and ash in a nearby cave in a limestone hill. In a 600-page treatise on the Plain of Jars, she ventured that remains were cremated in the cave, which has a meter-wide hole in its ceiling—a natural chimney. Ash and bone were then interred in the jars, while tools, jewelry, and other objects for use of the deceased in the afterlife were buried next to the jars, Colani proposed. Stone disks served as grave markers.

Before colleagues could probe this theory, Laos descended into conflict. After 3 decades of internal strife, the war in Vietnam spilled over the border in the 1960s. Central Laos bore the brunt of U.S.-backed carpet bombing—in all, some 2 million tons of munitions—to disrupt North Vietnamese supply lines. "It's a miracle that so

CREDIT: NIK WHEELER/CORBIS

many jars survived," Van Den Bergh says.

Not surprisingly, study of the jars languished. Things picked up again in 1994 when Thongsa Sayavongkhamdy, now director of Laos's Department of Museums and Archaeology, excavated several burials near the jars. His work supported Colani's view of the jar fields as cemeteries. But the bone fragments he uncovered were not charred. "Was Colani right, did he really cremate the dead? We're not sure," says Bellwood. Interestingly, even today villagers erect small stupa containing ash of deceased relatives near the jars.

UNESCO's working hypothesis is that bodies were placed in the jars to rot and dry out, a ritual decomposition, or, as Van Den Bergh calls it, "distilling the body of its human essence." (Lids found at other sites would have kept out scavengers.) She cites a compelling modern parallel: Cambodian, Lao, and Thai nobility for centuries have been interred in large urns before cremation. An official at Thailand's Royal Palace told *Science* that each previous king of the present dynasty, upon his death, has been placed in a sitting position in a large golden urn for 3 months before cremation. But hard evidence for such a practice in ancient Laos is elusive. "Whether bodies were lodged in the jars is probably unknowable," says Higham.

The Asian megalith makers too are inscrutable. Colani speculated that the jars were fashioned by a vigorous society that mined salt, a valuable commodity, and was situated favorably on caravan routes. Similar large stone jars have turned up in the Assam Province of northeastern India, suggesting a possible cultural connection. However, Van Den Bergh notes, no one has yet pinpointed a prehistoric settlement in Xieng Khouang.

The age of the jars is anyone's guess. Charcoal found just under some of them is 4000 years old, and bone fragments from a few burials are 900 to 1000 years old. The bulk of material is between 2500 and 1500 years old. Although there is no way to directly date the sandstone jars, Ciochon suggests using optically stimulated luminescence to date quartz crystals in sediments underneath. In this recent technique, light liberates trapped electrons from long-buried crystals; intensity depends on background radioactivity and duration of burial. For the quartz trapped directly beneath upright jars, "the last time these sediments were exposed to light was when the jars were put in place," Ciochon says. UNESCO hopes to find funding for such dating, Van Den Bergh says.

It's evident that the steely gray jars in Xieng Khouang were hewn from local rock. When first chiseled, they would have been white or cream-colored and sparkled in the sun, says Van Den Bergh. "They must have been stunning," she says. In 2000, in highlands near Site Three, Thai archaeologists documented the vestiges of a jar factory: unfinished vessels near an ancient sandstone quarry. The jars presumably were rolled on logs and perhaps ferried by boat part way. "Then furnished at the site," says Van Den Bergh. But there were no clues to the artisans' identities. Nor do the urns give much away. Of the roughly 2000 verified jars, just one has an image inscribed by its makers. Excavations at Thong Hai Hin in November 1994, Dip Nishimura, an archaeologist at Kagoshima University in Japan, uncovered a faded bas-relief image of the upper body of a human figure, with upturned arms near the base of one jar. "They are very functional," says Van Den Bergh. "Whoever made them had no personal creativity in it."

A handful of lids and disks have images of tigers and monkeys, and one disk at Site Two is adorned with a curious carving of a frog-like creature. Large stone jars on central Sulawesi Island in Indonesia "also have animals on the lids," says Bellwood. But there is no other evidence linking the two sites.

Bellwood believes that archaeology alone will not unmask the jar people. But comparative linguistics might. Presuming that the makers of the Sulawesi jars spoke an Austronesian language, he argues, those in Laos might have been an Austronesian enclave—perhaps from central Vietnam, where the Sa Huynh culture used burial pots some 2000 years ago. But Bellwood acknowledges that he has not been able to find any "linguistic descendents or identifiable place names in Laos today."

Scientific minefield

With plenty of puzzles left to solve, UNESCO and Laos authorities are endeavoring to keep Xieng Khouang's treasures intact—both for future study and to attract more tourism revenue to the impoverished province. Van Den Bergh's team has mapped the Xieng Khouang sites and is helping officials craft a management plan for the Plain of Jars. A new fence at Site Three is keeping out cattle, which had trod circles around jars, rubbing against them and compressing the soil so much that some jars subsided. Before UNESCO and Laos officials intervened, some jars had been cut to serve as troughs for feeding animals or collecting drinking water, while lids and disks became millstones. And during the Secret War, untold numbers of relics were blown to bits.

The scars of war are still plain to see. Thong Hai Hin and surrounding fields, studded with spiky wild aloe, are pockmarked with bomb craters a few meters deep and several meters across. The nonprofit Mines Advisory Group has cleared 175 UXO—including bombs, rockets, artillery shells, mortars, and 20-millimeter antiaircraft rounds—from around the jars and paths at the three main Xieng Khouang sites. Van Den Bergh has ensured that artifacts are not damaged during clearance, rescuing a dozen stone tools, pottery, iron knives, and bone fragments.

Although UXO make the surrounding countryside treacherous, the Xieng Khouang sites are becoming safer for research. That has emboldened Van Den Bergh to hunt for a partner on a ground-penetrating radar survey. Farther afield, newly identified jar sites near the capital, Vientiane, and the medieval city of Luang Prabang are wholly unexplored. If that's not enticement enough for archaeologists, the jars continue to defy analysis. When Van Den Bergh first arrived here 6 years ago, she admits, "I didn't know much about the jars. But there wasn't much to know." And there still isn't.

—RICHARD STONE

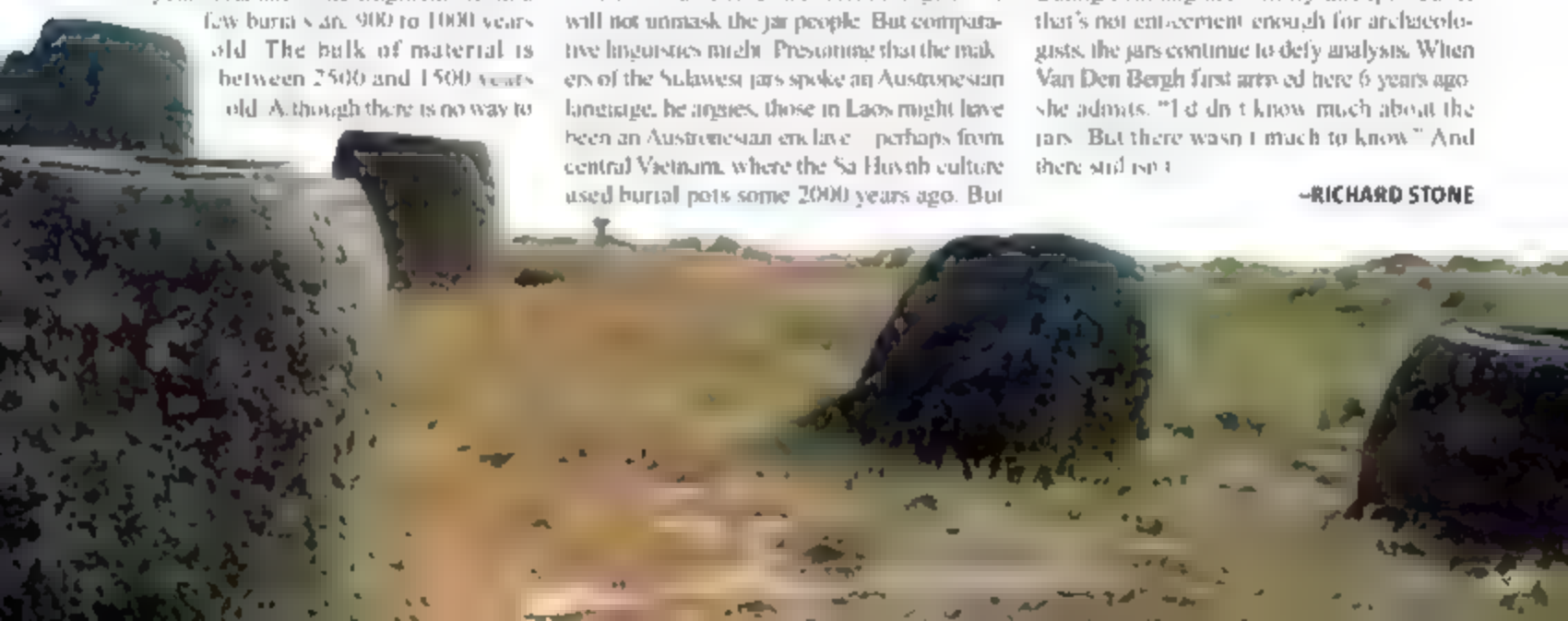

LETTERS

edited by Etta Kavanagh

A Voice over the Smoke for Academic Freedom

I CANNOT UNDERSTAND WHY THE PROPONENTS OF THE UNIVERSITY of California (UC) ban on funding from tobacco companies ("UC bulks at campus-wide ban on tobacco money for research," D. Grimm, News of the Week, 26 Jan., p. 447) constantly mischaracterize tobacco company–funded research as a "collective use of sponsored research by the manufacturers and distributors of tobacco products as an industry to support a public deception about its products." That statement in the preamble of the recent action item RI-89 of the UC Board of Regents is in itself a deception.

Only a handful of UC scientists, including myself, have competed successfully for tobacco company funds to conduct, as stated in the request for proposal guidelines, "the highest quality research that contributes to the fundamental scientific knowledge" and that "addresses the concern of public health regarding cigarette smoking."

I have not deceived the public, have not promoted tobacco use, and have not experienced any corporate intrusion in the collection or analysis of my research data. Yet neither I nor the other 107 awardees since 1995 have ever received the opportunity to defend ourselves against these charges.

The UC Board of Regents just has to apply the principles of academic freedom, give all awardees a voice to contest the allegations, and determine fairly if any public deception has actually occurred. They will discover that the hard evidence supports the 2006 UC Assembly of the Academic Senate resolution to assert academic freedom against a tobacco fund ban. Let's not squander the recent public health gains against smoking by attacking the foundation of freedom of speech and inquiry, which gave rise to the gains in the first place.

> "Let's not squander the recent public health gains against smoking by attacking the foundation of freedom of speech and inquiry, which gave rise to the gains in the first place."
>
> —Jue

THOMAS JUE*

Department of Biochemistry and Molecular Medicine, University of California Davis Medical School, Davis, CA 95616-8635, USA.

*The author recently completed a Philip Morris–funded project to develop noninvasive magnetic resonance techniques to measure vascular oxygen levels in tissue.

Debating Evidence for the Origin of Life on Earth

THERE ARE TWO MAIN THEORIES FOR THE origin of life on Earth: the "pioneer metabolic theory" (a hot, volcanic origin) and the "prebiotic soup theory" (a cold, oceanic origin). In their Report "α-hydroxy and α-amino acids under possible Hadean, volcanic origin-of-life conditions" (27 Oct. 2006, p. 630), C. Huber and G. Wächtershäuser describe prebiotic synthesis experiments that are claimed to "narrow the gap between biochemistry and volcanic geochemistry." However, no plausible geological environment could maintain the cited conditions of 0.1 to 0.2 M KCN at 100°C. As noted by Schwartz (1), in the "exceedingly improbable" case that all of Hadean Earth's nitrogen was converted to cyanide and dissolved in the oceans, a 0.2 M cyanide solution could be produced. Such high concentrations of cyanide in volcanic solutions would rapidly hydrolyze at 100°C (t$_{1/2}$ ~ 10 hours at pH 12) to formamide, which then quickly hydrolyzes to ammonia and formate (2). Huber and Wächtershäuser suggest that Ni-Fe-cyanide precipitates would have stabilized the cyanide, but robust sources of cyanide would be needed to produce a steady-state concentration of 0.1 to 0.2 M KCN at 100°C. No such robust sources are known.

The proposed 75 bars CO in volcanic solutions is also implausible, based on outgassing models using ordinary chondritic material (3). Nor are such elevated CO pressures necessary; previous experiments have demonstrated that a rich assortment of prebiotic organic compounds can be synthesized using a variety of energy sources from a modest ~1 bar CO_2 N_2 atmosphere [see (4) and references therein].

The compounds generated by Huber and Wächtershäuser, as well as their relative abundance, are remarkably similar to those generated previously in the "prebiotic soup" experiments they disparage. They claim that the lack of tar formation (from cyanide polymerization) makes their results distinct from earlier experiments, but this difference is easily explained by the reaction of cyanide with formaldehyde, produced by metal-catalyzed reduction reactions of formate (generated in this case by cyanide hydrolysis and the direct hydration of CO). As for their experiment 14, wherein they claim that no products were detected, we suspect that if they had acid-hydrolyzed the final solution, several products would have been identified (5). Finally, the results reported by Huber and Wächtershäuser are easily accommodated within the framework of an updated prebiotic soup heterotrophic theory in which pyrite and other metal sulfides are recognized as an important source of electrons for the reduction of organic compounds (6). In such a model, minera-

surfaces have the potential to select, concentrate, and organize these molecules (7).

JEFFREY L. BADA,[1] BRUCE FEGLEY JR.,[2] STANLEY L. MILLER,[3] ANTONIO LAZCANO,[4] H. JAMES CLEAVES,[1] ROBERT M. HAZEN,[5] JOHN CHALMERS[1]

[1]Scripps Institution of Oceanography, La Jolla, CA 92093–0212, USA. [2]Department of Earth and Planetary Science, Planetary Chemistry Laboratory, Washington University, St. Louis, MO 63130, USA. [3]Department of Chemistry and Biochemistry, University of California, San Diego, La Jolla, CA 92093–0506, USA. [4]Facultad de Ciencias, UNAM, Mexico D.F. 04510, Mexico. [5]Carnegie Institution, Washington, DC 20015–1305, USA.

References

1. A. W. Schwartz, in *Marine Organic Chemistry*, E. K. Duursma, R. Dawson, Eds. (Elsevier, Amsterdam, 1981), pp. 1–30.
2. S. Miyakawa *et al.*, *Org. Life Evol. Biosphere* **32**, 195 (2002).
3. L. Schaefer, B. Fegley, *Icarus* **186**, 462 (2007).
4. S. Miyakawa *et al.*, *Proc. Natl. Acad. Sci. U.S.A.* **99**, 14628 (2002).
5. J. P. Ferris *et al.*, *J. Mol. Evol.* **11**, 293 (1978).
6. J. L. Bada, A. Lazcano, *Science* **296**, 1982 (2002).
7. R. M. Hazen, *Am. Mineral.* **91**, 1715 (2006).

Response

THERE ARE TWO MUTUALLY EXCLUSIVE THEORIES on the origin of life. The "iron-sulfur organism" theory (1) claims a momentary, mechanistically definite origin by autocatalytic carbon fixation within a hot volcanic flow in contact with transition metal catalysts (1). The "prebiotic soup theory" claims a protracted, mechanistically obscure self-organization in a cold, primitive ocean, in which organic compounds accumulated over thousands or millions of years. The experiments under discussion have been designed to test the pioneer organism theory, and all experimental parameters have been chosen within this framework. The criticism presented by Bada *et al.* is made from the perspective of the prebiotic soup theory.

In agreement with the pioneer organism theory, we used Ni^{2+} or Fe^{2+} for catalytic purposes. These transition metals form extremely stable cyano complexes, which are similar to those found in volcanic field studies (2). This means that practically all cyanide ions become fixed as cyano ligands, with the effect that the concentration of dissolved free cyanide ions in the water phase is extremely low due to the high stability of the cyano complexes. It is a well-established fact of coordination chemistry that cyanide ions and cyano ligands have fundamentally different chemical properties. Bada *et al.* however seem to ignore this difference. They appear to work from the experience of previous prebiotic soup experiments with dissolved free cyanide, which did not yield products unless the cyanide concentration in water was sufficiently high (3). Therefore, this criticism is pointless.

We used 1 bar CO (Table 1, run 1), and we discussed at length that such CO pressure is in agreement with the volcanic setting of the pioneer organism theory. In other runs, we used 10 or 75 bar CO to shorten the reaction time. It is a well-established procedure to expedite reactions by increasing a parameter such as pressure. Therefore, the criticism of our use of 75 bar CO as pointless. We note that our use of 1 bar CO was not criticized.

Therefore, the above-mentioned geochemical criticisms do not cast a reasonable doubt on the ability of our reactions to have taken place within a volcanic hydrothermal flow system of early Earth.

We note that our critics differ from us as to the fate of reaction products we have found.

From the point of view of the pioneer organism theory, we see our reaction products, e.g., α-hydroxy acids or α-amino acids (or

peptides arising therefrom (4, 5)], as exhibiting positive autocatalytic feedback in situ by providing transition metal ligands for ligand-accelerated catalysis (6) of carbon fixation pathways, which constitutes evolvable reproduction (7). Reaction products that spill out into vast expanses of the ocean lose all chemical potential by dilution and are irreversibly lost for the circle of the pioneer organism (7).

From the point of view of the prebiotic soup theory, our critics see our reaction products as entering the primitive ocean to become additional ingredients of the prebiotic soup wherein after some thousand or million years and under all manner of diverse influences the magic of self-organization is believed to have somehow generated an unspecified first living cell.

The two theories are categorically different from the perspective of experimental science. The prebiotic soup theory is restricted to the testing of individual aspects of a long, protracted overall process (3). The pioneer organism, by contrast, is expected to be experimentally realizable in toto (7).

GÜNTER WÄCHTERSHÄUSER[1] AND CLAUDIA HUBER[2]

[1]Weinstraße 8, D-80333 München, Germany, and [redacted] Race Drive, Chapel Hill, NC 27514, USA. [2]Department for Organic Chemistry and Biochemistry, Technische Universität München, Lichtenbergstraße 4, D-85747 Garching, Germany.

1. G. Wächtershäuser, *Philos. Trans. R. Soc. B* **361**, 1787 (2006).
2. L. M. Mukhin, *Nature* **251**, 504 (1974).
3. J. P. Ferris, W. J. Hagan, *Tetrahedron* **40**, 1093 (1984).
4. C. Huber, G. Wächtershäuser, *Science* **281**, 670 (1998).
5. C. Huber, W. Eisenreich, S. Hecht, G. Wächtershäuser, *Science* **301**, 938 (2003).
6. D. E. Bergstrom, C. Bolm, K. B. Sharpless, *Angew. Chem. Int. Ed.* **34**, 1059 (1995).
7. G. Wächtershäuser, *Proc. Natl. Acad. Sci. U.S.A.* **87**, 200 (1988).

A Clarification on Global Access to Drugs

MARTIN ENSERINK'S ARTICLE "WHO PANEL weighs radical ideas" (News of the Week, 1 Dec. 2006, p. 1373) misrepresents the position of the European Commission in the important debate on global access to medicines.

In the final paragraph, there is a reference to the World Health Assembly (WHA) resolution establishing a World Health Organization (WHO) Intergovernmental Working Group (IGWG) on Public Health, Innovation, and Intellectual Property, followed by the sentence "(The drug companies and the European Commission opposed the plan.)"

In fact, the European Commission was a strong proponent of WHA Resolution 59.24 at last May's World Health Assembly. The Commission worked with the European Union (EU) to support the resolution, including the establishment of the WHO IGWG. The Commission was represented at the WHO IGWG in December by officials from five different Directorate Generals who worked closely with EU Member States at the meeting and actively intervened to support the process.

The three stated priorities of the European Union at the IGWG were (i) to promote research and development focused on products for diseases [for example, neglected diseases] that disproportionately affect developing countries, (ii) to ensure that these products are affordable and accessible within national health systems, and (iii) to ensure that all countries can use the flexibilities provided in international legal agreements on intellectual property rights.

The European Commission funds research into neglected diseases affecting developing countries, acts as a partner in clinical trials and issues development funding and policy to improve global access to medicines. A Commission legislative proposal for compulsory licensing was adopted by the European Parliament and Council earlier this year (Regulation 816/2006). The EU also fully respects the right of trading partners to use compulsory licensing in bilateral free trade agreements.

ANDRZEJ RYS

Health and Consumer Protection Directorate-General, European Commission, B-1049 Brussels, Belgium.

Who Is *et al.*?

ET AL.'S WORK IS REFERENCED IN DIVERSE journal articles demonstrating technical and research abilities that cross many scientific fields. *Et al.* does work in AIDS research, conserved noncoding elements, genetics, pathogenesis, astrophysics, and cancer research, to name a few. I'm left to wonder, "How does *et al.* do it?" I could benefit from having *et al.* as my next mentor, but who is *et al.*? Is *et al.* a professor at a university, what does *et al.* teach? What *et al.* the work *et al.* has published, maybe I can find *et al.*'s contact information by researching the patent and trademark office. To my surprise, I find no *et al.* listed on any patents or trademarks. I guess *et al.* wants all the work to remain in the public domain. Now I know I must have *et al.* as my next mentor, even at a distance. Maybe I can find *et al.*'s contact information on an NIH-sponsored research project. Annually, NIH-sponsored projects under *et al.*'s name (*et al.*) has more than 10,000 publications, a myriad of topics, so why is he/she not impressive for such scientific prestige, ordinary enough to receive funding? Does *et al.* lack focus in the eyes of peer reviewers? Are *et al.*'s projects too ambitious for peer reviewers to fund? I did notice that *et al.*'s author lines are generally fourth or sixth in the lack of first authorship the reason *et al.* does not receive government-sponsored funding? It is not that *et al.* is an author on all those papers, is because of supplying key reagents or involvement in patient care. The days of mammoth authorship as the reward for providing key components of a project are over. Such individuals are now consigned to the acknowledgment section. I am indebted to my former professors to secure their knowledge, but so far I have not received a reply. Does anyone know where *et al.* is?

RICHARD MCDONALD

Genovar Biosciences Ltd, 22963 California Street, St. Clair Shores, MI 48080, USA.

Letters to the Editor

Letters (~300 words) discussing articles published in *Science* in the previous 6 months or issues of general interest, may be submitted through the Web (www.submit2science.org) or by regular mail (1200 New York Ave., NW, Washington, DC 20005, USA). Letters are not acknowledged upon receipt, nor are authors generally consulted before publication. Whether published in full or in part, letters are subject to editing for clarity and space.

CORRECTIONS AND CLARIFICATIONS

Reports "Ultrahard bond softening in bismuth: Mapping a solid's interatomic potential with x rays" by O. M. Fritz *et al.* (2 Feb., p. 633): In the acknowledgments note 27, one of the funding groups was misidentified. FLASH stands for Understanding Fast Light Activated Structural Changes."

Reports "Global-scale similarities in nitrogen release patterns during long-term decomposition" by W. Parton *et al.* (19 Jan., p. 361): William Parton and Whendee L. Silver should have been listed as co-lead authors.

ECOLOGY

Voices from Bird Bones

Jared Diamond

Paleontologists study ancient bones excavated from early archaeological sites on Pacific islands to have identified many previously unknown bird species that evidently became extinct soon after human arrival. Those extinctions have implications for human history on the Pacific, biogeography, and evolutionary theory. Two recent books, which complement each other geographically and by chance of species, each summarize current knowledge of extinct birds on all Pacific island groups except Hawaii.

Alan Tennyson and Paul Martinson's *Extinct Birds of New Zealand* adds to Trevor Worthy and Richard Holdaway's excellent book (*1*) by illustrating New Zealand's 58 extinct bird species. Although the most famous of these are the giant flightless moas, nearly as remarkable were the world's largest eagle (up to 16 kg) and its smallest flightless bird (22 g). Martinson's gorgeous watercolor paintings bring home the tragic loss of form and ecological role that each species represents in a way that descriptions and museum specimens cannot achieve.

The New Zealand fossil record is by far the most completely sampled in the world: most of the extinct species are known from bones of hundreds or thousands of individuals, and almost all modern species have been recovered as fossils. Among the points made in Tennyson's text and by Worthy and Holdaway (*1*) is that the New Zealand extinctions were followed by the founding of New Zealand populations of at least 16 Australian species in response to human-induced habitat changes and to the absence of related former resident species. Small Australian swamphens, coots, and harriers replaced extinct, giant ecological equivalents; a coastal vegetarian shelduck spread inland after the extinction of the vegetarian Finsch's duck; and Australian pied stilts prospered as populations of New Zealand black stilts crashed.

In *Extinction and Biogeography of Tropical Pacific Birds*, David Steadman summarizes fossil avifaunas of Pacific islands other than New Zealand and Hawaii. His account is based in large part on his own discoveries over the past 22 years. He personally excavated dozens of sites, retrieved hundreds of thousands of bones, measured the bones of over 25,000 individual birds, and prepared uncounted skeletons of modern species for comparison. This monumental research program was accomplished mostly single-handedly, against obstacles in obtaining permits, finding sites, creating cooperation of local people, and obtaining funding from granting agencies that admire studies of museum scholars and scorn descriptions of species.

The resulting discoveries include over 70 previously unknown extinct species now named and described, dozens of others recognized but not yet named or described, and some large geographic range extensions. Bird species diversity and endemism prove to have been higher, sympatric congeneric species more frequent, and flightless species far more numerous than previously realized. Contrary to the former view of rare and instantaneous events treading lightly on their environments, human colonization of every well-studied Pacific island group was followed by a wave of vertebrate extinctions.

All these discoveries represent new data against which extant previous conclusions about biogeography, extinction, and community ecology. Throughout the book, Steadman criticizes conclusions reached by previous authors (especially Ernst Mayr, Robert H. MacArthur, and Edward O. Wilson) who worked before the impact of human-caused extinction in Oceania was recognized. Steadman concludes that "impact overwhelmingly characterizes avian biogeography on Pacific islands." One might therefore expect the book to be full of analyses of the new data, demonstrating how earlier interpretations are thereby altered. Sadly, such analyses are not offered for most of the obvious questions, and only crude analyses are offered for others, although the book often provides enough data to let others do the missing calculations.

For instance, two of Mayr's conclusions about Pacific island avian biogeography were that an Australian biogeographic component in the islands, mainly New Guinea, survived as fauna is strongest on New Caledonia, decreasing to the east and north (*2*), and that island endemism increases with island area and isolation (*3*). Other researchers have concluded that the body masses of an island's top herbivore and carnivore increase with island area and are also possibly a function of age and productivity (*4*, *5*). Steadman discusses none of these points. My preliminary impression is that his data confirm rather than overturn these conclu-

Done in by rats and cats. The smallest flightless bird, Lyall's wren (*Traversia lyalli*), depicted here in a colony of fairy prions (*Pachyptila turtur*), survived on Stephens Island until 1895.

CREDIT: PAUL MARTINSON/FROM *EXTINCT BIRDS OF NEW ZEALAND*

The reviewer is in the Department of Geography, UCLA, Los Angeles, CA 90095–1524, USA. E-mail: jdiamond@geog.ucla.edu

sions.) Ian Atkinson (6) and others have suggested that susceptibility of island birds to extermination by introduced mammalian predators depends on prior evolutionary exposure to native mammalian predators and also to nonmammalian predators such as land crabs and land crocodiles. Steadman provides much data suitable for quantitative evaluation of the idea, but he does not pursue the analysis beyond an anecdotal example (New Ireland) and some qualitative discussion. Another much-discussed topic of avian biogeography that Steadman does not explore is the trade-offs between costs and benefits that lead to the evolution of flightlessness in island birds. With the author's discoveries, the prehistoric avifaunas of the tropical Pacific now encompass the largest number of flightless birds in the world and, Steadman lists the 25 bird families that contain flightless species. Yet he does not discuss why flightlessness never appeared in so many other bird families, or why it evolved in several Pacific pigeons and megapodes, only three Pacific songbirds, and many ground-dwelling rails but no ground-dwelling quail.

The book's most glaring omissions are statistical analyses of island species numbers S and their control by area A, distance D, and elevation E—despite long discussions of those subjects. For all Pacific islands other than New Zealand, small sample sizes mean that their fossil avifaunas are incompletely known and that their actual S values must be estimated by statistical sampling models. In paleontology, such statistical calculations (e.g., ones that incorporate specimen numbers and relative species abundances recovered to date and known sampling biases (7)—are now routine and mandatory. Unfortunately, none appear in the book. Island biogeographers routinely tease apart effects of A, D, and E on S by multiple regression analyses and other statistical methods, but the book offers no such analyses of the prehistoric avifauna. There are no graphs of prehistoric S plotted against either D or E. Despite a whole chapter on species-area relations and their slope (termed z), the book presents only a single graph (e.g., 19-14) of new fossil data adequate for calculating z; that plot for prehistoric land birds among seven islands in Tonga yields a z of 0.07, virtually unchanged from the modern z of 0.06. Several graphs in the species-area chapter combine fossil and modern species on the assumption that all existed simultaneously. But Tennyson and Martinson's accounts of the far-better-known New Zealand avifauna warn us that many modern species arrived only as or after the original species declined. It's as if one combined the 1940 and 1980 Manhattan telephone directories and assumed that all people in one directory shared their island with all people in the other.

Despite this lack of supporting analyses, Steadman offers specific but implausible conclusions: e.g., that E has little or no effect on S of Pacific islands other than low atolls, that "inter-island distances less than ca. 100 km have had a minimal effect on species richness", and that S is virtually independent of island A for any island exceeding some threshold A (ranging from 1 to 5 km^2 in East Polynesia to 90 to 100 km^2 farther west). Where do these detailed conclusions come from?

Steadman's method throughout the book is to replace quantitative analyses with anecdotal examples that he then overgeneralizes, state the overgeneralizations as beliefs, and finally relabel the beliefs as conclusions. For instance, he often remarks that a certain species confined today to some particular large island has been found as a fossil on one or more smaller islands of the same archipelago, then concludes that this suggests that most or nearly all species were formerly present on most or nearly all islands of the archipelago. The verbs believe, expect, predict, speculate, and suspect and the adverbs possibly, presumably, probably, and undoubtedly are used throughout the book—e.g., on the average more than twice per page in the chapter on species-area relations—to precede statements that scientists normally draw as conclusions from analyses. In the final chapter, words like "I believe" and "probably" become scarce, and the former beliefs become stated as facts.

Why would someone spend 22 years excavating, cleaning, and microscopically scrutinizing 25,000 bird bones and then neglect modern analyses? The answer emerges on the first page of the Preface and appears repeatedly thereafter. Steadman states his disdain for many things, including computers, data transformations, dynamics, elegance, equations, generalizations, macroecology, overall frameworks, rules, statistics, and theory. He also repeatedly criticizes conclusions by biogeographers who used these approaches or concepts—not only MacArthur, Wilson, and Mayr but also James Brown, Stephen Hubbell, Mark Lomolino, Stuart Pimm, Robert Ricklefs, Dolph Schluter, Thomas Schoener, and (full disclosure) me. With these self-imposed blinders, it becomes tragically clear why Steadman did not undertake quantitative analyses of his own data, nor collaborate with others who could have complemented his expertise.

The data in *Extinction and Biogeography of Tropical Birds* are now available for others to analyze. But we shall have to look past Steadman's dismissals of surviving modern avifaunas as unnatural and resistant to interpretation at face value. Yes, answering some questions requires a historical perspective. However, biotas are buffeted today, and have been buffeted for hundreds of millions of years, by impacts other than those of humans. Living birds still eat, prey, compete, breed, disperse—and challenge our understanding. They remain the only birds in which we can study basic ecological processes directly.

References

1. T. H. Worthy, R. N. Holdaway, *The Lost World of the Moa. Prehistoric Life of New Zealand* (Indiana Univ. Press, Bloomington, 2002); reviewed by D. W. Steadman, *Science* **298**, 2136 (2002).
2. E. Mayr, *Proc. 6th Pacific Sci. Congr. 1939* **4**, 187 (1941).
3. E. Mayr, *Science* **150**, 1587 (1965).
4. P. A. Marquet, M. L. Taper, *Evol. Ecol.* **12**, 127 (1998).
5. G. P. Burnes *et al.*, *Proc. Natl. Acad. Sci. U.S.A.* **98**, 14518 (2001).
6. I. A. E. Atkinson, in *Conservation of Island Birds*, P. J. Moors, Ed. (International Council for Bird Preservation, Cambridge, 1985), pp. 35–81.
7. J. Cornell, S. Pimm, *Stud. Avian Biol.* **22**, 15 (2001).

10.1126/science.1137556

PHYSICS

Astronomers' Relativity

Peter Galison

Einstein's special and general theories of relativity span a century. People a century ago. Although the list of charges against them has fluctuated from year to year, many return to the same themes. Relativity is wrong, some insist. It is unintuitive, too geometrical, say others. The list goes on. General relativity uses unreasonably complicated mathematics. It violates Kantian philosophy. One or both theories of relativity are correct but were anticipated by the French mathematician-physicist Henri Poincaré, the German mathematician David Hilbert, or the Dutch theorist Hendrik Lorentz. Relativity's premature demise has been announced time and again. Its effects don't exist—or they do exist but have other explanations. The sun is oblate, thus causing the precession of the perihelion of Mercury. Or the ether can be detected by a souped-up Michelson-Morley experiment. Starlight isn't bent as Einstein predicted—or it is, but that is due to the atmosphere of the

The reviewer is at the Department of History of Science, Science Center, 1 Oxford Street, Harvard University, Cambridge, MA 02138, USA. E-mail: galison@fas.harvard.edu

Sun or Earth or some combination. When all else failed, there was always the charge that the theory was too much like its author: too German, or not German enough, or too Jewish, or too cosmopolitan.

Jeffrey Crelinsten's fascinating *Einstein's Jury: The Race to Test Relativity* tracks the ways in which one particular community—astronomers, handled Einstein's relativity theories, roughly between 1910 and 1935. Although German and British astronomers appear, Crelinsten's central and most illuminating focus is on American astronomers. Among these, despite the rise of a remarkable astronomical community (one of the first real powerhouses in U.S. science), there were some truly unpleasant types. One nasty piece of work, Thomas Jefferson Jackson See, quite hated Einstein's general theory ("too metaphysical") and did all he could—polemicizing, theorizing, and plagiarizing—to sink Einstein's boat. Fired both from the University of Chicago and Lowell Observatory, See nonetheless got a useful rise out of luminaries like James Jeans, who may have been pushed toward a more instrumental interpretation of the theory by See's vituperative remarks. Another angry boy was Heber Curtis, an astronomer who had worked at Lick Observatory and then went on to direct the Allegheny Observatory. One prominent astronomer, Charles Lane Poor, though unable to follow the mathematics of the theory, nonetheless detested it and wrote to Curtis that Einstein was "the Bolshevist of science." Curtis for his part confided to Poor in May 1923, "there is absolutely no doubt, in my own mind, that a deflection [of starlight] exists essentially as shown on his plates [1919]. This does not, however, make me a believer in the theory of relativity. I am still an irredeemable heretic, and it does not seem now that I shall ever swallow that theory unless chloroformed first."

Other Americans required less chemical assistance to back relativity. William Wallace Campbell, director of the Lick Observatory, shifted toward Einstein on the basis of meticulous observation. As presented by a colleague in 1923, those Lick results indicated a new view "that light is subject to gravitation and that Einstein's law of gravitation is more accurate than Newton's law." Observation and theory met with great precision—1919 predicted, 1922 measured. In a powerful consensus, observations from both Lick and Mt. Wilson agreed, turning the American astronomical tide toward a broad if not universal acceptance of general relativity. Additional support—if more complex, news came from the results of spectral-line measurements for the gravitational redshift.

There is something understandable—and right—about Crelinsten's decision to have his astronomical jury deliver its verdict in the late 1920s. With two mountains of eclipse results on the table, the double consensus of Lick and Mt. Wilson brought powerful support to relativity. As one American astronomer (Robert Aitken) put it in 1928, "the values are in substantial accord with the theory and . . . no other satisfactory explanation of the displacement is available. Whether we like it or not, we are obliged to admit that in these three instances [redshift, perihelion, starlight] the Einstein theory has successfully stood the test of astronomical observations." So once the jury passed its verdict, the theory, like an innocent man, walked. No double jeopardy. In law, yes, in science, not quite.

The problem is that closure in the matter of Einsteinian theory (or, indeed, other theo-

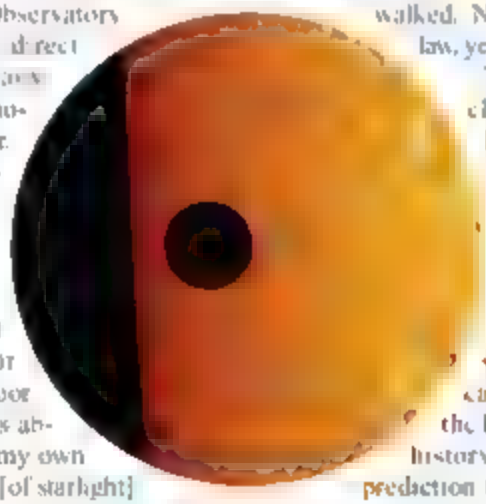

Orbital test. General relativity explained the motion of Mercury's perihelion.

ries) doesn't necessarily mean that the case stays closed. Take the long and troubled early history of the redshift, the prediction that light traveling out from a gravitating body would be moved toward the lower end of the spectrum. If, as Aitken claimed, the issue of the redshift was settled by 1928, then we would be hard put to understand the extraordinary importance accorded the Mössbauer effect measurements that R. V. Pound and G. A. Rebka obtained three decades later when they dropped light down the stairwell of Harvard's Jefferson Laboratory. Experimental conditions change: new and better technologies make possible the isolation and specification of effects.

This raises a larger point. American astronomers of the 1920s were keen to jettison high theory in favor of pragmatic measurements. As Crelinsten relates, the period's astronomers "never dealt with the deeper implications of Einstein's ideas. It was not necessary . . . apart from the few specialists who work the equations, we do not need to understand the underlying concepts, nor do many of the experts." But is this true? The redshift, for example, is really probing only the equivalence principle, not (for example) the curvature of space-time that is, in addition to the equivalence principle, put to the test by light deflection. So two of the "classic" three experiments do not, in fact, test the same aspects of the general theory of relativity. In order to render a verdict, the observational astronomical jury needed—and needs—a specific statement of the charge it is to adjudicate. And that requires a command of both experiment and theory.

Since the 1920s, a host of other experiments have gotten at other aspects of the theory. Bouncing radar beams off the surface of Venus in superior conjunction came, in the 1960s, to be a probe of the nonlocal velocity of light as it raced by the Sun. It was elegant because, unlike the precession of the perihelion of Mercury, it was not so sensitive to the precise oblateness or interior excitations of our favorite star. Tests of frame dragging by a precision satellite-borne gyroscope (the general relativity "equivalent" to magnetic interactions in electrodynamics) tested another aspect of relativity. The slowing of binary stars explored radiation through gravity waves—yet another and quite different aspect of general relativity.

Crelinsten has done a great service and deserves our thanks for tracking so beautifully the American astronomical response to relativity between the wars. But the once-and-for-all-time jurisprudential metaphor is notoriously dangerous for science, for history, and for philosophy. New judgments about general relativity have arisen again and again—and will continue to arise in the future as new charges and challenges appear, some from deep inside the theory, others from novel technologies or experiments. From astrophysical observations to string-theoretical calculations, the history of our understanding of general relativity is not yet finished. In the end, that is the greatest legacy Einstein has left us.

10.1126/science.1134451

PUBLIC HEALTH

911.gov

Web-based communication can provide better reporting on disasters, coordination of responses, dissemination of information, and social networking to deliver assistance

Ben Shneiderman and Jennifer Preece

When individuals need help for medical emergencies or fires, most U.S. residents reach for their phones to dial 911. But when natural disasters, public health threats, or terrorist attacks occur that affect thousands of individuals or more, 911 operators cannot handle all the requests. Such disasters may require massive coordination of public and private agencies, plus cooperation from millions of citizens.

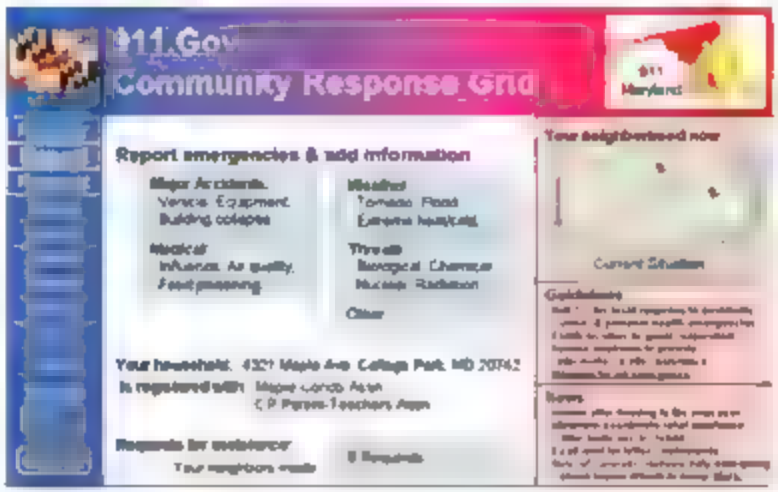

A community response grid. Mockup of a World Wide Web page that supports registering of households, reporting of incidents, requesting assistance, and responding to requests.

Public use of Web-based social computing services, such as MySpace or Facebook, has spread to hundreds of millions of users. This suggests that local, state, and federal agencies could build community response grids (CRGs) where residents could report incidents in seconds, receive emergency information, and request resident-to-resident assistance. The current Internet and World Wide Web have proven effective for many purposes, but government agencies have been slow to adopt social computing for national security, disaster response, and emergency relief (*1*).

CRGs should be more than an emergency reporting service as already proposed (*2*). They should also be more than the U.S. Department of Homeland Security (DHS) Information Network (*3*), which focuses, like some European (*4*) and Asian (*5*) initiatives, on networking for professionals. CRGs would not duplicate DHS's CitizenCorps.gov, which is designed to build local volunteer groups for emergency response but doesn't include online reporting or resident-to-resident assistance.

Community members (who would register in advance) could use Web-based computers, mobile devices, and cell phones to give and get text messages, photos, or videos. The site would support coordination as emerging software tools could enable agencies to integrate reports and promptly recognize patterns. Civic leaders could disseminate information on a street by street basis. A CRG would be most effective if it is used on a regular basis so that people know about it and develop closer community contacts. Such activities would build trust and increase social capital that will be needed during major emergencies.

Some catastrophes destroy infrastructure, but in many situations, such as avian flu, chemical and biological attacks, and temperature extremes, do not. Even when there is focused damage to communications infrastructure, the adjoining areas need to communicate to report and receive instructions. As the Internet matures, its reliability will improve, and if disrupted it is more likely to be easily restored than phone services (*6*, *7*).

In the aftermath of Hurricane Katrina, local libraries helped to rebuild neighborhoods (*8*). After the Kobe earthquake (*9*), British foot-and-mouth disease outbreak (*10*), and Indonesian tsunami (*11*), resident collaborations, Internet communications, and community networks were effective in coordinating local assistance, supplies, and information dissemination (*12*). An effective, regional model is Craigslist.com, which has tailored Web pages for all 50 U.S. states and 22 metropolitan regions. The California Web pages already disseminate earthquake and weather information, but have no reporting system.

Just as 911 emergency phone services are run and funded locally by phone service fees, CRGs could be maintained through user fees collected by Internet service providers. In smaller communities, CRGs could be run by trained volunteers with a few professionals, much as volunteer fire departments now operate. Local 911 phone centers have annual budgets of $200,000 to $3 million (*13*). A reasonable estimate is that adding 911.gov services would do no more than double these budgets.

There are many challenges to be faced. We need to understand the norms and policies that generate intense participation in groups such as the Wikipedia community and some health support groups (*14*). Many online communities fail, so we must learn what barriers reduce and what incentives create successful community interactions in which privacy is respected (*15*). It will be important to integrate with existing social networking sites and local community groups. However, developing a research agenda, pilot testing, and phased implementation could make CRGs a reality within 3 to 5 years.

References

1. Y. Kapiteni, N. Okada, H. Tatano, *Nat. Hazards Rev.* **6**, 61 (2005).
2. 107th U.S. Congress, House Resolution 3353.
3. DHS Information Network, www.dhs.gov/xinfoshare/.
4. European Union, Community Research and Development Information Service, Emergency Response Grid, http://cordis.europa.eu/ist/grid/emergency_response_grid.htm.
5. Grid-Enabled Disaster Prediction and Emergency Response, www.gridasia.net/content/view/44/70/.
6. J. Cox, "Communicating even when the network's down: Researchers seek disruption-tolerant nets" (2006), www.networkworld.com/news/2006/011406-dtn.html.
7. M. Turoff *et al.*, *J. Inf. Technol. Theory App.* **5**, 1 (2004).
8. E. L. Quarantelli, http://understandingkatrina.ssrc.org/Quarantelli (2005).
9. R. Shaw, K. Goda, *Disaster* **28**, 16 (2004).
10. C. Hagar, thesis, University of Illinois, Urbana-Champaign, IL (2005).
11. M. Stephenson, *Disasters* **29**, 337 (2005).
12. C. Jones, S. Minnick (2006), www.firstmonday.org/issues/issue11_5/jones/.
13. National Emergency Number Association, www.nena.org/.
14. D. Maloney-Krichmar, J. Preece, *ACM Trans. Comput. Hum. Interaction* **12**, 201 (2005).
15. J. Preece, *Online Communities: Designing Usability and Supporting Sociability* (Wiley, New York, 2000).

B. Shneiderman was the founding director of the Human-Computer Interaction Laboratory and is a professor in the Department of Computer Science, and J. Preece is professor and dean of the College of Information Studies, University of Maryland, College Park, MD 20742, USA.

*E-mail: ben@cs.umd.edu or preece@umd.edu

10.1126/science.1139088

PHYSICS

Two for the Price of One

Physicists need to come up with theories that explain unexpected energy changes during quantum-phase transitions

Andrew J. Schofield

Phase transitions are all around us, whether we boil a kettle or make some ice—changing the temperature drives matter from one form into another at a characteristic transition temperature. It can be an abrupt change like ice forming, or it can be smooth like the growth of magnetism in iron as the temperature drops below 770°C. Despite the rich variety of such transitions, we have known since the 1960s that there is a unifying principle that groups together the smooth or continuous transitions into a small number of "universality classes" (*1*). What distinguishes between the classes is related to the energy difference between the two phases. This energy difference defines a single energy scale that vanishes as the transition point is reached (that is, it becomes easier for one phase to change into the other). The particular way this single energy scale vanishes is enough to characterize each universality class of transition. This concept of a single energy scale was expected to be valid even for so-called quantum phase transitions (*2*, *3*), which are induced by changing pressure, magnetic field, or composition for a material held at absolute zero temperature. However, low-temperature studies by Gegenwart *et al.* on a metallic magnet reported on page 969 of this issue (*4*) demonstrate a serious failure of our understanding. They find not one but two energy scales vanishing at a quantum transition.

Quantum phase transitions have moved in recent years from mere theoretical curiosities to subjects of intense experimental and theoretical interest. Whereas previously it was thought that changes of phase at zero temperature would be of little practical relevance, it has become clear that the presence of a quantum critical point at absolute zero could nevertheless exert a profound influence on a material at higher temperatures. It could, for example, make magnets into superconductors (*5*) and superconductors into novel metals (*6*). Yet the more these transitions have been studied, the weaker appears our conventional framework for understanding quantum criticality in metals (*7*).

Within this conventional framework, even before the transition temperature is reached, bubbles of the matter's new form appear momentarily, presaging the coming change. These fluctuations require energy, but the "energy cost" for these fluctuations reduces to nothing as the temperature approaches the transition temperature. The fluctuations then become critical—ever larger in size and longer lived—until they dominate the physical properties. These properties tend to be proportional to powers of the difference between the temperature of the material and the transition temperature. It is these powers, or critical exponents, that characterize the universality classes.

The extension of this theory to quantum phase transitions includes the energy cost of a fluctuation caused by Heisenberg's quantum uncertainty principle. This uncertainty keeps quantum matter in constant motion even at absolute zero and can become so vigorous that it drives the melting of one form of order into another. At first glance, it appears that this is what is happening in the compound studied by Gegenwart and co-workers. $YbRh_2Si_2$ is a delicate antiferromagnet where the electron spins arrange themselves in an ordered alternating pattern, but applying a small magnetic field enhances the quantum agitation of the spins until magnetism is destroyed completely at the quantum critical point (*8*).

Yet despite being an ideal candidate for demonstrating this theory, the material studied by Gegenwart *et al.* is one of a growing number that seem to lie outside this established framework. Previous bad actors (*9*, *10*) have revealed themselves discretely through unusual combinations of critical exponents that don't quite fit with the theory. $YbRh_2Si_2$ does this and more. In addition to strange power laws, Gegenwart *et al.* see abrupt changes in physical properties, all of which emanate from the quantum critical point in a manner quite distinct from the magnetic ordering transition. The changes define a new energy scale different from that of the magnetic fluctuations, yet similar to it in vanishing at the quantum critical point. This tells us that the transitory appearance of bubbles of nascent order is not the only important physical process occurring at the critical point and that a theory that includes only fluctuating order will never be enough to characterize these transitions. They must therefore lie outside the universality classes we have known to date and require a new physical ingredient.

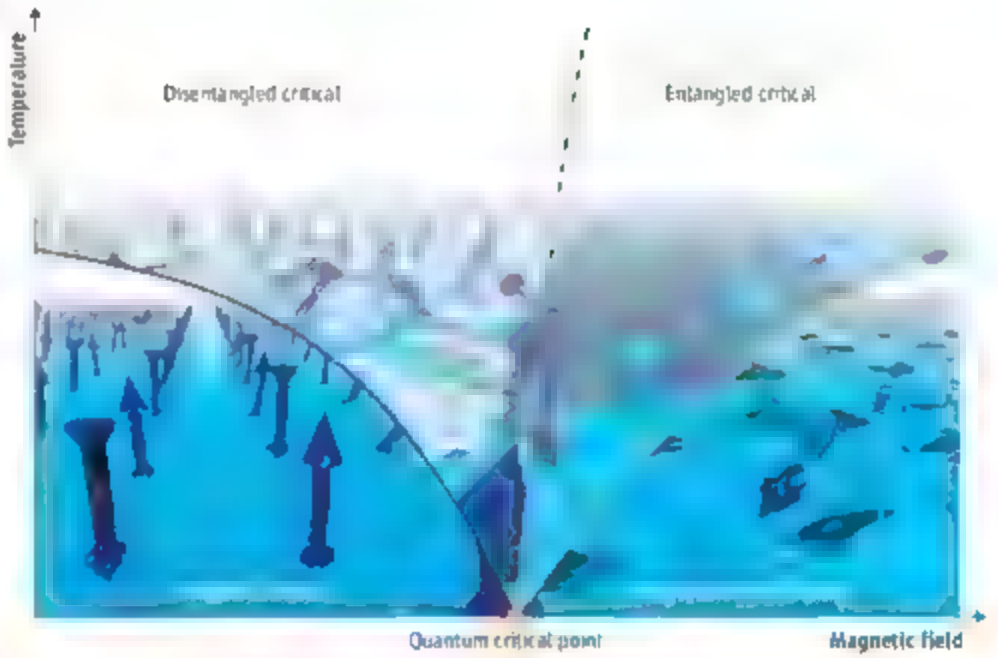

Quantum fates. One speculative interpretation of the collapsing energy scales observed around the quantum critical point is shown schematically. At high temperatures, fluctuating magnetic spins disrupt the electron fluid in a disentangled critical region. On cooling, the spins may order to form a magnetic metal. Alternatively, the spins can become locally entangled (*15*) with the electrons' fluctuating quantum fluid when, at a lower energy scale, it is destined to form a heavy electron liquid. Why all these regions should converge on the quantum critical point is the mystery.

The author is in the School of Physics and Astronomy, University of Birmingham, Birmingham B15 2TT, UK. E-mail: ajs@th.ph.bham.ac.uk

A number of recent theoretical suggestions might point to what we have missed. Theoretical work on insulating two-dimensional magnets has shown (*11*) that under certain circumstances, yet to be realized in a real material, but nevertheless entirely plausible excitations appear at the critical point that bear no resemblance to the fluctuations in the ordered phases. Extending this idea to the metal might suggest that it is the break-up of the electron itself that is being reflected in this new energy scale (*12*).

Alternatively, this new energy scale could be a reflection of the unusual nature of the metal in $YbRh_2Si_2$, which is a mixture of magnetic atoms like ytterbium bathed in a flood of metallic electrons. The fate of the spins in materials like these has long been known to lie in the balance between two extremes (*13*). Either the spins form an ordered magnetic state, leaving the conduction electrons alone, or the spins and conduction electrons can fuse to create a metallic state of apparently heavy electrons. Usually it is assumed that this second process happens and is followed by a weak magnetization of the resultant metal. These experiments could suggest that the quantum critical point is not primarily about magnetic order at all but rather is a transition between these two different fates of the spins (*14*) (see the figure). Whatever the underlying cause, the theorists now have a great task: To unravel the identity of the new energy scale.

References

1. See, for example, P. M. Chaikin and T. C. Lubensky, *Principles of Condensed Matter Physics* (Cambridge Univ. Press, Cambridge, UK, 1995).
2. J. A. Hertz, *Phys. Rev. B* **14**, 1165 (1976).
3. A. J. Millis, *Phys. Rev. B* **48**, 7183 (1993).
4. P. Gegenwart *et al.*, *Science* **315**, 969 (2007).
5. N. D. Mathur *et al.*, *Nature* **394**, 39 (1998).
6. J. Paglione *et al.*, *Phys. Rev. Lett.* **91**, 246405 (2003).
7. P. Coleman, A. J. Schofield, *Nature* **433**, 226 (2005).
8. O. Trovarelli *et al.*, *Phys. Rev. Lett.* **85**, 626 (2000).
9. G. R. Stewart, *Rev. Mod. Phys.* **73**, 797 (2001).
10. G. R. Stewart, *Rev. Mod. Phys.* **78**, 743 (2006).
11. T. Senthil, A. Vishwanath, L. Balents, M. P. A. Fisher, *Science* **303**, 1490 (2004).
12. T. Senthil, *et al.*, *Phys. Rev. B* **69**, 035111 (2004).
13. S. Doniach, *Physica B* **91**, 231 (1977).
14. P. Coleman, *et al.*, *J. Phys. Condens. Mat.* **13**, R723 (2001).
15. Q. Si, S. Rabello, K. Ingersent, J. L. Smith, *Phys. Rev. B* **68**, 115103 (2003).

10.1126/science.1139335

ANTHROPOLOGY

Some Like It Hot

Sandra Knapp

Studies of novel types of microfossils reveal new patterns and connections between human movement and the distribution and movement of plant species, both domesticated and wild.

Can you imagine some of the great world cuisines—such as Indian, Thai, and Korean—without chili peppers? This fiery spice has become an integral part of cooking and culture far from its native ranges. Chili peppers (*Capsicum*) come from the Americas and were introduced to places such as India and Thailand after Europeans explored the New World in the 15th century. On page 986 of this issue, Perry *et al.* (*1*) shed light on when and where chili peppers were first cultivated. Data from studies of this kind may also have potential use in the analysis of human transport and spread of invasive species.

Capsicum is a genus comprising about 25 species (*2*). It is a member of the plant family Solanaceae, which contains other economically important plants such as the potato, the tomato, and tobacco. Brazil is the center of species diversity for *Capsicum*, but many species are also found in the Andes. Humans have domesticated and today cultivate five species of *Capsicum*, all for their spicy flavor that comes from the long-chain amide capsaicin. Some varieties of the cultivated species (such as bell peppers) lack high quantities of capsaicin, but the sensation of hotness and the "endorphin rush" induced by eating chilis largely account for their universal appeal.

Capsaicin is a specialized metabolite that is produced in the fruits of some *Capsicum* species as a deterrent to seed predators. Great variation in capsaicin content has been introduced through plant breeding into cultivated species of peppers, but wild species of *Capsicum* also have hot and mild forms (*3*). Humans first exploited this metabolite in the Americas, and European explorers and colonists later transported this and other New World plants all over the world. But exactly when and where domestication of peppers first occurred have proved difficult to establish (*4*), in part due to a lack of macrofossil remains for these tropical plants.

Perry *et al.* now show that peppers were cultivated and in widespread use across the Americas 6000 years ago, not only as occasional condiments, but also as components of a complex and sophisticated diet. The authors recovered microfossils of starch grains from grinding stones and cooking pots in archaeological sites from the Caribbean, Venezuela, and the Andes. They found *Capsicum*-specific starch grains in association with maize and manioc. Their evidence suggests that three of the five species of domesticated *Capsicum* were cultivated together in Peru in both the coast and the highlands as long as 4000 years ago.

As humans moved around all over the face of the Earth, they carried with them their favorite foods and herbal medicines. *Capsicum* is notable in this regard, as it quickly became integral to a wide range of Old World disciplines, from Indian cuisine to Tibetan medicine (*5*). Other members of the Solanaceae, such as thornapple and tobacco, have also had their native distributions obscured by human transport. The scientific name *Datura* was given to the thornapples by Linnaeus from the Sanskrit *dhustura*, but all species of *Datura* are in fact only native to the Americas (*6*).

What is a native range when humans transport plants so far from their origins, and alter them through selection to suit their own purposes? Today's concern over invasive species and their threat to native biodiversity (*7*) highlights the importance of understanding how human movements and transport have

Diversity explained. These different kinds of *Capsicum* grown at the University of Wageningen (*8*), illustrate the diversity of shape and color in domesticated chili peppers. Perry *et al.* (*2*) show that peppers have been cultivated across the Americas for at least 6000 years.

CREDIT: REPRODUCED WITH PERMISSION FROM (8)

The author is in the Department of Botany, The Natural History Museum, Cromwell Road, London SW7 5BD, UK. E-mail: s.knapp@nhm.ac.uk

affected distributions of plants and animals. Species of plants introduced for a variety of reasons have come to invade ecosystems in alarming ways, witness Japanese knotweed in Britain or kudzu in the southern United States. Domesticated plants have always been taken by humans wherever they have traveled and are mostly (but not always) unproblematic, but these patterns can be among the most difficult of all distributions to unravel. New ways of studying ancient human use and transport of plants can contribute to our knowledge of the dynamics of introductions, including the effects of invasive species.

Perry *et al.*'s innovative use of starch grains from kitchen tools, coupled with their elegant unraveling of the specificity of these grains to domesticated *Capsicum*, reveals more ancient cultivation and widespread use of this crop plant than previously reported. It also opens up new avenues of research into how the peoples of the Americas transported and traded plants of cultural importance. The authors found no starch grains of wild species of *Capsicum* in any of the sites they examined, showing that domestication of chili peppers had occurred long before these sites were occupied and that cultivation was routine. Where domestication of the five species of *Capsicum* occurred is currently speculative, based on modern distribution and genetic analysis. *C. annuum* is thought to have been domesticated in Mexico or northern Central America, *C. frutescens* in the Caribbean, *C. chinense* in Amazonia, *C. baccatum* in Bolivia, and *C. pubescens* in the southern Andes. *C. baccatum* and *C. pubescens* are taxonomically distinct, but the other three are members of a species complex and perhaps not really "wild" species at all.

Humans have, in a very short time, radically altered both the characteristics and distributions of the organisms we value. New data types like the starch microfossils discovered by Perry *et al.* have enormous potential to help investigate the trajectories for domestication, cultivation, and trade in a wide variety of crops whose histories have remained difficult to unravel due to their lack of preservation or their tropical origins. Data like these will also be useful beyond the study of a few crop plants. They have the potential to help in efforts to understand the links between human transport and invasive species, thus contributing to the challenge of biodiversity conservation.

References

1. L. Perry *et al.*, *Science* **315**, 986 (2007).
2. G. Barboza, L. de B. Bianchetti, *Syst. Bot.* **30**, 863 (2005).
3. I. J. Tewksbury *et al.*, *J. Chem. Ecol.* **32**, 547 (2006).
4. B. Pickersgill *et al.*, in *The Biology and Taxonomy of the Solanaceae*, J. G. Hawkes, R. N. Lester, A. D. Skelding, Eds. (Academic Press, London, 1979), pp. 679–700.
5. A. M. De, *Capsicum* (Taylor & Francis, London, 2003).
6. D. E. Symon, L. Haegi, in *Solanaceae IV*, J. G. Hawkes, R. N. Lester, M. Nee, N. Estrada R., Eds. (Royal Botanic Gardens, Kew, Richmond, Surrey, UK, 1991), pp. 197–210.
7. Millennium Ecosystem Assessment, *Ecosystems and Human Well-Being: Biodiversity Synthesis* (World Resources Institute, Washington, DC, 2005); see www.maweb.org/documents/document.354.aspx.pdf.
8. S. Knapp, *J. Exper. Bot.* **53**, 2001 (2002).

10.1126/science.1138308

NEUROSCIENCE

Where Am I?

Studies in rats reveal that the key to interpreting spatial information—where we are compared to where we've already been—may lie in the hippocampus.

André A. Fenton

The Greek philosopher Heraclitus famously observed, "You can never step into the same river, for new waters are always flowing on to you." How do we recognize a place as the same, even when it is different? How do brains routinely activate the same representations in response to somewhat different experiences? When is experience the same but different, and when is it just plain different?

Neuroscientists are getting closer to obtaining answers by recording the activity of neurons in the rat hippocampus that signal the animal's location. One of these "place cells" (*1*) only discharges rapidly when the animal is in a specific part of the environment corresponding to the cell's "firing field." The collective discharging of place cells allows us to predict the rat's location (*2*) by, in a sense, reading its mind. Knowing a rat's location from the activity of its neurons is astonishing given that rats, like people, have no specific spatial sense organs analogous to, for example, the visual or auditory systems. Somehow spatial knowledge is assembled by the brain. On page 961 of this issue, Leutgeb *et al.* (*3*) provide the latest insight into how spatial information is computed and transformed into spatial awareness, or knowledge through distinct networks of neurons in the hippocampus.

Leutgeb *et al.* recorded hippocampal activity while rats foraged in seven boxes that systematically varied in shape between a circle and a square. Similar "morph boxes" were previously used by others to record from CA1 (*4*), the information output region of the hippocampus. The earlier study found that a rat forms distinct neural "representations" (patterns of activated place cells) when occupying either a circular or square box. Neither the fields of place cells nor their firing (activity) rates are related—that is, there is global remapping of neuronal activity in CA1 when a rat moves between the two different box shape environments. Moreover, only the circle or the square neural representation is activated for all the morph box shapes; boxes that are more circle-like activate the circle representation in the hippocampus, whereas square-like boxes activate the square representation. The activation state changes coherently across CA1 cells. These findings suggested that the CA1 region lumps spatial information into categories (in this case, circle or square categories). Thus, a rat perceives itself to be in either a circular or square box and the appropriate spatial memory gets activated by mechanisms with attractor network properties. The collective activity in a neural network defines its state. An equilibrium state, called an attractor, is akin to a memory (*5*). Attractor network responses to input are analogous to a ball on a bumpy surface. The network and the ball quickly settle into a nearby attractor until the inputs change enough to switch attractors.

In 2005, Leutgeb and colleagues (*6*) had done essentially the same experiment with morph boxes, but also recorded from CA3, the hippocampal region projecting to CA1. For unknown reasons, they got a somewhat different result from the earlier study. Global remapping occurred at a particular stage in the morph box sequence for only a subset of cells ("lumpers") in both hippocampal regions. Other neuronal subsets, so-called "splitters," changed by rate remapping—systematically increasing or decreasing discharge rates across the morph sequence while maintaining firing field locations (*6*, *7*). The result sug-

The author is in the Department of Physiology and Pharmacology, Robert F. Furchgott Center for Neural and Behavioral Science, State University of New York Downstate Medical Center, Brooklyn, NY 11203, USA. E-mail: afenton@downstate.edu

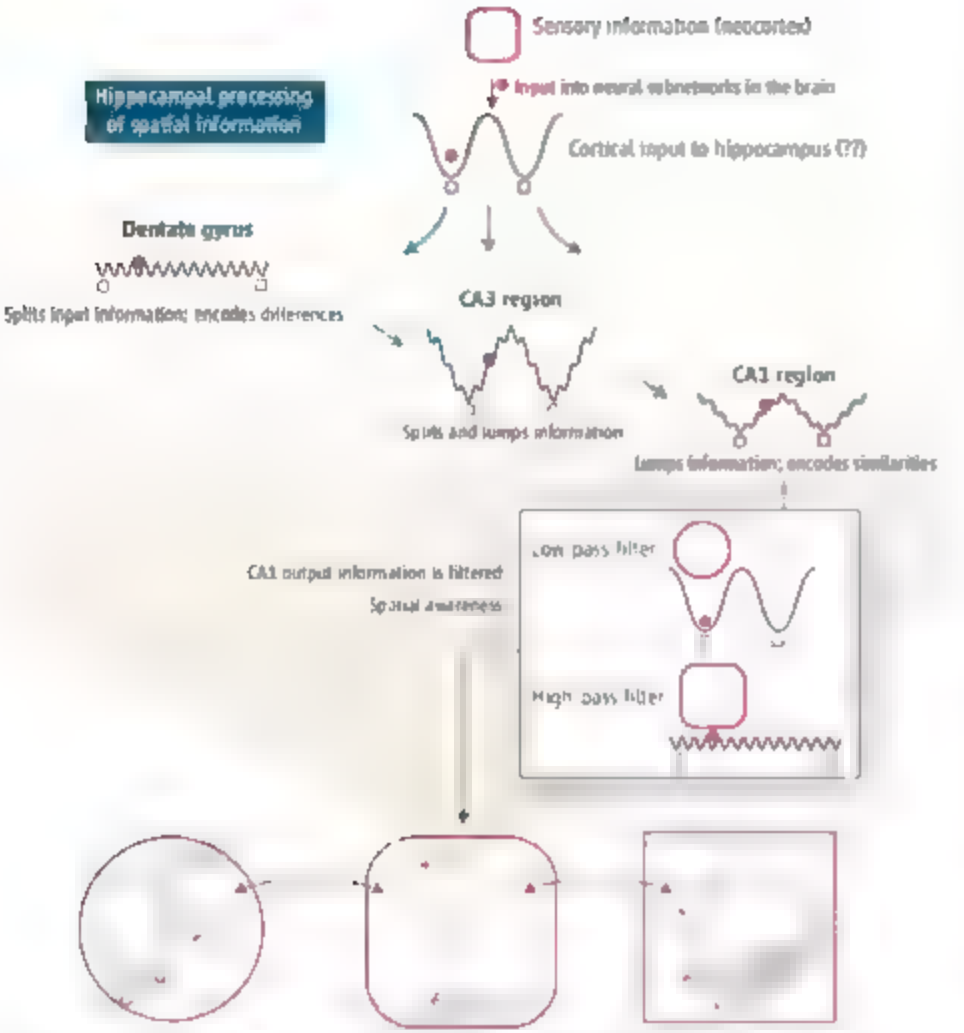

Thinking like a rat. Sensory information about a rat's spatial environment (square or square box or an intermediate-shape box) feeds into three hippocampal regions of the brain (dentate gyrus, CA3, and CA1) from the neocortex. Spatial information about the nature of the animal's environment is encoded in the activity patterns of neuron networks in these regions.

gested that hippocampal activity contains information that an environment is both the same and different relative to a previously experienced and remembered environment. But this posed another puzzle: To extract either a same or a different signal, the network must somehow coexist in the two corresponding attractors. This necessitates mechanisms to segregate neuronal activity into the appropriate lumper and splitter subgroups (*8*).

There is good understanding of how spatial information is associated and stored in the hippocampus (*9*, *10*), but a knowledge system must also segregate information and memories so that they can be recombined in arbitrary and useful ways. In the present study, Leutgeb *et al.* repeated the morph box experiment, this time recording from the rat's dentate gyrus and CA3. The dentate gyrus is a hippocampal region that projects to CA3 and is thought to transform slightly different input activity from the neocortex into more distinctly different patterns. Leutgeb *et al.*'s latest recordings provide evidence of two mechanisms by which the hippocampus segregates neuronal activity to assess the same and different nature of the animal's environment.

The authors confirm that CA3 place cells respond to small deviations in the spatial environment by lumping. In other words, the same neuronal discharge patterns were observed in CA3 regardless of whether the rat was in a morphed or unmorphed circular or square box. Larger deviations from either environment caused rate remapping in CA3. The dentate gyrus was quite different. Single dentate granule cells had more firing fields than did individual CA3 cells. Granule cells responded to small morph deviations in the rat's environment by changing both firing rates and firing fields unpredictably. Thus, the dentate gyrus proves a consummate information splitter and the CA3 more of a lumper (see the figure). Small changes in spatial input information caused large changes in dentate gyrus output to CA3 but virtually no changes in CA3 output to CA1.

These lumper and splitter behaviors were also evident in the temporal dimension of processing spatial information. In addition to place cell firing rates, the particular subset of place cells that do or do not fire together also signals the rat's position (*8*). The likelihood that a pair of cells will fire together during a short time window is measured by their coactivity. The difference between the coactivity of pairs of dentate gyrus cells grew larger as the shape distinction between two boxes occupied by the rat increased. The same was true for pairs of dentate gyrus–CA3 cells and pairs of cells within CA3, with a surprising exception. When a rat was moved between two boxes at the extremes of the morph sequence, coactivity in CA3 was more similar than that observed when the rat repeatedly occupied only a circular or square box. When a morph box was minimally different from the circle or square, CA3 temporal discharge seemed to lump, emphasizing similarity between the two environments, whereas dentate gyrus discharge seemed to split, enhancing the difference.

The second segregation mechanism is global remapping in response to large environmental changes. Dentate gyrus and CA3 cells also differed. Global remapping in CA3 and CA1 is characterized by a seemingly random selection of the active subset of cells; some cells turn on and others turn off (*11*). Although dentate gyrus discharge in one environment could not be predicted from its activity in another environment, the active subset of granule cells was constant. The same granule cells were active across all conditions, including different-sized boxes and rooms.

Beyond these recordings from all three major hippocampal subregions, what is now needed are rat brain recordings from the neocortex during the morph box experiment to characterize the location-specific neocortical inputs to the hippocampus (*12*). This will provide a complete description of how each connected part of the hippocampal circuit responds to spatial changes in an animal's environment. The fly in the ointment appears to be the fixed active subset of granule cells. Only 2 to 3% of dentate gyrus cells are active in conditions (*13*) like those used by Leutgeb *et al.* If spatial inputs do not activate the other 97% of the dentate gyrus, what does? This is especially puzzling because the dentate gyrus generates new neurons throughout life and this neurogenesis is modulated by learning.

(14). Future work will surely focus on why more or apparently the same neurons seem to have a different function.

References

1. J. O'Keefe, *Exp. Neurol.* **51**, 78 (1976).
2. M. A. Wilson, B. L. McNaughton, *Science* **261**, 1055 (1993).
3. J. K. Leutgeb, S. Leutgeb, M.-B. Moser, E. I. Moser, *Science* **315**, 961 (2007).
4. T. J. Wills, C. Lever, F. Cacucci, N. Burgess, J. O'Keefe, *Science* **308**, 873 (2005).
5. J. Hopfield, *Proc. Natl. Acad. Sci. U.S.A.* **79**, 2554 (1982).
6. J. K. Leutgeb *et al.*, *Neuron* **48**, 345 (2005).
7. R. M. Hayman, S. Chakraborty, M. I. Anderson, K. J. Jeffery, *Eur. J. Neurosci.* **18**, 2825 (2003).
8. K. D. Harris, D. Csicsvari, H. Hirase, G. Dragoi, G. Buzsáki, *Nature* **424**, 552 (2003).
9. E. Pastalkova *et al.*, *Science* **313**, 1141 (2006).
10. J. R. Whitlock, A. J. Heynen, M. G. Shuler, M. F. Bear, *Science* **313**, 1093 (2006).
11. R. U. Muller, J. L. Kubie, *J. Neurosci.* **7**, 1951 (1987).
12. M. H. Fyhn, T. F. Hafting, A. Treves, E. I. Moser, M. B. Moser, *Soc. Neurosci. Abstr.* **68**.9 (2006).
13. M. K. Chawla *et al.*, *Hippocampus* **15**, 579 (2005).
14. E. Gould, A. Beylin, P. Tanapat, A. Reeves, T. Shors, *Nat. Neurosci.* **2**, 260 (1999).

10.1126/science.1139146

COMPUTER SCIENCE

Where Are the Exemplars?

A fast way of finding representative examples in complex data sets may be applicable to a wide range of difficult problems.

Marc Mézard

As we build databases from scientific and medical experiments, researchers crave more efficient computational methods to organize and analyze it. When dealing with large, noisy, unstructured sets of data, a common computational method consists in looking for data clusters. In the case of gene expression, with hundreds of sequences for example, the clusters would be groups of genes with similar patterns of expression. On page 972 of this issue, Frey and Dueck propose a new method for finding an optimal set of clusters (*1*). Their algorithm detects special data points called exemplars, and connects every data point to the exemplar that best represents it. In principle, finding an optimal set of exemplars is a hard problem, but this algorithm is able to efficiently and quickly handle very large problems (such as grouping 75,000 DNA segments into 2000 clusters). An analysis that would normally take hundreds of hours of computer time might now be done in a few minutes.

Detecting exemplars goes beyond simple clustering, as the exemplars themselves store compressed information. An example with a broad range of possible applications is found in the statistical analysis of language. For instance, take your last scientific paper and (no, I don't really suggest that it's a large, noisy data set) and consider each sentence to be a data point. The similarity between any two sentences can be computed with standard information theory methods (that is, the similarity increases when the sentences include the same words). Knowing the similarities, one can select the exemplars (sentences) in the paper which provide an optimally condensed description. If you are a hasty reader, you can thus go directly to Fig. 4 of Frey and Dueck's report and find the best summary of their own paper in four sentences. But understanding the method requires a bit more effort.

Such methods start with the construction of a similarity matrix *s*, a list of numbers that establishes the relationship of each data point to every other data point. As we saw in the sentences example, *s*(B, A) is a number that measures how well the data point A represents point B (and it is not necessarily equal to *s*(A, B)). The optimal set of exemplars is the one for which the sum of similarities of each point to its exemplar is maximized. In the usual clustering methods, one decides *prior* on the number of exemplars, and then tries to find them by iterative refinement, starting from a random initial choice.

The method of Frey and Dueck, called affinity propagation, does not fix the number of exemplars. Instead, one gives a cause for each point B, a number *c*(B) that characterizes

Caravaggio's "Vocazione di San Matteo." How to choose an exemplar through message passing. The messages are exchanged in the directions of the fingers and of the glances, leading to the recognition of San Matteo as the exemplar.

CREDIT: SCALA/ART RESOURCE

The author is at the Centre National de la Recherche Scientifique and Laboratoire de Physique Theorique et Modeles Statistiques, Université Paris Sud, 91405 Orsay, France. E-mail: mezard@lptms.u-psud.fr

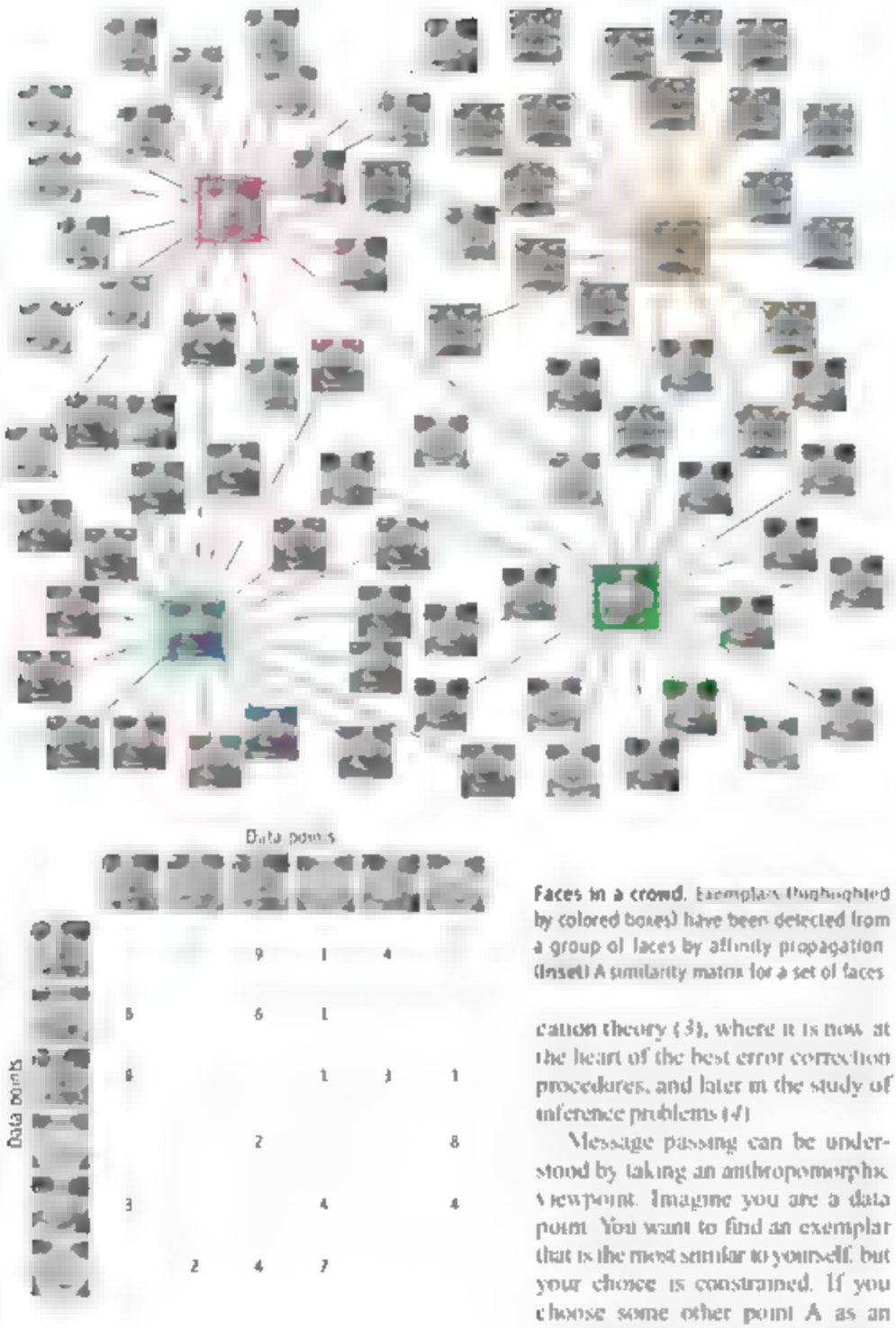

Faces in a crowd. Exemplars (highlighted by colored boxes) have been detected from a group of faces by affinity propagation (inset) A similarity matrix for a set of faces

the a priori knowledge of how good point B is as an exemplar. In most cases all points are equally suitable, so all the numbers take the same value P. This quantity provides a control parameter. The larger P, the more exemplars one is likely to find.

Affinity propagation is known in computer science as a message-passing algorithm (see the first figure) and it aims at maximizing the net similarity. It is in fact an application of a method called "belief propagation," which was invented at least twice: first in communication theory (*3*), where it is now at the heart of the best error correction procedures, and later in the study of inference problems (*4*).

Message passing can be understood by taking an anthropomorphic viewpoint. Imagine you are a data point. You want to find an exemplar that is the most similar to yourself, but your choice is constrained. If you choose some other point A as an exemplar, then A must also decide to be its own exemplar. This creates one constraint per data point, establishing a large network of constraints that must all be satisfied. When the net similarity is maximized with all constraints satisfied, the set of actual exemplars emerges.

Now imagine that next to each point stands a guardian angel telling whether someone else has chosen that point as an exemplar or not. An approximate solution of the complicated web of conflicting constraints is obtained by having all of these characters talk to each other. At a given time, all angels send messages to all points, and all points answer to all angels. One data point tells the angel of every other point his ranked list of favorite exemplars. An angel tells every other point the degree of compatibility of his list with the angel's constraints. Every sent message is evaluated through a simple computation on the basis of the received messages and the similarity matrix. After several message-passing rounds, all the characters reach an agreement and every point knows its exemplar. In practice, the running time of this algorithm scales linearly with the number of similarities.

As an example, affinity propagation can be a powerful method to extract representative faces from a gallery of images (see the second figure). The input is a list of numerical similarities between pairs of data points, which may be measured, computed using a model, or, in the present example, set by visual inspection (missing similarity values indicated with question marks are accepted by the algorithm). Each face is a data point, that exchanges messages with all other faces and their guardian angels. After a few iterations of message passing, a global agreement is reached on the set of exemplars.

Such message-passing methods have been shown to be remarkably efficient in many hard problems that include error correction, learning in neural networks, computer vision, and determining the satisfiability of logical formulas. In many cases they are the best available algorithms, and this new application to cluster analysis looks very powerful. Understanding their limits is a main open challenge. At the lowest level this means controlling the convergence properties or the quality of the approximate solutions that they find. A more ambitious goal is to characterize the problems where they can be useful. The concepts and methods developed in statistical physics to study collective behavior offer the most promising perspective in this respect. In physics terms, belief propagation (and therefore affinity propagation) is a mean field type method (*5*). That is, the complex interaction of a given object (a data point) with all of the others is approximated by an average effective interaction. Although this works well in most cases, it may get into trouble when the system gets close to a phase transition (*6*), where some correlations become extremely long-ranged. The appropriate modification, which requires using more sophisticated messages, has been worked out in some special cases (*7*), but again its full range of applicability is still to be found.

Along with its pedagogical virtue, the anthropomorphic explanation of message passing also underlines its main features. This

CREDIT: B. J. FREY, D. DUECK/UNIVERSITY OF TORONTO

strategy can find an excellent approximate solution to some of the most difficult computational problems with a very simple recipe. It uses basic messages which are exchanged in a distributed system, together with simple update rules that are purely local. This realizes in practice a new scheme of computation, based on distributed simple elements that operate in parallel, in the spirit of neurocomputation. One might expect to find that some of its principles are at work in living organisms or social systems. Each new successful application of message passing, such as affinity propagation, thus adds to our understanding of complex systems.

References

1. B. J. Frey, D. Dueck, *Science* **315**, 972 (2007); published online 11 January 2007 (10.1126/science.1136800)
2. *Proceedings of the Fifth Berkeley Symposium on Mathematical Statistics and Probability*, L. Le Cam, J. Neyman, Eds. (Univ. of California Press, Berkeley, CA, 1967), p. 281.
3. R. G. Gallager, *Low Density Parity Check Codes* (MIT Press, Cambridge, MA, 1963).
4. J. Pearl, *Probabilistic Reasoning in Intelligent Systems: Networks of Plausible Inference* (Morgan Kaufmann, San Mateo, CA, 1988).
5. J. S. Yedidia, W. T. Freeman, Y. Weiss, *IEEE Trans. Infor. Theory* **51**, 2282 (2005).
6. O. Dubois, R. Monasson, B. Selman, R. Zecchina, Eds., special issue on Phase Transitions in Combinatorial Problems, *Theor. Comp. Sci.* **265** (2001).
7. M. Mezard, G. Parisi, R. Zecchina, *Science* **297**, 812 (2002); published online 27 June 2002 (10.1126/science.1073287).

10.1126/science.1139678

GEOLOGY

On the Origins of Granites

Granites make up a large part of the continental crust. New data reveal their complex and diverse formation history, calling for a revision of the geological histories of many granites.

John M. Eiler

Geology spent the 19th and much of the 20th century in the throes of a scientific civil war over the origin of granites—the coarsely crystalline, feldspar-rich rocks that make such excellent building stones and kitchen counters. The ultimate losers (*1*) held that granites precipitated from aqueous fluids that percolate through the crust, or formed by reaction of preexisting rocks with such fluids. The winners (*2*) recognized that granites crystallized from silicate melts.

Yet, the resolution of this argument led to various others that remain almost as divisive. Are the silicate melts that give rise to granites partial melts of preexisting rocks in the continental crust, or are they instead the residues of crystallizing mantle-derived basalts, analogous to the brine that is left when ice freezes out of salty water? If granites form by crustal melting, do they come from the sediment-rich upper crust or from preexisting igneous rocks that dominate the lower crust? On page 980 of this issue, Kemp *et al.* (*3*) examine these questions through the lens of two of the newest analytical tools developed for the earth sciences.

Clear answers to the above questions have been found previously for some extreme types of granite. There is little debate that upper-crustal sediments are the sources of S-type granites (*4*) (where "S" stands for sediment) and that mantle-derived basalts give rise to M-type granites (*5*) ("M" for mantle). However, members of a third class, the I-type (*4*)—are abundant, widely distributed, and diverse, and their origins are up for grabs. A popular view holds that these granites are melts of deep-crustal igneous rocks (hence the "I" for igneous) (*4*, *6*). A minority dissenting view suggests that they are instead largely mantle-derived and only modified by passage through the crust (*7*).

The stakes in this argument are high. I-type granites (or their metamorphosed or eroded derivatives) make up a large fraction of the continental crust. Therefore, our thoughts regarding their origins are key to understanding the mechanisms by which the continents differentiate from the rest of the silicate earth and the consequences of that differentiation for the composition of the mantle. If I-type granites are descended from basalts, then their formation represents net growth of the continents and net removal from the mantle of elements that are highly concentrated in the crust (such as the heat-producing radioactive isotopes, ^{40}K and ^{238}U). If, instead, they form by melting preexisting crustal rocks, they represent a mechanism by which the continents internally redistribute their various sedimentary and igneous constituents.

One reason the origin of granite is such a difficult problem is that these rocks can be extremely complicated (see the figure) (*8*). Many are composed of minerals that represent only a component of the melts from which they formed, some are mixtures of minerals that grew from different melts; some contain unmelted remnants of their sources, and individual minerals often have heterogeneous chemical and isotopic compositions, reflecting the evolution of their parental magmas over the course of their crystallization.

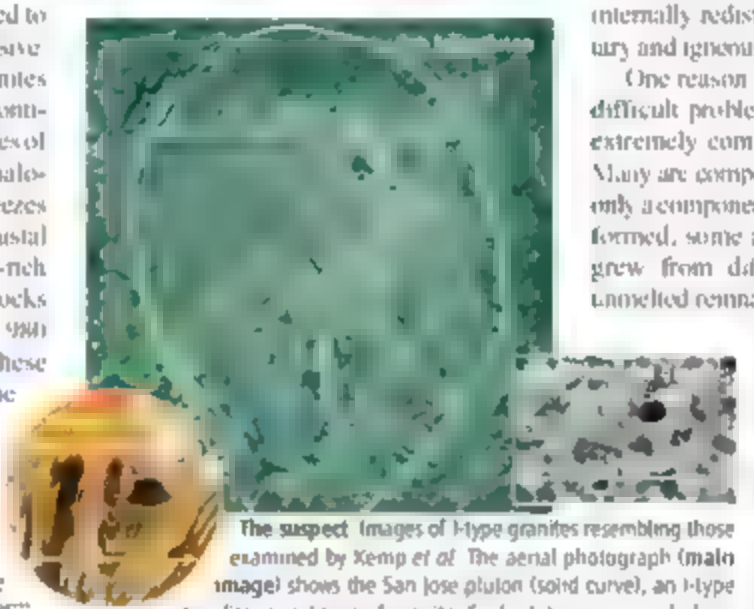

The suspect. Images of I-type granites resembling those examined by Kemp *et al.* The aerial photograph (**main image**) shows the San Jose pluton (solid curve), an I-type tonalite, or subtype of granite. Such plutons commonly form kilometer-scale bodies intruded into rocks of the upper crust. Kemp *et al.* suggest that assimilation of enveloping rocks influences the compositions of such bodies. The insets show a specimen of a similar tonalite from the Chihuahua Valley, California. The visible light photograph (**right inset**) reveals dark laths of amphibole and hexagonal crystals of biotite embedded in a white matrix of interlocking feldspar and quartz. The transmitted-light photomicrograph (**left inset**) shows twinning, compositional zoning, overgrowths, and inclusions in plagioclase (complex light and dark pattern), adjacent to a crystal of amphibole (brown). The micro-analytical techniques employed by Kemp *et al.* aim to avoid artifacts that arise from mixing different components of these compositionally and texturally complex rocks.

Kemp *et al.* (*3*) examine the origin and evolution of I-type granites from the Lachlan belt in Australia. Their work draws on several recent microanalytical innovations, including high-precision, in situ measurements of oxygen isotope ratios with a large-radius ion microprobe and in situ measurements of hafnium isotopes using laser ablation joined with an inductively coupled plasma mass spec-

The author is in the Division of Geological and Planetary Sciences, California Institute of Technology, Pasadena, CA 91125, USA. E-mail: eiler@gps.caltech.edu

CREDIT: MAIN IMAGE, J. D. MURRAY AND J. F. SLACK; INSETS, J. M. EILER

trometer. Sediments and weathered or hydrothermally altered rocks in the shallow crust have oxygen isotope compositions that differ strongly from those of the mantle and of deep-crustal igneous rocks. Hafnium isotopes evolve through time due to production of ^{176}Hf from radioactive decay of ^{176}Lu and generally differ strongly between the mantle (high in Lu-Hf ratio and thus relatively ^{176}Hf-rich) and ancient crust (low in Lu-Hf ratio and thus relatively ^{176}Hf-poor). Together, these geochemical systems can measure the proportions of recent mantle extracts versus ancient crust and the amounts of shallow sediment-rich crust versus deep, largely igneous crust in the sources of granites.

Kemp *et al.* make their oxygen and hafnium isotope measurements on zircon, a trace mineral common to most granites. Zircon has long been used to determine the crystallization ages of granites, and is increasingly used to constrain the compositions of their sources (*9*). Kemp *et al.* show that the oxygen and hafnium isotope compositions of zircons in Lachlan I-type granites correlate with one another over a wide range, from compositions characteristic of the mantle to those characteristic of upper-crustal sediments. These trends suggest that I-type granites form by mixing of differentiated mantle melts with melts of the upper crust. Thus, they represent both net crustal growth (and corresponding mantle depletion) and redistribution of existing parts of the continental crust.

The results reported by Kemp *et al.* present a powerful case that we must rethink the most popular explanation of the origins of I-type granites (*4*, *6*) and recognize that I-type granites are close relatives of both the M- and the S-type granites (*7*) rather than distant cousins (*4*, *6*). These conclusions will force revisions of the geological histories of the many places where such granites are found. Kemp *et al.* also suggest that common I-type granites represent net crustal growth and thus should factor more extensively into estimates of the rate and mechanisms of Earth's chemical differentiation. More generally, the authors expose the complex, multicomponent origin of granites and argue forcefully against the rigid either/or approach most earth scientists have taken to granite classification.

Kemp *et al.*'s argument that the Lachlan I-type granite suite is derived from partial melts of the mantle depends crucially on their interpretation of the major element compositions of the most primitive members of that suite. These rocks are broadly basaltic suggesting that they are partial melts of peridotite (the dominant mantle rock type). However, these compositions might also be formed by high-degree melting of preexisting igneous rocks in the lower continental crust (*10*). This alternative scenario is more consistent with common interpretations of the origins of I-type granites (*4*, *6*). This question could be resolved more conclusively with geochemical measurements that are sensitive to the time at which crust is first extracted from the mantle (for example, osmium isotopes).

Kemp *et al.*'s model suggests that portions of the continental crust that are rich in I-type granites should evolve in composition through time. The degree of melting of the sediment-rich upper crust should increase, and the crust as a whole should become progressively richer in juvenile mantle-derived material. This prediction could be tested with larger-scale studies using the same methods as Kemp *et al.* Such work would be an attractive next step in one of geology's oldest debates.

References

1. A. G. Werner, *an Short Classification and Description of the Various rocks*, A. M. Ospovat, Ed. (Hafner, New York, 1971), pp. 38–95.
2. J. Hutton, *System of the Earth, 1785. Theory of the Earth, 1788. Observations on Granite, 1794. Together with Playfair's Biography of Hutton* (Hafner, Darien, CT, 1970).
3. A. I. S. Kemp *et al.*, *Science* **315**, 980 (2007).
4. A. J. R. White, B. W. Chappell, *Geol. Soc. Am. Mem.* **159**, 21 (1983).
5. M. R. Perfit, H. Brueckner, J. R. Lawrence, R. W. Kay, *Contrib. Mineral. Petrol.* **73**, 69 (1980).
6. A. J. R. White, B. W. Chappell, *Tectonophysics* **43**, 7 (1977).
7. C. M. Gray, *Earth Planet. Sci. Lett.* **70**, 47 (1984).
8. A. Castro, I. Moreno-ventas, J. D. De-la-Rosa, *Earth Sci. Rev.* **31**, 237 (1991).
9. J. W. Valley, J. R. Chiarenzelli, , M. McLelland, *Earth Planet. Sci. Lett.* **126**, 187 (1994).
10. B. W. Chappell, A. J. R. White, I. S. Williams, D. Wyborn, *Trans. R. Soc. Edinburgh. Earth Sci.* **95**, 125 (2004).
11. I thank J. D. Muhay and L. T. Silver for use of the photonegative used to generate the main image and L. T. Silver for use of the hand specimens and thin sections used to create the insets. I also thank L. T. Silver for his guidance and advice in writing this article.

10.1126/science.1138065

BIOMEDICINE

Every Joint Has a Silver Lining

Therapy directed at a nonimmune cell that is unique to joints could suppress rheumatoid arthritis

Gary S. Firestein

For millions of patients that suffer from rheumatoid arthritis, simple tasks of daily life such as tying shoes and climbing steps are painful and perhaps even impossible. Symptoms range from sore, stiff joints to chest pain or shortness of breath from inflammation around the heart and lungs. The myriad of problems result from an immune system that has become confused and attacks normal tissues. Despite new treatments for rheumatoid arthritis that focus on controlling overactive immunity, joint destruction and disability progress in many patients. In fact, the response rates to these approaches are surprisingly similar, even though they target distinct routes to the disease such as hormone-like molecules or distinct immune cell types, emphasizing the complexity of the condition. On page 1006 of this issue, Lee and colleagues (*1*) propose an alternative therapeutic approach that targets a cell not generally considered part of the body's immune arsenal but is unique to the joint—the fibroblast-like synoviocyte.

Susceptibility to rheumatoid arthritis is caused by both genetic and environmental components. Patients with genetically programmed immune hyperactivity often produce rheumatoid factors—autoantibodies that bind to normal antibodies—sometimes years before the onset of clinical disease. Production of anti-citrullinated peptide antibodies is another early disease hallmark. Little is known about how the preclinical state evolves to the full-blown disease, although stochastic events such as repeated activation of innate immunity might contribute (*2*).

The synovium, or lining of the joint, provides nutrients to cartilage and produces lubricants to facilitate movement (see the figure). It normally includes a relatively acellular sublining layer that is sparsely populated by connective tissue cells and immune cells (mononuclear lymphocytes) and a thin discontinuous intimal lining composed of cells that resemble macrophages of the immune system and fibroblast-like synoviocytes. In rheumatoid arthritis, the intimal lining is hyperplastic, exhibiting a marked increase in

The author is in the Division of Rheumatology, Allergy and Immunology, University of California, San Diego, School of Medicine, 9500 Gilman Drive, MC 0656, La Jolla, CA 92093–0656, USA. E-mail: gfirestein@ucsd.edu

both cell types. The rheumatoid sublining is often heavily infiltrated with mononuclear lymphocytes including $CD4^+$ T cells, CD20 B cells, macrophages, and antibody-secreting plasma cells. Macrophage-like cells in the intimal lining express many of the proinflammatory cytokines that contribute to the disease. Synoviocytes produce prodigious amounts of proteases, prostaglandins, and certain cytokines (most notably interleukin-6) that also perpetuate inflammation.

Unlike synoviocytes in a healthy joint, those in rheumatoid arthritis are invasive and aggressive, reminiscent of transformed (malignant) cells (*3*). For instance, they express many proto-oncogenes characteristic of tumors, can proliferate without adhering to a substrate, and can escape growth inhibition that contact with other cells normally imparts. When synoviocytes have been implanted with human cartilage into mice that lack an adaptive immune system (and therefore cannot reject the human cells), synoviocytes isolated from rheumatoid arthritis patients invade the implanted cartilage whereas normal synoviocytes do not (*4*). This process occurs even though the synoviocytes have not been exposed to proinflammatory rheumatoid synovial cytokines or cells of the adaptive immune system for many months while they survive in the mouse.

The pathogenesis of this unusual aggressive behavior by synoviocytes is not well-defined but it could simply represent a normal response to the rich rheumatoid cytokine environment. On the other hand, permanent imprinting in response to the genotoxic environment of the rheumatoid synovium might account for this behavior—that is, events such as somatic mutations and oncogene expression could permanently alter cell behavior. Such genetic changes in synoviocytes are reflected by dysregulated modification of proteins (such as sumoylation), defective apoptosis, and mutations of the p53 tumor suppressor gene (*5*). Abnormal regulation of genes that regulate cell survival, such as *PTEN* and *sentrin* (*6*), might also contribute. However, in rheumatoid arthritis, synoviocytes are not truly transformed, they ultimately senesce when grown in culture and do not behave like malignant cells in vivo by metastasizing to other organs.

Despite these observations, investigators have been unable to assess synoviocytes as a therapeutic target in rheumatoid arthritis because no agents have been available to target this cell type. An opportunity arose with the the identification of cadherin-11 as a key adhesion molecule that regulates formation of the synovial lining and functional synoviocytes.

Lee and colleagues used several elegant methods to validate synoviocytes as a target in an animal model of arthritis, including genetically modified mice that lack the gene encoding cadherin-11, cadherin-11 specific antibodies, and a cadherin-11 fusion protein. In each case, they show that synovial inflammation is suppressed by blocking cadherin-11 function. Cartilage destruction, but less so bone erosion, was also reduced in mice treated with the antibody or the fusion protein, thereby confirming the seminal role of synoviocytes in the former. These data are supported by in vitro studies showing that cadherin-11 facilitates synoviocyte invasion into cartilage-like extracellular matrix in an in vitro model.

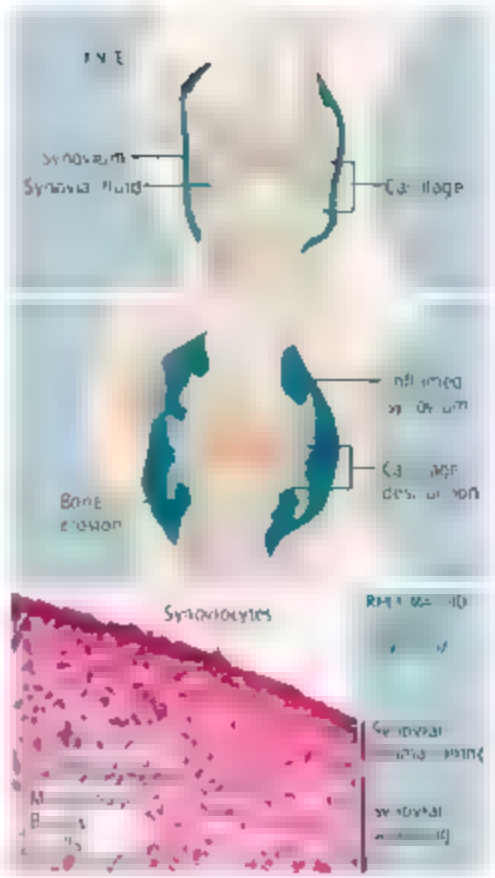

Rheumatoid arthritis. Synoviocytes, which express cadherin-11, comprise an inner membrane that lines the synovial cavity of joints (**top**). When activated by cytokines, lymphocytes, and environmental stresses (such as reactive oxygen species and nitrogen), they perpetuate disease by producing proinflammatory mediators and by invading cartilage (**middle, bottom**). Therapy directed at cadherin-11 could interrupt this cascade by blocking synoviocyte function.

Animal models are not the same as human rheumatoid arthritis, and the applicability of cadherin-11–targeted therapy to this disease still needs to be evaluated. Furthermore, it is not clear which synoviocyte functions might be linked to therapeutic benefit. One interesting observation is that preventive protocols are somewhat more effective than treating mice that are already afflicted with arthritis. Because the particular arthritis model used by the authors requires precise localization of autoantibodies in the joint as well as activation of synovial innate immunity (e.g., proinflammatory mast cells), disrupting normal synovial architecture by interfering with cadherin-11 might block events that initiate the disease (*7*). The effect of cadherin-11–based therapy in established disease, however, could involve other complex mechanisms such as suppressing interleukin-6 production or metalloproteinase expression by synoviocytes or by direct effects on synoviocyte invasiveness.

Distinguishing between these possibilities will require additional work in animal models that reflect other pathogenic features of rheumatoid arthritis besides autoantibody localization to joints. It will also be important to determine the fate of synoviocytes in cadherin-11–based treatment protocols. Do they undergo apoptosis, migrate out of the joint, or simply deactivate?

Another consideration is that synoviocytes in murine arthritis models do not display many of the unique aggressive features of rheumatoid synoviocytes. They are generally not imprinted and rapidly deactivate when cultured in vitro. This portends well for the potential efficacy of cadherin-11–targeted therapy in humans because of the possible added benefit gained by blocking the more aggressive rheumatoid synoviocyte phenotype that is not a feature of short-term animal models.

One challenge in rheumatoid arthritis is that complete remissions from the available targeted therapies occur in only a minority of patients. Using a series of individual biological agents that target different cell lineages (B cells, T cells) or proinflammatory cytokines (tumor necrosis factor) has improved outcomes and decreased the number of patients with uncontrolled disease. Combination therapy, however, has been fraught with problems due to suppressed host defense without additional clinical benefit. One intriguing possibility for cadherin-11–directed therapy is that the effects on adaptive immunity will probably be minimal. Hence, combination of an agent that interferes with immune function along with another that targets synoviocytes might achieve the elusive goals of safety and synergy.

References

1. D. M. Lee *et al.*, *Science* **315**, 1006 (2007).
2. G. S. Firestein, *Nature* **423**, 356 (2003).
3. G. S. Firestein, *Arthritis Rheum.* **39**, 1781 (1996).
4. U. Muller-Ladner *et al.*, *Am. J. Pathol.* **149**, 1607 (1996).
5. G. S. Firestein, F. Echeverri, M. Yeo, N. J. Zvaifler, D. R. Green, *Proc. Natl. Acad. Sci. U.S.A.* **94**, 10895 (1997).
6. J. K. Franz *et al.*, *Arthritis Rheum.* **43**, 599 (2000).
7. X. Valencia *et al.*, *J. Exp. Med.* **200**, 1673 (2004).
8. L. Mandik-Nayak, P. M. Allen, *Immunol. Res.* **32**, 5 (2005).
9. Y. Yamanishi *et al.*, *Proc. Natl. Acad. Sci. U.S.A.* **99**, 10025 (2002).

10.1126/science.1139574

PHOTO CREDIT: YAMANISHI ET AL. (9)

Applications of Modern Ferroelectrics

J. F. Scott

Long viewed as a topic in classical physics, ferroelectricity can be described by a quantum mechanical, ab initio theory. Thin-film nanoscale device structures integrated onto Si chips have made inroads into the semiconductor industry. Recent prototype applications include ultrafast switching, cheap room-temperature magnetic-field detectors, piezoelectric nanotubes for microfluidic systems, electrocaloric coolers for computers, phased-array radar, and three-dimensional trenched capacitors for dynamic random-access memories. Terabit-per square-inch ferroelectric arrays of lead zirconate titanate have been reported on Pt nanowire interconnects and nanorings with 5 nanometer diameters. Finally, electron emission from ferroelectrics yields cheap, high-power microwave devices and miniature x-ray and neutron sources.

From their discovery by Valasek in 1920 until about 1945, ferroelectrics were academic curiosities, of little application or practical interest, mostly water-soluble and toxic. They were all hydrogen bonded and were thought to be essential for ferroelectricity. During the war years, this changed, upon the discovery of the robust ferroelectric oxide $BaTiO_3$ (*1*), whose structural simplicity encouraged theoretical work and whose physical properties stimulated engineering advances. Soon ferroelectrics became an "electronic ceramics" industry. Billions of $BaTiO_3$ "condensers" are still made annually at a cost of less than one cent per capacitor, even including expensive Ag-Pd electrodes.

Before 1970, the most exciting challenges in ferroelectrics was modeling ferroelectric phase transitions (*2*) and discovering new ones. There are now 700 ferroelectric materials, many of which are neither hydrogen bonded nor oxides, such as $GeTe$, $SrAlF_4$, or $SbSI$ (*3*, *4*). Because of the high cost of single crystals, devices were limited to bulk ceramics. These were very successful for actuators and piezoelectric transducers as well as for pyroelectric detectors. The application to sonar was especially well funded.

The focus changed after 1984, when thin-film ferroelectrics were developed and first integrated into semiconductor chips (*5*). In 1994, a ferroelectric bypass capacitor for 2.3-GHz operation in mobile digital telephones won the Japan Electronic Industry "Product of the Year" award, with 6 million chips per month in production. The polarization of a typical ferroelectric is reversed in a coercive field $E_c \approx 50$ kV/cm. In a 5-mm bulk device, this is a 5-kV voltage unsuitable for a mobile telephone; however, for submicrometer films it is ~5 V, compatible with integration into most silicon chips. It is in the era of "integrated ferroelectrics" that the renaissance of ferromaterials occurred. The first Review in *Science* of integrated ferroelectrics (*5*) was published in 1989, and the first text on ferroelectric memories (*6*) was published in 2000 and then translated into Japanese (2003) and Chinese (2004), reflecting the locations of greatest current activity. Ferroelectricity is now treated by a quantum mechanical Berry-phase formalism, such an ab initio approach is compatible with magnetic calculations in the same materials, stimulating a renaissance in magnetoelectric materials that are simultaneously ferromagnetic and ferroelectric (*7*, *8*).

There are several directions for ferroelectrics research: substrate-film interfaces and high-strain states, Janus size effects, nanotubes and nanowires, electrocaloric devices, ferroelectric random access memories (FeRAMs), dynamic random access memory (DRAM) capacitors, electron emitters, weak magnetic field sensors, magnetoelectrics, and self-assembly. Ferroelectric liquid crystals (smectic thin films) probably have a more mature commercial product line (spatial light modulators and video camera view-finders) but are not included in this Review.

A ferroelectric is generally defined as a material whose intrinsic lattice polarization P can be reversed through the application of an external electric field E that is greater than the coercive field E_c. Ferroelectrics usually have a phase-transition temperature T_0 above which they are paraelectric, but some do not (they melt first). All ferroelectrics are also pyroelectric, and all pyroelectrics are piezoelectric. (The reverse is not true: Pyroelectric ZnO is not ferroelectric.) Hence, ferroelectrics cannot have a center of symmetry, nor can they be glasses. In their paraelectric phase, some are centrosymmetric ($BaTiO_3$) and some are not (KH_2PO_4). Most ferroelectric thin films are not oxides, though these are most studied because of their robustness and practical applications. Not all solids with electrical hysteresis are ferroelectric. Electrets have an extrinsic hysteresis due to mobile charged defects, and pn-junctions also exhibit hysteresis. Measuring polarization P is often contaminated with artifacts. For perfectly insulating capacitors, apply E and measure switched charge $Q = 2PA$, where P is polarization and A is electrode area. However, in semiconducting or lossy dielectrics ($Q = \sigma AEt/d < 2PA$, where σ is conductivity, t is time, and V is voltage across thickness d. Real charge is ejected. Losses result in a cigar-shaped loop that is unrelated to ferroelectricity. Although one looks for flat, saturated hysteresis curves, these can be artifacts also, resulting from saturated amplifiers. dP/dE in a hysteresis curve cannot be perfectly flat; that would imply an unphysical dielectric constant of zero.

Ferroelectric Nanostructures

There are two research and development (R&D) thrusts in nanoferroelectrics. First, are there physical phenomena such as crystallographic phases or domain structures that are stable only at these sizes? Second, are the nanoscale device properties qualitatively different? One might examine ferroelectric quantum dots and confinement energies, direct electron tunneling, unusual phases resulting from substrate-interface strain, and transport properties of semiconducting ferroelectrics. Typical oxide ferroelectrics are wide-gap semiconductors with $E_g \approx 3.5$ to 4.1 eV and both electronic and hole conduction. Most are p-type as grown. Electron mobilities are low (0.1 to 3.0 cm^2/Vs); hole mobilities (e.g., oxygen vacancies) are about 10^{-12} cm^2/Vs, and effective masses are high ($m^* = 5.0$ to 6.7 m_e). Lead zirconate-titanate (PZT), strontium bismuth tantalate (SBT), and bismuth titanate (BIT) are switching-device favorites (*9*), and barium strontium titanate (BST) is used for nonswitching applications.

Exactly 60 years ago, Kittel published a paper (*10*) showing that 180° magnetic domains exhibit stripe widths w that are proportional to the square root of the crystal thickness d: $w^2 = ad$, where a expresses a balance between domain wall energy and surface energy. More recently, Catalan *et al.* (*11*) and Lukyanchuk *et al.* (*12*) have shown that $w^2 = adT$, where T is the domain wall thickness and $a = [2\pi^3 |21\zeta(3)|] |\chi(z)\chi(z)^{1/2} \approx 3.455 \chi(z)\chi(0)|^{1/2}$, where $\chi(x,y,z)$ are the susceptibilities and $\zeta(3)$ is the Riemann zeta function of power 3. This dimensionless equation is universal, applying equally to magnets and ferroelectrics (Fig. 1A).

The Kay-Dunn Law similarly describes the coercive field $E_c = bd^{-2/3}$ and coercive voltage $V_c = bd^{1/3}$. Both of these laws hold from macroscopic millimeter thickness d down to about 2 nm. Thus, surprisingly much of the behavior of nanoferroelectric domains can be derived from bulk classical physics. Domains are usually studied in flat planes, but some three-dimensional (3D) nanodomains are shown in Fig. 1B. Domain switching in submicrometer ferroelectrics is rate-limited by nucleation rather than by domain wall velocities, unlike bulk, and can be <280 ps.

Figure 1, C and D, shows nanostructures in thin ceramic films. Figure 1C shows nanotubes and Fig. 1D shows a 0.3 terabit/inch^2 (Tb/in^2) nanoarray of Pt nanowires per PZT (1 Tb in^2 = 1600 Tb/m^2). In Fig. 2, more complex nanodevice structures are shown. Figure 2A is a magnetoelectric composite electron micrograph

Centre for Ferroics, Earth Sciences Department, University of Cambridge, Cambridge CB2 3EQ, UK. E-mail: jsco99@esc.cam.ac.uk

(3), and Fig. 2B shows nanowriting of patterns with an atomic force microscopy (AFM) tip (14).

Terabit ferroelectric memories are not quite a reality. The state-of-the-art hard-wired device is a 0.3 Tb in^2 PZT array (15) on Pt nanowires encased in mesoporous Al_2O_3. These unregistered 30-nm-diameter capacitors switch a reliable 2000 electrons per bit, and fully registered alumina pores are available. Figure 2 shows nanoferroelectrics fabricated as composites (Fig. 2A), from AFM writing (Fig. 2B), and by focused ion beam (FIB) (Fig. 2, C and D). Scientists in Belfast have fabricated complicated 3D nanostructures, including 16-, FIB-cut free standing microrings (Fig. 2C), and a 5-nm-inside-diameter PZT nanotube (Fig. 2D), solution-deposited within a pore of mesoporous Si (17). Using synchrotron sources (Fig. 2A), one can study the domain structure of such very thin films. The 2004 32 megabit (Mb) FeRAMs from Samsung (PZT) or Matsushita (SBT) are still ahead of the commercial magnetic random access memory (MRAM) development (4-Mb MRAM from Freescale Q3 July 2006), and Samsung now has a 64-Mb FeRAM. A more advanced ferroelectric-gate field-effect transistor (FeFET) offers nondestructive read operation, but short retention times have thus far precluded commercial products.

Symetrix and Matsushita Electronics Corporation (MEC) have produced SBT FeRAMs with breakdown of 1.5 MV cm for the semiconductor 45-nm node (DRAM half-pitch, 2010 target). FeRAMs are produced at 25,000 on each 8-inch Si wafer, with 6 million per month shipped for applications such as Japanese Railroad "smart" fare cards. Ramtron and Fujitsu are at 0.35-μm strap-cell PZT design. MEC has produced 500 million units of SBT thin-film integrated ferroelectrics (chip-on, including nonvolatile BST-on-GaAs capacitors) and is at 0.13-μm stacked 4-level-metal design. The Symetrix 5-ns access-time "Transnor" cell is the first nonvolatile cache memory. On 15 December 2006, Fujitsu announced production of a Mn-doped $BiFeO_3$ memory for the 65-nm node.

Self-Patterning

The two basic ways of fabricating nanoferroelectric devices are "top down" (submicrometer lithography) and "bottom up" (self-assembly). The development of mesoporous Si, Al_2O_3, GaN, and GaAs has presented experimentalists with templates for the latter, and other techniques for coating nanowires have developed. Self-assembly of nanoelectrodes on ferroelectric films (18) (Fig. 3B) is based on the model of Andreev that such islands would repel each other through their mutual strain interactions with the substrate. Complete registration that is satisfactory for commercial RAM memory devices can be achieved through deposition with inert spacers, such as submicrometer silicon spheres.

True finite-size depolarization effects were once thought incorrectly to occur at dimensions slightly less than 100 nm. In nanospheres of $BaTiO_3$, the outside shell is cubic (paraelectric) and the interior is (19) tetragonal and ferroelectric (thus resembling a M&M candy). As diameter is reduced, the nanosphere is all cubic and not ferroelectric, but this is not a surface chemistry effect and not a finite size effect. Real finite size effects may occur for diameters that are very small.

Most readers are familiar with carbon nanotubes. These are generally good conductors, either metallic or semiconducting. By comparison, ferroelectric nanotubes are fairly good insulators. When a voltage is applied to them, they expand, contract, or bend (piezoelectric). First fabricated by Hernandez in Colorado and Mishina in Moscow, such oxide nanotubes have recently been characterized by Morrison *et al.* (20). Notably, the size distribution of self-assembled nano-islands of PZT in Fig. 3B is not a phase diagram (it is not a system in thermodynamic equilibrium). Figure 3, C to E, shows true phase diagrams for nanoferroelectrics.

The distribution function for fractional percentage of volume of crystallites of volume V has

$$\log(v) = a_0 V + b_0 V^{1/3} + c_0 V^{1/6} \quad (1)$$

assumed, with empirical parameters a_0, b_0, and c_0.

Magnetoelectrics

Crystals whose Hamiltonians contained linear coupling between electric polarization P and

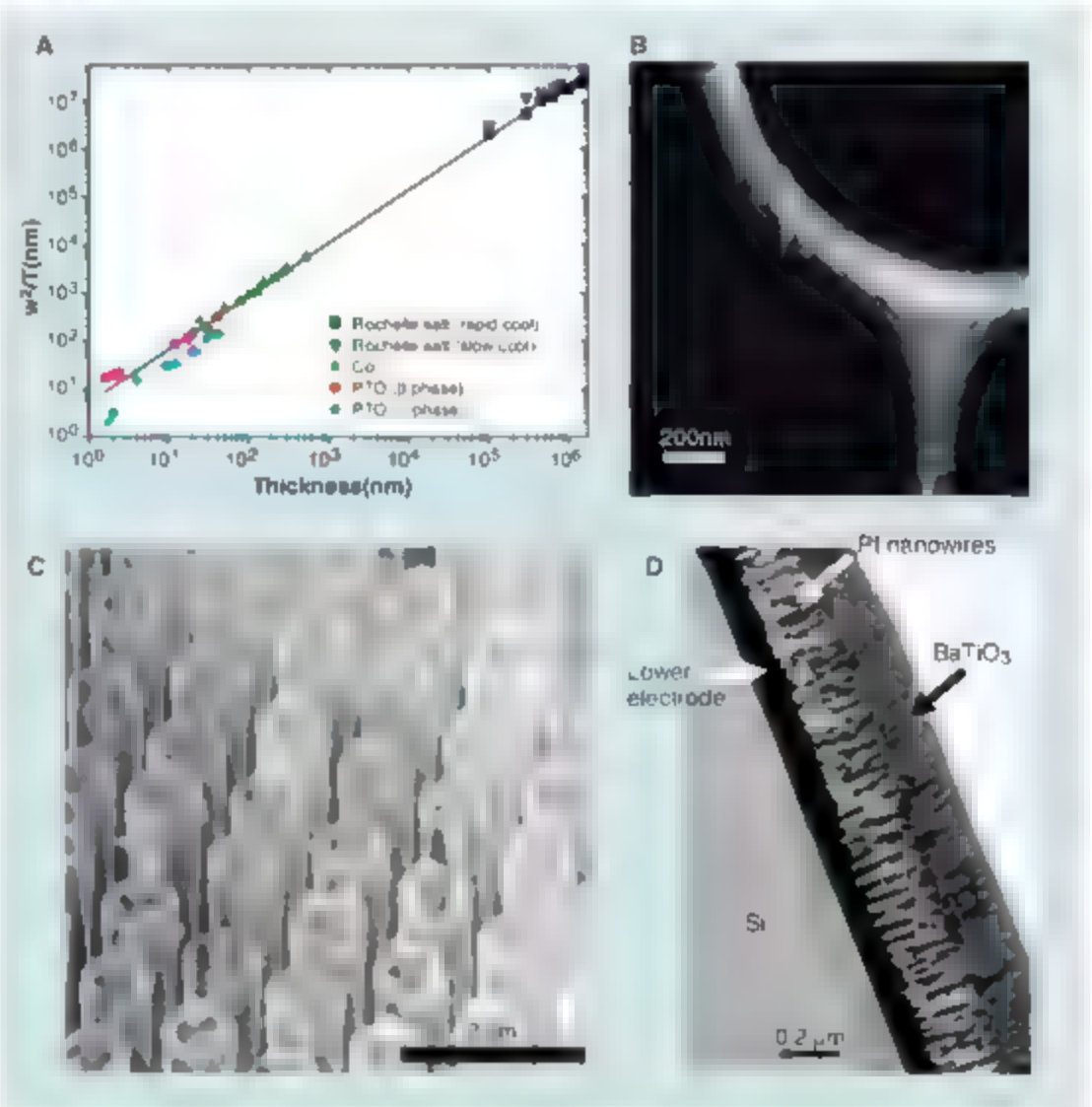

Fig. 1. Nanostructures in thin ceramic films. (**A**) Stripe width squared divided by domain wall thickness t versus film thickness d, showing that w^2/dT is constant in ferroelectrics $PbTiO_3$ and $BaTiO_3$ and in Rochelle Salt and ferromagnet Co, demonstrating a universal law over 6 decades (*49*). (**B**) Plan view micrograph of 3D nanodomains in $BaTiO_3$ (*16*). (**C**) Scanning electron microscopy (SEM) micrograph of $SrBi_2Ta_2O_9$ nanotubes at oblique incidence (*20*). (**D**) SEM cross-sectional view of 0.5 Tb/in^2 nanoarray of Pt nanowires and PZT (*15*).

magnetization M were thought to be discovered in France in the 1920s. However, after subsequent data showed that the effect was forbidden in the materials used, it was believed impossible, causing a hiatus in "magnetoelectricity" R&D until 1957, when Moscow groups resurrected the problem. Dzyaloshinskii predicted magnetoelectricity in Cr_2O_3, rapidly confirmed by Astrov, and also Antiferromagnetism, quickly found by Borovik-Romanov. During the 1970s, a successful search for linear magnetoelectrics ("multiferroics") was led by Hans Schmid in Geneva. The primary device interest was multistate logic elements for computer bit storage that could be greater than binary. As such, it was imperative to show switching of magnetic states with electric fields and of ferroelectric states with magnetic fields and the interaction between magnetic and electric domain walls. This work has had a renaissance since 2000, emphasizing thin films and heterostructures (2–5).

Magnetoelectric studies emphasize two terms, which are expanded as (1)

$$F = \alpha_{ij} E_i M_j + \beta_{ijk} P_i M_j M_k + \ldots \quad (1)$$

where P is electric polarization and M is magnetization. The first term is not time-reversal invariant. Here, the linear magnetoelectric effect due to α_{ij} vanishes above T_N (the Neel temperature) or T_c (the Curie temperature), because $\langle M \rangle = 0$; however, the quadratic term due to β_{ijk} is proportional to $\langle M^2 \rangle$ and remains finite well above T_N (until $T \approx 3T_N$ in magnets such as $BaMnF_4$ with 2D planar spin ordering).

To switch a magnetic domain with an electric field, we need to know how much the magnetization M depends on the polarization P. Does reversing P influence M by 1, 10, or 100%? The idea that ferroelectricity could actually cause ferromagnetism (a 100% effect) was explained by Fox and Scott in 1977 (6) and exemplified with the $BaMF_4$ family (of Mn, Ni, Co, and Fe). By producing a weak ferromagnetic moment (canting of antiferromagnetic spin sublattices M_1 and M_2) parallel to Dzyaloshinskii-Moriya antisymmetric exchange D, reversal of polarization produces this weak ferromagnetism in some crystals (e.g., M_2 in $BaMnF_4$) but not others (e.g., 2 in $BaCoF_4$). The angle of spin canting (3 mrad = 0.17°) in $BaMnF_4$) implies a plausible value for the anisotropic exchange J (comparable with the diagonal α_{ij} in other Mn^{+2} compounds). This Fox-Scott model has recently been discussed for $BaNiF_4$ (7).

There are artifact problems in the recent magnetoelectric literature. Strong magnetoresistance (dielectric constant change with applied magnetic field) can occur merely through Maxwell-Wagner space charge in any magnetoresistive material (8). This is not intrinsic and requires no ferroelectricity at all. The effects can be huge and may explain the 45% anomaly in cadmium (or mercury) chromium spinel (9).

Brown, Bonnerich, and Shiranian showed that the static magnetoelectric susceptibility cannot exceed the product of the electric susceptibility and the magnetic susceptibility ($\alpha_{max} = \chi_e \chi_m$) (10). This is a key result for devices, however, that require interfacial coupling through strain. Strain coupling can be via a substrate or, if all components are nanoscale, via nanoscale proximity. By choosing two materials in a laminated or nanostructured bimorph, one can cause large magnetostriction in, for example, terfenol-D, and large piezoelectricity in, for example, PZT. The result is a prototype room-temperature detector of weak magnetic fields—a low-cost (uncooled) replacement for superconducting quantum interference device (SQUID) detectors. Unfortunately, the "Holy Grail" of multiferroics—a strong (uncanted) ferromagnet that is also ferroelectric at room temperature—has yet to be found. As a memory element, it would permit electric write operations and magnetic read, eliminating the need for a destructive read (and reset) for present-day FeRAMs and making possible fatigue-free memories. This attractive possibility requires a ferroelectric that is also a strong ferromagnet and has low electrical conductivity at ambient temperatures. Although $BiFeO_3$ doped to increase resistivity remains a possible candidate, ferroelectric-ferromagnetic fluorides such as $AgMF_4$ or $KaFeF_4$ merit much more study (5), where A is Sr or Pb and M is any 3d metal (Ti, V, Cr, or Fe); these are apparently ferroelectric with dielectric peaks at $550\ K < T_c < 740\ K$.

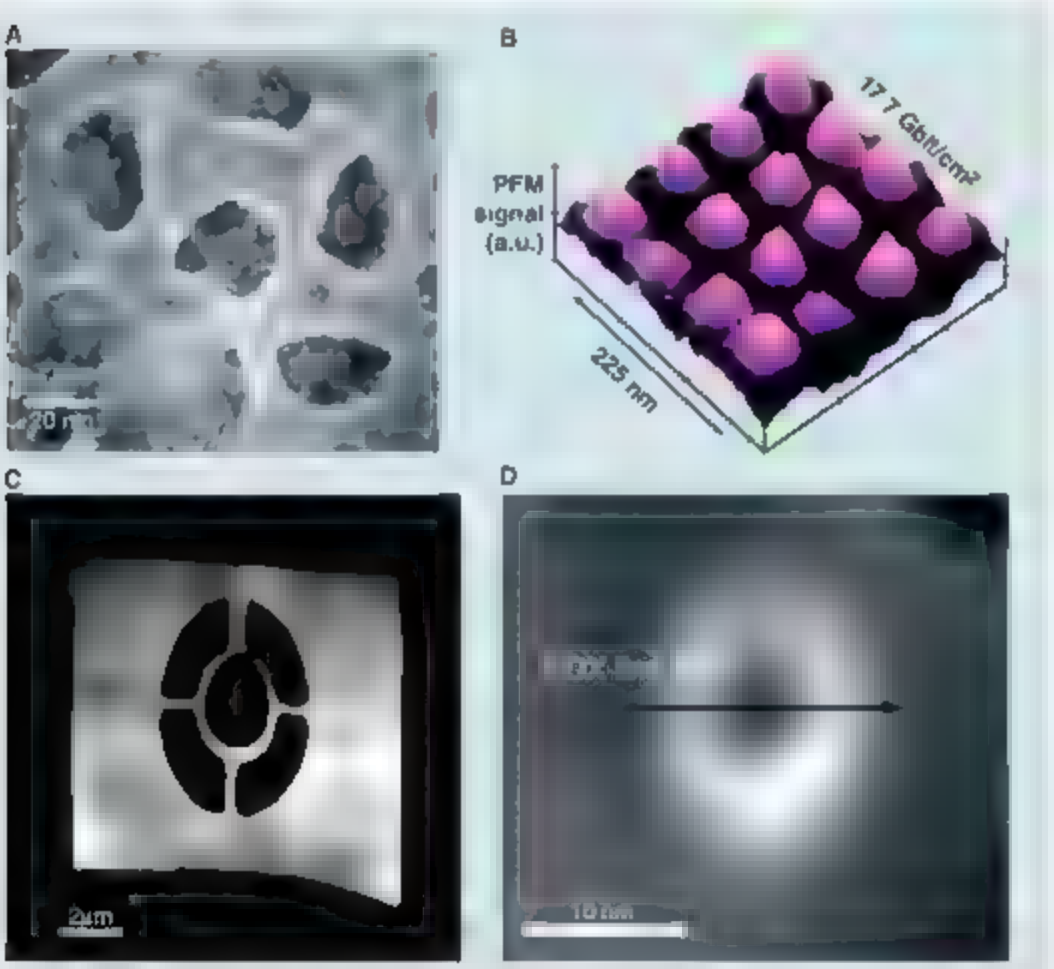

Fig. 2. FIB nanoscience. (**A**) SEM plan view of magnetoelectric composite of $CoFe_2O_4$ pillars in a $BaTiO_3$ matrix (*13*). (**B**) Nanodomains produced by AFM nanowriting on PZT (*50*). a.u., arbitrary units. (**C**) Electron micrograph of nanotoroid of single crystal $BaTiO_3$ (*15*). (**D**) Micrograph of ultra-nanotoroid of PZT inside a mesoporous Al_2O_3 pore (*17*). EDX, energy-dispersive x-ray analysis.

Toroidal and Circular Ordering of Ferroelectric Domains

Most ferroelectrics or antiferroelectrics order with polarizations that are parallel or antiparallel, respectively. However, circular or toroidal patterns can occur. As Kittel first pointed out (*11*), ferromagnets in nanosize diameters will order with four 90° do-

mains, forming a circle. This kind of topological spin defect (vortex) was treated theoretically by Mermin (*24*) in terms of winding numbers and is commonly found in nanomagnets, including both naturally occurring minerals and synthetics (*25*).

A completely different origin for circular or toroidal domains occurs in magnetoelectrics, even in bulk. First analyzed in detail by Ginzburg and by Samulkov, this is reviewed by several authors (*7*, *8*) and subject to a flurry of recent papers, but not yet unambiguously observed. Such a system offers the possibility of very high-density (Tb in^2) memory and storage with electrical write (fast) and magnetic read (no loss).

Ab Initio Theory

A veritable renaissance in theoretical ferroelectricity has resulted from the work by Resta, Vanderbilt, Rabe, Cohen, Krakauer, and others on ab initio models. These replace the semiclassical ball-and-stick model with fully quantum mechanical calculations. They have proved particularly insightful in calculating temperature-strain phase diagrams for thin films (*26*), in which the large strains result from coherent (epitaxial) growth onto substrates with slightly different lattice constants from those of the ferroelectric film (Fig. 3, C to E). The technique suffers from four limitations. (i) It generally works for zero applied field E, although Wu *et al.* have done finite field calculations (*27*). (ii) Most work is at zero temperature. (iii) The number of atoms in the programs are still too small even for nanodevice simulations. (iv) It is not easy to incorporate the semiconducting character of the ferroelectric oxides, nor defects such as oxygen vacancies, nor gradients near the electrode interface.

One of the most important qualitative things to learn from these new models is the kind of phase shown in Fig. 3 from Pertsev and Tagantsev *et al.* (*28*) that a new *ac* phase occurs with polarization lying between the *a* and *c* faces of a pseudo-tetragonal $BaTiO_3$ crystal. If correct, this would have been new physics. Unfortunately, the ab initio work of Vanderbilt (*29*) (Fig. 3E) shows that both models of Pertsev and Tagantsev *et al.* (Fig. 3, C and D) are qualitatively wrong and that there is no *ac* phase (*27*). This shows the power of ab initio modeling over more primitive free-energy theories. Although the Pertsev-Tagantsev model was unsuccessful for barium titanate, a more successful example is $PbTiO_3$, which in bulk has only cubic and tetragonal phases but in thin film exhibits both an orthorhombic phase (*aa*, meaning that polarization P lies at a 45° angle between each of the two *a* axes of the tetragonal precursor phase, along [110]) and a rhombohedral (*r*) phase (P along 111]). For $BaTiO_3$, the initial model predictions were that a new *ac* phase would be stable in thin-film form at zero stress, but ab initio calculations (*29*) showed that this is unlikely. The most extreme experimental result is that $SrTiO_3$, which in bulk is paraelectric down to absolute zero, can be made ferroelectric at room temperature in thin-film form (*30*) with the use of a rather new substrate material: $DyScO_3$.

Interfacial phenomena. Ferroelectrics are more complicated than ferromagnets because electrical measurements must be made on a sandwich consisting of two electrodes and a dielectric. The interface is very complex, involving screening at the metal (*31*) and instabilities at about 3 nm of dielectric thickness (*32*). The resulting leakage current in PZT films can be Schottky-limited or Poole-

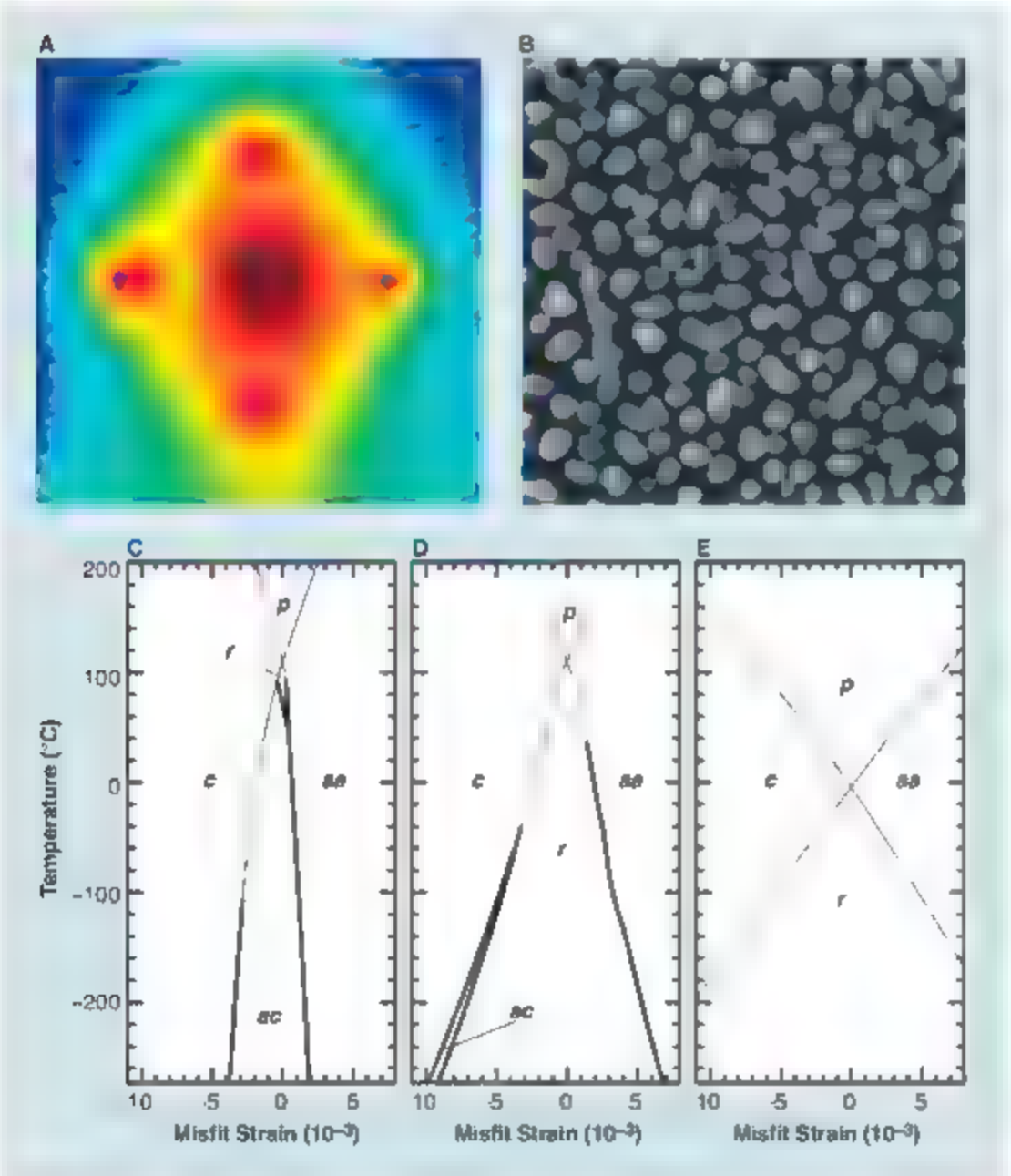

Fig. 3. Storage devices. (**A**) In-plane diffuse x-ray scattering profiles around the $PbTiO_3$ <303> Bragg peak at 549 K (*33*). The four satellite reflections are not Bragg peaks but instead are due to periodic stripe domains in orthogonal directions, and the geometry reveals that polarization P lies out of the plane of the film. (**B**) PZT self-assembly. AFM scan shows PZT on $SrTiO_3$ (*18*). Scale, 2.5 by 2.5 μm from left to right edge and from top to bottom edge of panel. (**C** to **E**) $BaTiO_3$ temperature-stress diagram with ab initio results (*29*) (**E**) and results from Pertsev and Tagantsev in 1998 (*28*) (**C**) and 1999 (*51*) (**D**).

Frenkel and the films can be fully or partially depleted. Interfacial phenomena were recently reviewed (33). Early problems with fatigue partially due to perovskite-pyrochlore conversion (34) in FeRAMs, have been overcome. Replacement of Pt by oxide electrodes to eliminate fatigue spawned a lot of good research, but Matsushita and Panasonic find the metallic Pt electrodes on SBT to be very satisfactory.

Ferroelectric superlattices. Artificially layered ferroelectric superlattices, such as $BaTiO_3$/$SrTiO_3$ can produce enhanced polarization P and dielectric constant ε. $PbTiO_3$/$SrTiO_3$ is particularly notable because it has a near-perfect lattice constant match (35). Surprisingly, the $SrTiO_3$ polarization in $BaTiO_3$/$SrTiO_3$ flops from along [001] to [110] in the relaxed superlattice (36, 37), with strain energy overcoming electrostatics.

A related topic is periodically poled crystals of $LiNbO_3$ and other nonlinear optical materials (38). Here, the superlattice consists not of different chemical compositions such as $BaTiO_3$/$SrTiO_3$, but of P and $\bar{P}$ domains, providing efficient phase matching for nonlinear optics. The quest at present is to produce sub-micrometer wavelengths and to understand domain widths and stability.

Ultrathin single crystals. The use of focused ion beams to cut nanoelectronics was pioneered by Ramesh's group in Maryland for ceramic films but recently extended to single crystals of $BaTiO_3$ (39) to characterize single-crystal capacitors of thickness down to about 65 nm. This has shown that effects of Curie temperature shift or dielectric peak broadening are extrinsic, contrary to the previous conventional wisdom.

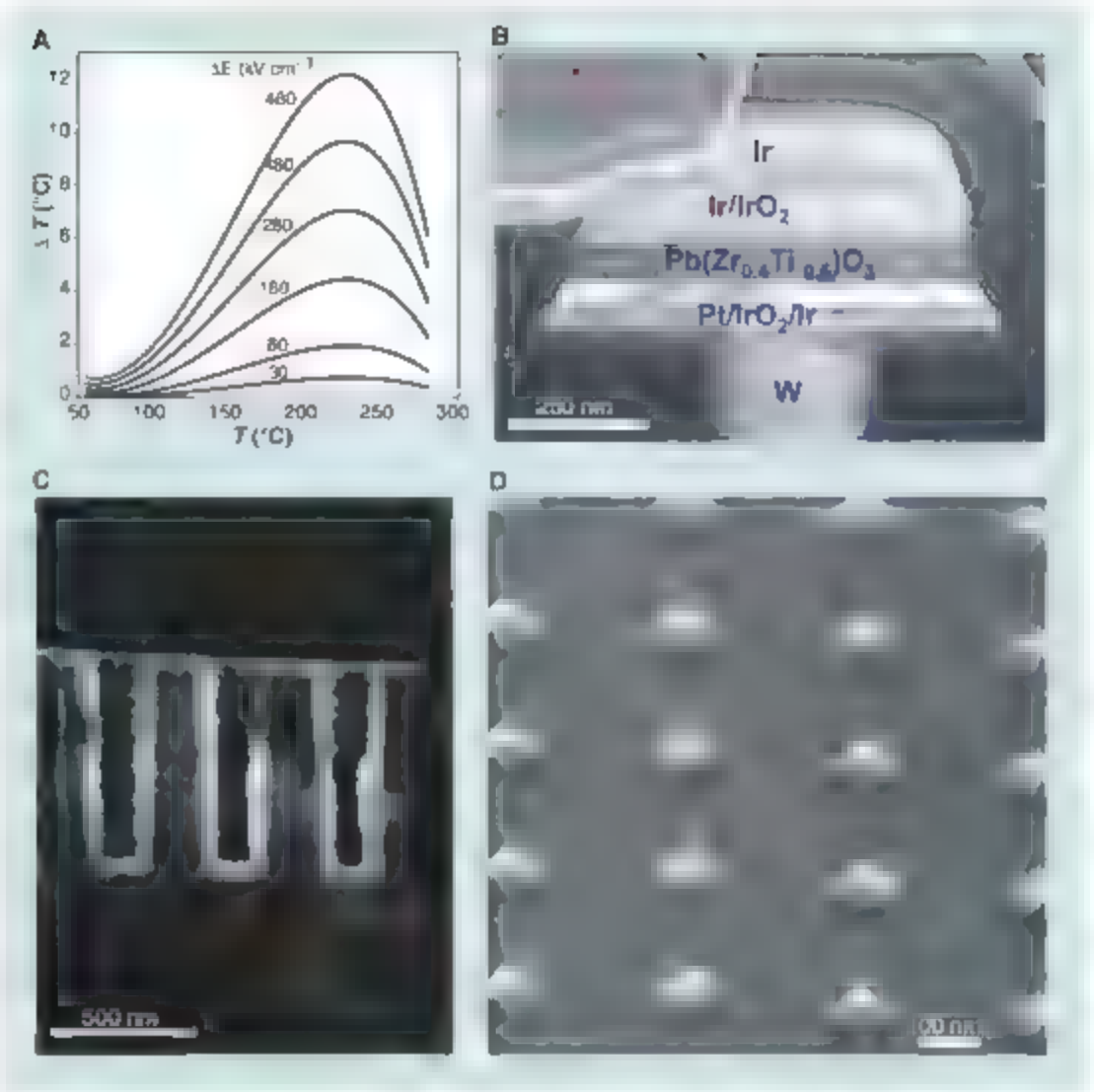

Fig. 4. Applications. (**A**) Electrocaloric effect in PZT (39). (**B**) SEM cross-section of 32 Mb Samsung PZT FeRAM (52). (**C**) SEM cross-section of ruthenium nanotrenches in Si (53). (**D**) e-beam lithography. Plan view shows PZT capacitor array (54).

Short-Term Applications

Electrocaloric cooling for membranes and microelectric motors. The fact that ferroelectrics can be cooled by applying an electric field to them under certain conditions is termed the electrocaloric effect. Using thermodynamics and the idea that entropy decreases under applied field E, one finds a temperature cooling of

$$\Delta T = T_1 - T_2 = \int_{E_1}^{E_2} (T_1/c)(\partial P/\partial T)_E \, dE \quad (3)$$

where c is specific heat at constant polarization P and β is the P^4 coefficient in the free energy $G(T,P) = \alpha(T - T_0)P^2 + \beta P^4$, so that ΔT is often measured from P rather than directly. Electrocaloric cooling was studied in the 1960s to 1970s, but the effect was small in bulk (a few millidegrees per volt). Recently, however, Mischenko *et al.* measured $\Delta T = 12$ K at 25 V across 350 nm lead scandium tantalate (PST) thin films (40), sufficient to design a prototype cooling for computer membranes.

Electron emission from ferroelectrics. The fact that ferroelectrics emit copious electrons from their surfaces during switching has been known for many years. First discovered at Michigan by Rosenblum, this phenomenon was later investigated extensively at Centre European pour la Recherche Nucleaire (CERN) (41) and in France, Poland, Israel, and the United States. The prototype use as a synchronized, pulsed electron source for accelerators was investigated, including the extension to flat channel-plate structures. Currents of tens of amperes have been obtained with synchronized, monoenergetic pulse lengths of 100 ns to 1 μs. These are superior to thermionic cathodes in that they have higher current densities and lifetimes and also have instant turn-on (thermionic cathodes require a warm-up). The ferroelectric electron emitters can be operated in a poor vacuum and require no separate activation process. The commercial drawbacks are that the intense electric fields cause electrode cracking and device failure and that the effect is poorer in thin films than in bulk. Moreover, no unambiguous theoretical model has been accepted for the basic emission process. Microscopic mechanisms remain debatable. Although fields of $E = 10^7$ V/cm are required, this is only 50 V across 50 nm, readily obtainable in good films.

This is an unexploited device area for which commercial development of miniature high-power microwave devices could be made within a few years. Samsung explored in the 1990s the use of this phenomenon for nanolithography (42). Most recently (in 2005), this effect was used by Futerman's group for a kind of cold fusion (43), as a miniaturized source of x-rays and neutrons.

Bias multilayer-electrode capacitors. Barium titanate based ceramic capacitors are a commodity and account for the bulk of all capacitors used in electronics (billions per year). These are

multilayer capacitors with Ag:Pd electrode stacks. Present efforts are to increase high-voltage performance to higher breakdown voltages and to further reduce costs by replacing silver-palladium with base metals, especially nickel. The electrode separation d varies from submicrometer to about 70 μm. Recently Milliken *et al.* have shown (*44*) that the breakdown field varies as the dc thermal model predicts (ignoring transient effects of applied field ramp rate): $E_B = c_1 d^{-1/2}$ for thicknesses above 1 μm, but no theory exists for the submicrometer-spaced devices, for which electrode surface roughness may be the limiting parameter. Progress can be expected in this high-volume commercial area in the next 5 years. No replacement, higher-breakdown devices, and a reliable theory for both Ni-$BaTiO_3$ interfaces and the nonmonotonic dependence of breakdown voltage on the electrode separation d. This has not been a trendy research area in universities, but the financial pay-off is potentially huge. Another major commercial area, not reviewed here, is piezoelectric actuators. Most piezoelectrics are ferroelectric, and new "relaxor" ferroelectrics such as lead magnesium niobate compounds achieve 2% strain, about 10 times that in conventional ferroelectrics. The most valuable application area is fuel injectors for automobile engines.

Phased-array radar. Thin-film ferroelectrics exhibit a large decrease in dielectric constant with application of modest voltages. This suggested that they could be used as the active phase-shift element in phased-array radar, a project studied carefully by researchers at Grumman and TRW in the United States and by Veraldi's group in Leningrad. Unfortunately the dielectric loss tangent in these films remains too large for acceptable insertion losses in such devices, so nothing has been made commercially. A status report was published recently by Miranda *et al.* (*45*).

Future Prospects

Hybrid devices combining piezoelectric nanotubes with carbon nanowires will appear in 2007. Si_3N_4 dielectric capacitor tips on carbon nanotubes exist (*46*), and my group has put PZT tips on a registered array of carbon nanotubes. Commercial ferroelectric cells (up to 64 Mb) in FeRAMs are 0.4 μm (0.12 μm thick) in ceramic form (Samsung; Fig. 4B), 0.35 μm (Fujitsu), and 0.13 to 0.18 μm (Matsushita); thinner samples suffer from tunneling currents but may be useful for 3D DRAMs (Fig. 4C). Single crystals of ~50 to 70 nm and films of ~2 nm are under study, as are piezoelectric 3D nanotubes for microfluidics. Atomizers for insulin inhalers (e.g., Pfizer "Exubera," 2006) require small particles or droplets of uniform diameter, and the U.S. market for diabetes products (190 million cases worldwide) is $25 billion per year. Although microfluidics (including ink-jet printers) favor piezoelectric tubes of micrometer-sized diameters, microelectronics may exploit the smaller 5- to 10-nm-diameter rings and tubes shown here for DRAM trenching, with PZT Pt-nanowire arrays recently giving nearly 1 Tb/in^2 nonvolatile memory arrays. Read-write speeds are already as fast as 200 ps for laboratory devices, but sense amplifier realities and bit-line capacitance limit commercial FeRAMs to about 5-ns access time. e-beam lithography (Fig. 4D) still leads self-assembly techniques for the registration required for commercial random access memories, but self-assembly with high registration will eventually win out. FeRAMs are way ahead of MRAMs, but multiferroic memories with electrical write and magnetic read operations may yet blossom.

References and Notes

1. A. von Hippel, U.S. National Defense Research Committee Report 300 (NDRC, Boston, MA, 1944).
2. M. E. Lines, A. M. Glass, *Principles and Applications of Ferroelectrics and Related Materials* (Clarendon, Oxford, 1977).
3. Hence the fashionable question "Why are there so few magnetic ferroelectrics?" cannot have an answer limited to d^0-orbitals in transition-metal oxides (*47*).
4. Abrahams (*48*) indicates that several families of d-electron transition-metal fluorides are probably ferroelectric ferromagnets.
5. J. F. Scott, C. A. Araujo, *Science* **246**, 1400 (1989).
6. J. F. Scott, *Ferroelectric Memories* (Springer, Heidelberg, Germany, 2000).
7. M. Fiebig, *J. Phys. D* **38**, R123 (2005).
8. W. Eerenstein, N. D. Mathur, J. F. Scott, *Nature* **442**, 759 (2006).
9. C. A. Paz de Araujo, J. D. Cuchiaro, L. D. McMillan, M. C. Scott, J. F. Scott, *Nature* **374**, 627 (1995).
10. C. Kittel, *Phys. Rev.* **70**, 965 (1946).
11. G. Catalan, *Appl. Phys. Lett.* **88**, 102902 (2006).
12. V. A. Stephanovich, I. A. Luk'yanchuk, M. G. Karkut, *Phys. Rev. Lett.* **94**, 047601 (2005).
13. H. Zheng *et al.*, *Science* **303**, 661 (2004).
14. P. Paruch, T. Giamarchi, J.-M. Triscone, *Phys. Rev. Lett.* **94**, 197601 (2005).
15. R. Pollard *et al.*, personal communication.
16. M. M. Saad *et al.*, *IEEE Trans. Ultrason. Ferroelectr. Freq. Control* **53**, 2208 (2006).
17. X. H. Zhu *et al.*, *Appl. Phys. Lett.* **89**, 129913 (2006).
18. M. Dawber, I. Szafraniak, M. Alexe, J. F. Scott, *J. Phys. Condens. Mat.* **15**, 4667 (2003).
19. M. Tanaka, Y. Makino, *Ferroelectr. Lett.* **24**, 13 (1998).
20. F. D. Morrison, L. Ramsay, J. F. Scott, *J. Phys. Condens. Mat.* **15**, L527 (2003).
21. D. L. Fox, J. F. Scott, *J. Phys. C* **10**, L329 (1977).
22. C. Ederer, N. Spaldin, *Phys. Rev. B* **74**, 020401 (2006).
23. J. Heidberger *et al.*, *Nature* **434**, 364 (2005).
24. N. D. Mermin, *Rev. Mod. Phys.* **51**, 591 (1979).
25. R. J. Harrison, R. E. Dunin-Borkowski, A. Putnis, *Proc. Natl. Acad. Sci. U.S.A.* **99**, 16556 (2002).
26. M. Dawber, K. M. Rabe, J. F. Scott, *Rev. Mod. Phys.* **77**, 1083 (2005).
27. X. Wu, D. Vanderbilt, D. R. Hamann, *Phys. Rev. B* **72**, 035105 (2005).
28. N. A. Pertsev, A. G. Zembilgotov, A. K. Tagantsev, *Phys. Rev. Lett.* **80**, 1988 (1998).
29. O. Dieguez, K. M. Rabe, D. Vanderbilt, *Phys. Rev. B* **72**, 144101 (2005).
30. Y. L. Li *et al.*, *Phys. Rev. B* **73**, 184112 (2006).
31. M. Dawber, P. Chandra, P. B. Littlewood, J. F. Scott, *J. Phys. Condens. Mat.* **15**, L393 (2003).
32. J. Junquera, P. Ghosez, *Nature* **422**, 506 (2003).
33. O. Auciello, *J. Appl. Phys.* **100**, 051614 (2006).
34. X. Lou, M. Zhang, S. A. T. Redfern, J. F. Scott, *Phys. Rev. Lett.* **97**, 177601 (2006).
35. M. Dawber *et al.*, *Phys. Rev. Lett.* **95**, 177601 (2005).
36. A. Q. Jiang, J. F. Scott, H. Lu, Z. Chen, *J. Appl. Phys.* **93**, 1180 (2003).
37. K. Johnston, X. Huang, B. Neaton, K. M. Rabe, *Phys. Rev. B* **71**, 100103 (2005).
38. D. Walker *et al.*, *J. Phys. D Appl. Phys.* **38**, A55 (2005).
39. M. M. Saad *et al.*, *J. Phys. Condens. Mat.* **16**, 4451 (2004).
40. A. S. Maschenko, O. Zhang, J. F. Scott, R. W. Whatmore, N. D. Mathur, *Science* **311**, 1270 (2006).
41. H. W. Gundel, *Ferroelectrics* **184**, 89 (1996).
42. D. C. Kim, W. Jo, H. M. Jang, K. Y. Kim, *Integ. Ferroelectr.* **18**, 137 (1997).
43. R. Naranjo, J. K. Glimzewski, S. Putterman, *Nature* **434**, 1115 (2005).
44. A. O. Milliken, A. J. Bell, J. F. Scott, *Appl. Phys. Lett.* in press.
45. A. L. Morales-Cruz *et al.*, *Integ. Ferroelectr.* **77**, 51 (2005).
46. T. Ren *et al.*, *Integ. Ferroelectr.* **14**, 95 (1997).
47. N. Hill, *J. Chem. Phys. B* **104**, 6694 (2000).
48. S. C. Abrahams, *Acta Crystallogr. B* **55**, 494 (1999).
49. G. Catalan, J. F. Scott, A. Schilling, J. M. Gregg, *J. Phys. Condens. Matter* **19**, 022201 (2007).
50. M. Dawber, N. Stucki, C. Lichtensteiger, J.-M. Triscone, personal communication.
51. N. A. Pertsev, A. G. Zembilgotov, A. K. Tagantsev, *Ferroelectrics* **223**, 79 (1999).
52. J. F. Scott, *J. Phys. Condens. Mat.* **18**, R361 (2006).
53. K. Kawano, H. Kosuge, N. Oshima, H. Funakubo, *Electrochem. Sol. St. Lett.* **9**, C175 (2006).
54. M. Alexe, C. Harnagea, D. Hesse, U. Gösele, *Appl. Phys. Lett.* **79**, 242 (2001).

25 July 2006; accepted 1 November 2006
10.1126/science.1129564

Predation Risk Affects Reproductive Physiology and Demography of Elk

Scott Creel,* David Christianson, Stewart Liley, John A. Winnie Jr.

Inducible defenses (changes in morphology or behavior in response to predation or herbivory) reduce an individual's vulnerability to predation but carry costs that select against their expression when predation risk is low. For plants and invertebrates, the costs of inducible defenses have important effects on demography and community structure (*1*). Elk (like most vertebrates) alter their behavior in response to predation risk, and these antipredator responses are analogous to inducible defenses in plants and aquatic invertebrates. Nonetheless, analyses of wolf-elk systems have focused on direct predation, ignoring nonconsumptive effects of antipredator behavior on dynamics (*2*). This is surprising because the effects of changes in elk behavior on plant communities has been discussed extensively [e.g., (*3*)].

Elk behavior responds to the presence of wolves on a spatial scale of several kilometers and a time scale of minutes to days (*4*–*8*). Wolves were reintroduced to the Greater Yellowstone Ecosystem (GYE, United States) in 1995 and 1996, followed by rapid growth and geographic expansion of the wolf population and a concurrent decline in most elk populations (*9*). In the Gallatin Canyon portion of the GYE (*10*), predation risk from wolves varies spatially and temporally (*7*), and elk respond to the presence of wolves by altering patterns of aggregation, habitat selection, vigilance, foraging, and sensitivity to environmental conditions (*4*–*8*). For all of these behaviors, females produce significantly stronger antipredator responses than males (*7*, *8*), and females fall prey to wolves less often than males [in fig. S1, χ^2 = 194.8, degrees of freedom (df) = 2, N = 124, and P < 0.0001]. Here we show that these antipredator responses are associated with costs that can be measured by changes in reproductive physiology and demography.

In the GYE, elk populations mix in the summer but occupy discrete winter ranges with relatively little movement between populations (*8*). Elk-wolf ratios vary substantially across winter ranges (Fig. 1). Elk-wolf ratios are generally low in the center of the ecosystem and high at its edge where wolf culling is common and wolf occupancy is sporadic. We assessed elk reproductive physiology by using enzyme-linked immunosorbent assay (ELISA) to measure progesterone concentrations for 1495 fecal samples from populations on five winter ranges, 2002–2006 (*10*). Across populations and years, mean fecal progesterone concentrations correlated strongly with elk-wolf ratios. Low progesterone values were associated with heavier predation pressure (in Fig. 1A, adjusted correlation (r^2_{adj}) = 0.54, $F_{1,13}$ = 17.6, and P = 0.0011).

The recruitment of calves declined significantly in two of these populations since local recolonization by wolves (*4*, *8*), and progesterone concentrations were correlated with calf recruitment in the subsequent year (in Fig. 1B, r^2_{adj} = 0.32, $F_{1,11}$ = 6.08, and P = 0.032). The lowest observed progesterone concentration was associated with the lowest calf-cow ratio (8 calves per 100 cows), which was the lowest of 20 calf-cow ratios measured for that site over a period of 37 years. The highest progesterone concentrations were associated with calf-cow ratios above 30 (typical of growing populations) and with estimated pregnancy rates near 100% (*10*). Lastly, calf-cow ratios correlate directly with predation pressure (in Fig. 1C, r^2_{adj} = 0.58, $F_{1,11}$ = 12.95, and P = 0.004).

Although correlative, these results suggest that wolf predation has indirect effects on elk dynamics, driven by costs of behavioral defenses that alter reproductive physiology and demography. Recent declines in calf recruitment (*2*, *4*, *8*) are not well explained by density dependence, because these populations have recently been stable or declining. We have previously found that local winter severity is not a good predictor of recent shifts in elk demography and dynamics, and winters were locally mild over all years of this study (*8*). Lastly, data from radiotagged elk calves on the Gallatin Canyon site showed that none were killed by wolves in their first summer and fall (N = 30 calves, 13 mortalities). A larger sample of radiotagged calves on Northern Range of the GYE also showed little wolf predation on calves before their first winter (*11*). Together these studies detected very few rates of direct wolf predation on calves before early-winter calf:cow estimates.

The benefit of antipredator behavior is a decreased risk of predation, and this is incorporated automatically into measures of the direct rate of predation. In contrast, most analyses of vertebrate predator-prey dynamics do not account for the costs of antipredator behavior. Without consideration of the indirect effects of predation, it is likely that decreased reproduction would be mistaken for bottom-up limitation by resources. Our data show that the reproductive costs of antipredator behavior can be large, with important consequences for prey dynamics.

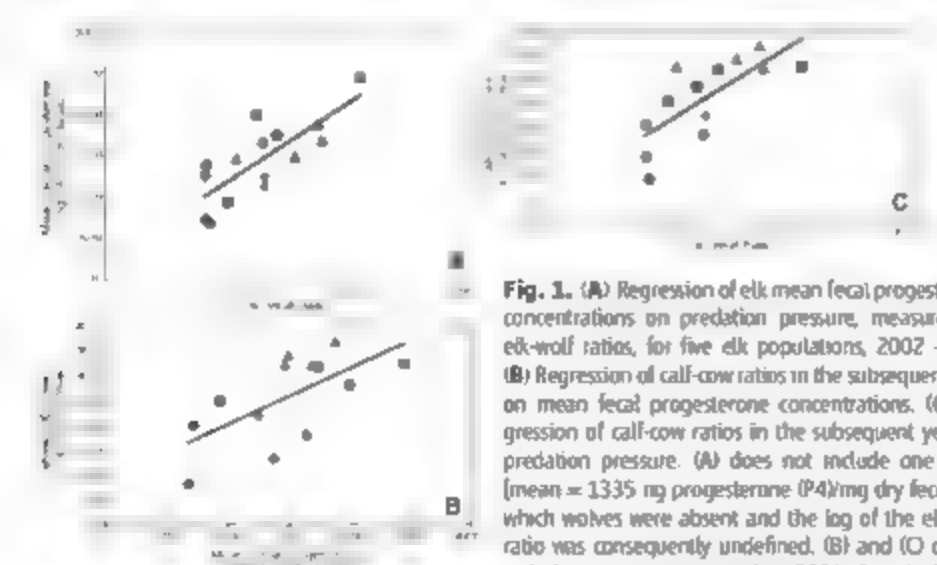

Fig. 1. (**A**) Regression of elk mean fecal progesterone concentrations on predation pressure, measured by elk-wolf ratios, for five elk populations, 2002–2006. (**B**) Regression of calf-cow ratios in the subsequent year on mean fecal progesterone concentrations. (**C**) Regression of calf-cow ratios in the subsequent year on predation pressure. (**A**) does not include one point [mean = 1335 ng progesterone (P4)/mg dry feces] for which wolves were absent and the log of the elk-wolf ratio was consequently undefined. (**B**) and (**C**) do not include two points sampled in 2006, for which subsequent calf-cow ratios are not known. Data point shapes denote different elk winter ranges within the GYE.

References and Notes

1. R. Tollrian, C. D. Harvell, in *The Ecology and Evolution of Inducible Defenses*, R. Tollrian, C. D. Harvell, Eds. (Princeton Univ. Press, Princeton, NJ, 1999), chap. 17, pp. 306–321.
2. N. Varley, M. S. Boyce, *Ecol. Model.* **193**, 315 (2006).
3. M. Hebblewhite, D. Pletscher, P. C. Paquet, *Can. J. Zool.* [illegible].
4. P. J. White, R. A. Garrott, *Biol. Conserv.* **125**, 141 (2005).
5. W. J. Ripple, E. J. Larsen, R. A. Renkin, D. W. Smith, *Biol. Conserv.* **102**, 227 (2001).
6. J. Wyman, D. Christianson, B. Maxwell, S. Creel, *Behav. Ecol. Sociobiol.* **61**, 277 (2006).
7. S. Creel, J. Winnie, *Anim. Behav.* **69**, 1181 (2005).
8. S. Creel, J. Winnie, B. Maxwell, K. L. Hamlin, M. Creel, *Ecology* **86**, 3387 (2005).
9. D. W. Smith, R. O. Peterson, D. B. Houston, *Bioscience* **53**, 330 (2003).
10. Materials and methods are available on *Science* Online.
11. S. M. Barber, L. D. Mech, P. J. White, *Yellowstone Sci.* **13**, 37 (2005).

12. We thank K. Hamlin and C. Jourdonnais for aerial count data and assistance with collection of fecal pellets, R. Garrott and P. J. White for samples used to validate the ELISA, and E. Bonar for assistance in the lab. Supported by NSF grant DBI-0238369 and the Montana Department of Fish, Wildlife and Parks.

Supporting Online Material

www.sciencemag.org/cgi/content/full/315/5814/960/DC1
Materials and Methods
Fig. S1
References

4 October 2006; accepted 4 December 2006
10.1126/science.1135918

Department of Ecology, Montana State University, 310 Lewis Hall, Bozeman, MT 59717, USA.

*To whom correspondence should be addressed. E-mail: screel@montana.edu

Pattern Separation in the Dentate Gyrus and CA3 of the Hippocampus

Jill K. Leutgeb, Stefan Leutgeb, May-Britt Moser, Edvard I. Moser*

Theoretical models have long pointed to the dentate gyrus as a possible source of neuronal pattern separation. In agreement with predictions from these models, we show that minimal changes in the shape of the environment in which rats are exploring can substantially alter correlated activity patterns among place-modulated granule cells in the dentate gyrus. When the environments are made more different, new cell populations are recruited in CA3 but not in the dentate gyrus. These results imply a dual mechanism for pattern separation in which signals from the entorhinal cortex can be decorrelated both by changes in coincidence patterns in the dentate gyrus and by recruitment of nonoverlapping cell assemblies in CA3.

The ability to form distinct representations of highly similar experiences is thought to depend on a pattern separation process by which cortical inputs are decorrelated before they are stored in the hippocampus (*1*–*3*). The hippocampus itself is also thought to perform pattern separation, but the neural circuit mechanisms that could be responsible for such a function remain unclear. In the associative CA3 network (*4*–*6*), pattern separation could be enhanced by the sparse connectivity of the granule cells, which provide the major excitatory input to the CA3 cells, via recurrent collaterals. In CA3 areas on its own it has been suggested to promote new representations in response to weak changes in cortical input because small changes in such input can result in a reversal of similar patterns that were already stored in the network (*pattern completion*) (*2*, *3*, *5*). Yet, for patterns of stored discrete representations would remain stored, the existence of an additional layer upstream of CA3 with small differences between incoming signals could be important before the input is essential for the associative network. The dentate gyrus is well-suited to serve such a function (*2*, *3*). On the basis of anatomical and physiological data (*7*–*11*), it has been suggested that in the dentate gyrus, input from the entorhinal cortex is expressed onto a more extensive layer of sparsely firing granule cells, enabling each granule cell to carry only a small and limited fraction of the total input (*2*). It is also because of the low level of firing of the granule cell population (*12*–*14*) and the sparse connections between the granule cells and the pyramidal cells in CA3 (*15*), the segregation of incoming inputs from the cortex might be relatively independent of the inputs of the CA3 network. Encouraged by the idea that the dentate gyrus is perfect separator can be tested experimentally by the ability of dentate neurons to discriminate small differences in cortical input patterns. In both the dentate gyrus and the CA areas, the principal cells have spatial receptive fields, i.e., they discharge only when the animal is in particular places (*13*, *16*, *17*). In the CA areas, pattern separation is expressed in place cells as a substantial reorganization of the collective firing pattern ("remapping") that is induced when sensory or motivational inputs to the network exceed a certain difference threshold (*18*–*25*). To establish whether a similar ability to distinguish overlapping input patterns is expressed in the dentate gyrus, we compared the configurations of representations in the dentate gyrus and CA3 under conditions where sensory input patterns were made progressively more different.

Six rats were trained to run for a food reward in different enclosures, during which spikes were recorded from multiple granule cells in CA3 and dentate gyrus (see fig. S1 and table S1) (*26*). Most of the animals were tested in a familiar environment. Was the number of cells was lower in the dentate gyrus than in CA3 (*25*), which confirmed previous indications of sparse firing in the granule cell population (*13*, *14*), but among those neurons that were active, the peak firing rates were similar in the two hippocampal regions ($t = 0.95$, $df = 94$, not significant).

Centre for the Biology of Memory, Norwegian University of Science and Technology, 7489 Trondheim, Norway

*To whom correspondence should be addressed. E-mail: edvard.moser@ntnu.no

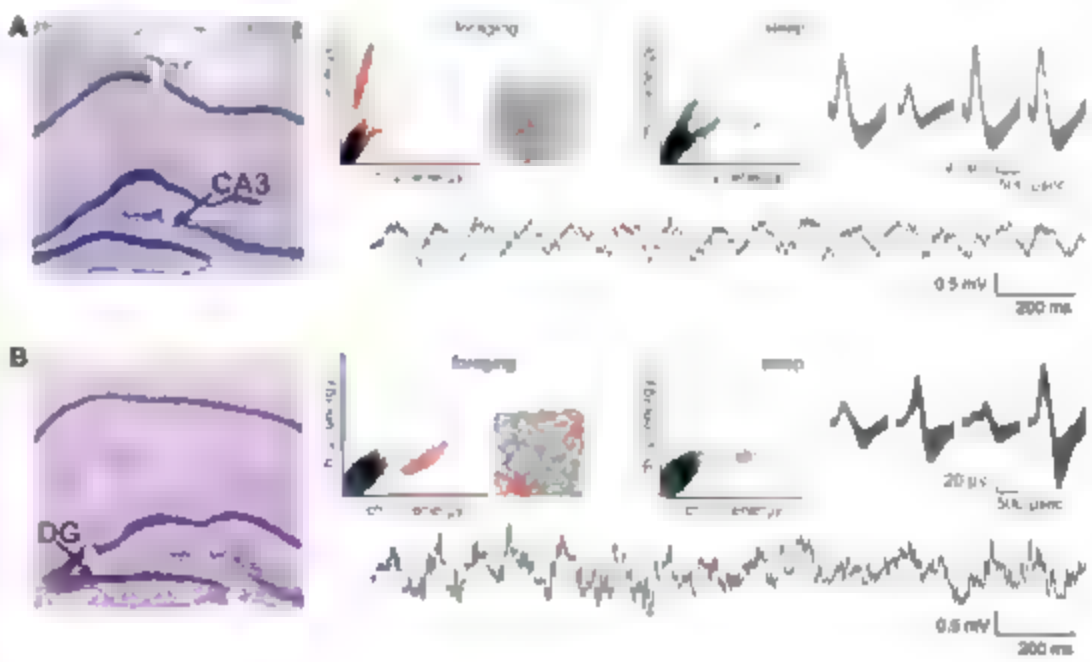

Fig. 1. Place-specific firing in (**A**) the pyramidal layer of CA3, and (**B**) the granule layer of the dentate gyrus. (A) and (B) were recorded simultaneously (rat 11215) (See fig. S1 for additional electrode positions from this animal). (Left) Recording locations (arrow) identified by following the electrode tracts through serial cresyl violet stained sections. DG, dentate gyrus. (Middle) Cluster diagrams showing separation of extracellular action potentials (spikes) when the animal foraged in a square box for 10 min or when the animal slept. Scatterplots show energies (sum of squares) of waveforms on two recording channels. Each dot represents one sampled spike. Distinct spike clusters (each corresponding to one putative cell) are assigned a unique color that is consistent across pairs of cluster diagrams. Insets show the spikes from the red cluster superimposed on the rat's trajectory (gray) during food-motivated running in a square enclosure. (Right) Waveforms of spikes from the red clusters (means ± standard deviation). Bottom of each panel: representative EEG trace from the indicated recording site during foraging in the box.

(table S1)]. The majority of active cells exhibited strongly localized firing in both areas. Of the 71 active CA3 cells, 62 (87.3%) had localized firing: 58 cells had a single field and only 4 had more than one firing field (Fig. 1A). Of the 44 active dentate cells, 41 had firing fields. The majority of these cells fired at multiple places: 6 had single fields, 13 double fields, 8 triple fields, and 4 quadruple fields (Fig. 1B and fig. S2)] (*13*, *14*). The distribution of the multiple firing fields was generally irregular (Fig. 1A).

Pattern separation by changes in spatial and temporal coincidence. We compared the activity of simultaneously recorded principal neurons from dentate gyrus and CA3 during incremental transformation of the recording environment. Five rats were first trained in square and circular versions of a recording enclosure with flexible walls, with the two versions presented in random order (*26*) (fig. S3). The box was then transformed, through a series of five intermediate shapes, from the square shape to the circular shape (n = 57 dentate and 170 CA3 cells) or vice versa (n = 66 dentate and 186 CA3 cells) (Fig. 2A, fig. S4 and S5). The transformation was accompanied by a progressive change in the firing rate distribution of cells in both CA3 and dentate gyrus. In the dentate gyrus, the multiple firing fields of each cell changed noncoherently: some were most active in the initial shape, others in the middle or final shapes (Fig. 2, B and C). These differential changes resulted in a strong decorrelation of the rate distribution of individual cells between even the closest shapes of the morph box. The rate distribution changed independently of the order of the box shapes (fig. S6), unlike the firing rates in CA3, which exhibited hysteresis (Fig. 2B and fig. S6) (*26*).

To examine how the decorrelation of rate change patterns in the dentate gyrus might influence CA3, we estimated the cumulative change in population output from the dentate gyrus as increasing degrees of dissimilarity were introduced between pairs of test boxes

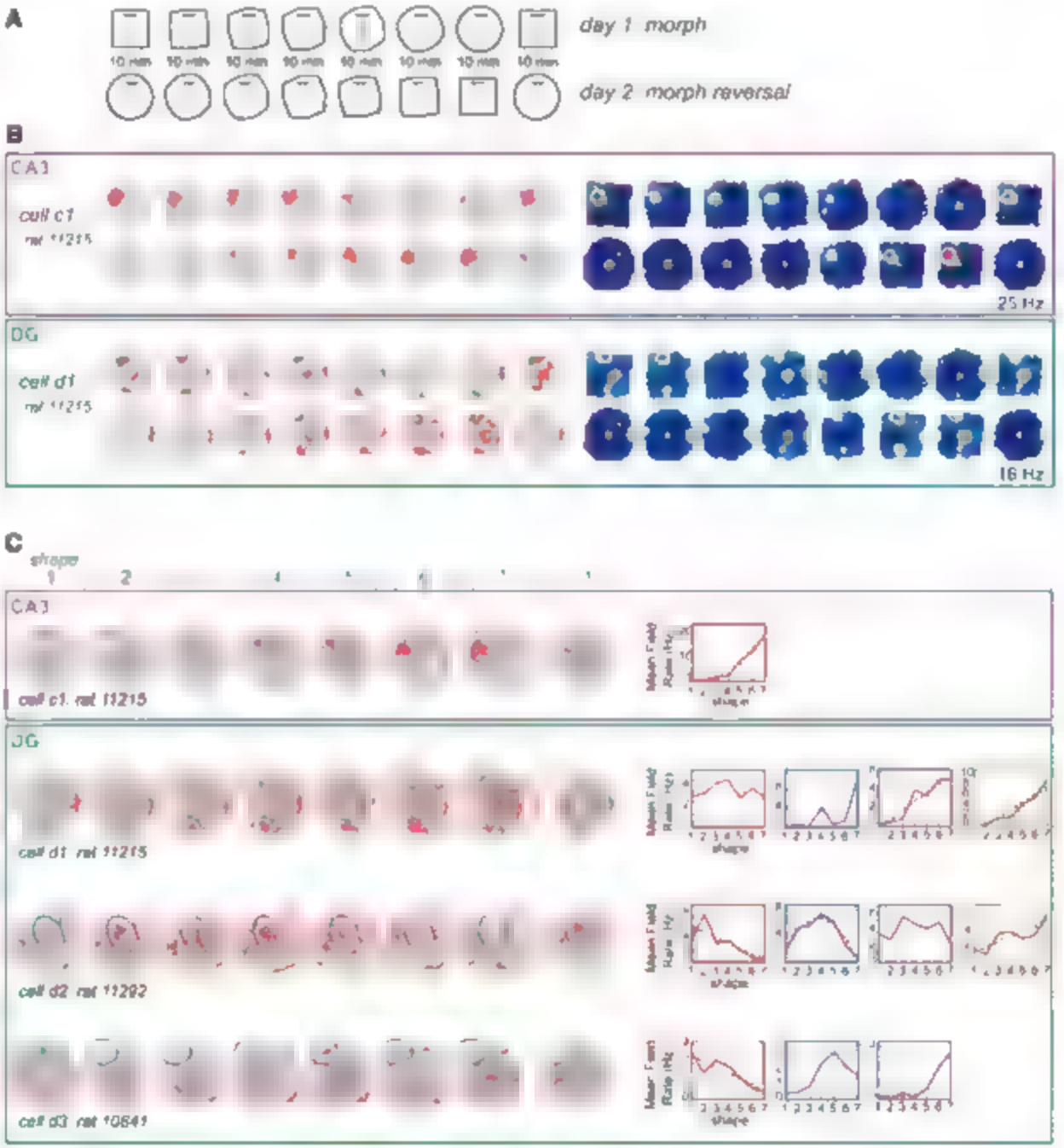

Fig. 2. Changes in rate distribution in CA3 and dentate gyrus during progressive transformation of the recording environment. (**A**) Cells were recorded consecutively in seven shapes of an enclosure with flexible walls, starting with a square (1) and ending with a circle (7), or vice versa. The initial shape was finally repeated (1′). (**B**) Firing fields for a representative CA3 cell (top, purple box) and a simultaneously recorded cell in the dentate gyrus (bottom, green box). (Left) Trajectories with spike locations; (right) corresponding color-coded rate maps. The color scale is from blue (silent) to red (peak rate), with pixels not visited shown in white. The rate maps were scaled to the maximum firing rate within the entire testing sequence. Peak rates are indicated to the right. The complete set of active cells is shown in fig. S4. (**C**) Differential rate changes in individual firing fields of the cell in (B) and two additional representative cells from the dentate gyrus (from different animals). Individual fields of each cell are outlined in different, but consistent, colors throughout the morph sequence. (Right) Line diagrams for the mean firing rate (red curve) in each individual firing field (box outlines have the same color as the corresponding firing fields). The rates were fitted to sigmoid, linear or quadratic functions. Curve fits are only shown when significant (in black). The best fit was linear for 30 fields, sigmoidal for 21 fields, and quadratic for 8 fields (n = 122).

Composite population vectors were constructed for each box by stacking the rate maps of all cells into a three-dimensional matrix with the two spatial dimensions discretized along the x and y axes and cell identity represented on the z axis (Fig. 3A). For each pair of environments, the firing rates of the active cells were correlated for each spatial bin shared by the two box shapes. Population activity in the dentate gyrus was highly sensitive to small changes in the shape of the environment (Fig. 3A). The smallest difference gave a highly significant decrease in the correlation of the population vectors for the dentate gyrus (0.75 ± 0.01 for shape 1 versus 2 and 0.87 ± 0.004 for shape 1 versus 1′; mean correlation ± SEM; $t = 15.1$, $P < 0.001$). A similar decrease was not observed in CA3, where the population vector correlations for neighboring shapes and identical shapes were about the same (0.92 ± 0.004 and 0.92 ± 0.003, respectively; $t = 1.96$, n.s.). As the shapes became more different, the correlations decreased in both hippocampal subfields, but the decrease was initially more pronounced in the dentate gyrus (Fig. 3A). The advance of the dentate gyrus disappeared toward the end of the morph sequence. Because the impact of decorrelation processes in the dentate gyrus is likely to be constrained by the limited convergence of granule cells on CA3 neurons (*15*, *27*), we asked whether a similar distinction between adjacent shapes would be possible with sparser inputs. The change in spatial population vectors in the dentate gyrus was thus calculated after subsampling from the recorded cell population. Small changes in box shape (1 versus 2) led to a similar drop in correlation even when the cell sample was reduced to less than 30 (Fig. 3B and fig. S7).

The differentiation of the spatial rate maps could be improved by decorrelation in the temporal domain (*28*). For each pair of simultaneously recorded cells, we thus determined the rate of coincident firing within time windows of 30 ms, 150 ms, and 300 ms (*25*). The coincidence rates, averaged across cell pairs, were compared for successive shapes of the morph sequence by dividing the rates by each other, giving a coactivity ratio. The coactivity ratio decreased across morph trials and, in the dentate gyrus, dropped significantly even between adjacent shapes (Fig. 3C and fig. S8). The decrease between shapes 1 and 2 was significant for all three time windows ($t > 2.14$, $P < 0.05$). For larger shape differences, the dissimilarity reached the level of a shuffled distribution (0 in Fig. 3C). Cell pairs in CA3 were more correlated than cell pairs with one cell from the dentate gyrus and one from CA3 (fig. S8).

We next asked whether the change in the representation of the environment in the dentate gyrus bears any qualitative similarity to remapping processes in the CA fields. In place cells in CA3, and to some extent in CA1, remapping

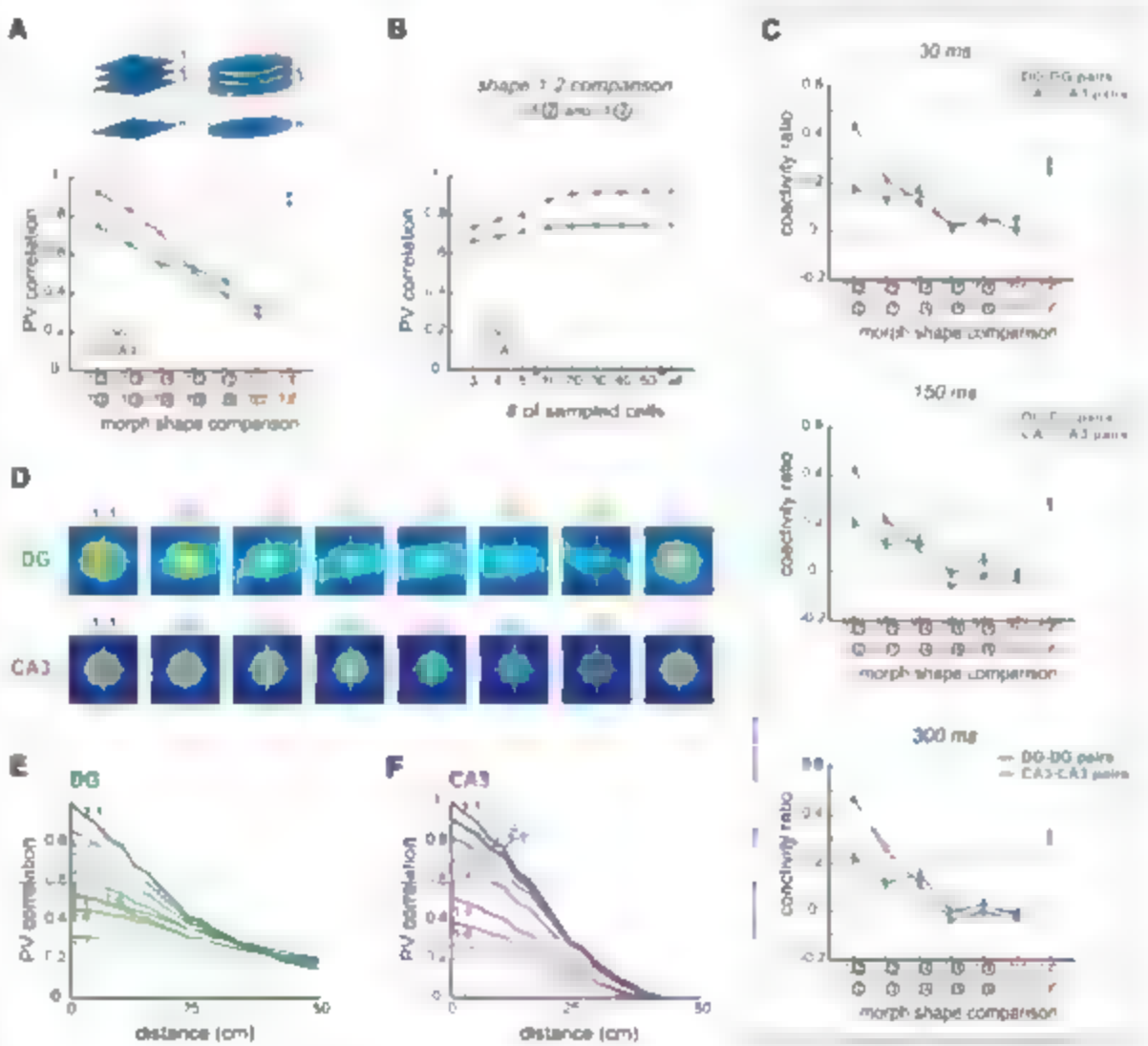

Fig. 3. Quantitative assessment of spatial and temporal coincidence reduction in the dentate gyrus. (**A**) (Top) Procedure for calculating population vector correlations. The rates of all CA3 or dentate cells were stacked into 256 population vectors (PVs), one for each of the 5 cm by 5 cm bins that were shared between the morph square and the morph circle. The correlation between the population vectors was computed for each pair of pixels. (Bottom) Mean population vector correlations for pairs of increasingly divergent morph shapes. Unlike the population output from CA3, population vectors in the dentate gyrus showed dissimilarities already at the smallest change of the box configuration, shape 1 versus 2). (Gray stippled lines highlight the difference between this comparison and repeated recordings in shape 1.) (**B**) Population vector correlations after random subsampling from the recorded cell sample. Subsets of cells were chosen from either dentate gyrus or CA3, and correlation coefficients were calculated as in (A). Corresponding data points in (A) and (B) are circled in red. (**C**) Change in temporal correlation of cell pairs as a function of difference between morph shapes. The degree of change across morph shapes was expressed as the ratio, for each cell pair, of coactive spikes in one environment divided by coactive spikes in the other, within three time windows as noted. The ratio is averaged and linearly transformed such that randomly shuffled cell pairs have a ratio of 0. Symbols as in (A). (**D**) Color-coded spatial cross-correlation matrices for composite rate maps, one for each pair of morph shapes. The scale is from red (+1) to blue (≤0); yellow corresponds to 0.5 to 0.7. (**E** and **F**) Line diagrams showing cross-correlations as a function of distance from the center of the cross-correlogram for pairs of trials with increasing dissimilarity in box shape [one line for each pair (E), dentate gyrus; (F), CA3].

occurs as a complete change in both firing fields and firing rates ("global remapping") or as a selective change in firing rates within a fixed set of firing locations ("rate remapping") (*24*, *29*). In the present study, the CA3 neurons exhibited consistent rate remapping throughout the morph sequence (*26*), whereas cells from the dentate gyrus fired at different locations in the most different shapes of the box (Fig. 2B). Yet, the redistribution of the firing locations was non-random. In all individual fields of a dentate neuron, firing increased and decreased gradually across multiple trials, sometimes throughout the entire morph sequence (Fig. 2C). To estimate the extent to which the place code was retained, as in the CA3 cells, we cross-correlated the composite rate maps of the dentate cells for each pair of shapes in the morph sequence by shifting the stack from one of the shapes in 5-cm steps along the *x* and *y* axes. This resulted in a map of the average similarity of the population vectors, at various offsets of one stack relative to the other. A central peak was observed for all pairs of shapes, but the peak decreased progressively as the shapes became more different (Fig. 3, D to F), which suggested that the rate distribution was altered smoothly, as during rate remapping in CA3 (*26*). Even the smallest shape change caused a decrease in the central peak in the dentate gyrus (see also Fig. 3A).

The expression of a coactivity-based pattern separation process in the dentate gyrus raises the question of whether the underlying computations take place locally in the dentate gyrus or are mediated from afferent regions. If the dentate gyrus contributes actively to pattern separation, its sensitivity to small changes in input patterns should be substantially larger than in the entorhinal cortex, which mediates the majority of cortical inputs to this area. We tested this prediction by recording from three cells in the perforant-path termination area of the hippocampus while the shape of the recording box was increased in small steps (Fig. 4 and fig. S9). These cells had grid-like firing fields similar to those of principal cells in the medial entorhinal cortex (*30*, *31*). The spikes may have originated from intact or punctured axons of grid cells or, perhaps, but less likely, from local interneurons activated by grid cells with identical firing locations. The three cells were recorded simultaneously with cells in the granule cell layer on other tetrodes. None of the grid cells exhibited detectable changes in the rate or the location of firing that could be attributed to the incremental transformation of the recording environment (Fig. 4, B and C, and fig. S9). Whereas the magnitude of the cross-correlation between pairs of environments decreased progressively in the simultaneously recorded dentate neurons, the correlation did not change systematically for the grid cells (Fig. 4C). These recordings confirm observations from studies with larger numbers of entorhinal grid cells, which show that the distribution of activity between firing fields in entorhinal neurons does not change detectably in response to environmental reconfiguration under conditions where hippocampal CA3 assemblies undergo rate remapping (*32*).

Pattern separation by recruitment of new cell assemblies. Although changes in the shape of the morph box strongly influenced the coactivity of already active neurons in the dentate gyrus, there was no replacement of the active subset of the population. In CA3, such replacement can be induced by further increasing the differences between the environments, either by moving the animal to a different recording room (*24*, *33*) or by making the enclosures more dissimilar (*18*, *19*, *23*, *32*). We asked whether such changes, sufficient to induce global remapping in the CA3 (*24*), would cause new and independent cell ensembles to be recruited also in the dentate gyrus. Rats were tested in boxes of different size, color, and shape in three different rooms (Fig. 5, and figs. S10 and S11). As expected, in CA3, statistically independent subpopulations were recruited in a pair of similarly shaped rooms (*33*) (Fig. 5). With a rate threshold of 0.1 Hz, only 20 (18.3%) of the 109 CA3 cells that were active in one room were also active in the second room. Of the 23 active CA3 cells recorded simultaneously with dentate cells, only 3 (13.0%) were active in both rooms (table S1). In striking contrast, 17 out of 20 active neurons in the dentate gyrus (85.0%) were active in both room 1 and room 2, only three (each from a different animal) fired exclusively in one of the environments (Fig. 5). The regional difference

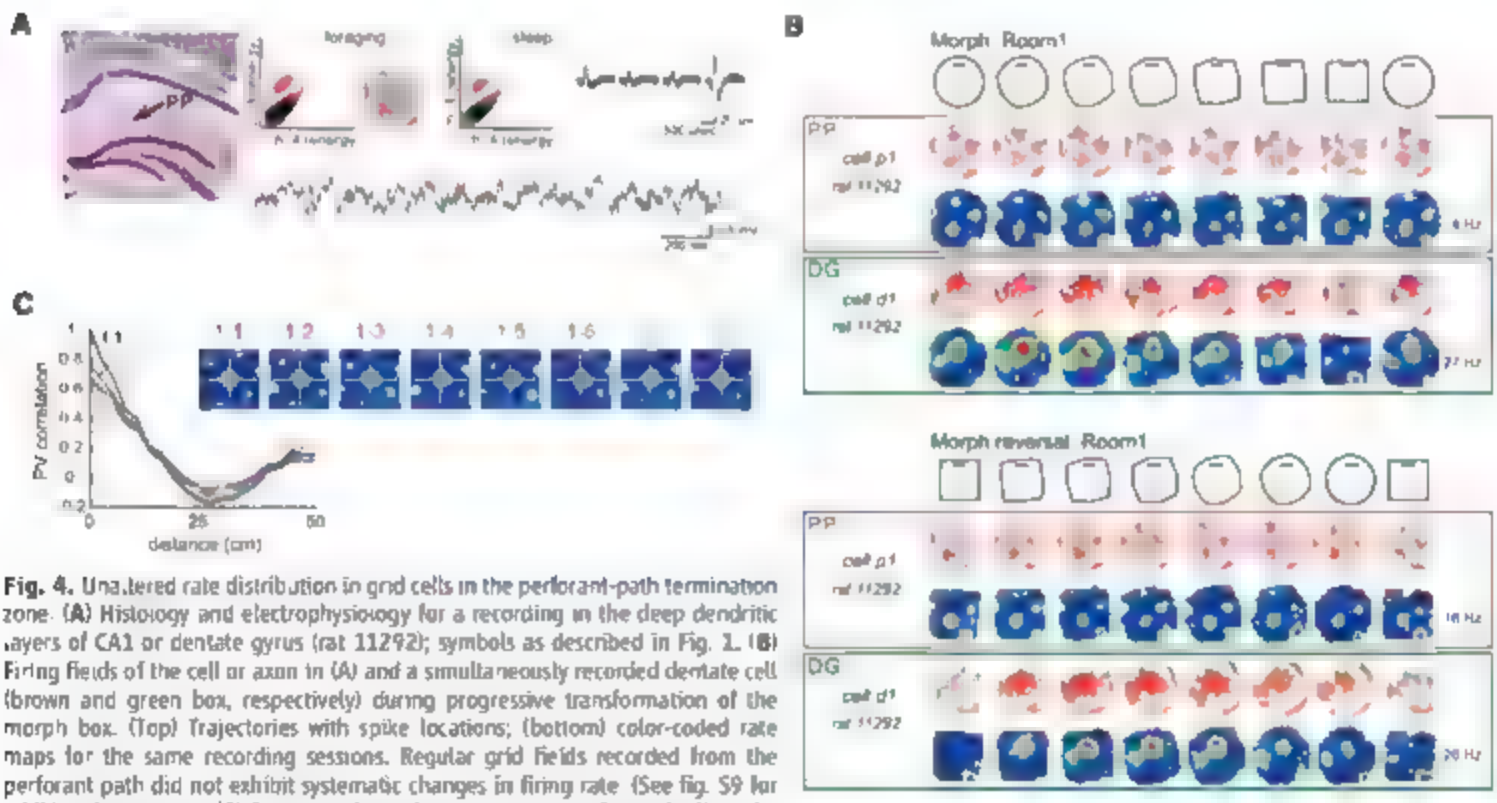

Fig. 4. Unaltered rate distribution in grid cells in the perforant-path termination zone. (**A**) Histology and electrophysiology for a recording in the deep dendritic layers of CA1 or dentate gyrus (rat 11292); symbols as described in Fig. 1. (**B**) Firing fields of the cell or axon in (A) and a simultaneously recorded dentate cell (brown and green box, respectively) during progressive transformation of the morph box. (Top) Trajectories with spike locations; (bottom) color-coded rate maps for the same recording sessions. Regular grid fields recorded from the perforant path did not exhibit systematic changes in firing rate. (See fig. S9 for additional examples.) (**C**) Cross-correlation between rate maps for grid cells in the perforant-path termination zone, calculated as in Fig. 3, D to F, and shown for incremental changes in box shape. The line diagram shows a central peak, as expected if the fields remain stable, and a second peak at 45 to 50 cm from the center, which is a consequence of the similar grid spacing (40 to 60 cm) of the recorded grid cells. PP, perforant path.

was highly significant ($Z = 22.0$, $P < 0.001$ simultaneously recorded cells only). The difference was maintained with a higher rate threshold [0.25 Hz, $Z = 20.8$; $P < 0.00$, (table S1)] and with a rate overlap measure where, for each cell, the mean firing rate in the less-active setting was divided by the mean rate in the more-active setting (3.3) [$t = 4.77$, $P < 0.001$ (fig. S10)]. Moreover, in two animals that were tested in a third room where the enclosure was substantially larger, 11 out of 12 dentate cells that were active in rooms 1 and 2 were active also in room 3 (fig. S 1). Although the active subset was generally the same in all three rooms, there was no similarity in the relative locations of their firing fields. Irrespective of the relative orientation of the stacks, cross-correlation maps for simultaneously recorded dentate neurons in rooms 1 and 2 were flat and the coactivity of cell pairs was not higher than that of a shuffled rate distribution (Fig. 5D and fig. S12).

Discussion. This study provides experimental support for a role of the initial stages of the hippocampus in pattern separation and suggests that a dual set of network mechanisms is involved. These mechanisms, implemented in the dentate gyrus and CA3, are both able, in different ways, to completely orthogonalize the collective firing pattern of cell assemblies in CA3. Together they provide a potential neuronal substrate for disambiguation of overlapping memories in the hippocampus.

Which mechanism is recruited depends on the nature of changes in inputs to the hippocampus. When the environment is only slightly modified, at a fixed spatial location, pattern separation is expressed in dentate gyrus and CA3 as a change in the pattern of correlated activity within the active cell assembly. The divergent direction of the rate changes in the different firing fields of dentate cells accentuates the decorrelation of the ensemble activity, which allows each environment to be represented by a unique rate pattern in a small number of granule cells. Sparse connections between granule cells in the dentate gyrus and pyramidal cells in CA3 (*15*) may allow the disambiguation of firing patterns to be translated to the CA fields, although the smallest differences may be opposed by pattern completion processes in the CA3 network (*5*, *9*). Whether decorrelation in the dentate gyrus is necessary for rate redistribution in the CA fields remains to be determined. When the changes in input to the hippocampus are more substantial, pattern separation is accomplished also by recruitment of a statistically independent cell population in CA3 (*24*, *33*, *34*).

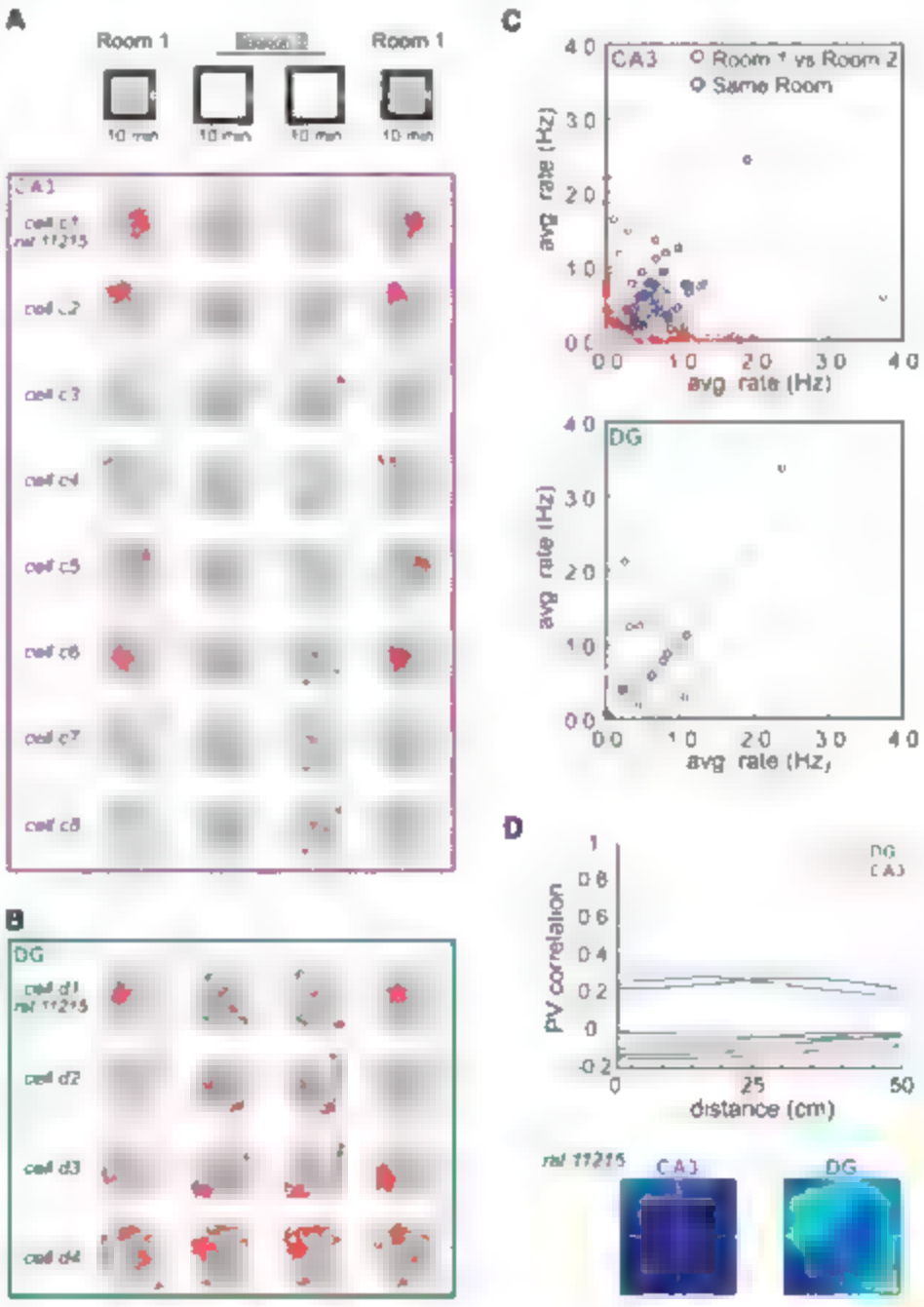

Fig. 5. Recruitment of statistically independent cell ensembles in CA3, but not in dentate gyrus, after large changes in the recording environment. (**A** and **B**) Firing fields of all cells recorded simultaneously from CA3 (A) and the dentate gyrus (B) in an animal exploring boxes of varied size and color in two different rooms (rat 11215). (A) Recording sequence schematic and spatial firing correlates for active cells recorded from tetrodes in CA3. The rat's trajectory (gray) with superimposed spike locations (red dots) is shown for each cell. Silent cells are not shown ($n = 8$). (B) Trajectories with spike locations for dentate cells recorded simultaneously with the CA3 cells in (A). (See fig. S10 for color-coded rate maps.) (**C**) Relation between firing rates on repeated tests in the same room (blue symbols) or in different rooms (red symbols) for the entire sample of cells recorded in CA3 (top) and dentate gyrus (bottom) ($n = 11$ animals, three with simultaneous recordings). Circles of lighter color indicate cells from trials with simultaneous recording in dentate gyrus and CA3; darkened circles indicate cells that were recorded separately in one brain region. (**D**) Cross-correlation between rate maps for cells with firing fields in both rooms, calculated as in Fig. 3D, but with prior rotation of the maps relative to each other and with analyses performed separately for individual animals. The line diagrams show cross-correlations for individual experiments as a function of distance from the center of the cross-correlogram (one line for each animal with more than three simultaneously recorded cells in either subfield). Cross-correlation maps (at the bottom) are only shown for rat 11215 [corresponding to (A) and (B)]. (See fig. S12 for the remaining maps.)

A similar replacement of the active subset is not apparent in the dentate gyrus, which suggests that the change in the CA3 code is triggered by direct projections from entorhinal grid cells to the CA3 (*32*).

Pattern separation in the dentate gyrus is thus different from separation processes in the cerebellum (*10*, *11*), where signals from the brain stem spread out on a layer of granule cells whose cell numbers exceed those of the input layer by a factor of several million. The number of granule cells in the dentate gyrus and pyramidal cells in the CA3 only marginally outnumbers the projection neurons from layer II of the entorhinal cortex (in the rat, 1,000,000, 300,000, and 200,000, respectively (*35*, *35*, *36*)), which suggests that the same hippocampal cells must participate in many representations even when the population activity is sparse (*13*, *14*). In such networks, orthogonalization of coincidence patterns may be more effective.

The decorrelated firing of the dentate cells contrasts with the invariant discharge structure of grid cells upstream in the medial entorhinal cortex (*30*–*32*) (Fig. 4). The reduction in spatio-temporal coincidence could be derived from the lateral entorhinal cortex, but not by a straightforward relay mechanism, because cells in this area do not exhibit reliable place modulation (*37*). It is thus likely that many of the underlying computations take place within the dentate gyrus itself. The use of a dedicated neuronal population for orthogonalization of small differences in input to the CA3 circuits enables the hippocampal network to encode the full variety of experience in a more diversified manner than what could be accomplished with attractor networks alone.

References and Notes

1. B. L. McNaughton, L. Nadel, in *Neuroscience and Connectionist Theory*, M. A. Gluck and D. E. Rumelhart, Eds. (Lawrence Erlbaum, Hillsdale, NJ, 1989), pp. 1–63.
2. A. Treves, E. T. Rolls, *Hippocampus* **2**, 189 (1992).
3. R. C. O'Reilly, J. L. McClelland, *Hippocampus* **4**, 661 (1994).
4. P. E. Gilbert, R. P. Kesner, I. Lee, *Hippocampus* **11**, 626 (2001).
5. D. Marr, *Philos. Trans. R. Soc. Lond. B Biol. Sci.* **262**, 23 (1971).
6. M. E. Hasselmo, E. Schnell, E. Barkai, *J. Neurosci.* **15**, 5249 (1995).
7. M. Tsodyks, *Hippocampus* **9**, 481 (1999).
8. K. Nakazawa *et al.*, *Science* **297**, 211 (2002).
9. I. Lee, D. Yoganarasimha, G. Rao, J. J. Knierim, *Nature* **430**, 456 (2004).
10. D. Marr, *J. Physiol.* **202**, 437 (1969).
11. J. Albus, *Math. Biosci.* **10**, 25 (1971).
12. P. Chadderton, T. W. Margrie, M. Häusser, *Nature* **428**, 856 (2004).
13. M. W. Jung, B. L. McNaughton, *Hippocampus* **3**, 165 (1993).
14. M. K. Chawla *et al.*, *Hippocampus* **15**, 579 (2005).
15. D. G. Amaral, N. Ishizuka, B. Claiborne, *Prog. Brain Res.* **83**, 1 (1990).
16. J. O'Keefe, J. Dostrovsky, *Brain Res.* **34**, 171 (1971).
17. R. U. Muller, J. L. Kubie, J. B. Ranck Jr., *J. Neurosci.* **7**, 1935 (1987).
18. R. U. Muller, J. L. Kubie, *J. Neurosci.* **7**, 1951 (1987).
19. G. J. Quirk, R. U. Muller, J. L. Kubie, *J. Neurosci.* **10**, 2008 (1990).
20. E. Bostock, R. U. Muller, J. L. Kubie, *Hippocampus* **1**, 193 (1991).
21. E. J. Markus *et al.*, *J. Neurosci.* **15**, 7079 (1995).
22. C. Lever, T. Wills, F. Cacucci, N. Burgess, J. O'Keefe, *Nature* **416**, 90 (2002).
23. T. J. Wills, C. Lever, F. Cacucci, N. Burgess, J. O'Keefe, *Science* **308**, 873 (2005).
24. S. Leutgeb *et al.*, *Science* **309**, 619 (2005).
25. Materials and Methods and other supporting material are available on *Science* Online.
26. J. K. Leutgeb *et al.*, *Neuron* **48**, 345 (2005).
27. D. A. Henze, L. Wittner, G. Buzsáki, *Nat. Neurosci.* **5**, 790 (2002).
28. K. D. Harris, J. Csicsvari, H. Hirase, G. Dragoi, G. Buzsáki, *Nature* **424**, 552 (2003).
29. R. M. Hayman, S. Chakraborty, M. I. Anderson, K. J. Jeffery, *Eur. J. Neurosci.* **18**, 2825 (2003).
30. M. Fyhn, S. Molden, M. P. Witter, E. I. Moser, M.-B. Moser, *Science* **305**, 1258 (2004).
31. T. Hafting, M. Fyhn, S. Molden, M.-B. Moser, E. I. Moser, *Nature* **436**, 801 (2005).
32. M. H. Fyhn, T. F. Hafting, A. Treves, E. I. Moser, M.-B. Moser, *Nature*, in press.
33. S. Leutgeb, J. K. Leutgeb, A. Treves, M.-B. Moser, E. I. Moser, *Science* **305**, 1295 (2004).
34. A. Vardanjanova, J. F. Guzowski, *J. Neurosci.* **24**, 6489 (2004).
35. P. R. Rapp, P. S. Deroche, Y. Mao, R. D. Burwell, *Cereb. Cortex* **12**, 1171 (2002).
36. R. D. Boss, G. M. Peterson, W. M. Cowan, *Brain Res.* **338**, 144 (1985).
37. E. L. Hargreaves, G. Rao, I. Lee, J. J. Knierim, *Science* **308**, 1792 (2005).

38. We thank A. Treves, C. A. Barnes, and M. B. Mehta for discussion and A. M. Amundsgård, K. Haugen, K. Jensen, E. Spildrad, R. Skjerpeng, and H. Waade for technical assistance. This work was supported by a Centre of Excellence grant from the Norwegian Research Council.

Supporting Online Material

www.sciencemag.org/cgi/content/full/315/5814/961/DC1
Materials and Methods
SOM Text
Figs. S1 to S12
Tables S1 and S2
References

2 October 2006; accepted 15 December 2006
10.1126/science.1135801

REPORTS

Experimental Realization of Wheeler's Delayed-Choice Gedanken Experiment

Vincent Jacques,[1] E Wu,[1,2] Frederic Grosshans,[1] François Treussart,[1] Philippe Grangier,[1] Alain Aspect,[1] Jean-François Roch[1]*

Wave-particle duality is strikingly illustrated by Wheeler's delayed-choice gedanken experiment, where the configuration of a two-path interferometer is chosen after a single photon pulse has entered it: Either the interferometer is closed (that is, the two paths are recombined) and the interference is observed, or the interferometer remains open and the path followed by the photon is measured. We report an almost ideal realization of that gedanken experiment with single photons, allowing unambiguous which-way measurements. The choice between open and closed configurations, made by a quantum random number generator, is relativistically separated from the entry of the photon into the interferometer.

Young's double-slit experiment, realized with particles sent one at a time through an interferometer, is at the heart of quantum mechanics (*1*). The striking feature is that the phenomenon of interference, interpreted as a wave following two paths simultaneously, is incompatible with our common-sense representation of a particle following one route or the other but not both. Several single-photon interference experiments (*2*–*6*) have confirmed the wave-particle duality of the light field. To understand their meaning, consider the single-photon interference experiment sketched in Fig. 1. In the closed interferometer configuration, a single-photon pulse is split by a first beamsplitter BS_{input} of a Mach-Zehnder interferometer and travels through it until a second beamsplitter BS_{output} recombines the two interfering arms. When the phase shift Φ between the two arms is varied, interference appears as a modulation of the detection probabilities at output ports 1 and 2, respectively, as $\cos^2 \Phi$ and $\sin^2 \Phi$. This result is the one expected for a wave, and as Wheeler pointed out, "[this] is evidence … that each ar-

[1]Laboratoire de Photonique Quantique et Moléculaire, Ecole Normale Supérieure de Cachan, UMR CNRS 8537, 94235 Cachan, France. [2]Key Laboratory of Optical and Magnetic Resonance Spectroscopy, East China Normal University, 200062 Shanghai, China. [3]Laboratoire Charles Fabry de l'Institut d'Optique, Campus Polytechnique, UMR CNRS 8501, 91127 Palaiseau, France.

*To whom correspondence should be addressed. E-mail: roch@physique.ens-cachan.fr

...ving light quantum has arrived by both routes (7). If BS_{output} is removed (the open configuration), each detector D1 or D2 on the output ports is then associated with a given path of the interferometer, and provided one uses true single-photon light pulses, "[either one counter goes off, or the other. Thus the photon has traveled only one route" (7). Such an experiment supports Bohr's statement that the behavior of a quantum system is determined by the type of measurement performed on it (8). Moreover, it is clear that for the two complementary measurements considered here, the corresponding experimental settings are mutually exclusive; that is, BS_{output} cannot be simultaneously present and absent.

In experiments where the choice between the two settings is made long in advance, one could reconcile Bohr's complementarity with Einstein's local conception of the physical reality. Indeed, when the photon enters the interferometer, it could have received some "hidden information" on the chosen experimental configuration and could then adjust its behavior accordingly (9). To rule out that too naive interpretation of quantum mechanical complementarity, Wheeler proposed the "delayed-choice" gedanken experiment in which the choice of which property will be observed is made after the photon has passed BS_{input}: "Thus one decides the photon shall have come by one route or by both routes after it has already done that" (10).

Since Wheeler's proposal, several delayed-choice experiments have been reported (10–15). However, none of them fully followed the original scheme, which required the use of the single-particle quantum state as well as relativistic space-like separation between the choice of interferometer configuration and the entry of the particle into the interferometer. We report the realization of such a delayed-choice experiment in a scheme close to the ideal original proposal (Fig. 1). The choice to insert or remove BS_{output} is randomly decided through the use of a quantum random number generator (QRNG). The QRNG is located close to BS_{output} and is far enough from the input so that no information about the choice can reach the photon before it passes through BS_{input}.

Our single photon source, previously developed for quantum key distribution (16, 17), is based on the pulsed, optically excited photoluminescence of a single nitrogen-vacancy (N-V) color center in a diamond nanocrystal (18). At the single-emitter level, these photoluminescent centers, which can be individually addressed with the use of confocal microscopy (19), have shown unsurpassed efficiency and photostability at room temperature (20, 21). In addition, it is possible to obtain single photons with a well-defined polarization (16, 22).

The delayed-choice scheme is implemented as follows. Linearly polarized single photons are sent by a polarization beamsplitter BS_{input} through an interferometer (length 48 m) with two spatially separated paths associated with orthogonal S and P polarizations (Fig. 2). The movable output beamsplitter BS_{output} consists of the combination of a half-wave plate, a polarization beamsplitter BS, an electro-optical modulator (EOM) with its optical axis oriented at 22.5° from input polarizations, and a Wollaston prism. The two beams of the interferometer, which are spatially separated and orthogonally polarized, are first overlapped by BS but can still be unambiguously identified by their polarization. Then, the choice between the two interferometer configurations, closed or open, is realized with the EOM, which can be switched between two different configurations within 40 ns by means of a homebuilt fast driver (16). Either no voltage is applied to the EOM or its half-wave voltage V_π is applied to it. In the first case, the situation corresponds to the removal of BS_{output} and the two paths remain uncombined (open configuration). Because the original S and P polarizations of the two paths are oriented along prism polarization eigenstates, each "click" of one detector D1 or D2 placed on the output ports is associated with a specific path (path S or path P, respectively). When the V_π voltage is applied, the EOM is equivalent to a half-wave plate that rotates the input polarizations by an angle of 45°. The prism then recombines the two rotated polarizations that have traveled along different optical paths, and interference appears on the two output ports. We then have the closed interferometer configuration (22).

To ensure the relativistic space-like separation between the choice of the interferometer configuration and the passage of the photon at BS_{input}, we configured the EOM switching process to be randomly decided in real time by the QRNG located close to the output of the interferometer (48 m from BS_{input}). The random number is generated by sampling the amplified shot noise of a white-light beam. Shot noise is an intrinsic quantum random process, and its value at a given time cannot be predicted (23). The timing of the experiment ensures the required relativistic space-like separation (22). Then, no information about the interferometer configuration choice can reach the photon before it enters the interferometer.

The single-photon behavior was first tested using the two output detectors feeding single-photon

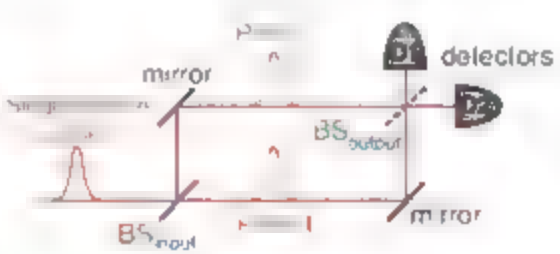

Fig. 1. Wheeler's delayed-choice gedanken experiment proposal. The choice to introduce or remove beamsplitter BS_{output} (closed or open configuration) is made only after the passage of the photon at BS_{input}, so that the photon entering the interferometer "cannot know" which of the two complementary experiments (path difference versus which-way) will be performed at the output.

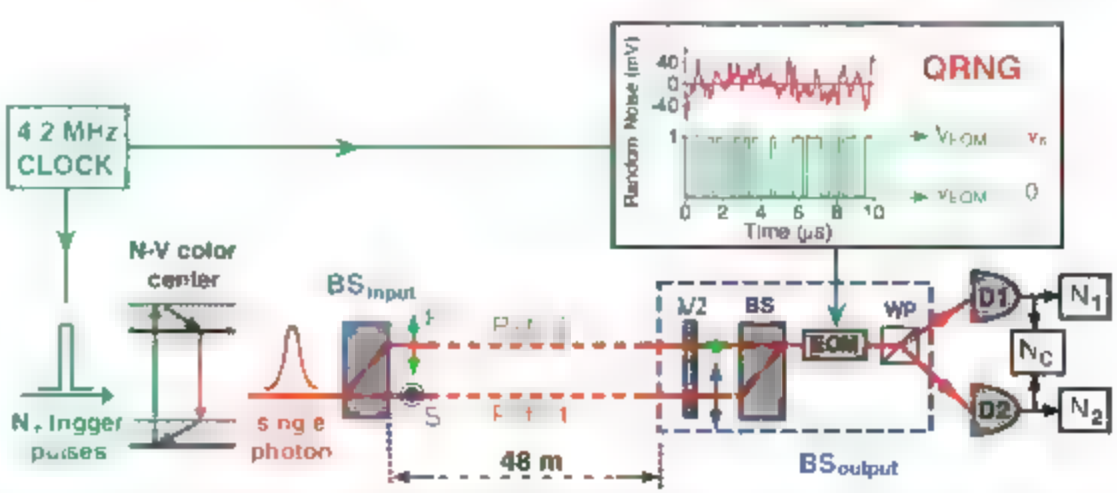

Fig. 2. Experimental realization of Wheeler's gedanken experiment. Single photons emitted by a single N-V color center are sent through a 48-m polarization interferometer, equivalent to a time of flight of about 160 ns. A binary random number 0 or 1, generated by the QRNG, drives the EOM voltage between $V = 0$ and $V = V_\pi$ within 40 ns, after an electronic delay of 80 ns. Two synchronized signals from the clock are used to trigger the single-photon emission and the QRNG. In the laboratory frame of reference, the random choice between the open and the closed configuration is made simultaneously with the entry of the photon into the interferometer. Taking advantage of the fact that the QRNG is located at the output of the interferometer, such timing ensures that the photon enters the future light cone of the random choice when it is at about the middle of the interferometer, long after passing BS_{input}.

coincidence counters with BS_{output} removed (open configuration). We used an approach similar to the one described in (2) and (6). Consider a run corresponding to N_T trigger pulses applied to the emitter, with N_1 counts detected in path 1 of the interferometer by D1, N_2 counts detected in path 2 by D2, and N_C detected coincidences corresponding to joint photodetections on D1 and D2 (Fig. 2). Any description in which light is treated as a classical wave, such as the semiclassical theory with quantized photodetectors (24), predicts that these numbers of counts should obey the inequality

$$\alpha \equiv \frac{N_C N_T}{N_1 N_2} \geq 1 \qquad (1)$$

Violation of this inequality thus gives a quantitative criterion that characterizes nonclassical behavior. For a single-photon wavepacket, quantum optics predicts perfect anticorrelation (i.e., $\alpha = 0$) in agreement with the intuitive image that a single particle cannot be detected simultaneously in the two paths of the interferometer (2). We measured $\alpha = 0.12 \pm 0.01$, hence we are indeed close to the pure single-photon regime. The nonideal value of the α parameter is due to residual background photoluminescence of the diamond sample and to the two-photon Raman scattering line, which both produce uncorrelated photons with Poissonian statistics (6).

With single photon pulses in the open configuration, we expected each detector D1 and D2 to be unambiguously associated with a given path of the interferometer. To test this point, we evaluated the "which-way" information parameter $I = (N_1 - N_2)/(N_1 + N_2)$ (25, 26) by blocking one path (e.g., path 2) and measuring the counting rates at D1 and D2. A value of I higher than 0.99 was measured, limited by detector dark counts and residual imperfections of the optical components. The same value was obtained when the other path was blocked (e.g., path 1). In the open configuration, we thus have an almost ideal which-way measurement.

The delayed-choice experiment itself is performed with the EOM randomly switched for each photon sent into the interferometer, corresponding to a random choice between the open and closed configurations. The phase shift Φ between the two interferometer arms is varied by tilting the second polarization beamsplitter BS′ with a piezoelectric actuator (PZT). For each photon, we recorded the chosen configuration, the detection events, and the PZT position. All raw data were saved in real time and were processed only after a run was completed. For each PZT position, detection events on D1 and D2 corresponding to each configuration were sorted (Fig. 3). In the closed configuration, we observed interference with 0.94 visibility. We attribute the departure from unity to an imperfect overlap of the two interfering beams. In the open configuration, interference totally disappears, as evidenced by the absence of modulation in the two output ports when the phase shift Φ was varied. We checked that in the delayed-choice configuration, parameters α and I kept the same values as measured in the preliminary tests presented above.

Our realization of Wheeler's delayed-choice gedanken experiment demonstrates that the behavior of the photon in the interferometer depends on the choice of the observable that is measured, even when that choice is made at a position and a time such that it is separated from the entrance of the photon into the interferometer by a space-like interval. In Wheeler's words, as no signal traveling at a velocity less than that of light can connect these two events, "we have a strange inversion of the normal order of time. We, now, by moving the mirror in or out have an unavoidable effect on what we have a right to say about the already past history of that photon" (7). Once more, we find that nature behaves in agreement with the predictions of quantum mechanics even in surprising situations where a tension with relativity seems to appear (29).

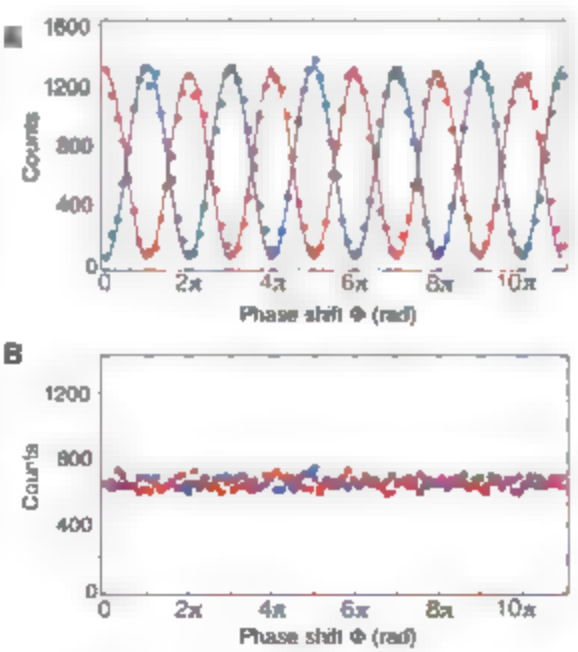

Fig. 3. Results of the delayed-choice experiment. The phase shift Φ (indicated with arbitrary origin) is varied by tilting BS′. Each point, recorded with acquisition time of 1.9 s, corresponds to the detection of about 2600 photons. The detector dark counts, 59 s^{-1} for D1 (blue points) and 70 s^{-1} for D2 (red points), have been subtracted from the data. (**A**) Cases when V_π is applied on the EOM (closed configuration): interference with 94% visibility is obtained. (**B**) Cases when no voltage is applied on the EOM (open configuration): no interference is observed and equal detection probabilities (0.50 ± 0.01) on the two output ports are measured, corresponding to full knowledge of the complementary which-way information (I parameter greater than 99%).

References and Notes

1. R. P. Feynman, R. B. Leighton, M. L. Sands, *Lectures on Physics* (Addison-Wesley, Reading, MA, 1965).
2. P. Grangier, G. Roger, A. Aspect, *Europhys. Lett.* **1**, 173 (1986).
3. F. Jelezko, A. Volkmer, I. Popa, K. K. Rebane, J. Wrachtrup, *Phys. Rev. A* **67**, 041802 (2003).
4. A. Zeilinger, G. Weihs, T. Jennewein, M. Aspelmeyer, *Nature* **433**, 230 (2005).
5. T. Aichele, U. Herzog, M. Scholtz, O. Benson, *AIP Conf. Proc.* **750**, 35 (2005).
6. V. Jacques *et al.*, *Eur. Phys. J. D* **35**, 561 (2005).
7. J. A. Wheeler, in *Quantum Theory and Measurement*, J. A. Wheeler, W. H. Zurek, Eds. (Princeton Univ. Press, Princeton, NJ, 1984), pp. 182–213.
8. N. Bohr, in *Quantum Theory and Measurement*, J. A. Wheeler, W. H. Zurek, Eds. (Princeton Univ. Press, Princeton, NJ, 1984), pp. 9–49.
9. G. Greenstein, A. G. Zajonc, *The Quantum Challenge* (Jones and Bartlett, Sudbury, MA, 1997).
10. C. O. Alley, O. G. Jakubowicz, W. C. Wickes, in *Proceedings of the Second International Symposium on the Foundations of Quantum Mechanics*, H. Narani, Ed. (Physics Society of Japan, Tokyo, 1987), pp. 36–47.
11. T. Hellmuth, H. Walther, A. G. Zajonc, W. Schleich, *Phys. Rev. A* **72**, 2533 (1987).
12. J. Baldzuhn, E. Mohler, W. Martienssen, *Z. Phys. B* **77**, 347 (1989).
13. B. J. Lawson-Daku *et al.*, *Phys. Rev. A* **54**, 5042 (1996).
14. Y.-H. Kim, R. Yu, S. P. Kulik, Y. Shih, M. O. Scully, *Phys. Rev. Lett.* **84**, 1 (2000).
15. T. Kawai *et al.*, *Nucl. Instr. Methods A* **410**, 259 (1998).
16. A. Beveratos *et al.*, *Phys. Rev. Lett.* **89**, 187901 (2002).
17. R. Alléaume *et al.*, *New J. Phys.* **6**, 92 (2004).
18. A. Beveratos *et al.*, *Eur. Phys. J. D* **18**, 191 (2002).
19. A. Gruber *et al.*, *Science* **276**, 2012 (1997).
20. C. Kurtsiefer, S. Mayer, P. Zarda, H. Weinfurter, *Phys. Rev. Lett.* **85**, 290 (2000).
21. R. Brouri, A. Beveratos, J.-P. Poizat, P. Grangier, *Opt. Lett.* **25**, 1294 (2000).
22. See supporting material on *Science* Online.
23. H.-A. Bachor, T. C. Ralph, *A Guide to Experiments in Quantum Optics* (Wiley-VCH, Weinheim, Germany, [illegible]).
24. W. E. Lamb, M. O. Scully, in *Polarization, Matière et Rayonnement, Volume in Honour of A. Kastler* (Presses Universitaires de France, Paris, 1969), pp. 363–369.
25. P. Grangier, thesis, Institut d'Optique et Université Paris 11 (1986); available at http://tel.ccsd.cnrs.fr/tel-00009436.
26. B.-G. Englert, *Phys. Rev. Lett.* **77**, 2154 (1996).
27. S. Dürr, T. Nonn, G. Rempe, *Phys. Rev. Lett.* **81**, 5705 (1998).
28. P. D. Schwendt, P. G. Kwiat, B.-G. Englert, *Phys. Rev. A* **60**, 4285 (1999).
29. J. S. Bell, *Speakable and Unspeakable in Quantum Mechanics* (Cambridge Univ. Press, Cambridge, 1987).

30. We thank A. Clouqueur and A. Villing for the realization of the electronics of the experiment, J.-P. Madrange for the mechanical realization of the interferometer, and A. Browaeys, I. Jacubowiez, and D. Chauvat for their constant help and many enlightening discussions. Supported by Institut Universitaire de France.

Supporting Online Material

www.sciencemag.org/cgi/content/full/315/5814/966/DC1
Materials and Methods
Figs. S1 to S4
References

13 October 2006; accepted 3 January 2007
10.1126/science.1136303

Multiple Energy Scales at a Quantum Critical Point

P. Gegenwart,[1]*† T. Westerkamp,[1] C. Krellner,[1] Y. Tokiwa,[1]‡ S. Paschen,[1]§ C. Geibel,[1] F. Steglich,[1] E. Abrahams,[2] Q. Si[3]*

We report thermodynamic measurements in a magnetic field–driven quantum critical point of a heavy fermion metal, $YbRh_2Si_2$. The data provide evidence for an energy scale in the equilibrium excitation spectrum that is in addition to the one expected from the slow fluctuations of the order parameter. Both energy scales approach zero as the quantum critical point is reached, thereby providing evidence for a new class of quantum criticality.

Quantum criticality encodes the strong fluctuations of matter undergoing a second-order phase transition at zero temperature. It underlies the unusual properties observed in a host of quantum materials. A basic question that remains unsettled concerns its proper theoretical description, which is challenging because the fluctuations are both collective and quantum mechanical. One class of theory, based on the traditional formulation of classical critical phenomena (*1*), considers the fluctuations of a classical variable, Landau's order parameter, in both spatial and temporal dimensions (*2*–*5*). The slowing down of the order-parameter fluctuations accompanies the divergence of a spatial correlation length at each value of the tuning parameter; the equilibrium many-body spectrum contains a single-excitation energy scale, which vanishes at the quantum critical point (QCP) (*6*). An unconventional class of theory (*7*–*9*), by contrast, is inherently quantum mechanical; it explicitly invokes quantum entanglement effects, which are manifested through vanishing energy scales that are in addition to the one associated with the slowing down of order-parameter fluctuations. The nature of quantum criticality can therefore be experimentally elucidated by determining whether single or multiple energy scales vanish as the QCP is reached.

We consider the heavy-fermion metal $YbRh_2Si_2$ (YRS) and show that multiple energy scales vanish as its QCP is approached and, in addition, suggest that critical electronic modes coexist with the slow fluctuations of the magnetic order parameter. A direct way to probe the intrinsic energy scales in the equilibrium spectrum near a QCP is to measure thermodynamic properties. Another approach is to measure the fluctuation spectrum in equilibrium, for example by inelastic neutron scattering experiments. Such equilibrium methods are in contrast to transport experiments, which are influenced by electronic relaxational properties, especially for anisotropic and multiband systems.

As extraction of critical energy scales requires measurements through fine steps of the control parameter, which is nearly impossible for inelastic neutron scattering, we report here measurements of thermodynamic properties of YRS across its magnetic QCP.

We chose to work with the tetragonal heavy fermion compound YRS because it presents a clean and stoichiometric material that is well characterized (*10*). In the absence of an external magnetic field, YRS shows very weak antiferromagnetic (AF) order at $T_N = 70$ mK, with an ordered moment of only $\sim 10^{-3}\,\mu_B$/Yb (*11*). A small magnetic field ($H_{c,ab} = 0.06$ T for the field applied within the easy *ab* plane, and $H_{c,c} = 0.66$ T along the hard *c* axis) suppresses the transition temperature and accesses the QCP (*12*). The ability to use such a small magnetic field to access the QCP makes YRS suited for our purpose: the determination of energy scales requires scanning across the phase transition, and an external magnetic field can be tuned with relative ease and continuously. Hall effect measurements ($I \perp H$) on YRS have shown a large and rapid crossover in the Hall constant at a temperature-dependent magnetic field away from the antiferromagnetic transition. In the zero-temperature limit, this crossover extrapolates to a jump across the QCP, which has been interpreted as a large change of the Fermi surface volume. This represents yet another advantage of measuring the thermodynamic properties in YRS because they can be compared with their transport counterparts.

We measured the isothermal linear magnetostriction $\lambda = \Delta l/l$, where l is the length along the [110] direction within the tetragonal *ab* plane and the magnetic field H is applied along the same direction ($H \perp I$). Figure 1 shows the magnetostriction as a function of the magnetic field, at temperatures ranging from 0.02 K to 0.8 K. For temperatures below 0.075 K, a clear discontinuity is observed when suppressing the AF order by a critical magnetic field. At $T = 0.075$ K, it is seen that, for a small magnetic field, the isothermal magnetostriction linearly depends on the magnetic field, as is the case in typical metals (*13*). Beyond a crossover field, however, there is a change to a high-field region with a different slope. The crossover field decreases as the temperature is reduced.

To understand this crossover, we compare it with the field-dependent isothermal behavior of other thermodynamic and transport quantities. Figure 2A illustrates the similarity of the crossover in the magnetostriction to that seen in the field-dependent isothermal Hall resistivity ρ_H (measured with $H \perp I$). The Hall coefficient was described (*13*) by an empirical crossover

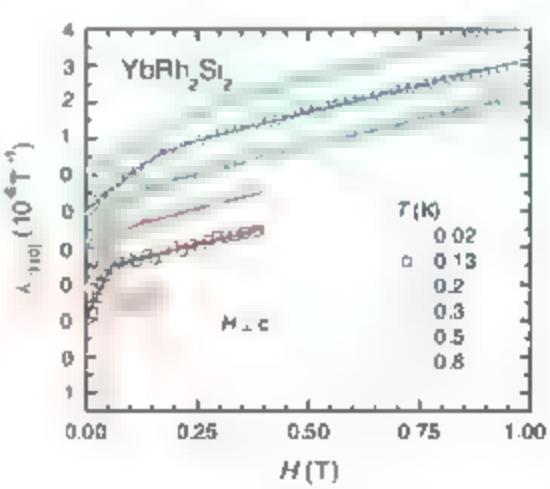

Fig. 1. Magnetic-field dependence of the magnetostriction of $YbRh_2Si_2$. The symbols represent the linear coefficient $\lambda_{[110]} = \Delta l/l$ of l/H (where l is the sample length along the [110] direction within the tetragonal *ab* plane) versus H at various temperatures. Note that $\lambda_{[110]} < 0$ and that the data sets have been shifted by different amounts vertically. The sharp feature in the 0.02 K data corresponds to a discontinuity in λ (as is more clearly seen in the measured length versus H, which shows a change in slope but does not contain any discontinuity), demonstrating the continuous nature of the magnetic transition at the critical field of 0.05 T. Similar behavior is observed at various different temperatures below 0.075 K, for example, at 0.03 K and 0.05 K. The solid lines for $T = 0.13$ K are fits using the integral of the crossover function $f(H,T)$, which reveal a characteristic field scale $H_0(T)$ along which the magnetostriction shows a drastic change in slope.

[1]Max Planck Institute for Chemical Physics of Solids, D-01187 Dresden, Germany. [2]Center for Materials Theory, Department of Physics and Astronomy, Rutgers University, Piscataway, NJ 08855, USA. [3]Department of Physics and Astronomy, Rice University, Houston, TX 77005, USA.

*To whom correspondence should be addressed. E-mail: pgegenw@gwdg.de (P.G.); qmsi@rice.edu (Q.S.)

†Present address: First Physics Institute, University of Goettingen, 37077 Goettingen, Germany.

‡Present address: Los Alamos National Laboratory, Los Alamos, NM 87545, USA.

§Present address: Institute of Solid State Physics, Vienna University of Technology, 1040 Vienna, Austria.

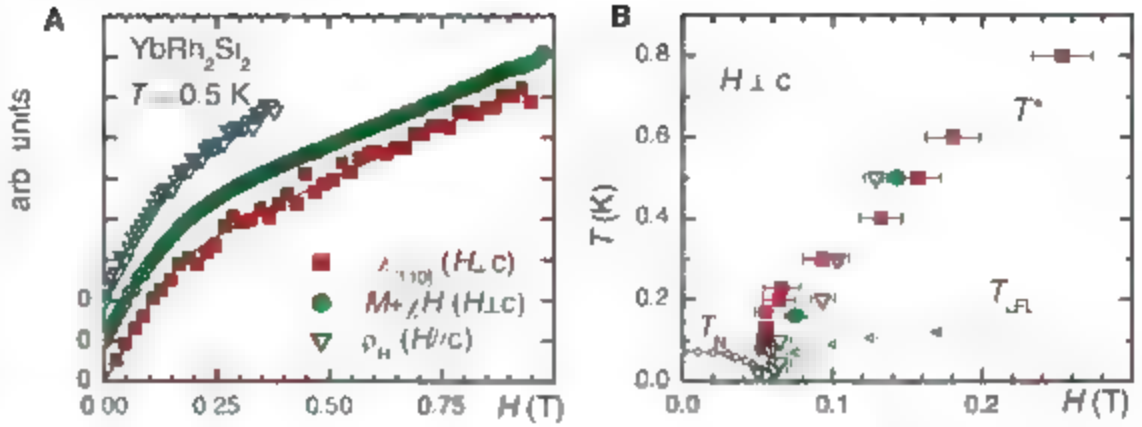

Fig. 2. Energy scales in $YbRh_2Si_2$ determined from thermodynamic, magnetic, and transport measurements. (**A**) The field dependence ($H \perp c$) of the magnetostriction $\lambda_{[110]}$, $\tilde{M} = M + \chi H$ (where $\chi = \partial M/\partial H$), and the Hall resistivity ρ_H for $H \| c$ (for the latter, the field values have been divided by the anisotropy factor 13.2, which corresponds to the ratio of the critical fields in the Hall and magnetostriction measurements), respectively, all at $T = 0.5$ K; similar behavior is observed at other temperatures. For $\lambda_{[110]}(H \perp c)$, the sample has a residual resistivity $\rho_0 = 0.5\ \mu\Omega$ cm and $H_c = 0.05$ T; for $\tilde{M}$ ($H \perp c$), the sample has $\rho_0 = 1.0\ \mu\Omega$ cm and $H_c = 0.06$ T; and for $\rho_H(H \| c)$, the sample has $\rho_0 = 1.0\ \mu\Omega$ cm and $H_c = 0.66$ T. The solid lines correspond to fits using the integral of the same crossover function $f(H,T)$. Each data set has been normalized by its initial slope. For clarity, the three data sets have been shifted by different amounts vertically. This is represented by the three separate zero marks along the vertical axis for the three quantities. $\rho_H - \rho_{H,a}$, where $\rho_{H,a}$ is the anomalous Hall resistivity (*13*), behaves similarly to ρ_H. We analyzed $\tilde{M}(H)$, which is the field derivative of the magnetic free energy contribution ($-M \times H$); fitting $M(H)$ leads to similar conclusions, although the quality of the fit is somewhat poorer because M versus H is not as linear as $\tilde{M}$ at high fields (fig. S2). (**B**) The crossover field scale H_0 as determined from magnetostriction, $\tilde{M}$, and Hall resistivity using the same symbols as in A. It is equivalent to the energy scale $T^*(H)$. The gray diamonds and triangles represent, respectively, the Néel ordering temperature (T_N) and the crossover temperature (T_{FL}), below which the electrical resistivity has the Fermi liquid form $\rho = \rho_0 + AT^2$, as determined from measurements on a single crystal with $\rho_0 = 0.5\ \mu\Omega$ cm and $H_c = 0.05$ T. The solid and dotted lines are guides to the eye; for the latter, data points outside the plotted field regime have also been used. The horizontal error bars represent the fitting error rather than the width of the crossover.

function of the form $f(H,T) = A_2 - (A_2 - A_1)/[1 + (H/H_0(T))^n]$; the crossover field scale $H_0(T)$ is equivalent to an energy scale $T^*(H)$. We have analyzed the magnetostriction data, as well as the existing magnetization data ($H_{\perp c}$) (*15*, *16*), with the same crossover function. No corresponding anomalies can be resolved in the magnetization data for $H \| c$ (*16*), which is almost linear in H. The solid curves in Fig. 1 and Fig. 2A correspond to fits of $\lambda_{[110]}$, $\tilde{M} = M + \chi H$, and the Hall resistivity ρ_H. Figure 2B shows the three sets of $H_0(T)$ obtained from such fits. Their overlap represents a key conclusion of the present work: It suggests that they define one energy scale $T^*(H)$. This scale is seen to be distinct from either the transition temperature (T_N) for the magnetic ordering at $H < H_c$ or the scale (T_{FL}) for the establishment of the Landau Fermi liquid state at $H > H_c$. For all three quantities, the width of the crossover extrapolates to zero at $T = 0$, implying that the differentials of the magnetostriction, magnetization, and Hall resistivity have a jump at the zero-temperature limit (supporting online text).

The results raise the important question of the causal relation between the thermodynamic and electronic transport properties. One might argue (*17*) that the Hall-effect evolution as a function of the magnetic field (*13*) is caused by the Zeeman splitting of the Fermi surface induced by the magnetization (and reflected in the magnetostriction). However, the magnetization only displays a smeared kink, and the corresponding Fermi surface change would at most produce a smeared kink in the evolution of the Hall coefficient, such a kink is too weak compared with the smeared jump seen experimentally. Moreover, along the c axis, even such a smeared kink feature is absent in the magnetization versus the magnetic field. Instead, it is more natural to view the nonanalyticities in both the magnetostriction and magnetization as thermodynamic manifestations of the large Fermi surface jump caused by an f-electron localization.

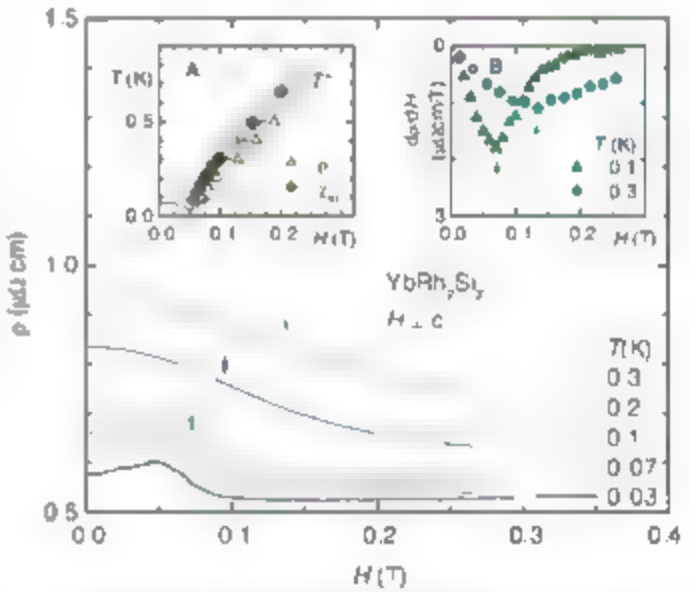

Fig. 3. Longitudinal magnetoresistivity of $YbRh_2Si_2$ at ρ versus H ($H \perp c$) at various temperatures. The maxima in the 0.03 and 0.07 K data indicate the boundary of the AF ordered state [$T_N(H = 0) = 0.075$ K]. The arrows mark the positions of inflection points in $\rho(H)$. The inset A displays the phase diagram, where the gray shaded area represents the range of $H_0(T)$ values shown in Fig. 2B. Open yellow triangles mark the positions of the inflection points in the longitudinal electrical resistivity. The smeared kink behavior in the isothermal M versus H corresponds to a peak in the T dependence of χ. The latter has been observed (*20*); the corresponding peak temperature versus H for a sample with $\rho_0 = 0.5\ \mu\Omega$ cm and $H_c = 0.05$ T is displayed by the dark blue diamonds and found to be consistent with $H_0(T)$. Inset B displays the derivative $d\rho/dH$ versus H at both $T = 0.1$ K and $T = 0.3$ K. Arrows mark the minima, corresponding to the inflection points in $\rho(H)$.

To explore this issue further, we have also studied the longitudinal magnetoresistivity. Figure 3 shows the electrical resistivity ρ as a function of the magnetic field ($H \perp c$) at various temperatures. The broadened steplike decrease, observed at all temperatures, corresponds to the crossover observed in the other properties. Indeed, as shown in inset A, the crossover fields determined from the maxima of the derivative $d\rho/dH$ (inset B) fall on the same $T^*(H)$ line determined from the magnetostriction, magnetization, and Hall effect. In addition, inset B shows that the width of the crossover decreases as the temperature is lowered. A detailed analysis shows that the crossover width goes to zero in the zero-temperature

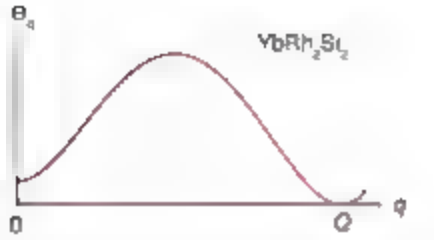

Fig. 4. Sketch of the suggested **q** dependence of the Weiss temperature Θ_q, which enters the magnetic susceptibility. As H reaches H_c, it vanishes at the antiferromagnetic wave vector **Q**, as shown. In addition, Θ_q has a second minimum at **q** = 0. Ferromagnetic fluctuations at **q** = 0 remain important as $\Theta_{q=0}$ goes to zero.

limit (supporting online text), implying a jump in the residual resistivity across the magnetic QCP. This is in accordance with the theoretical expectations (*18*, *19*) associated with an *f*-electron localization transition.

Figure 3, inset A, also shows the temperature scale as a function of field, extracted from the peak in the *T*-dependence of the differential susceptibility $\chi_{dc} = \partial M/\partial H$; the latter, observed earlier (*20*), necessarily accompanies the sharpened kink behavior in the isothermal *M* versus *H*. It is clearly seen that this scale too falls on the same $T^*(H)$ line.

Our results shed light on the overall phase diagram of this clean stoichiometric quantum critical material. Nuclear magnetic resonance (NMR) measurements (*21*), while signaling the dominance of AF fluctuations in the quantum critical regime, have also revealed enhanced ferromagnetic fluctuations. The Korringa ratio $\mathcal{R} = T_1TK^2$ is small—on the order of 0.15—where K is the corresponding ratio for non-interacting electrons. Further evidence for enhanced ferromagnetic fluctuations has come from magnetization measurements (*20*). The Wilson ratio $R_W = \pi k_B^2/(\mu_0\mu_{eff}^2) \times \chi_0/\gamma_0$, with $\mu_{eff} = 1.4\,\mu_B$/Yb (*22*), is strongly enhanced for an extended region of the phase diagram. It is already large (~20) for magnetic fields of a few teslas and further increases as the field is reduced toward H_c. Therefore, it could be tempting to consider the **q** = 0 magnetic fluctuation as the dominant critical fluctuation (*17*), especially because a conventional ferromagnetic QCP would yield a Grüneisen exponent (*23*) of $\Gamma = \nu z = 2/3$, close to what is observed in YRS (*24*). This picture is problematic for a number of reasons, however. First, neither three-dimensional (3D) nor 2D ferromagnetic spin fluctuations can generate the fractional exponent observed in the temperature dependence of the uniform spin susceptibility (*20*). Second, ferromagnetic spin fluctuations would lead to a divergent $1/T_1 (\sim) T^x$, with $x = 1/3$ and $-1/2$ for 3D and 2D cases, respectively) that is in contrast to the observation that $1/T_1$ is approximately constant when the NMR measurement field is extrapolated to the quantum critical regime (*11*). Third, because ferromagnetic spin fluctuations are inefficient in affecting charge transport, this picture contradicts the observation of a nearly *H*-independent ratio A/χ^2 that accompanies a strongly *H*-dependent *A* and χ (*20*). Here, *A* is the coefficient of the T^2 component of the resistivity.

The data presented here show that the uniform magnetization (**q** = 0) depends on the same underlying physics as that for the charge transport. Because the transport is dominated by large **q** fluctuations, the results imply that the **q** = 0 magnetic fluctuations are a part of overall fluctuations in an extended range of wave-vector scales. It is then more natural to assume that the dynamical spin susceptibility at different wave vectors obeys the same form (*8*, *25*) as that observed in another prototypical quantum critical heavy fermion metal, $CeCu_{5.9}Au_{0.1}$: $\chi(\mathbf{q},\omega,T,H) = \chi_{\mathbf{q}-\mathbf{Q}}(T,H) + \chi_{\mathbf{q}-0}(T,H) - \chi_0$. At the QCP, the Weiss field at the antiferromagnetic wave vector ($\mathbf{q} = \mathbf{Q}$) vanishes: $\Theta_{\mathbf{Q}} = 0$. At the same time, and unlike for $CeCu_{5.9}Au_{0.1}$, $\Theta_{q=0}$ is very small in YRS. Based on the saturation scale seen in the temperature dependence of the uniform magnetic susceptibility (*20*) and the NMR Knight shift data (*21*) near H_c, we estimate $\Theta_{q=0}$ to be on the order of 0.3 K (*26*). When **q** moves away from either 0 or **Q**, $\Theta_{\mathbf{q}}$ increases to the order of the Ruderman-Kittel-Kasuya-Yosida (RKKY) interaction or bare Kondo scale [about 25 K for YRS (*10*)], as illustrated in Fig. 4. The enhanced uniform magnetic susceptibility, the concomitant enhanced Wilson ratio (*20*), and the small $S = 1/T_1TK^2$ naturally follow from this picture. Moreover, both $\chi_{q=0}$ and $\chi_{q=Q}$ scale similarly with *H*, and the observation that A/χ^2 is nearly *H*-independent is in fact a manifestation of an *H*-independent A/χ_0^2. All this leads to the conclusion that the origin of the T^* line lies in an electronic slowing down and, for YRS, the strong **q** = 0 fluctuations happen to be a consequence of the latter as well.

We now turn to more detailed theoretical implications of our results. Our measurements establish that the energy scale T^* is associated with the equilibrium many-body spectrum (which alone determines thermodynamics). Moreover, this scale is distinct from the Landau Fermi liquid scale, T_{FL}, because physical quantities manifest rather different behavior across the two scales (supporting online text). Finally, both of these scales vanish at the QCP. These findings contradict the conventional order-parameter fluctuation theory in at least two respects. First, the only low-energy scale in that theory is associated with the magnetic slowing down which, for $H > H_c$, is T_{FL} (*2*–*5*). Second, within that theory, a sharp feature in thermodynamics and transport quantities might arise near T_N only.

Our results are instead consistent with magnetic quantum criticality accompanied by the destruction of Kondo entanglement. In the form of local quantum criticality (*7*, *8*), a collapse of a large Fermi surface as *H* decreases leads to an added energy scale characterizing an electronic slowing down and, in addition, yields a zero-temperature jump in the Hall coefficient and in the field differentials of the thermodynamic quantities. An additional vanishing energy scale also exists in the "deconfined" quantum criticality scenario for insulating quantum magnets (*9*), as well as in its extension to itinerant electron systems (*27*–*28*) that are argued to be relevant to quantum critical heavy fermion metals.

References and Notes

1. K. G. Wilson, *Rev. Mod. Phys.* **55**, 583 (1983).
2. J. A. Hertz, *Phys. Rev. B* **14**, 1165 (1976).
3. A. J. Millis, *Phys. Rev. B* **48**, 7183 (1993).
4. T. Moriya, T. Takimoto, *J. Phys. Soc. Jpn.* **64**, 960 (1995).
5. N. D. Mathur *et al.*, *Nature* **394**, 39 (1998).
6. S. Sachdev, *Quantum Phase Transitions* (Cambridge Univ. Press, Cambridge, 1999).
7. P. Coleman, C. Pépin, Q. Si, R. Ramazashvili, *J. Phys. Condens. Matter* **13**, R723 (2001).
8. Q. Si, S. Rabello, K. Ingersent, J. L. Smith, *Nature* **413**, 804 (2001).
9. T. Senthil, A. Vishwanath, L. Balents, S. Sachdev, M. P. A. Fisher, *Science* **303**, 1490 (2004).
10. O. Trovarelli *et al.*, *Phys. Rev. Lett.* **85**, 626 (2000).
11. K. Ishida *et al.*, *Phys. Rev. B* **68**, 184401 (2003).
12. P. Gegenwart *et al.*, *Phys. Rev. Lett.* **89**, 056402 (2002).
13. S. Paschen *et al.*, *Nature* **432**, 881 (2004).
14. B. S. Chandrasekhar, E. Fawcett, *Adv. Phys.* **20**, 775 (1971).
15. Y. Tokiwa *et al.*, *Phys. Rev. Lett.* **94**, 226402 (2005).
16. P. Gegenwart, Y. Tokiwa, J. Custers, C. Geibel, F. Steglich, *J. Phys. Soc. Jpn.* **75** (suppl.), 155 (2006).
17. H. v. Löhneysen, A. Rosch, M. Vojta, P. Wölfle, http://arxiv.org/abs/cond-mat/0606317 (2006).
18. P. Coleman, J. B. Marston, A. J. Schofield, *Phys. Rev. B* **72**, 245111 (2005).
19. Q. Si, S. Rabello, K. Ingersent, J. L. Smith, *Phys. Rev. B* **68**, 115103 (2003).
20. P. Gegenwart, J. Custers, Y. Tokiwa, C. Geibel, F. Steglich, *Phys. Rev. Lett.* **94**, 076402 (2005).
21. K. Ishida *et al.*, *Phys. Rev. Lett.* **89**, 107202 (2002).
22. J. Custers *et al.*, *Nature* **424**, 524 (2003).
23. L. Zhu, M. Garst, A. Rosch, Q. Si, *Phys. Rev. Lett.* **91**, 066404 (2003).
24. R. Küchler *et al.*, *Phys. Rev. Lett.* **91**, 066405 (2003).
25. A. Schröder *et al.*, *Nature* **407**, 351 (2000).
26. More specifically, the data over the temperature range of $0.3\,K < T < 10\,K$ are fitted with $\alpha = 0.6$ and $\Theta_{q=0} = 0$, whereas those for $T < 0.3\,K$ by $\alpha = 1$ and $\Theta_{q=0} = 0.3\,K$ (*27*).
27. T. Senthil, M. Vojta, S. Sachdev, *Phys. Rev. B* **69**, 035111 (2004).
28. T. Senthil, S. Sachdev, M. Vojta, *Physica B* **359–361**, 9 (2005).

29. We would like to thank P. Coleman, J. Custers, Z. Fisk, S. Friedemann, K. Ishida, S. Kirchner, D. Natelson, N. Oeschler, and S. Wirth for useful discussions. This work has been supported by the Fonds der Chemischen Industrie, NSF grant DMR-0424125, and the Robert A. Welch Foundation.

Supporting Online Material

www.sciencemag.org/cgi/content/full/315/5814/969/DC1
SOM Text
Figs. S1 and S2

6 October 2006; accepted 8 January 2007
10.1126/science.1136020

Clustering by Passing Messages Between Data Points

Brendan J. Frey* and Delbert Dueck

Clustering data by identifying a subset of representative examples is important for processing sensory signals and detecting patterns in data. Such "exemplars" can be found by randomly choosing an initial subset of data points and then iteratively refining it, but this works well only if that initial choice is close to a good solution. We devised a method called "affinity propagation," which takes as input measures of similarity between pairs of data points. Real-valued messages are exchanged between data points until a high-quality set of exemplars and corresponding clusters gradually emerges. We used affinity propagation to cluster images of faces, detect genes in microarray data, identify representative sentences in this manuscript, and identify cities that are efficiently accessed by air travel. Affinity propagation found clusters with much lower error than other methods, and it did so in less than one-hundredth the amount of time.

Clustering data based on a measure of similarity is a critical step in scientific data analysis and in engineering systems. A common approach is to use data to learn a set of centers such that the sum of squared errors between data points and their nearest centers is small. When the centers are selected from actual data points, they are called "exemplars." The popular k-centers clustering technique (1) begins with an initial set of randomly selected exemplars and iteratively refines this set so as to decrease the sum of squared errors. k-centers clustering is quite sensitive to the initial selection of exemplars, so it is usually rerun many times with different initializations in an attempt to find a good solution. However, this works well only when the number of clusters is small and chances are good that at least one random initialization is close to a good solution. We take a quite different approach and introduce a method that simultaneously considers all data points as potential exemplars. By viewing each data point as a node in a network, we devised a method that recursively transmits real-valued messages along edges of the network until a good set of exemplars and corresponding clusters emerges. As described later, messages are updated on the basis of simple formulas that search for minima of an appropriately chosen energy function. At any point in time, the magnitude of each message reflects the current affinity that one data point has for choosing another data point as its exemplar, so we call our method "affinity propagation." Figure 1A illustrates how clusters gradually emerge during the message-passing procedure.

Affinity propagation takes as input a collection of real-valued similarities between data points, where the similarity $s(i,k)$ indicates how well the data point with index k is suited to be the exemplar for data point i. When the goal is to minimize squared error, each similarity is set to a negative squared error (Euclidean distance): For points x_i and x_k, $s(i,k) = -\|x_i - x_k\|^2$. Indeed, the method described here can be applied when the optimization criterion is much more general. Later, we describe tasks where similarities are derived for pairs of images, pairs of microarray measurements, pairs of English sentences, and pairs of cities. When an exemplar-dependent probability model is available, $s(i,k)$ can be set to the log-likelihood of data point i given that its exemplar is point k. Alternatively, when appropriate, similarities may be set by hand.

Rather than requiring that the number of clusters be prespecified, affinity propagation takes as input a real number $s(k,k)$ for each data point k so that data points with larger values of $s(k,k)$ are more likely to be chosen as exemplars. These values are referred to as "preferences." The number of identified exemplars (number of clusters) is influenced by the values of the input preferences, but also emerges from the message-passing procedure. If a priori, all data points are equally suitable as exemplars, the preferences should be set to a common value—this value can be varied to produce different numbers of clusters. The shared value could be the median of the input similarities (resulting in a moderate number of clusters) or their minimum (resulting in a small number of clusters).

There are two kinds of message exchanged between data points, and each takes into account a different kind of competition. Messages can be combined at any stage to decide which points are exemplars and, for every other point, which exemplar it belongs to. The "responsibility" $r(i,k)$, sent from data point i to candidate exemplar point k, reflects the accumulated evidence for how well-suited point k is to serve as the exemplar for point i, taking into account other potential exemplars for point i (Fig. 1B). The "availability" $a(i,k)$, sent from candidate exemplar point k to point i, reflects the accumulated evidence for how appropriate it would be for point i to choose point k as its exemplar, taking into account the support from other points that point k should be an exemplar (Fig. 1C). $r(i,k)$ and $a(i,k)$ can be viewed as log-probability ratios. To begin with, the availabilities are initialized to zero: $a(i,k) = 0$. Then, the responsibilities are computed using the rule

$$r(i,k) \leftarrow s(i,k) - \max_{k' \text{ s.t. } k' \neq k} \{a(i,k') + s(i,k')\} \quad (1)$$

In the first iteration, because the availabilities are zero, $r(i,k)$ is set to the input similarity between point i and point k as its exemplar, minus the largest of the similarities between point i and other candidate exemplars. This competitive update is data-driven and does not take into account how many other points favor each candidate exemplar. In later iterations, when some points are effectively assigned to other exemplars, their availabilities will drop below zero as prescribed by the update rule below. These negative availabilities will decrease the effective values of some of the input similarities $s(i,k')$ in the above rule, removing the corresponding candidate exemplars from competition. For $k = i$, the responsibility $r(k,k)$ is set to the input preference that point k be chosen as an exemplar, $s(k,k)$, minus the largest of the similarities between point i and all other candidate exemplars. This "self-responsibility" reflects accumulated evidence that point k is an exemplar, based on its input preference tempered by how ill-suited it is to be assigned to another exemplar.

Whereas the above responsibility update lets all candidate exemplars compete for ownership of a data point, the following availability update gathers evidence from data points as to whether each candidate exemplar would make a good exemplar:

$$a(i,k) \leftarrow \min\left\{0, r(k,k) + \sum_{i' \text{ s.t. } i' \notin \{i,k\}} \max\{0, r(i',k)\}\right\} \quad (2)$$

The availability $a(i,k)$ is set to the self-responsibility $r(k,k)$ plus the sum of the positive responsibilities candidate exemplar k receives from other points. Only the positive portions of incoming responsibilities are added, because it is only necessary for a good exemplar to explain some data points well (positive responsibilities), regardless of how poorly it explains other data points (negative responsibilities). If the self-responsibility $r(k,k)$ is negative (indicating that point k is currently better suited as belonging to another exemplar rather than being an exemplar itself), the availability of point k as an exemplar can be increased if some other points have positive responsibilities for point k being their exemplar. To limit the influence of strong

Department of Electrical and Computer Engineering, University of Toronto, 10 King's College Road, Toronto, Ontario M5S 3G4, Canada.

*To whom correspondence should be addressed. E-mail: frey@psi.utoronto.ca

incoming positive responsibilities, the total sum is thresholded so that it cannot go above zero. The "self-availability" $a(k,k)$ is updated differently:

$$a(k,k) \leftarrow \sum_{i' \neq k} \max[0, r(i',k)] \quad (3)$$

This message reflects accumulated evidence that point k is an exemplar, based on the positive responsibilities sent to candidate exemplar k from other points.

The above update rules require only simple, local computations that are easily implemented (2), and messages need only be exchanged between pairs of points with known similarities. At any point during affinity propagation, availabilities and responsibilities can be combined to identify exemplars. For point i, the value of k that maximizes $a(i,k) + r(i,k)$ either identifies point i as an exemplar if $k = i$, or identifies the data point that is the exemplar for point i. The message-passing procedure may be terminated after a fixed number of iterations, after changes in the messages fall below a threshold, or after the local decisions stay constant for some number of iterations. When updating the messages, it is important that they be damped to avoid numerical oscillations that arise in some circumstances. Each message is set to λ times its value from the previous iteration plus $1 - \lambda$ times its prescribed updated value, where the damping factor λ is between 0 and 1. In all of our experiments (3), we used a default damping factor of $\lambda = 0.5$, and each iteration of affinity propagation consisted of (i) updating all responsibilities given the availabilities, (ii) updating all availabilities given the responsibilities, and (iii) combining availabilities and responsibilities to monitor the exemplar decisions and terminate the algorithm when these decisions did not change for 10 iterations.

Figure 1A shows the dynamics of affinity propagation applied to 25 two-dimensional data points (3), using negative squared error as the similarity. One advantage of affinity propagation is that the number of exemplars need not be specified beforehand. Instead, the appropriate number of exemplars emerges from the message-passing method and depends on the input exemplar preferences. This enables automatic model selection, based on a prior specification of how preferable each point is as an exemplar. Figure 1D shows the effect of the value of the common input preference on the number of clusters. This relation is nearly identical to the relation found by exactly maximizing the squared error (2).

We next studied the problem of clustering images of faces using the standard optimiza-

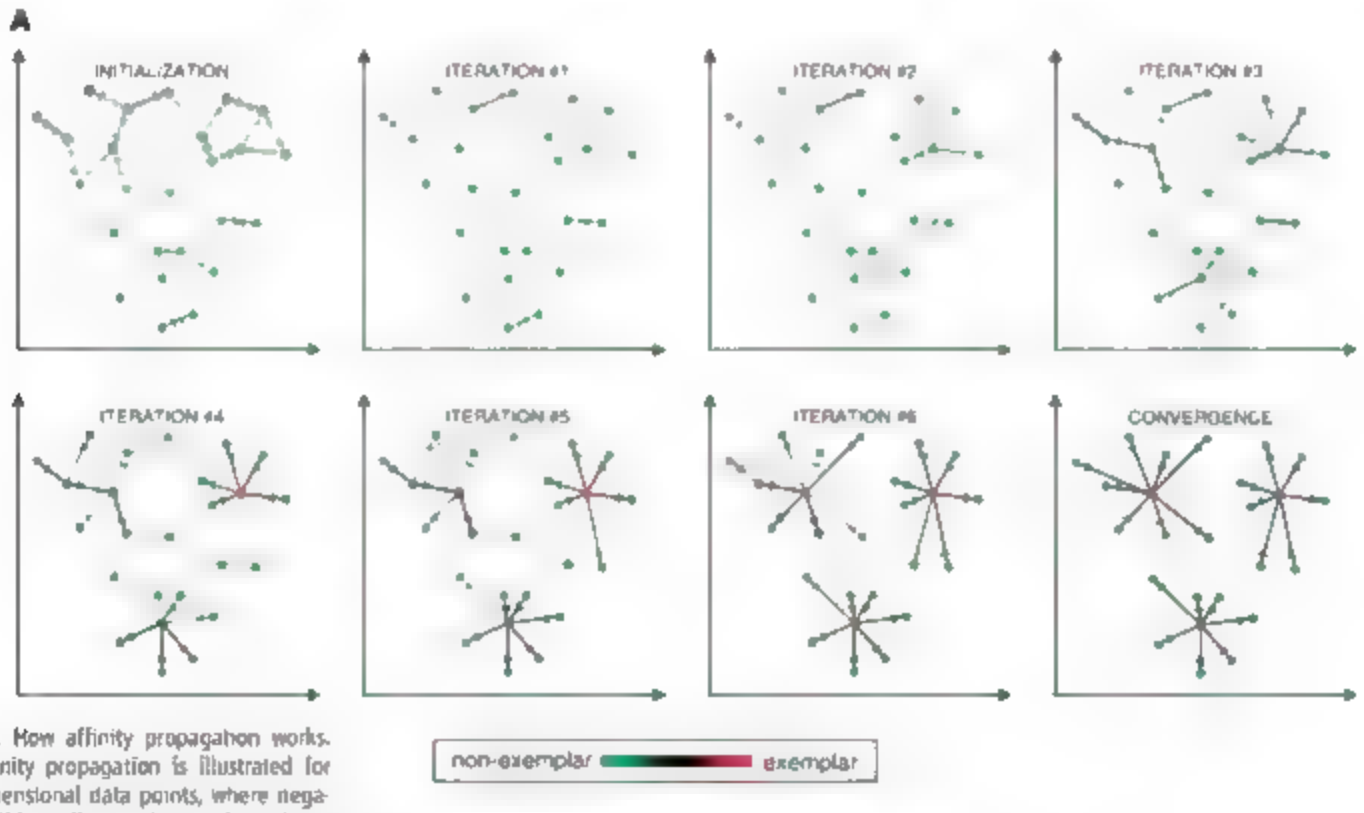

Fig. 1. How affinity propagation works. **(A)** Affinity propagation is illustrated for two-dimensional data points, where negative Euclidean distance (squared error) was used to measure similarity. Each point is colored according to the current evidence that it is a cluster center (exemplar). The darkness of the arrow directed from point i to point k corresponds to the strength of the transmitted message that point i belongs to exemplar point k. (**B**) "Responsibilities" $r(i,k)$ are sent from data points to candidate exemplars and indicate how strongly each data point favors the candidate exemplar over other candidate exemplars. (**C**) "Availabilities" $a(i,k)$ are sent from candidate exemplars to data points and indicate to what degree each candidate exemplar is available as a cluster center for the data point. (**D**) The effect of the value of the input preference (common for all data points, on the number of identified exemplars (number of clusters) is shown. The value that was used in (A) is also shown, which was computed from the median of the pairwise similarities.

tion criterion of squared error. We used both affinity propagation and *k*-centers clustering to identify exemplars among 900 grayscale images extracted from the Olivetti face database (3). Affinity propagation found exemplars with much lower squared error than the best of 100 runs of *k*-centers clustering (Fig. 2A), which took about the same amount of computer time. We asked whether a huge number of random restarts of *k*-centers clustering could achieve the same squared error. Figure 2B shows the error achieved by one run of affinity propagation and the distribution of errors achieved by 10,000 runs of *k*-centers clustering, plotted against the number of clusters. Affinity propagation uniformly achieved much lower error in more than two orders of magnitude less time. Another popular optimization criterion is the sum of absolute pixel differences (which better tolerates outlying pixel intensities), so we repeated the above procedure using this error measure. Affinity propagation again uniformly achieved lower error (Fig. 2C).

Many tasks require the identification of exemplars among sparsely related data, i.e., where most similarities are either unknown or large and negative. To examine affinity propagation in this context, we addressed the task of clustering putative exons to find genes, using the sparse similarity matrix derived from microarray data and reported in (4). In that work, 75,066 segments of DNA (60 bases long) corresponding to putative exons were mined from the genome of mouse chromosome 1. Their transcription levels were measured across 12 tissue samples, and the similarity between every pair of putative exons (data points) was computed. The measure of similarity between putative exons was based on their proximity in the genome and the degree of coordination of their transcription levels across the 12 tissues. To account for putative exons that are not exons (e.g., introns), we included an additional artificial exemplar and determined the similarity of each other data point to this "non-exon exemplar" using statistics taken over the entire data set. The resulting 75,067 × 75,067 similarity matrix (3) consisted of 99.73% similarities with values of $-\infty$, corresponding to distant DNA segments that could not possibly be part of the same gene. We applied affinity propagation to this similarity matrix, but because messages need not be exchanged between point i and k if $s(i,k) = -\infty$, each iteration of affinity propagation required exchanging messages between only a tiny subset (0.27% or 15 million) of data point pairs.

Figure 3A illustrates the identification of gene clusters and the assignment of some data points to the non-exon exemplar. The reconstruction errors for affinity propagation and *k*-centers clustering are compared in Fig. 3B. For each number of clusters, affinity propagation was run once and took 6 min, whereas *k*-centers clustering was run 10,000 times and took 208 hours. To address the question of how well these methods perform in detecting bona fide gene segments, Fig. 3C plots the true-positive (TP) rate against the false-positive (FP) rate, using the labels provided in the RefSeq database (5). Affinity propagation achieved significantly higher TP rates, especially at low FP rates, which are most important to biologists. At a FP rate of 3%, affinity propagation achieved a TP rate of 39%, whereas the best [illegible] was 2%. [illegible] comparison, at the same FP rate, the best TP rate for hierarchical agglomerative clustering (2) was 19%, and the engineering tool described in (4), which accounts for additional biological knowledge, achieved a TP rate of 43%.

Affinity propagation's ability to operate on the basis of nonstandard optimization criteria makes it suitable for exploratory data analysis using unusual measures of similarity. Unlike metric-space clustering techniques such as *k*-means clustering (1), affinity propagation can be applied to problems where the data do not lie in a continuous space. Indeed, it can be applied to problems where the similarities are not symmetric [i.e., $s(i,k) \neq s(k,i)$] and to problems where the similarities do not satisfy the triangle inequality [i.e., $s(i,k) < s(i,j) + s(j,k)$]. To identify a small number of sentences in a draft of this manuscript that summarize other sentences, we treated each sentence as a "bag of words" (6) and computed the similarity of sentence i to sentence k based on the cost of encoding the words in sentence i using the words in sentence k. We found that 97% of the resulting similarities (2, 3) were not symmetric. The preferences were adjusted to identify (using $\lambda = 0.8$) different numbers of representative exemplar sentences (2), and the solution with four sentences is shown in Fig. 4A.

We also applied affinity propagation to explore the problem of identifying a restricted number of Canadian and American cities that are most easily accessible by large subsets of other cities, in terms of estimated commercial airline travel time. Each data point was a city, and the similarity $s(i,k)$ was set to the negative time it takes to travel from city i to city k by airplane, including estimated stopover delays (3). Due to headwinds, the transit time was in many cases different depending on the direction of travel, so that 36% of the similarities were asymmetric. Further, for 97% of city pairs i and k, there was a third city j such that the triangle inequality was violated, because the trip from i to k included a long stopover delay

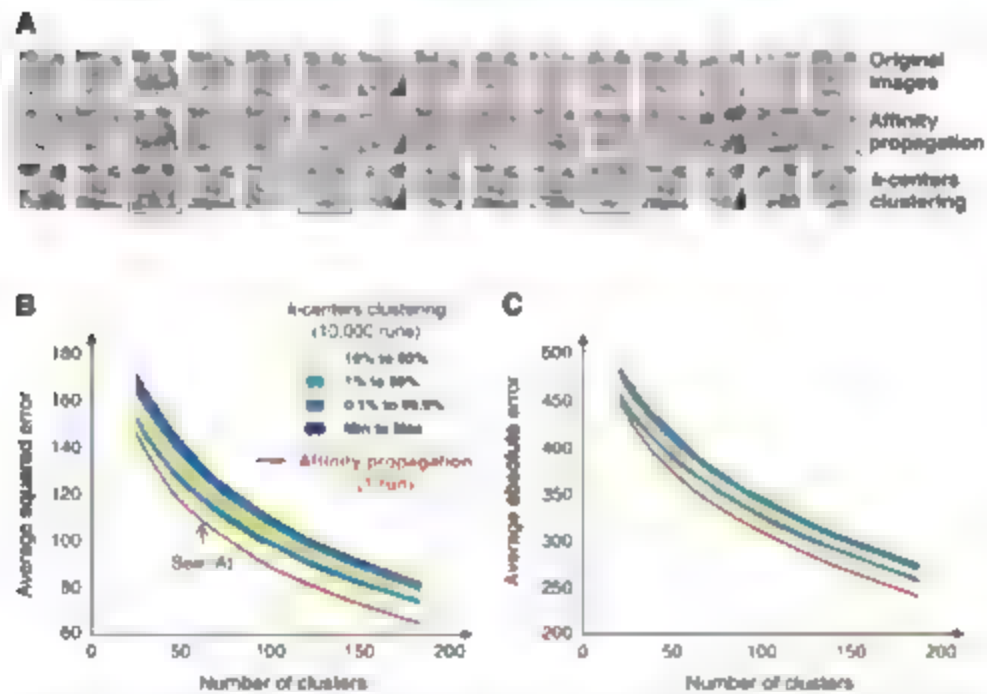

Fig. 2. Clustering faces. Exemplars minimizing the standard squared error measure of similarity were identified from 900 normalized face images (3). For a common preference of −600, affinity propagation found 62 clusters, and the average squared error was 108. For comparison, the best of 100 runs of *k*-centers clustering with different random initializations achieved a worse average squared error of 119. (**A**) The 15 images with highest squared error under either affinity propagation or *k*-centers clustering are shown in the top row. The middle and bottom rows show the exemplars assigned by the two methods, and the boxes show which of the two methods performed better for that image in terms of squared error. Affinity propagation found higher-quality exemplars. (**B**) The average squared error achieved by a single run of affinity propagation and 10,000 runs of *k*-centers clustering, versus the number of clusters. The colored bands show different percentiles of squared error, and the number of exemplars corresponding to the result from (A) is indicated. (**C**) The above procedure was repeated using the sum of absolute errors as the measure of similarity, which is also a popular optimization criterion.

in city j so it took longer than the sum of the durations of the trips from i to j and j to k. When the number of "most accessible cities" was constrained to be seven (by adjusting the input preference appropriately), the cities shown in Fig. 4, B to E, were identified. It is interesting that several major cities were not selected, either because heavy international travel makes them inappropriate as easily accessible domestic destinations (e.g., New York City, Los Angeles) or because their neighborhoods can be more efficiently accessed through other destinations (e.g., Atlanta, Philadelphia, and Minneapolis account for Chicago's destinations, while avoiding potential airport delays).

Affinity propagation can be viewed as a method that searches for minima of an energy function (7) that depends on a set of N hidden labels, $c_1, \ldots, c_N$, corresponding to the N data points. Each label indicates the exemplar to which the point belongs, so that $s(i,c_i)$ is the similarity of data point i to its exemplar ($c_i = i$ as a special case indicating that point i is used as an exemplar, so that $s(i,c_i)$ is the input preference for point i). Not all configurations of the labels are valid: a configuration $\mathbf{c}$ is valid when for every point i, if some other point i' has chosen i as its exemplar (i.e., $c_{i'} = i$), then i must be an exemplar (i.e., $c_i = i$). The energy of a valid configuration is $E(\mathbf{c}) = -\sum_{i=1}^{N} s(i,c_i)$. Exactly minimizing the energy is computationally intractable, because a special case of this minimization problem is the NP-hard k-median problem (8). However, the update rules for affinity propagation correspond to fixed-point recursions for minimizing a Bethe free-energy (9) approximation. Affinity propagation is most easily derived as an instance of the max-sum algorithm in a factor graph (10) describing the constraints on the labels and the energy function (2).

In some degenerate cases, the energy function may have multiple minima with corresponding multiple fixed points of the update rules, and these may prevent convergence. For example, if $s(1,2) = s(2,1)$ and $s(1,1) = s(2,2)$, then the solutions $c_1 = c_2 = 1$ and $c_1 = c_2 = 2$ both achieve the same energy. In this case, affinity propagation may oscillate, with both data points alternating between being exemplars and nonexemplars. In practice, we found that oscillations could always be avoided by adding a tiny amount of noise to the similarities to prevent degenerate situations, or by increasing the damping factor.

Affinity propagation has several advantages over related techniques. Methods such as k-centers clustering (11), k-means clustering (1), and the expectation maximization (EM) algorithm (11) store a relatively small set of estimated cluster centers at each step. These techniques are improved upon by methods that begin with a large number of clusters and then prune them (12), but they still rely on random sampling and make hard pruning decisions that cannot be reconsidered. In contrast, by simultaneously considering all data points as candidate centers and gradually identifying clusters, affinity propagation is able to avoid many of the poor solutions caused by unlucky initializations and hard decisions. Markov chain Monte Carlo techniques (13) randomly search for good solutions, but do not share affinity propagation's advantage of considering many possible solutions all at once.

Hierarchical agglomerative clustering (14) and spectral clustering (15) solve the quite different problem of recursively comparing pairs of points to find partitions of the data. These techniques do not require that all points within a cluster be similar to a single center and are thus not well-suited to many tasks. In particular, two points that should not be in the same cluster may be grouped together by an unfortunate sequence of pairwise groupings.

In (16), it was shown that the related metric k-median problem could be relaxed to form a

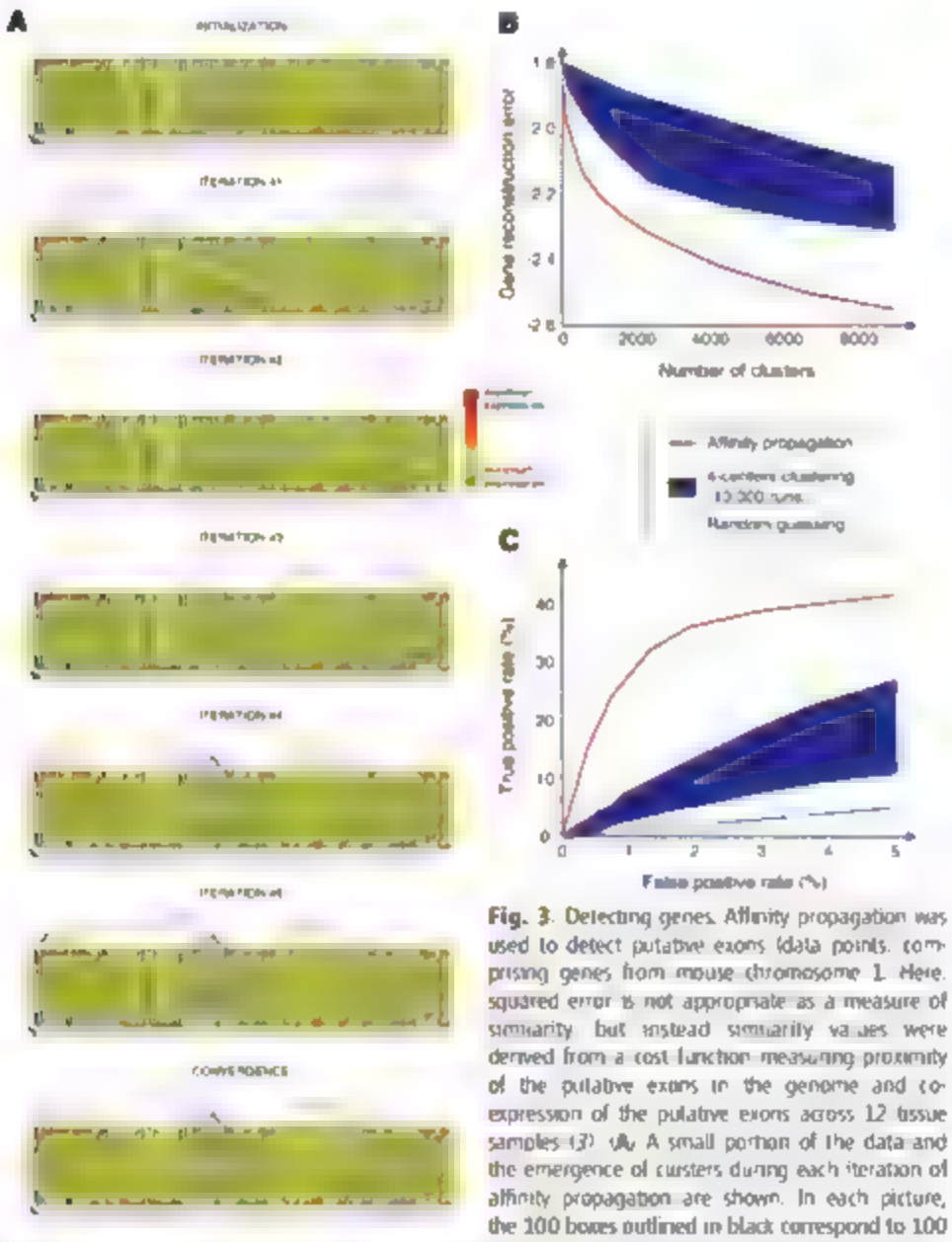

Fig. 3. Detecting genes. Affinity propagation was used to detect putative exons (data points, comprising genes from mouse chromosome 1. Here, squared error is not appropriate as a measure of similarity, but instead similarity values were derived from a cost function measuring proximity of the putative exons in the genome and coexpression of the putative exons across 12 tissue samples (3). (**A**) A small portion of the data and the emergence of clusters during each iteration of affinity propagation are shown. In each picture, the 100 boxes outlined in black correspond to 100 data points (from a total of 75,066 putative exons), and the 12 colored blocks in each box indicate the transcription levels of the corresponding DNA segment in 12 tissue samples. The box on the far left corresponds to an artificial data point with input preference that is used to account for nonexon regions (e.g., introns). Lines connecting data points indicate potential assignments, where gray lines indicate assignments that currently have weak evidence and solid lines indicate assignments that currently have strong evidence. (**B**) Performance on minimizing the reconstruction error of genes, for different numbers of detected clusters. For each number of clusters, affinity propagation took 6 min, whereas 10,000 runs of k-centers clustering took 208 hours on the same computer. In each case, affinity propagation achieved a significantly lower reconstruction error than k-centers clustering. (**C**) A plot of true-positive rate versus false-positive rate for detecting exons (using labels from RefSeq (5)) shows that affinity propagation also performs better at detecting biologically verified exons than k-centers clustering.

linear program with a constant factor approximation. There, the input was assumed to be metric, i.e., nonnegative, symmetric, and satisfying the triangle inequality. In contrast, affinity propagation can take as input general nonmetric similarities. Affinity propagation also provides a conceptually new approach that works well in practice. Whereas the linear programming relaxation is hard to solve and sophisticated software packages need to be applied (e.g., CPLEX), affinity propagation makes use of intuitive message updates that can be implemented in a few lines of code (*2*).

Affinity propagation is related in spirit to techniques recently used to obtain record-breaking results in quite different disciplines (*16*). The approach of recursively propagating messages (*17*) in a "loopy graph" has been used to approach Shannon's limit in error-correcting decoding (*18*, *19*), solve random satisfiability problems with an order-of-magnitude increase in size (*20*), solve instances of the NP-hard two-dimensional phase-unwrapping problem (*21*), and efficiently estimate depth from pairs of stereo images (*22*). Yet, to our knowledge, affinity propagation is the first method to make use of this idea to solve the age-old, fundamental problem of clustering data. Because of its simplicity, general applicability, and performance, we believe affinity propagation will prove to be of broad value in science and engineering.

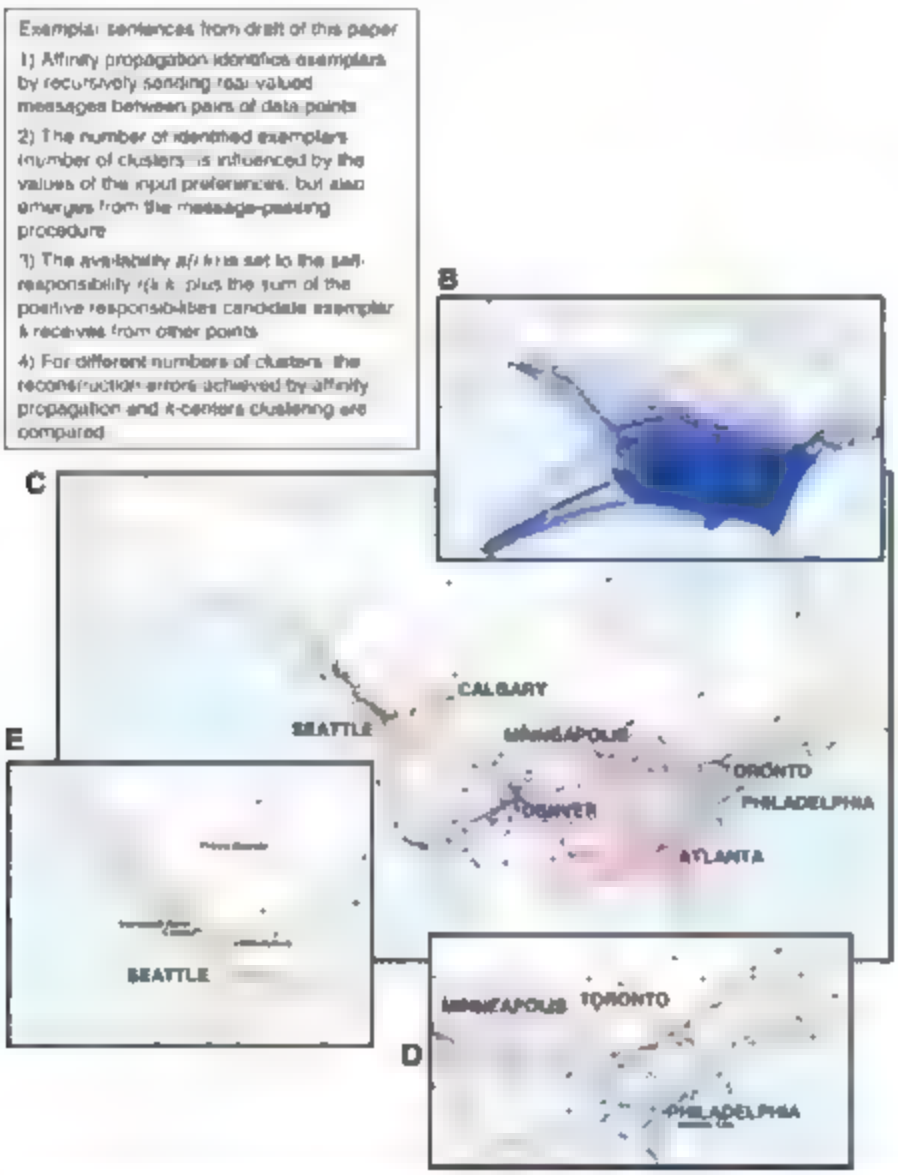

Fig. 4. Identifying key sentences and air-travel routing. Affinity propagation can be used to explore the identification of exemplars on the basis of nonstandard optimization criteria. (**A**) Similarities between pairs of sentences in a draft of this manuscript were constructed by matching words. Four exemplar sentences were identified by affinity propagation and are shown. (**B**) Affinity propagation was applied to similarities derived from air-travel efficiency, measured by estimated travel time between the 456 busiest commercial airports in Canada and the United States—the travel times for both direct flights (shown in blue) and indirect flights (not shown) including the mean transfer time of up to a maximum of one stopover were used as negative similarities (*3*). (**C**) Seven exemplars identified by affinity propagation are color-coded, and the assignments of other cities to these exemplars is shown. Cities located quite near to exemplar cities may be members of other more distant exemplars due to the lack of direct flights between them (e.g., Atlantic City is 100 km from Philadelphia, but is closer in flight time to Atlanta). (**D**) The inset shows that the Canada-USA border roughly divides the Toronto and Philadelphia clusters due to a larger availability of domestic flights compared to international flights. However, this is not the case on the west coast as shown in (**E**) because extraordinarily frequent airline service between Vancouver and Seattle connects Canadian cities in the northwest to Seattle.

References and Notes

1. J. MacQueen, in *Proceedings of the Fifth Berkeley Symposium on Mathematical Statistics and Probability*, L. Le Cam, J. Neyman, Eds. (Univ. of California Press, Berkeley, CA, 1967), vol. 1, pp. 281–297.
2. Supporting material is available on *Science* Online.
3. Software implementations of affinity propagation, along with the data sets and similarities used to obtain the results described in this manuscript, are available at www.psi.toronto.edu/affinitypropagation.
4. B. J. Frey *et al.*, *Nat. Genet.* **37**, 991 (2005).
5. K. D. Pruitt, T. Tatusova, D. R. Maglott, *Nucleic Acids Res.* **31**, 34 (2003).
6. C. D. Manning, H. Schütze, *Foundations of Statistical Natural Language Processing* (MIT Press, Cambridge, MA, 1999).
7. J. J. Hopfield, *Proc. Natl. Acad. Sci. U.S.A.* **79**, 2554 (1982).
8. M. Charikar, S. Guha, A. Tardos, D. B. Shmoys, *J. Comput. Syst. Sci.* **65**, 129 (2002).
9. J. S. Yedidia, W. T. Freeman, Y. Weiss, *IEEE Trans. Inf. Theory* **51**, 2282 (2005).
10. F. R. Kschischang, B. J. Frey, H.-A. Loeliger, *IEEE Trans. Inf. Theory* **47**, 498 (2001).
11. A. P. Dempster, N. M. Laird, D. B. Rubin, *Proc. R. Stat. Soc. B* **39**, 1 (1977).
12. S. Dasgupta, L. J. Schulman, *Proc. 16th Conf. UAI* (Morgan Kaufman, San Francisco, CA, 2000), pp. 152–159.
13. S. Jain, R. M. Neal, *J. Comput. Graph. Stat.* **13**, 158 (2004).
14. R. R. Sokal, C. D. Michener, *Univ. Kans. Sci. Bull.* **38**, 1409 (1958).
15. J. Shi, J. Malik, *IEEE Trans. Pattern Anal. Mach. Intell.* **22**, 888 (2000).
16. M. Mézard, *Science* **301**, 1685 (2003).
17. J. Pearl, *Probabilistic Reasoning in Intelligent Systems* (Morgan Kaufman, San Mateo, CA, 1988).
18. D. J. C. MacKay, *IEEE Trans. Inf. Theory* **45**, 399 (1999).
19. C. Berrou, A. Glavieux, *IEEE Trans. Commun.* **44**, 1261 (1996).
20. M. Mézard, G. Parisi, R. Zecchina, *Science* **297**, 812 (2002).
21. B. J. Frey, R. Koetter, N. Petrovic, in *Proc. 14th Conf. NIPS* (MIT Press, Cambridge, MA, 2002), pp. 737–743.
22. T. Meltzer, C. Yanover, Y. Weiss, in *Proc. 10th Conf. ICCV* (IEEE Computer Society Press, Los Alamitos, CA, 2005), pp. 428–435.

23. We thank B. Freeman, G. Hinton, R. Koetter, Y. LeCun, S. Roweis, and Y. Weiss for helpful discussions and P. Dayan, G. Hinton, D. MacKay, M. Mezard, S. Roweis, and C. Tomasi for comments on a previous draft of this manuscript. We acknowledge funding from Natural Sciences and Engineering Research Council of Canada, Genome Canada/Ontario Genomics Institute, and the Canadian Institutes of Health Research. B.J.F. is a Fellow of the Canadian Institute for Advanced Research.

Supporting Online Material

www.sciencemag.org/cgi/content/full/1136800/DC1
SOM Text
Figs. S1 to S3
References

26 October 2006; accepted 26 December 2006
Published online 11 January 2007
10.1126/science.1136800
Include this information when citing this paper.

Reversible Concerted Ligand Substitution at Alternating Metal Sites in an Extended Solid

Darren Bradshaw,[1] John E. Warren,[2] Matthew J. Rosseinsky[1]*

We report a synthetic material, $[Co_2(bipy)_3(SO_4)_2(H_2O)_2](bipy)(CH_3OH)$, (**1**, where bipy = 4,4′-bipyridyl) that contains discrete reactive and inert structural motifs that undergo a reversible substitution reaction involving the concerted and spatially controlled introduction of bipyridine and methanol molecules at the reactive sites. This reaction defines the pore geometry of the resulting open-framework structure and controls the manner in which this structure sorbs small molecules. The molecules involved in the reaction are positioned by an array of well-defined interactions during their path to binding to the metal centers.

Extended crystalline solid arrays based on the coordination of polydentate organic ligands to metal centers have produced materials with high surface areas (*1*), including structures that can undergo reversible guest sorption and reactivity between network and guest species (*2*–*5*). Additionally, classes of organic solids can undergo topochemical reactions to form a different transport through components solids (*6*). Designed linkers can be combined with organic ligands in the coordination of these materials (*7*–*11*), and extended arrays are to be used further to direct multiple small molecules cooperatively in concerted reactions and transform in a manner reminiscent of enzymes (*12*). This would probably require complex organization of sites to accommodate the necessary electronic motifs in the solid. We show that the crystalline solid $[Co_2(bipy)_3(SO_4)_2(H_2O)_2](bipy)(CH_3OH)$ **1**, where bipy = 4,4′-bipyridyl) has discrete reactive and inert structural motifs that undergo a reversible substitution reaction that involves the concerted and spatially discrete introduction of two different molecules at the reactive sites. This process is accommodated without the retention of long-range order by cooperative structural rearrangements within the motifs.

The control of the reaction in the structure of **1** can be precisely understood because of the single-crystal nature of both reagent and product. The entering groups in the substitution reaction are located in their pre-reaction positions in **1** by a diverse array of weak interactions. The resulting material **1′** is porous, with a porosity defined structurally and functionally by the topology of the substitution reaction.

A controlled reaction of methanolic solutions of $Co(SO_4)\cdot 7H_2O$ and 4,4′-bipyridine with a metal:ligand ratio of 1:0.75 under ambient conditions resulted in pink block-shaped crystals of **1** after several weeks. Structural analysis by single-crystal x-ray diffraction at 298 K revealed that **1** is composed of two distinct coordination structural units that are cross-linked into three dimensions via bidentate bridging SO_4^{2-} anions to give a hybrid framework of composition $[Co_2(bipy)_3(SO_4)_2(H_2O)_2](bipy)(CH_3OH)$. Both inorganic and organic framework-defining ligands (Fig. 1) are present. The first structural unit is a Co(bipy)$_2$ square grid that is decorated on two of the four sides by independent bipy molecules that constitute the overall framework. This two-dimensional (2D) grid stacks along the [001] direction to give ABAB… sheets with alternate grids offset by ½ *b*, where *b* is the repeat distance along the *b* axis (Fig. S1) (*19*). Coordination at these Co(1) centers is octahedral with four bipy nitrogens in the plane of the grid and two sulfate oxygens (O from symmetry-equivalent sites) from SO_4^{2-} anions completing the octahedral coordination. The second structural unit, a 1D Co(bipy) chain (Fig. 1, A and B), is also octahedral, with N atoms from the two chain-forming bipyridyl ligands and two trans water molecules and two trans O atoms from the bridging SO_4^{2-} anions forming the metal coordination sphere. The chains connect one square grid to another via two bridging SO_4^{2-} anions (Fig. 1B). The key difference between

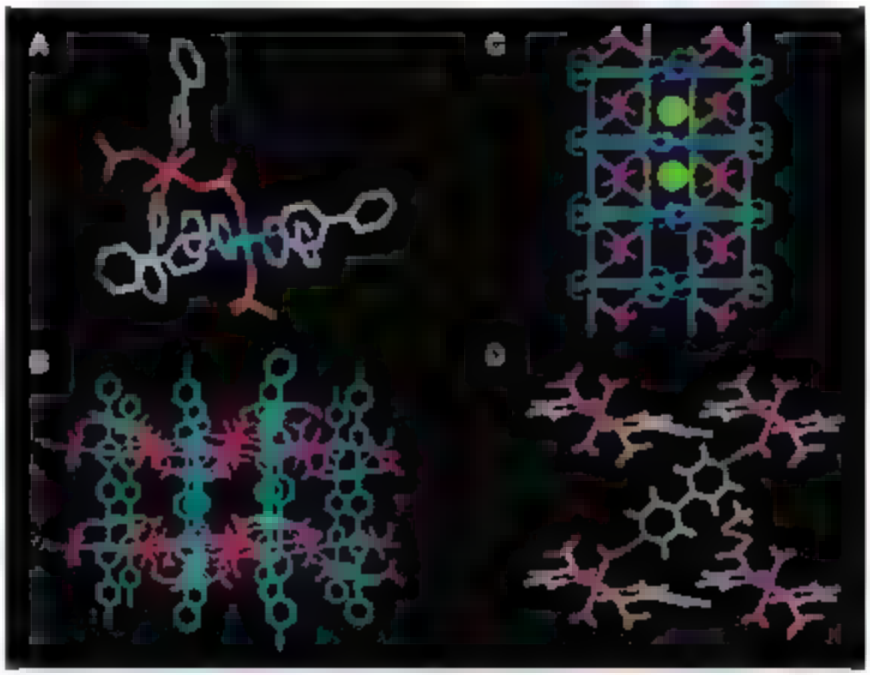

Fig. 1. (**A**) Coordination about the two structurally distinct Co centers in **1**, which are linked by the SO_4^{2-} anion. The metal associated with the square-grid network is light blue and that associated with the 1D chains is purple. O from the linking SO_4^{2-} anion and the water bound to the chain metal sites are red; S, yellow; C, gray; N, dark blue. (**B**) The extended structure of **1** viewed along the 100 direction. The bipy ligands from the square grids are light blue and those from the chains are purple, emphasizing the relation between the two distinct components of the structure linked by the SO_4^{2-} anions (S, yellow; O, red). The chains pass through the grids at an angle of 129.3°. All H atoms and guest species are omitted for clarity. Double interpenetration of this structural motif is seen in nonporous $[Co_2(bpe)_3(SO_4)_2(H_2O)_2]\cdot 2H_2O$, where bpe is *trans*-1,2-bis-(4-pyridyl)ethylene (*20*). (**C**) The extra-framework bipyridines (dark blue) form a 2D hydrogen-bonded layer by interaction with the Co-bipy) chains (viewed along the 101 direction). The location of the channels, occupied by CH_3OH molecules in **1**, is marked by the green circles. Bipyridyls from the Co(bipy)$_2$ square grids are light blue, those from the Co(bipy) chains are purple, and H atoms are omitted. (**D**) Each extra-framework bipyridine in **1** closely interacts with two Co(bipy) chains, forming two hydrogen bonds (dashed yellow lines) to the metal-bound water molecules. The CH_3OH guests are held in position by hydrogen bonding to the framework-forming SO_4^{2-} anions.

[1]Department of Chemistry, University of Liverpool, Liverpool L69 7ZD, UK. [2]Synchrotron Radiation Source, Council for the Central Laboratory of the Research Councils, Daresbury Laboratory, Warrington WA4 4AD, UK.

*To whom correspondence should be addressed. E-mail: m.rosseinsky@liv.ac.uk

the two structural units is that the chains in the second unit contain additional vacant metal centers.

The extended framework of **1** has an open 3D pore structure composed of large voids of 945 Å^3 that represent 46% of the unit-cell vol-

Fig. 2. The Co(bipy) chains in **1** undergo a reversible bimolecular substitution reaction upon heating to 368 K. The bipyridine and CH_3OH guest molecules (purple) occupy hydrogen bonding positions in the channels of solvated **1**. The incoming guest species displace metal-bound water upon heating to produce a chain that has bipyridine and CH_3OH bound to alternate metal centers along the chains in **1'**. When **1'** is cooled back to 298 K and exposed to the laboratory atmosphere, water is taken up to give a rehydrated phase, **1''**, the water displaces the substituted ligands at the chain sites in **1'** to return the structure to that of **1**. **1''** and not **1**, is used to denote the rehydrated material. Although the extra-framework ligands in **1''** are no longer bound to the Co(bipy) chains, thus demonstrating the reversibility of the substitution reaction, the solvent composition in the channels will clearly be different from the parent solvated phase **1**, hence the distinction between the two phases is made. The inset pictures show how the color of the crystal changes as the substitution process evolves.

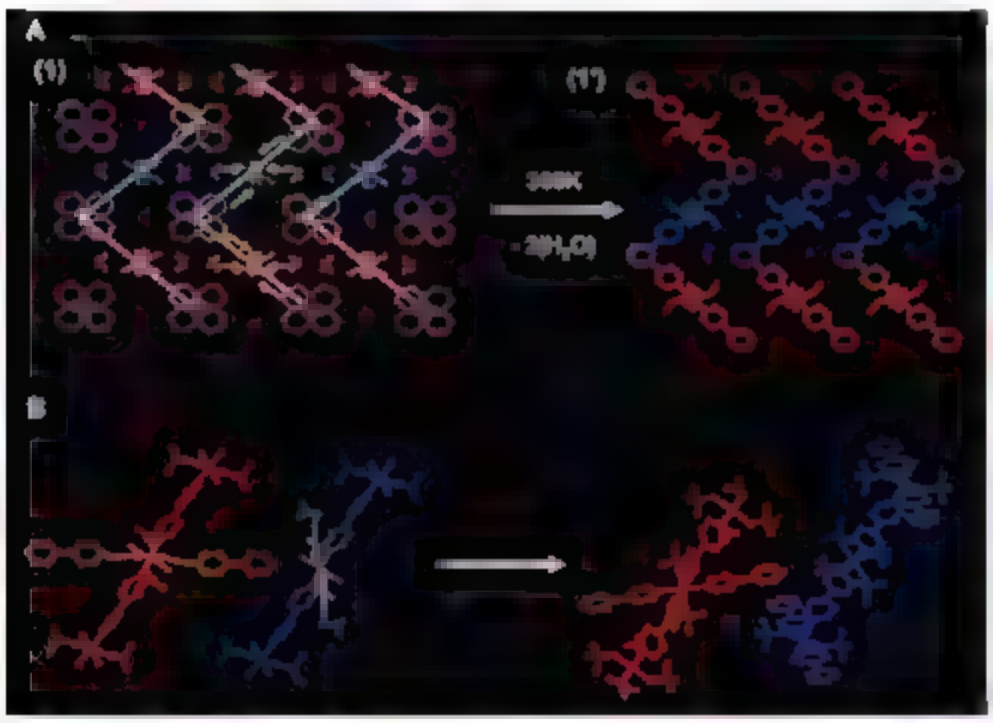

Fig. 3. (A) The CH_3OH and extra-framework bipyridine guest species move in a cooperative manner to substitute labile water ligands at the Co(bipy) chains in the transformation from **1** to **1'** (viewed close to the 101 direction). The bipyridine that was initially hydrogen-bonded symmetrically must select one of two initially equivalent chains, shown in dark blue and red. The extra-framework bipyridine and CH_3OH guests are colored according to which chain they are associated with in **1** and which they are bound to in **1'**. The white lines are shown as a guide to the eye to illustrate the perpendicular motion of two neighboring bipyridine molecules, and the yellow arrows in **1** indicate the guest molecules that bind to the chains in **1'**. Figure S3 (*15*) shows the evolution of the structure along the 001 and 101 directions. **(B)** The evolution of the positions of the CH_3OH and bipyridine guest molecules between two neighboring chains in the substitution reaction to form **1'** from **1**, producing a chain with alternating metal sites.

ume. At 298 K, partial desolvation of crystals of **1** places one CH_3OH molecule and one extra-framework bipyridyl ligand that are not coordinated to the metal centers in this solvated framework space (Fig. 1C and fig. S2) (*15*). The noncoordinated bipyridyl ligand occupies a hydrogen-bonded position (N···O 2.809 Å) (*16*) interacting with the metal-bound water molecules from two neighboring Co(bipy) chains (Fig. 1D) to form a well-ordered-bonded layer (Fig. 1C) within the 3D framework. This interaction ties the bipyridine molecule in the secondary coordination sphere of the metal centers of the chain components of the structure. The position of the CH_3OH guest is also well-defined (Fig. 1D) because of its hydrogen bonding to the SiF_6^{2-} anion (O···F 3.08 Å) and a non-classical interaction with the bipyridine (C···O 3.20 Å). The two guest molecules are thus precisely located by anion-directed interactions with the framework.

When a single crystal of **1** was heated to 368 K for 1 hour, the crystal changed color from pink to purple without the loss of crystallinity or long-range order, and could be used to collect data on **1'**. Determination of the structure of **1'** at 368 K (as established by repeated with new crystals on three different occasions) revealed that the two guest molecules were translocated into the extended framework to give a framework composition of $Co(bipy)_2SiF_6[CH_3OH]_{0.5}$ for **1'**. This change is accompanied by the displacement of the metal centers in which a pair of **1** chains (the two labile coordinated water ligands are displaced by the two pendant nitrogen atoms of a spatially correlated bipyridine molecule from neighboring metal centers. Substitution can be envisaged to occur at one CH_3OH and two bipyridine molecules were moved to alternate Co centers along the chains to form **1'** (Fig. 2).

The substitution of labile water molecules at two CH_3OH molecules at each metal center is driven by entropy as between the pairs of guests and a supposed structural relaxation of the chain. The extra-framework bipyridine ligands must move by ~2.8 Å to bind to one of the two nearest metal centers, which destroys the symmetrical environment of the bipyridine molecule as it moves from its position midway between two chains to substitute a water molecule at one chain metal site. A cooperative perpendicular motion of neighboring bipyridine molecules takes place in order to complete a substitute two water molecules on either side of the centers of inversion. The two centers in the transformation from **1** to **1'** (Fig. 3A and fig. S3) (*15*). The coordinated bipyridine in **1'** is bound to the metal centers in a monodentate manner (Fig. 3A and fig. S3) (*15*), and the second aromatic N atom extends into the void space to provide a basic site.

As in **1'**, each entering bipyridine makes one coordinate bond in the primary coordination sphere of a single Co center and two hydrogen bonds in the secondary coordi-

...rahedral spheres of two carbons (as in **1**) corresponds to substitution of the bound water molecules requires the introduction of one further ligand per metal center: the CH_3OH guest molecule. The CH_3OH molecules move by 4.41 Å to affect concerted substitution of all of the water ligands at the chain sites in a spatially correlated manner (Fig. 3B). The breaking of the symmetry of the bipyridine environment in **1** produces the free N function that weakly interacts with the methyl groups (N···H–C 3.10 Å) of the CH_3OH molecules coordinating to the Co centers of adjacent chains. This interaction would not be possible because of distances considerations if a water molecule remained bound at these sites.

The substitution reaction illustrates the role of the framework in affording a single metal site that will accommodate metal ions of increased steric demand of the ethylene bipyridine ligand. A comparison with the desolvated water molecule (Fig. 3A) (*14*), produces an elongation of the bond lengths at the Co site to which it coordinates and a change of the N–Co–O angle to the linking sulfate from 139.1° in **1** to 86.2° in **1'**, whereas this angle remains at 133.1° at the less crowded methanol-coordinated site in **1'**. The orientation of the ethylene bipyridine is imposed by the sulfate groups binding the chains to the grids via short C–H···O contacts of 2.39 and 2.43 Å (Fig. 3A) (*14*). The spatial requirements of the pyridyl C–H units adjacent to the metal-binding N are considerably greater than those of the O atoms of the water molecule, and these requirements force the pyridyl ring to detach at the metal. The bipyridine ligand therefore binds above the chain to a greater extent than either of the pyridine rings in **1** or the rings coordinating to the neighboring methanol-bound Co sites in **1'** (Fig. 4).

This steric requirement necessarily imposes irregularities on the two ends of the chain bridges in **1'** and it results in the closest C···H–C contacts of equivalent length at both metal sites on the chain (2.87 Å at the bipy-bound Co and 2.83 Å at the methanol-bound Co). The alternate displacement of the pyridyl rings in the chain on either side of the bipyridyl-coordinated Co accommodates all of the steric crowding at one metal center and drives the orientation of the alternate other than exactly substituted chain in **1'**. The chains in **1'** thus become substantially puckered as compared to those in **1** and they impose a periodic constriction on the pore ends that more closely approach the dimensions of the guest molecules (Fig. 4 and fig. S6). Structure relaxation of both the framework and the structural grid components (Fig. 4 and fig. S6) is also expected to accommodate the steric strain of the reaction.

Architecture may confer not substantial selectivity of the channels in **1'** at 300 K. Isosteric heat of adsorption has thus far not a proven tool to probe the channel structure directly determined by the guest species and have values for the extent of pore space.

The molecular binding event at accessible metal centers leading to **1'** is reversible. After the crystal was removed from the CH_3OH solution and allowed to stand at room temperature overnight, evaporation of the uptake of the methanol-water (replaced the bipyridyl) and CH_3OH leaves ordered to the Co sites to give a desolvated phase, **1''** (Fig. 2) (*15*). If however the crystal was cooled to 298 K in the dry gas stream, the extra-framework bipyridine did not return to its original position upon cooling but remained bound to the metal. This difference in behavior is a consequence of the process. Ligand desorption and binding are driven by the entropically induced compositional change of the channel species as in the absence of excess water bipyridyl is able to displace the metal-bound CH_3OH in **1'**. The substitution reaction is irreversible (*15*). The bipyridyl ligand is thus conceivably a guest species or a component of the framework.

PLATON (*17*) analysis of **1'** revealed an extra-framework volume of 24.3%, with a pore structure consisting of 1D channels with narrow constrictions aligned along the 101 direction (Figs. S6 and S7) (*15*). The cross section of the narrowest point of the channels in **1'** is 7.48 × 3.07 Å. The exposed group I (Lewis) metal-bound CH_3OH creates more wide space to accommodate with the incorporated bipyridyl N that projects the widening of the channels at these bonds upon displacement of the water (Figs. 3 and 4). Measurement at 77 K (vs. 198 K on bulk samples which form with a reduced crystal size concentration as compared to the three-axis single-crystal) revealed a type I nitrogen sorption isotherm (fig. S8) (*15*). A Brunauer-Emmett-Teller (BET) derived surface area of 221(3) m^2 g, where the number in parentheses indicates the estimated SD of the measured surface area corresponds with that expected from the pore size (*18*).

Hysteretic isotherm measurements at 77 K reveal excess upon desorption (fig. S9) (*15*). A very similar type of behavior for guests of comparable dimensions (Ar, fig. S10) (*15*), consistent with the 3D pore structure of **1** but the narrow constrictions along the channel length. The presence of the extra-framework bipyridyl in **1** is a prerequisite for this trapping behavior as in its absence the 3D pore structure of **1** would be too open to allow the ... of the guest molecules in **1** into the framework in **1'** that constitutes the pore dimensions and hence the detailed sorption response.

The structure of **1** is modular because two distinct metal-organic nets (the primary structural motifs) are connected by a rigid organic linker. The ease with which substitution at even coordinatively saturated metal centers affords the grids form a robust scaffold that ensures that the structural integrity of the material is retained. The distinct reactivities of the grids and the flexing of the flexible organic bipyridyl linker accommodates the structural rearrangements from a change of coordination at the chain metal sites. The reactivity of the grids here depends on the preorganization of the binding molecules at the metal center by diverse weak interactions with the framework structural motif (*7*). The targeted synthesis of materials with this design will be necessary to generalize this observation.

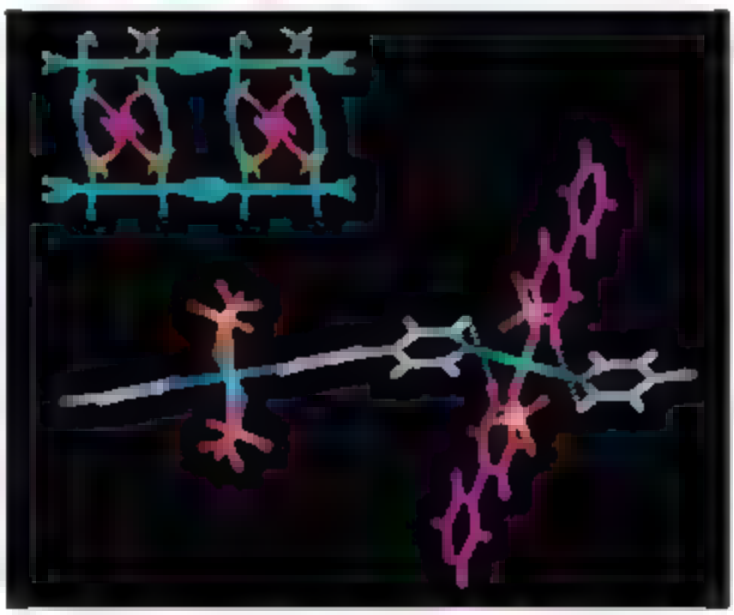

Fig. 4. The binding of CH_3OH and bipyridine molecules (highlighted in purple) at adjacent metal sites on the chain in **1'** makes the two pyridyl units in the chain-forming bipyridyl inequivalent. The pyridyl ring bound to the Co site coordinated by the entering bipyridine is displaced above and below the chain, causing puckering in order to prevent steric clashes between the C–H groups indicated with white dotted lines. The structure at the top left shows that this puckering of the chains induces a distortion in the bipyridyl linkers in one arm of the unreactive grid component of **1'** (viewed along the 101 direction as in Fig. 1C). Figure S5 (*15*) is a schematic of the coupled distortions at the grid and chain components. Bond lengths about the meta centers along the chain are Co–N_{chain} 2.172(7); Co–O_{CH_3OH} 2.130(5); Co–O_{SO_4} 2.089(5) Å for CH_3OH-bound Co and Co–N_{chain} 2.231(7); Co–N_{guest} 2.207(5); and Co–O_{SO_4} 2.130(5) Å for bipy-bound Co, where N_{chain} is from the chain-forming bipyridyl ligands, and N_{guest} is from the guest bipyridyl that is now bound to the chain.

References and Notes

1. G. K. H. Shimizu, *J. Solid State Chem.* **178**, 2519 (2005).
2. R. Kitaura, K. Seki, G. Akiyama, S. Kitagawa, *Angew. Chem. Int. Ed.* **42**, 428 (2003).
3. T. Loiseau *et al.*, *Chem. Eur. J.* **10**, 1373 (2004).
4. G. J. Halder, C. J. Kepert, *J. Am. Chem. Soc.* **127**, 7891 (2005).
5. K. Hanson, N. Calin, D. Bugaris, M. Scancella, S. C. Sevov, *J. Am. Chem. Soc.* **126**, 10502 (2004).
6. P. D. C. Dietzel, B. Panella, M. Hirscher, R. Blom, H. Fjellvåg, *Chem. Commun.* **2006**, 959 (2006).
7. E. Y. Lee, S. Y. Jang, M. P. Suh, *J. Am. Chem. Soc.* **127**, 6374 (2005).
8. C.-L. Chen, A. M. Goforth, M. D. Smith, C.-Y. Su, H.-C. zur Loye, *Angew. Chem. Int. Ed.* **44**, 6673 (2005).
9. D. Maspoch *et al.*, *Nat. Mater.* **2**, 190 (2003).
10. L. G. Beauvais, M. P. Shores, J. R. Long, *J. Am. Chem. Soc.* **122**, 2763 (2000).
11. M. H. Li, E. E. David, T. L. Gray, D. G. Kelley, O. M. Yaghi, *J. Am. Chem. Soc.* **120**, 2186 (1998).
12. K. Takaoka, M. Kawano, M. Tominaga, M. Fujita, *Angew. Chem. Int. Ed.* **44**, 2151 (2005).
13. J. L. Atwood, L. J. Barbour, A. Jerga, B. L. Schottel, *Science* **298**, 1000 (2002).
14. D. J. Chesnut *et al.*, *Coord. Chem. Rev.* **190–192**, 737 (1999).
15. Materials and methods are available as supporting material on *Science* Online.
16. L. Carlucci, G. Ciani, D. M. Proserpio, A. Sironi, *J. Chem. Soc. Dalton Trans.* **1997**, 1801 (1997).
17. A. L. Spek, PLATON (University of Utrecht, Utrecht, Netherlands, 1999).
18. Cycling between 1 and 1′ (via formation of the rehydrated phase 1‴ by exposure of the outgassed material to laboratory air), followed by further outgassing and CO_2 uptake, reveals that the porosity remains [BET surface area for cycle 2 is 2170(40) m^2/g], confirming the reversibility of the substitution reaction.
19. X. Zhao *et al.*, *Science* **306**, 1012 (2004).
20. O. Hagman, R. P. Hammond, R. Haushalter, J. Zubieta, *Chem. Mater.* **10**, 2091 (1998).

21. We thank the Engineering and Physical Sciences Research Council (EPSRC) for funding under grant EPSRC/C511794 and access to the Synchrotron Radiation Source. We thank B. Carter and S. Maraska for assistance with the synchrotron experiments. The Intelligent Gravimetric Analyzer instrument is funded by the EPSRC Molecular Materials Centre. Crystallographic data have been submitted to the Cambridge Crystallographic Database with reference numbers CCDC 617201 (1) and CCDC 617202 (1′) and are available free of charge at www.ccdc.cam.ac.uk/data_request/cif.

Supporting Online Material

www.sciencemag.org/cgi/content/full/315/5814/977/DC1
Materials and Methods
Figs. S1 to S9

22 September 2006; accepted 13 December 2006
10.1126/science.1135445

Magmatic and Crustal Differentiation History of Granitic Rocks from Hf-O Isotopes in Zircon

A. I. S. Kemp,[1,2]* C. J. Hawkesworth,[1] G. L. Foster,[1] B. A. Paterson,[1] J. D. Woodhead,[3] J. M. Hergt,[3] C. M. Gray,[4] M. J. Whitehouse[5]

Granitic plutonism is the principal agent of crustal differentiation, but linking granite emplacement to crust formation requires knowledge of the magmatic evolution, which is notoriously difficult to reconstruct from bulk rock compositions. We unlocked the plutonic archive through hafnium (Hf) and oxygen (O) isotope analysis of zoned zircon crystals from the classic hornblende-bearing I-type granites of eastern Australia. This granite type forms by the reworking of sedimentary materials by mantle-like magmas instead of by remelting ancient metamorphosed igneous rocks as widely believed. I-type magmatism thus drives the coupled growth and differentiation of continental crust.

Earth's veneer of continental crust is [illegible] granites and attests to a distinctive mode [illegible] differentiation (*1*). The vast granitic batholiths and their erupted analogs that dominate [illegible] landmasses are an obvious manifestation of such differentiation. Yet how granites relate to crustal growth processes remains puzzling, because the majority of these rocks have isotope signatures that preclude a direct mantle ancestry (*2*–*6*). The paradigm from studies in the Lachlan Fold Belt (eastern Australia) is that granitic magmas derive from preexisting sources that are fundamentally either supracrustal (formed originally at Earth's surface) or infracrustal (igneous rocks that solidified at depth) in character as reflected in the S- and I-type notation used to describe them (*7*). Granites of I-type affinity are globally prevalent. A corollary of the I-S type concept is that the isotope compositions of granites reflect the crustal residence prehistory of their protoliths (*4*), constraining the age and architecture of the deep crust as well as the timing of ancient crust-forming episodes. In contrast, other studies attribute the isotope variations to interaction between older crust and mantle-derived magma (*2*, *5*, *6*, *8*), implying that crustal growth is intrinsic to granitic emplacement. Mixing models are controversial (*9*), because ascertaining the timing and magnitude of mantle input is impeded by difficulties with retrieving the record of magmatic evolution from bulk granite compositions. This record is, however, preserved within the chemical and isotope stratigraphy of certain minerals (*10*–*13*). The robust accessory mineral zircon has the advantage that its intricate growth zoning can be dated by U-Pb isotopes, and it tracks changing melt chemistry in its Hf and O isotope ratios (*13*, *14*). We report an integrated in situ U-Pb, Hf, and O isotope study of zircons from granites, in this case the Lachlan I-types, to decipher the crustal evolutionary processes attending silicic magmatism.

We examined zircon crystals from three granitic suites (groups of rocks related through common geochemical trends): Jindabyne (415 million years ago (Ma)), Why Worry (400 Ma), and Cobargo (380 Ma). The Jindabyne plutons intrude Silurian (~425 Ma) S-type granites, whereas the Why Worry and Cobargo rocks are emplaced into Ordovician metasedimentary units at a depth of around 10 to 12 km. Rocks of each granitic suite have hallmark I-type features in their abundance of hornblende and in having higher concentrations of Ca, Na, and Sr than do S-type granites of similar silica content (*7*). Samples at either end of the compositional range of each suite were targeted. Zircons were also separated from a mafic rock associated with each suite, these being a gabbro (Jindabyne), synplutonic dolerite dyke (Why Worry), and diorite enclave (Cobargo). The mafic rocks are coeval with the respective granitic suites and share the same distinctive chemical features (*15*, *16*), implying consanguinity.

The zircons of all samples were first dated by [illegible] Pb isotope analysis (table S1). [illegible] (pre-Lachlan) component in some samples (*15*), but the discussion below focuses on data obtained from the magmatic portion of each zircon. O isotope compositions ($^{18}O/^{16}O$, expressed as $\delta^{18}O$) (*17*) were determined from the same zircon growth zone using a Cameca IMS [illegible] (*18*) (table S2). Unlike bulk rock samples, zircon is extremely retentive of the magmatic O isotope ratio (*19*), and zircons in equilibrium with pristine mantle-derived melts have a narrow range of $\delta^{18}O$ [5.3 [illegible] J. This range is insensitive to magmatic differentiation, because the attendant rise in bulk rock $\delta^{18}O$ is compensated for by an increase in zircon-liquid $\delta^{18}O$ fractionation from −0.5‰ for mafic melts to +1.5‰ for silicic derivatives (*14*). Values of $\delta^{18}O$ in zircon above 5.6‰ thus fingerprint an ^{18}O-enriched supracrustal component in the magma from which the zircon crystallized, this being either sedimentary rock (10 to 30‰) or altered volcanic rock (to 20‰) (*20*). The $^{176}Hf/^{177}Hf$ ratios were measured by laser

[1]Bristol Isotope Group, Earth Sciences Department, University of Bristol, Bristol BS8 1RJ, UK. [2]School of Earth and Environmental Sciences, James Cook University, Townsville, 4811, Australia. [3]School of Earth Sciences, University of Melbourne, Victoria, 3010, Australia. [4]Centre for Theoretical Isotope Studies, Greensborough, Victoria, 3088, Australia. [5]Swedish Museum of Natural History, Box 50007, SE-104 05 Stockholm, Sweden.

*To whom correspondence should be addressed. E-mail: tony.kemp@jcu.edu.au

ablation multicollector inductively coupled plasma mass spectrometry (*18*) (table S3), targeting, wherever possible, the pits generated by ion microprobe analysis.

An important feature of the Hf isotope data (Fig. 1) is the spectrum of εHf values exhibited by zircons of the same rock (up to 10 ε units) (*7*). Such variations within a single sample can only be reconciled by the operation of open-system processes that are capable of shifting the $^{176}Hf/^{177}Hf$ ratio of the melt from which the zircons precipitated. To identify these processes, it is necessary to deduce the polarity of Hf isotope change during zircon growth. This can be accomplished by examination of intracrystal isotope zoning trends and by pairing the isotope variations with trace element ratios (such as Th/U) that are proxies for the degree of differentiation. In cases where isotope zoning is pronounced, $^{176}Hf/^{177}Hf$ generally decreases toward zircon rims, although some grains show the opposite pattern. Trace element microanalysis has established that Th/U ratios typically fall from core to rim in the studied zircons (table S1), and the εHf values of the zircons also decrease systematically with Th/U (Fig. 2). We interpret this as evidence for a progressive reduction in the $^{176}Hf/^{177}Hf$ ratio during the magmatic evolution of each suite, as would be induced by the addition of an unradiogenic (continental crust like) component. The reversely zoned zircons manifest episodic input from material with higher εHf values.

Coupling the $^{176}Hf/^{177}Hf$ ratios of the zircons with their O isotope compositions reveals the nature of the crustal component. Zircons of individual samples exhibit a $\delta^{18}O$ range of 2 to 4‰, and, although rarely resolvable, intragrain heterogeneity can exceed 1‰ and involves a rise in $\delta^{18}O$ from core to rim (table S2). εHf and $\delta^{18}O$ are correlated for zircons of each suite and define curved arrays that extend to much higher $\delta^{18}O$ values than those of zircons precipitated from mantle melts (Fig. 3). These elevated $\delta^{18}O$ values diagnose a substantial supracrustal component in the Lachlan I-type granites. The isotope array defined by zircons of each suite has a distinctive trajectory anchored by a different low-$\delta^{18}O$ end member that is in equilibrium with mantle O. For Jindabyne and Why Worry this corresponds to zircons of the associated mafic intrusives. At higher $\delta^{18}O$ values, the arrays converge toward the field defined by magmatic zircons of S-type granites and the inferred Hf-O isotope composition of the metasedimentary country rocks.

The covariant εHf-$\delta^{18}O$ zircon arrays are therefore tracking the progressive interaction between two end-member components during zircon crystallization, these being parental low-$\delta^{18}O$ magmas and metasedimentary-derived materials. Such interaction could involve either mixing and hybridization with crustal partial melts or the digestion of supracrustal rock (assimilation) by low-$\delta^{18}O$ magmas. The origin of the low-$\delta^{18}O$ magmas is not uniquely constrained by the zircon isotope arrays. The data are permissive of an enriched mantle heritage or an intracrustal progenitor, or of variable combinations of the two (*8*). A predominantly mantle derivation accords with the mafic character of the inferred low-$\delta^{18}O$ components. These mafic magmas were subsequently modified by crustal contamination, as is evident in the spread of zircon εHf and $\delta^{18}O$ values in the Jindabyne gabbro and Why Worry basalt (Fig. 3), but zircon crystallized sufficiently early to retain vestiges of the original isotope signature.

Although long suspected (*5*), a mixed and partly supracrustal source for the Lachlan I-type granites is now incontrovertible. Major supracrustal input has also recently been inferred for other ^{18}O-enriched circum-Pacific I-type plutons (*22*). The remaining task is to quantify the metasedimentary component of each Lachlan suite and to determine the conditions under which this was incorporated. Assuming that assimilation-fractional crystallization equations (*23*) are a reasonable approximation of magmatic evolution, most zircons in the Cobargo Suite

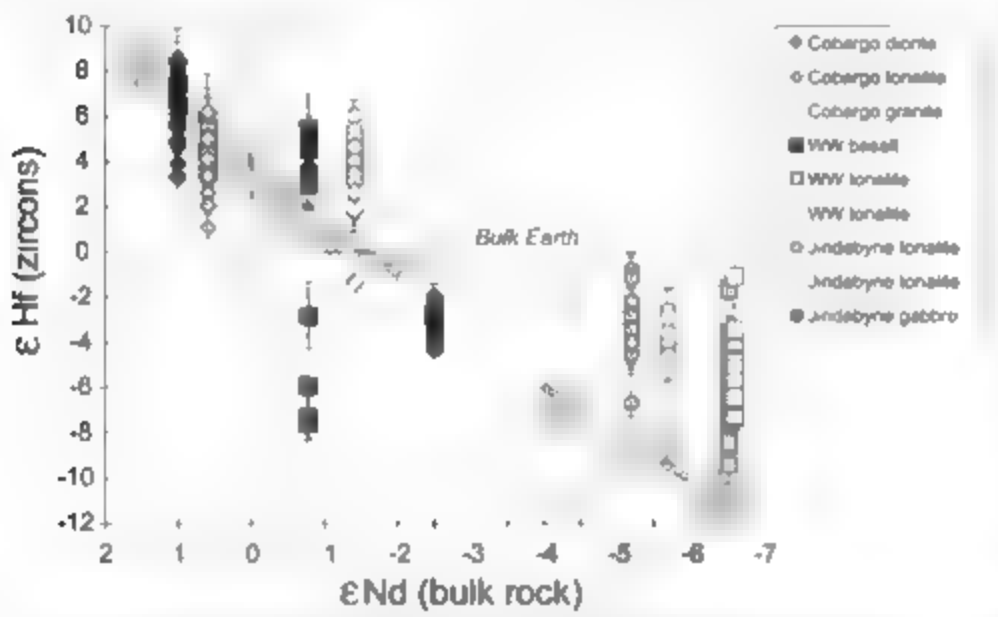

Fig. 1. The Hf isotope composition of melt-precipitated zircons from samples of each suite as a function of whole-rock Nd isotope composition at the time of crystallization (WW, Why Worry). Error bars represent 2 SEM.

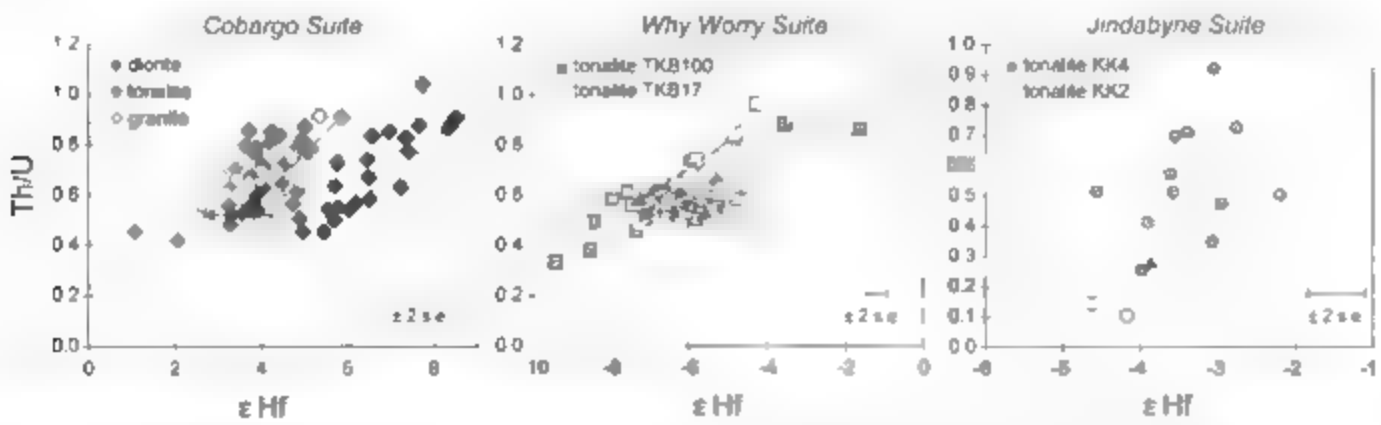

Fig. 2. Hf isotopic compositions of zircons from each suite plotted against the Th/U ratio measured for the same part of the crystal. Arrowed lines show the sense of core-to-rim zonation for individual zircons.

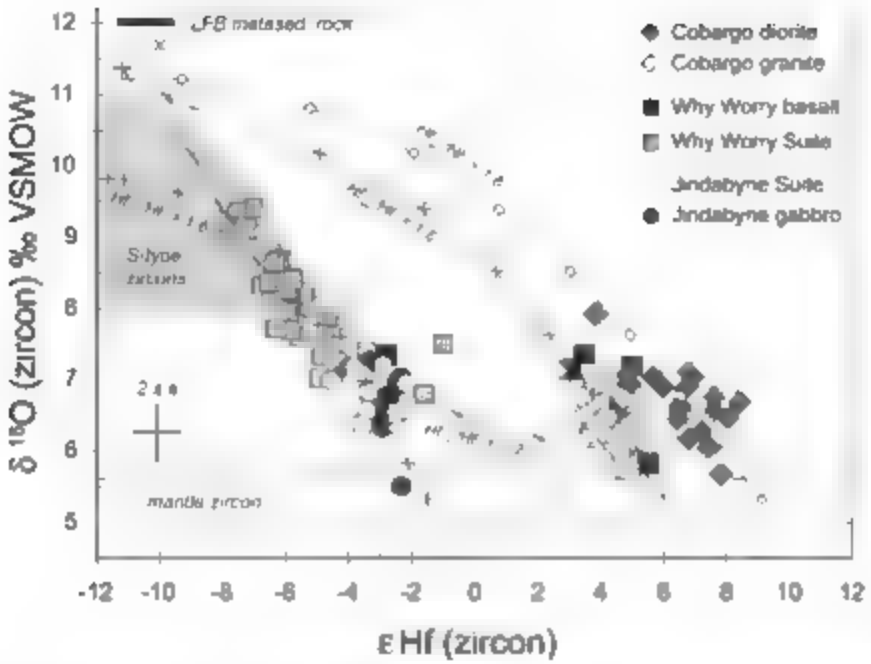

Fig. 3. Plot of $\delta^{18}O$ versus εHf for zircons of this study, showing the putative curves corresponding to magma evolution by crustal assimilation–crystallization (AFC) (*23*). Data from samples of each suite are assigned the same symbol (error bars depict the average 2 SEM uncertainty). The $\delta^{18}O$ value of Lachlan metasedimentary rock is taken from (*33*), and the shaded field depicts the isotope compositions of zircons from the Lachlan S-type granites. Ticks on the curves represent 10% AFC increments, and the ratio of Hf concentrations in the parental magma (pm) and crustal (c) end members (Hf_{pm}/Hf_c) is indicated for each. VSMOW, Vienna standard mean ocean water; LFB metased. rock, Lachlan Fold Belt metasedimentary rock.

precipitated from melts containing up to 25% supracrustal material, the corresponding figures being around 40% for Jindabyne and 60% for Why Worry (Fig. 3 and supporting online text). The geometry of the εHf-$\delta^{18}O$ arrays places additional constraints on the mixing or assimilation process, because the curvature of these arrays is controlled by the relative Hf concentrations of the end members. For Cobargo and Jindabyne, the Hf content of the low-$\delta^{18}O$ magma must have exceeded that of the crustal component, as would be the case if the latter were a partial melt with residual zircon. Conversely, the concave-up trend defined by the Why Worry suite zircons requires that the supracrustal ingredient had the higher Hf concentration, which is consistent with bulk assimilation. Partially disaggregated metasedimentary enclaves in these plutons provide evidence for this process (*32*).

Petrogenetic models for the Lachlan I-type granites must reconcile two key aspects of the new data. First, the Hf-O isotope arrays extend to high $\delta^{18}O$ values, indicating that zircon crystallization commenced before the ingestion of supracrustal material. However, the inferred temperatures of the parental low-$\delta^{18}O$ magmas were inevitably higher than the zircon stability field, typically >800°C (*24*), and crustal incorporation is more effective for hot liquid magmas (*25*). We therefore infer that crustal assimilation and zircon precipitation occurred at different temperatures, and thus crustal levels, for part of the magma system. Second, the Hf and $\delta^{18}O$ variations recorded by zircons in each granite sample radically disrupt their compositions, as if they are now juxtaposed within the same rock volume. This demands a process in the plutonic environment that can mix the crystals with disparate petrogenetic histories. Many volcanic rocks also comprise aggregates of crystals formed at different times from evolving melt compositions (*10*, *12*, *26*).

The following scenario is proposed (Fig. 4), accommodating the view that plutons are assembled incrementally (*27*, *28*). We envisage a dynamic dual-level process involving the incomplete solidification of basaltic magmas in a deep crustal hot zone (~35 to 40 km, constrained by the absence of a garnet signature in the Lachlan I-types), with batches of differentiated melt being extracted to ascend, coalesce, and crystallize in shallow magma reservoirs (*29*, *30*). The isotope systematics of each melt aliquot reflect the parental basalt composition and the degree of supracrustal input, thus commencing at depth before zircon saturation and continuing to higher crustal levels where zircon begins to crystallize (Fig. 4). Thermal simulations predict increased crustal anatexis with hot zone maturation (*29*), promoting higher rates of metasedimentary rock assimilation by the crystallizing basalts with time (*25*) and greater blending between the basalt-derived liquids and crustal melts draining the hot zone.

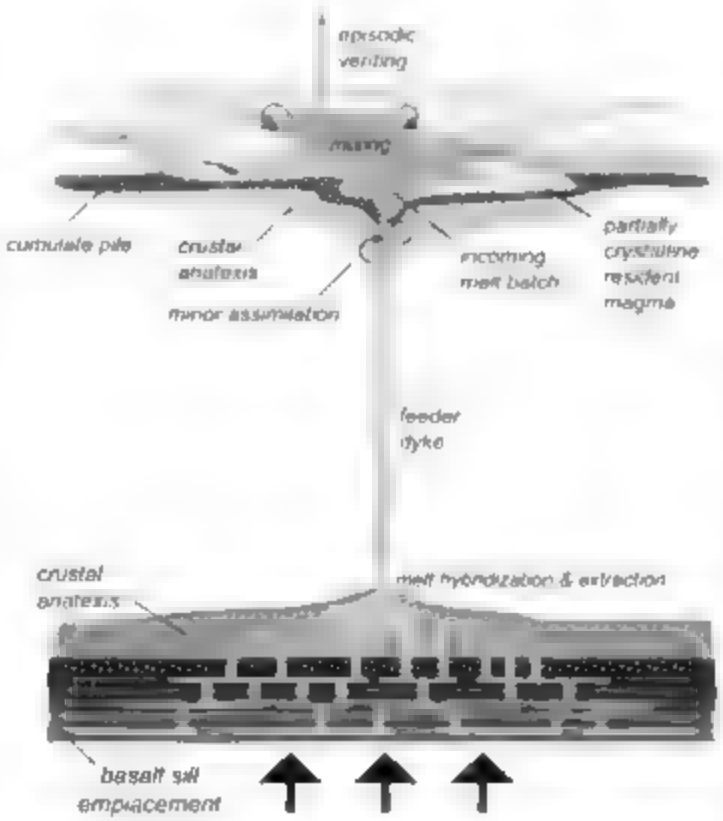

Fig. 4. A schematic model for the formation of I-type granites in eastern Australia based on the analysis of Hf-O isotopes in zircon. Silicic melts are generated at depth through interaction between residual liquids from basalt crystallization and melts derived from the overlying supracrustal assemblage (*29*). These hybrid magmas are extracted to ascend and pond in the shallow crust to crystallize zircons whose isotopic signature records the progress of supracrustal incorporation at depth. Mingling and amalgamation of melt batches during protopluton assembly accumulate zircons with different isotope characteristics. Basaltic emplacement is localized at the interface between the mafic (oceanic) substrate to the eastern Lachlan Fold Belt and the overlying turbidite pile; the interface is likely to represent a substantial rheological contrast.

Successive infusions of hybrid melt into the nascent pluton would therefore precipitate zircons with higher $\delta^{18}O$ and lower εHf values, as recorded by the zircon isotope arrays. Zircons with disparate isotope signatures are juxtaposed by mingling and crystal exchange between melt batches during pluton assembly and intrareservoir crystal-liquid sorting (*37*, *38*). Mixing with the recharge melt would also drive the resident magma and its crystallizing zircon cargo toward higher $\delta^{18}O$ and lower εHf values, explaining the intrazircon isotope zoning. Isotope reversals in some zircons and basalt injection in the Why Worry plutons suggest that this evolution was punctuated by juvenile magma replenishments.

The refined view of granite genesis captured by the zircon isotope data compels a reappraisal of the I-S type concept and its implications for crustal evolution. In revealing the reworking of supracrustal material by juvenile magmas, our study suggests that I-type magmatism critically involves continental growth, this being camouflaged to some extent by the non-mantle-like isotope ratios of the bulk rocks. The overall proportion of new material added by the Lachlan I-type suites was near 85% for Cobargo, 70% for Jincabbyne, and 50% for Why Worry. These estimates imply that Phanerozoic crust generation rates may have been higher than hitherto appreciated from studies of plutonic terranes (*6*, *32*), modifying global continental growth curves through time.

References and Notes

1. I. H. Campbell, S. R. Taylor, *Geophys. Res. Lett.* **10**, 1061 (1983).
2. D. J. DePaolo, *Science* **209**, 684 (1980).
3. E. J. Hamilton, R. K. O'Nions, R. J. Pankhurst, *Nature* **287**, 279 (1980).
4. M. T. McCulloch, G. W. Chappell, *Earth Planet. Sci. Lett.* **58**, 51 (1982).
5. C. M. Gray, *Earth Planet. Sci. Lett.* **70**, 47 (1984).
6. B.-M. Jahn, F. Wu, B. Chen, *Trans. R. Soc. Edinb. Earth Sci.* **91**, 181 (2001).
7. A. J. R. White, G. W. Chappell, *Tectonophysics* **43**, 7 (1977).
8. S. M. Keay, W. J. Collins, M. T. McCulloch, *Geology* **25**, 307 (1997).
9. G. W. Chappell, *J. Petrol.* **37**, 449 (1996).
10. J. P. Davidson, F. J. Tepley, *Science* **275**, 826 (1997).
11. T. E. Waight, R. Maas, I. A. Nicholls, *Contrib. Mineral. Petrol.* **139**, 227 (2000).
12. J. R. Vazquez, M. R. Reid, *Science* **305**, 991 (2004).
13. W. L. Griffin *et al.*, *Lithos* **61**, 237 (2002).
14. J. W. Valley *et al.*, *Contrib. Mineral. Petrol.* **150**, 561 (2005).
15. A. I. S. Kemp, M. J. Whitehouse, C. J. Hawkesworth, M. K. Alarcon, *Contrib. Mineral. Petrol.* **150**, 230 (2005).
16. R. Hine, I. S. Williams, G. W. Chappell, A. J. R. White, *J. Geol. Soc. Aust.* **25**, 219 (1978).
17. The $\delta^{18}O$ notation signifies deviation of the measured $^{18}O/^{16}O$ value from Vienna standard mean ocean water in parts per thousand.
18. Materials and methods are available as supporting material on *Science* Online.
19. W. H. Peck, J. W. Valley, C. M. Graham, *Am. Mineral.* **88**, 1003 (2003).
20. J. M. Eiler, *Rev. Mineral.* **43**, 319 (2001).
21. The epsilon notation signifies deviation of the isotope ratio [$^{176}Hf/^{177}Hf$] and [$^{143}Nd/^{144}Nd$] from a chondritic reference in parts per ten thousand.
22. J. S. Lackey, J. W. Valley, J. B. Saleeby, *Earth Planet. Sci. Lett.* **235**, 315 (2005).
23. D. J. DePaolo, *Earth Planet. Sci. Lett.* **53**, 189 (1981).
24. J. W. Valley, A. J. Cavosie, B. Fu, W. H. Peck, S. A. Wilde, *Science* **312**, 1139a (2006).
25. A. B. Thompson, L. Matile, P. Ulmer, *J. Petrol.* **43**, 403 (2002).
26. C. J. Hawkesworth, S. Turner, B. George, G. Zellmer, *Earth Planet. Sci. Lett.* **218**, 1 (2004).
27. R. A. Wiebe, W. J. Collins, *J. Struct. Geol.* **20**, 1273 (1998).
28. A. F. Glazner, J. M. Bartley, D. S. Coleman, W. Gray, R. Z. Taylor, *GSA Today* **14**, 4 (2004).
29. C. Annen, J. D. Blundy, R. S. J. Sparks, *J. Petrol.* **47**, 505 (2005).
30. M. D. Jackson, M. J. Cheadle, M. P. Atherton, *J. Geophys. Res.* **108**, 2332 (2003).
31. S. Couch, R. S. J. Sparks, M. R. Carroll, *Nature* **411**, 1037 (2001).
32. C. J. Hawkesworth, A. I. S. Kemp, *Nature* **443**, 811 (2006).
33. J. R. D. Reid, G. W. Chappell, *J. Geol. Soc. London* **133**, 559 (1977).

34. We are indebted to J. Craven for guidance with oxygen isotope analysis at the Edinburgh Ion Microprobe Facility and to C. Coath for assistance with Hf isotope analysis at Bristol. R. Arculus, N. Pearson, and C. Graham generously provided advice at the outset of the study. Constructive comments by S. Sparks, B. Collins, and two reviewers are gratefully acknowledged. Funded by NERC grants NER/I/S/00942 and IMF/250/505.

Supporting Online Material

www.sciencemag.org/cgi/content/full/315/5814/980/DC1
Materials and Methods
SOM Text
Tables S1 to S5
References

31 October 2006; accepted 11 January 2007
10.1126/science.1136154

Fracture-Controlled Paleo-Fluid Flow in Candor Chasma, Mars

Chris H. Okubo* and Alfred S. McEwen

Color observations from the High Resolution Imaging Science Experiment on board the Mars Reconnaissance Orbiter reveal zones of localized fluid alteration (cementation and bleaching) along joints within layered deposits in western Candor Chasma, Mars. This fluid alteration occurred within the subsurface in the geologic past and has been exposed at the surface through subsequent erosion. These findings demonstrate that fluid flow along fractures was a mechanism by which subsurface fluids migrated through these layered deposits. Fractured layered deposits are thus promising sites for investigating the geologic history of water on Mars.

The High Resolution Imaging Science Experiment (HiRISE) camera (*1*, *2*) on board the Mars Reconnaissance Orbiter (MRO) has returned images of the surface of Mars that have exceptional clarity and resolution. One of the first images of Mars returned by HiRISE in the low (250 to 315 km) mapping orbits of the layered deposits within western Candor Chasma (Fig. 1 and fig. S1), one of the larger canyons of the Valles Marineris system, in the western equatorial region of Mars (fig. S2). Surface features ≥0.26 m (equivalent to one pixel) are detectable, and the shapes of objects ≥0.78 m across are resolved (*3*).

The layered deposits appear as alternating light- and dark-toned bands (Fig. 1 and fig. S1) and may be volcanic, eolian, or lacustrine in origin (*3*, *6*). The dark bands appear to be flat-lying in many areas at the 10-m scale. Many of the dark-toned bands consist of a mixture of meter-scale boulders of light-toned material and finer grained dark material (figs. S3 and S4). The patches of fine-grained dark material commonly have a hummocky texture that is consistent with ripples of 2 to 5 m wavelength (fig. S3). Evidence of recent eolian activity is pervasive throughout the scene (supporting online material (SOM) text). Therefore, this flat-lying dark material is interpreted as surficial deposits of sediment composed of eolian sand, with a possible component of lag. Dark material within the underlying bedrock may also contribute to the tone of the dark bands.

The source of the dark-toned sediment is unconstrained by the present study, but it may be present within the underlying bedrock and became mobilized through eolian erosion or persists in place as lag deposits. Dark material may also have been transported from a distant source.

Local topography and high surface roughness of select layers within the light-toned bedrock apparently contribute to the accumulation of the dark sediment in distinct bands (Figs. S3 to S5). The dark-toned bands are commonly found within topographic depressions in the underlying bedrock. Accumulations of boulders also act to trap dark-toned sediment within the bands (SOM text). Thus, the dark-toned bands appear to consist of sediment that has accumulated within the troughs between ridges of light-toned bedrock.

This ridge-and-trough morphology is consistent with differential erosion, which can be

Lunar and Planetary Laboratory, University of Arizona, Tucson, AZ 85721, USA.

*To whom correspondence should be addressed. E-mail: chriso@lpl.arizona.edu

expected if the bedrock is mechanically layered. That is, the mechanically weaker, more-resistant rock layers have lower erosion rates than the stronger layers. Assuming a homogeneous and genetic history, fine-grained layers are stronger than coarse-grained layers within the same sedimentary deposit (*7*). Lower-strength layers could be due to the incorporation of dust, the resulting in a ridge-and-trough morphology as suggested here. Local heterogeneities in cementation and chemical weathering may also influence rock strength (*8*, *10*). Thus, the ridges and troughs within the bedrock may reflect local variations in either grain size or diagenetic history, or both.

Also present are sets of fractures that are hundreds of meters to several kilometers in length (Figs. 1 and 2 and fig. S3). Shear displacements of crosscut bedding and other depositional contrasts are not observed along these fractures. Small, horizontal displacements of more than 0.52 m (two pixels) would be clearly observed at the resolution of this HiRISE image. Therefore these fractures are identified as joints rather than faults (SOM text).

Many joints are surrounded by a nearly continuous "halo" of light-toned bedrock that cuts across the dark-toned bands (Fig. 2 and figs. S3 and S4). These joint halos are interrupting the background pattern of sediment patches or topographic depressions, and any layers of bedrock that are dark. The lack of dark material points to a negligible accumulation of dark sediment along these halos, as well as a systematic lightening of any dark layers of bedrock within these halos.

The negligible amount of dark material along the joint halos indicates that these areas are unfavorable for sediment deposition. A lack of meter-scale topographic shading along the bedrock within the halos reveals that these surfaces are smooth at the meter scale. In contrast, the adjacent light-toned bands show clear topographic shading that is due to observable low-albedo variations through HiRISE's color capability (Fig. 2 and figs. S3 and S4). The surface along the joint halos is therefore interpreted to be smoother at the meter scale relative to the adjacent light- and dark-toned bands. A smoother ground surface creates a lack of small-scale topography that can act to trap sediment.

Patterns of topographic shading also indicate that the joint halos often have a positive relief with inclined surfaces that would tend to impede sediment accumulation. By analogy with the light-toned bands, the accumulation of dark sediment along the trace of the joint can be inhibited where the halos are ridgelike. A ridgelike topography for the joint halos requires the bedrock along the joints to have been strengthened against erosion. Ridgelike segments of the halos that crosscut thin, dark-toned bands of sediment especially need to be strengthened because, presumably, these dark bands lie along mechanically weaker (more-eroded) layers of bedrock.

The combination of a smooth surface and positive relief along the joint halos accounts for the lack of accumulated dark sediment and indicates that the bedrock within these halos is stronger (more indurated) than the more readily eroded bedrock around it. Chemical precipitation of minerals (e.g., Fe-bearing minerals) (*11*, *13*) from fluids circulating within pore spaces of the rock along the haloed joints is a likely mechanism of wall-rock strengthening. These minerals act to cement the wall rock and thereby increase the rock's resistance to pitting and erosion.

These halos most plausibly formed after the joints were present. Had the halos formed first as noncontracted mechanically stronger ridges, the joints would have preferentially propagated within the weaker rock adjacent to those halos, rather than through the center of the halos as is observed. Previous joints would also facilitate the localization of cracking and cementation with distinct morphologies by acting as conduits for circulating fluids. In the absence of fracture-controlled fluid flow, diagenetic alteration would be distributed throughout the rock mass rather than being localized in discrete zones that crosscut bedding (e.g., *11*, *16*).

The systematic lightening in tone of any dark bedrock layers along the halos points to geochemical bleaching of the bedrock. As previously mentioned, dark material may contribute to the appearance of the dark-toned bands, especially on slopes. However, dark bedrock is lacking within the joint halos. Thus, any dark material originally present within the bedrock appears to have been dissolved or geochemically altered within the halos.

On Earth, the bleaching of the rock surrounding a fracture is a clear indication of chemical interactions between the fluids circulating within that fracture and the host rock (*11*, *12*). Additionally, interactions between the wall rock and the fluids flowing through the fracture induce changes in the strength of the wall rock (*8*, *10*). Fracture-supported flow is recognized as an important process that facilitates the large-scale subsurface migration of fluids and chemical interactions between these fluids and the host rock (*8*, *9*, *15*, *16*).

The strengthening of the joints' wall rock, as well as the geochemical bleaching of this rock, provides strong evidence of subsurface fluids having circulated through this section of the layered deposits. These episodes of bleaching and cementation probably reflect episodes

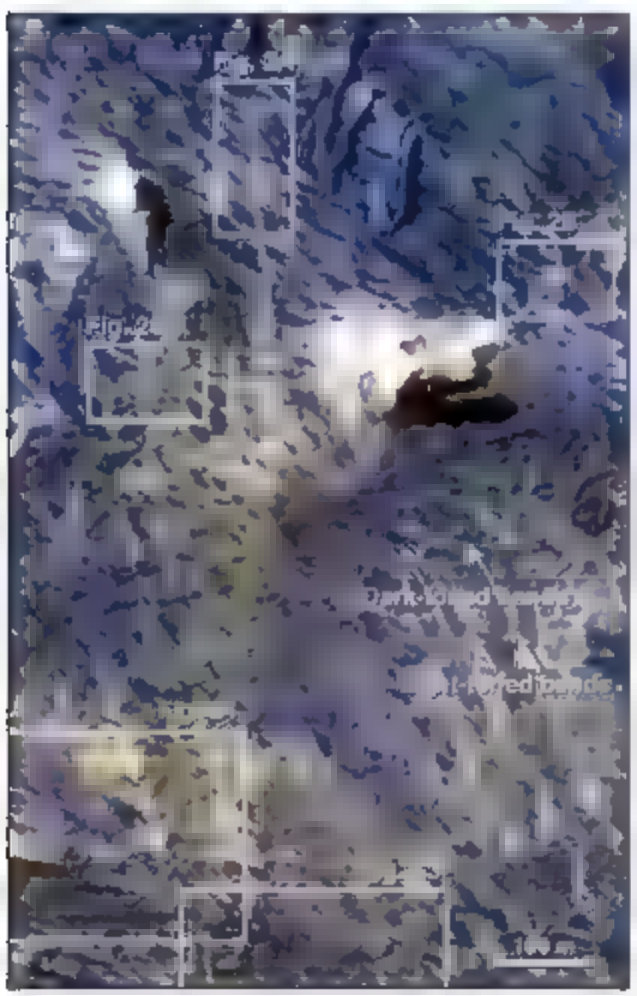

Fig. 1. High-resolution enhanced-color image showing a landscape of sand dunes and buttes against a background of light-toned (tan) and dark-toned (blue) bands in Candor Chasma. This is a subscene from HiRISE image ITRA_000836_1740, which was acquired on 30 September 2006 (Mars southern winter). The image was taken at the local Mars time of 3:29 p.m., and the scene was illuminated from the west with a solar incidence angle of 58.5°. The HiRISE camera collected image data in three band passes (blue-green, red, and near-infrared; 400 to 1000 nm) (*1*, *2*). The image scale is 0.26 m per pixel, which is equivalent to the scale of the red band-pass image. The other band passes were acquired with two-by-two pixel binning to 0.52 m per pixel. The complete image is centered at −5.7° latitude, 284.6°E longitude (planetocentric, International Astronomical Union 2000).

of reducing and oxidizing fluid flow, as is commonly observed on Earth (*11*, *13*) and also on Mars (*17*, *19*). These results support previous findings from the Observatoire pour la Mineralogie, l'Eau, les Glaces, et l'Activite (OMEGA) hyperspectral imager on board Mars Express. OMEGA observations of this region of the layered deposits reveal the spectral signature of hydrated sulfates, which is viewed as evidence of past aqueous activity (*20*, *21*).

Not all joints in this scene have halos (fig. S5). This is probably because of a difference in age for the haloed versus "non-haloed" joints. Halos developed around joints that were present when subsurface fluids were circulating through the currently exposed level of the bedrock. Once the bulk of the subsurface fluids drained from this area, any new joints that formed would not have supported adequate fluid flow for a sufficient amount of time to allow for the strengthening and bleaching of the wall rock to occur, thus no halo is present. Therefore, the presence of halos may be a proxy for relative fracture age, with the haloed fractures being the oldest and the non-haloed fractures being the youngest and having formed after the subsurface fluids drained from this level of the bedrock.

The presence of non-haloed joints that apparently postdate the haloed joints indicates that halo formation, and thus circulation of subsurface fluids within these joints, was not a geologically recent event. Further, had the haloed joints supported geologically recent near-surface fluid flow, fluvial erosional and depositional structures would be apparent (*22*, *23*). Such morphologic evidence for recent subaerial fluid flow (e.g., gullies and spring mounds) is not observed. Thus, the present-day exposures of the haloed joints initially formed within the subsurface as fluids circulated through the layered deposits. These fluids subsequently drained away, and the haloed joints were exposed at the surface through erosion. Therefore, evidence of geochemical processes that once occurred within the subsurface is currently exposed at the surface in the form of these haloed joints.

A current focus of Mars surface exploration is the investigation of areas that show evidence of past hydrologic activity, with the intent of characterizing the past habitability of these areas and their potential to support life. Much attention has been paid to clay-bearing and sulfate-bearing materials such as dry river and lakebeds and paleo-springs. This study demonstrates that exhumed joints and faults are also promising areas in which to investigate past hydrologic activity. In addition to Fig. 1, haloed joints are observed in other HiRISE images of equatorial layered deposits in Valles Marineris and elsewhere. Further analyses of these fractures may yield additional insight into the geochemistry that drives the bleaching and cementation of the wall rock.

Detailed surface observations of fracture-controlled fluid flow may be possible with the Mars Exploration Rover Opportunity. A separate HiRISE image of Victoria Crater in Meridiani Planum reveals a set of subparallel linear ridges along the crater's eastern rim and floor (fig. S6). These ridges are stratigraphically located within the regional layered sedimentary bedrock. The linearity, common orientation, and positive relief of these features suggest that these are fractures that are surrounded by bedrock that has been chemically cemented or otherwise indurated, similar to the joints described here in Candor Chasma. Opportunity is currently at Victoria Crater, and detailed studies of these ridges may provide additional insight into the mechanics and chemistry of paleo-fluid flow through the regional sedimentary bedrock.

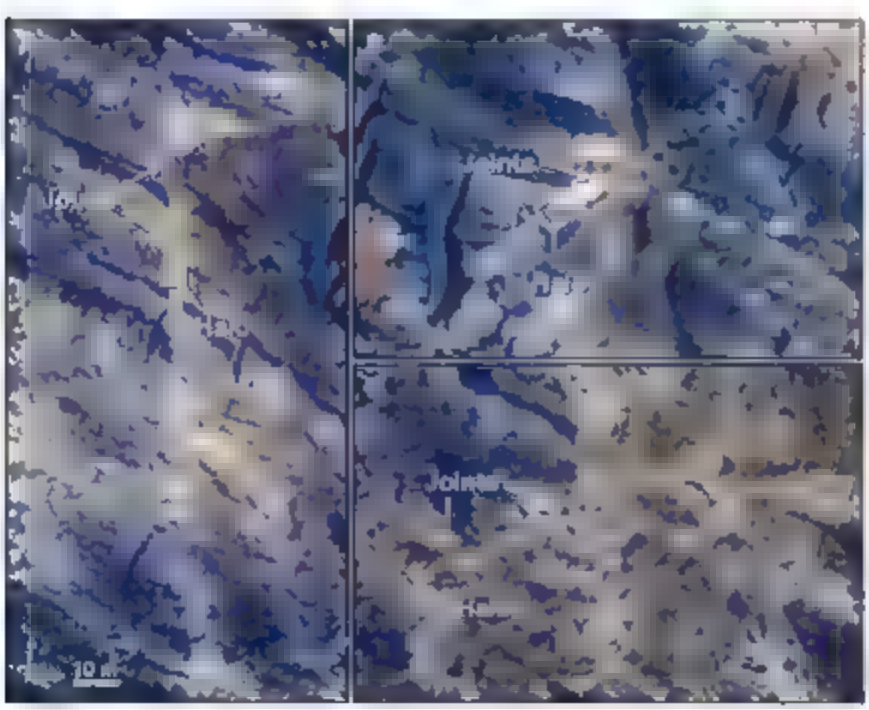

Fig. 2. (**A** to **C**) Examples of joints and surrounding halos of light-toned bedrock. The joints are the thin dark lineations. The scale bar and north arrow apply to each panel.

References and Notes

1. A. S. McEwen *et al.*, *J. Geophys. Res.*, in press.
2. For more information on HiRISE, see http://hirise.lpl.arizona.edu
3. M. E. Witbeck, K. L. Tanaka, D. H. Scott, *Geologic Map of the Valles Marineris Region of Mars*, scale 1:2,000,000, *U.S. Geol. Surv. Misc. Geol. Invest. Map I-2010* (U.S. Geological Survey, Denver, CO, 1991).
4. B. K. Lucchitta *et al.*, *Mars* (Univ. of Arizona Press, Tucson, AZ, 1992), pp. 453–492.
5. S. Murchie, L. Kirkland, S. Erard, J. Mustard, M. Robinson, *Icarus* **147**, 444 (2000).
6. M. G. Chapman, K. L. Tanaka, *Icarus* **155**, 324 (2002).
7. T.-F. Wong, C. David, W. Zhu, *J. Geophys. Res.* **102**, 3009 (1997).
8. K. J. W. McCaffrey, L. Lonergan, J. J. Wilkinson, *Fractures, Fluid Flow and Mineralization* (Special Publication 155, Geological Society of London, London, 1999).
9. B. Jamtveit, B. Yardley, *Fluid Flow and Transport in Rocks* (Chapman & Hall, London, 1997).
10. National Research Council, *Rock Fractures and Fluid Flow: Contemporary Understanding and Applications* (National Academy Press, Washington, DC, 1996).
11. M. A. Chan, B. B. Bowen, W. T. Parry, J. Ormö, G. Komatsu, *Geol. Soc. Am. Today* **15** (no. 8), 4 (2005).
12. M. A. Chan, W. T. Parry, J. R. Bowman, *Am. Assoc. Pet. Geol. Bull.* **84**, 1281 (2000).
13. M. A. Chan, B. Beitler, W. T. Parry, J. Ormö, G. Komatsu, *Nature* **429**, 731 (2004).
14. B. Beitler, W. T. Parry, M. A. Chan, *J. Sediment. Res.* **75**, 547 (2005).
15. W. T. Parry, M. A. Chan, B. Beitler, *Am. Assoc. Pet. Geol. Bull.* **88**, 175 (2004).
16. B. Beitler, M. A. Chan, W. T. Parry, *Geology* **31**, 1041 (2003).
17. B. C. Clark *et al.*, *Earth Planet. Sci. Lett.* **240**, 73 (2005).
18. S. M. Mcennan *et al.*, *Earth Planet. Sci. Lett.* **240**, 95 (2005).
19. N. J. Tosca *et al.*, *Earth Planet. Sci. Lett.* **240**, 122 (2005).
20. J.-P. Bibring *et al.*, *Science* **312**, 400 (2006).
21. A. Gendrin *et al.*, *Science* **307**, 1587 (2005).
22. Z. K. Shipton *et al.*, *Geological Storage of Carbon Dioxide* (Geological Society of London, London, 2004), pp. 43–58.
23. M. C. Malin, K. S. Edgett, L. V. Posiolova, S. M. McColley, E. Z. Noe Dobrea, *Science* **314**, 1573 (2006).

24. We are grateful to the science, operations, and engineering teams of HiRISE and the MRO project, whose diligent efforts made this work possible. Comments by HiRISE team members and two anonymous reviewers are also appreciated. Portions of this work were conducted under contract with NASA, with additional support by a grant from NASA's Mars Data Analysis Program.

Supporting Online Material

www.sciencemag.org/cgi/content/full/315/5814/983/DC1
SOM Text
Figs. S1 to S6
References

27 October 2006; accepted 19 December 2006
10.1126/science.1136855

Starch Fossils and the Domestication and Dispersal of Chili Peppers (*Capsicum* spp. L.) in the Americas

Linda Perry,[1] Ruth Dickau,[2] Sonia Zarrillo,[2] Irene Holst,[3] Deborah M. Pearsall,[4] Dolores R. Piperno,[1,3] Mary Jane Berman,[5] Richard G. Cooke,[3] Kurt Rademaker,[6] Anthony J. Ranere,[7] J. Scott Raymond,[2] Daniel H. Sandweiss,[6,8] Franz Scaramelli,[9] Kay Tarble,[10] James A. Zeidler[11]

Chili peppers (*Capsicum* spp.) are widely cultivated food plants that arose in the Americas and are now incorporated into cuisines worldwide. Here we report a genus-specific starch morphotype that provides a means to identify chili peppers from archaeological contexts and trace both their domestication and dispersal. These starch microfossils have been found at seven sites dating from 6000 years before present to European contact and ranging from the Bahamas to southern Peru. The starch grain assemblages demonstrate that maize and chilies occurred together as an ancient and widespread Neotropical plant food complex that predates pottery in some regions.

Chili peppers, members of the genus *Capsicum*, have been cultivated extensively in the Americas and, after Columbus, around the globe (*1*, *2*). The lack of a comprehensive archaeobotanical record has hindered accurate reconstructions of the origins, domestications, and dispersals of these plants. Macroremains of the fruits are confined to rare sites in arid environments, and reports of seeds and pollen are even less common (Table 1). We found that a widespread, but previously unidentified, archaeological starch morphotype is derived from chili pepper fruits and is commonly preserved on artifacts. We documented this microfossil from seven archaeological sites ranging [illegible] the Bahamas archipelago to Andean South America (Fig. 1) spanning 6000 years ago (Table 2).

The five most economically notable species of chili pepper are *C. annuum*, *C. baccatum*, *C. chinense*, *C. frutescens*, and *C. pubescens*. Although it is generally agreed that the genus *Capsicum* originated in Bolivia (*2*), the centers of domestication and dispersal patterns of these species remain speculative. A combination of archaeological evidence, genetic analyses, and modern plant distributions have led researchers to suggest that *C. annuum* was initially domesticated in Mexico or northern Central America, *C. frutescens* in the Caribbean, *C. baccatum* in lowland Bolivia, *C. chinense* in northern lowland Amazonia, and *C. pubescens* in the mid-elevation southern Andes (*2*, *3*).

All five species of domesticated chili peppers produce large, flattened lenticular starch grains with a shallow central depression, not unlike a red blood cell in appearance (Fig. 2, A to C). When rotated into side view, a central linear figure—a cleft, line or split figure with sharp edges—runs parallel to the long axis of the grain. This figure can extend for the entire length of the grain or just a part of it (Fig. 2, E and F). Ranging from about 13 to 45 μm in length, the starches of domesticated peppers are easily distinguishable from smaller wild types in the microfossil record (Fig. 2D and table S1). Although the basic three-dimensional morphology is consistent among all species of *Capsicum*, micromorphological characters differ between species.

Three of the species—*C. baccatum*, *C. frutescens*, and *C. pubescens*—can be identified on the basis of diagnostic morphotypes that have unique features of the central depression. However, these features are rare even in modern starch grain assemblages. Otherwise, the morphologies of starch grain assemblages from *C. annuum* and *C. frutescens* are so similar that, in the absence of a diagnostic, it is not possible to assign grains to a single species. The morphology of starch from *C. chinense* is similar to but not identical to that of *C. annuum* or *C. frutescens*, and the morphologies of all three starches differ significantly from those of *C. baccatum* and *C. pubescens* which, in turn, differ from one another. Because similar types occur in all congeneric species of *Capsicum*, either a diagnostic or a large archaeobotanical assemblage is required for a secure species identification.

The presence of a basic genus-diagnostic starch morphotype for *Capsicum* is predictable because of the lack of perfect barriers to interspecific hybridization (*4*). *C. annuum*, *C. chinense*, and *C. frutescens* have been described as a species complex, with a single ancestral gene pool (*4*). Therefore, it is not surprising that the starches of these three species are morphologically similar to one another. In contrast, *C. baccatum* and *C. pubescens* are distinct domesticated species in South America (*4*). Starches derived from other economically significant species in the Solanaceae including *Lycopersicon*, the genus that recent phylogenetic studies indicate is the most closely related to *Capsicum* (*5*), differ from those of chili peppers (table S1 and fig. S1) (*6*). Thus, we have eliminated those plant species with the potential to confuse the source of the microfossils.

We recovered securely identified genus-diagnostic *Capsicum* starch microfossils from seven sites throughout the Americas. The oldest positively identified starches were found at the contemporaneous sites of Loma Alta and Real Alto in southwestern Ecuador. Interpreted as a village-sized, permanent settlement, Loma Alta was occupied for more than a millennium beginning about 6100 years before present (yr B.P.) (*7*). We recovered chili pepper starches from sediment samples, milling stones, and food residues from ceramic sherds of cooking vessels, all of which were excavated from the lower levels of the site.

Similar to Loma Alta, Real Alto was a village site at about 6100 yr B.P. However, by about 4750 yr B.P., it had expanded into a regional ritual-ceremonial center (*8*, *9*). The chili starches were extracted from milling stones from two house floors dating to the period of expansion. Microfossil evidence of maize, *Canna edulis* (achira), *Maranta arundinacea* (arrowroot), *Calathea* sp.

[1]Archaeobiology Program, Department of Anthropology, Smithsonian National Museum of Natural History, Post Office Box 37012, Washington, DC 20013-7012, USA. [2]Department of Archaeology, University of Calgary, 2500 University Drive, NW, Calgary, Alberta, T2N 1N4, Canada. [3]Smithsonian Tropical Research Institute, Apartado Postal 0843-03092, Balboa, Republic of Panama. [4]Department of Anthropology, 107 Swallow Hall, University of Missouri, Columbia, MO 65211, USA. [5]Center for American and World Cultures, 105 MacMillan Hall, Miami University, Oxford, OH 45056, USA. [6]Climate Change Institute, University of Maine, 120 Alumni Hall, Orono, ME 04469-5773, USA. [7]Department of Anthropology, Temple University, 1115 West Berks Street, Philadelphia, PA 19122, USA. [8]Department of Anthropology, South Stevens 5773, University of Maine, Orono, ME 04469-5773, USA. [9]Centro de Antropología, Instituto Venezolano de Investigaciones Científicas, Carretera Panamericana, Kilometer 11, Altos de Pipe, Venezuela. [10]Departamento de Arqueología, Etnohistoria y Ecología Cultural, Escuela de Antropología, Facultad de Ciencias Económicas y Sociales, Universidad Central de Venezuela, Caracas 1041, Venezuela. [11]Center for Environmental Management of Military Lands, Colorado State University, Fort Collins, CO 80523, USA.

Table 1. Published reports of archaeological *Capsicum* from well-dated sites with clearly defined stratigraphy.

Species	Plant part	Region	Site(s)	Date(s) (yr B.P.)	Source
C. annuum	Fruits	Mexico	Tehuacan Valley	500–6000	(*24*)
C. annuum	Seeds and peduncles	El Salvador	Ceren	1400	(*25*)
C. baccatum	Fruits	Peru	Huaca Prieta, Punta Grande	4000	(*26*)
C. chinense	Fruits	Peru	Huaca Prieta, Punta Grande	4000	(*26*)
C. chinense	Fruits	Peru	Casma Valley	Ca. 2500–3500	(*3*)
Capsicum sp.	Seeds	Haiti	En Bas Saline	600	(*27*)
Capsicum sp.	Pollen	Venezuela	La Tigra	450–1000	(*28*)

lerén), manioc, cucurbits (squash), *Canavalia* sp. (jack bean), and the Arecaceae family (palms) has also been recovered from Real Alto (*10*, *12*). A combination of evidence, including plant remains and site proximity to seasonally flooded bottomland, indicates that agriculture was important in the economies of both Ecuadorian sites. Ecuador is not considered to be the center of domestication for any of the five major economic species of chili peppers. Therefore, the presence of domesticated chilies within this early, complex, agricultural system indicates that these plants must have been domesticated elsewhere earlier than 6000 yr B.P. and brought into the region from either the north or the south.

In central Panama, the Aguadulce Rock Shelter was occupied from about 13,000 to 9200 yr B.P. during both the Preceramic and Early Ceramic periods (*13*). The site has yielded evidence for the cultivation of other plants not native to southern Central America, including maize, manioc, and squashes dating from about 9000 to 5800 yr B.P. We identified chili pepper starch on a groundstone tool recovered from the top of the preceramic deposits; the tool and thus its associated starch residues have a stratigraphic date of about 5600 yr B.P. This artifact also yielded starch grains from maize and domesticated yam (*13*).

The occupation of the coastal shell-midden site of Zapotal coincides with the Early Ceramic period of this region of Panama, beginning about 4800 yr B.P. (*14*). We recovered starches of chilies from groundstone tools, indicating that the peppers were processed and consumed alongside a number of other domesticates at the site, including maize, manioc, and yams (*14*). By this time, swidden cultivation of several domesticated species, including maize and manioc, was well established in the region, and farmers had significantly deforested the foothills near both Panamanian sites (*16*). Thus, the Panamanian record documents the use of domesticated chilies as components of the diet of swidden agriculturists in both Preceramic and Ceramic era groups.

Farther south at 3600 m on the Peruvian Andes lies the site of Waynuna, a Late Preceramic house occupied beginning about 4000 yr B.P. At Waynuna, we found chili starches on processing tools in association with maize, arrowroot, and the remains of what is likely *Solanum* sp. (potato) (*17*). These data indicate that the residents of Waynuna were cultivating maize, tubers, and peppers and were processing them into food on site. Waynuna yielded the only starch assemblage that contained a species-diagnostic morphotype. These chili pepper starches appeared to be derived from *C. pubescens*, the species that includes varieties such as the rocoto pepper, a chili that is cultivated at mid-altitude in the Andes (*2*). When combined with macrofossil evidence (Table 1), the starch data indicate that the cultivation of three domesticated species of chili pepper was contemporaneous on the coast and in the highlands of Peru as early as 4000 yr B.P. in the Late Preceramic period. The presence of numerous other cultivars within the assemblages of each region indicates that sophisticated agriculture was practiced in both regions before the introduction of pottery.

We also found starches of chili peppers at the Three Dog site located on San Salvador Island in the Bahamas. This site was occupied by a group of fisher-horticulturists about 1000 yr B.P. Representing the material remains of at least one household, the site consists of a midden, two activity areas, and a low-density (well-swept) area. Fifty-eight chert microliths, all typical of the morphology commonly described as manioc grater flakes (*18*, *19*), have been recovered, as were ceramic griddle sherds. The microliths yielded the starchy remains of both maize and unidentified roots or tubers. We recovered chili starches from two flakes that also contained starches of maize.

Lastly, we recovered microfossil evidence for chili pepper at Los Mangos del Paguaza in Venezuela, a large habitation site occupied about

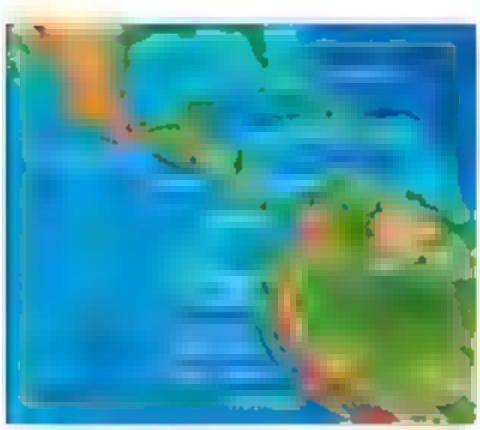

Fig. 1. Archaeological sites mentioned in the text. Red sites yielded starch grains of chili pepper. Blue sites yielded all other classes of remains of chili pepper.

Table 2. Summary of Neotropical archaeological starches of *Capsicum*. F, flaked tool; G, groundstone tool; C, ceramic sherd; S, sediment sample.

Sample	#	Size (μm)	Source	Date in yr B.P. (Ref.)
		Los Mangos, Venezuela (Arauquinoid, Valloid)		
Lev 1, 1	1	15	G	~500–1000 (*21*)
Lev 2, 1	1	17	F	~500–1000 (*21*)
Lev 3, 1	1	15	F	~500–1000 (*21*)
Lev 3, 2	1	22	F	~500–1000 (*21*)
Lev 5, 2	2	19, 20	F	~500–1000 (*21*)
Lev 7, 1	2	20, 20	F	~500–1000 (*21*)
		Three Dog, Bahamas (Lucayan)		
Z87-89	1	19	F	969–1265 Cal* (*29*)
Z1032-1035	1	21	F	969–1265 Cal* (*29*)
		Waynuna, Peru (Preceramic)		
Tool 10	2	18,24	F	3564–3837 Cal† (*17*)
Tool 11	6	14–34	G	3564–3837 Cal† (*17*)
Tool 29	2	24,25	G	3564–3837 Cal† (*17*)
Tool 30	6	19–28	G	3564–3837 Cal† (*17*)
Cat 36	1	18	S	3689–3969 Cal† (*17*)
		Zapotal, Panama (Early Ceramic)		
C2N8F4	4	20-28	G	3560–4850 Cal‡ (*14*)
C7N2	1	25	G	3560–4850 Cal‡ (*14*)
C32N7	1	32.5	G	3560–4850 Cal‡ (*14*)
		Real Alto, Ecuador (Valdivia 3)		
Structure 1	1	20	G	4400–4800 Cal† (*9*)
Structure 1	3	24–26	G	4400–4800 Cal† (*9*)
Structure 10	3	18–24	G	4400–4800 Cal† (*9*)
Structure 10	1	24	G	4400–4800 Cal† (*9*)
		Aguadulce, Panama (Late Preceramic)		
350	3	24–28	G	5600 Cal (*30*)
		Loma Alta, Ecuador (Early Formative)		
S5275	5	22–26	G	5050–6250 Cal† (*9*)
S5275-2	6	16–24	G	5050–6250 Cal† (*9*)
S5292	2	19, 20	G	4550–6050 Cal† (*9*)
Sample 13	2	24, 28	C	4830–5280 Cal† (*9*)
Sample 7	1	27	C	4080–4410 Cal† (*9*)
Level 12	2	24, 28	S	4990–5310 Cal† (*9*)
Sample 11	1	18	C	4250–4860 Cal† (*9*)
Sample 10	1	22	C	4990–5310 Cal† (*9*)
Level 14	2	24, 24	S	4990–5310 Cal† (*9*)
Sample 9	1	28	C	4990–5310 Cal† (*9*)

*Standard and AMS radiocarbon dates from associated charcoal, 2σ calibrated result. †Standard radiocarbon date from associated charcoal, 2σ calibrated result. ‡Standard radiocarbon dates from associated shell, adjusted for 12C/13C ratio, 2σ calibrated results.

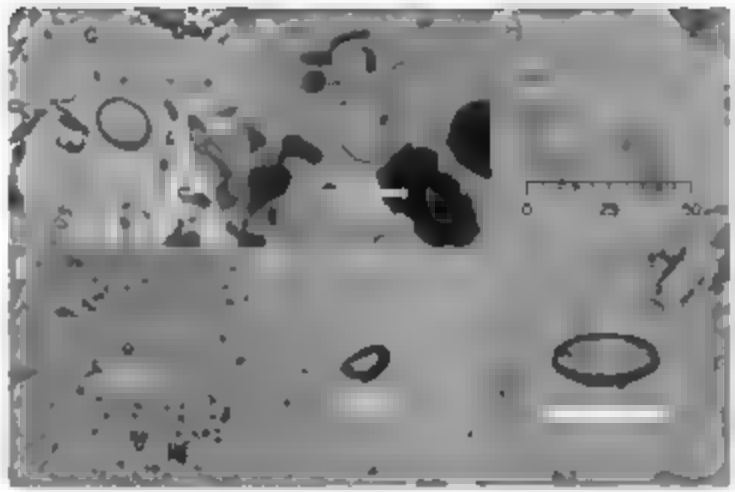

Fig. 2. Modern and archaeological starch granules from *Capsicum*. (**A**) Starch granule from the fruit of modern *Capsicum baccatum* var. *pendulum* (aji mirasol) showing typical morphology. Note the rounded lenticular form and large, flat, central depression. (**B**) Archaeological *Capsicum* starch granule from Loma Alta. (**C**) Archaeological starch granule of *Capsicum* from Real Alto. (**D**) Starch granule from a modern specimen of *Capsicum annuum* var. *minimum*. This starch granule is typical of those from wild peppers. (**E**) Side view of a modern starch granule from *Capsicum baccatum*. Note the linear figure. (**F**) Side view of an archaeological starch granule of *Capsicum* from Zapotal.

5100 to 1000 yr B.P. (*21*). Several large, deep storage pits were scattered over the surface of the site. Excavation of a midden deposit yielded ceramic griddle sherds and microlithic flakes that are often associated with manioc processing (*22*). As at the Three Dog site, the remains of manioc are conspicuously absent from an excavation that yielded artifacts usually associated with manioc processing (*22*). The same processing tools that contained starches of chili pepper also contained remains of maize. Root crops, including arrowroot, *Myrosma* sp. (guapo), and a member of the Zingiberaceae family (ginger) also left their starchy remains. When combined with the data from the Three Dog site, the chili pepper microfossils from Los Mangos del Paraguaza support the notion that a crop-centered mixed subsistence economy of both root and seed crops occurred at these sites that were initially categorized as being occupied by manioc-based cultivators (*21*).

Neither microfossils typical of wild species nor transitional forms of *Capsicum* were recovered from any site. The presence of domesticated plants used as condiments rather than as staple foods during the Preceramic period indicates that sophisticated agriculture and complex societies arose early throughout the Americas and that the exploitation of manioc, root crops, and chili peppers spread before the introduction of pottery. Evidence from both macrobotanical and microbotanical remains indicates that once chili peppers became incorporated into the diet, they persisted. Apart from the chili peppers, maize is present at every site we sampled. Maize and chilies occur together from the onset of this record until European contact and, thus, represent an ancient Neotropical plant food complex.

References and Notes

1. C. B. Heiser Jr., in *Evolution of Crop Plants*, N. W. Simmonds, Ed. (Longman, London, 1976), pp. 265–268.
2. W. H. Eshbaugh, in *New Crops*, J. Janick, J. E. Simon, Eds. (Wiley, New York, 1993), pp. 132–139.
3. B. Pickersgill, in *Pre-Columbian Plant Migration*, D. Stone, Ed. (Harvard Univ. Press, Cambridge, MA, 1984), pp. 105–123.
4. B. Pickersgill, *Biol. Zent.* **107**, 381 (1988).
5. L. Bohs, R. G. Olmstead, *Syst. Bot.* **22**, 5 (1997).
6. Materials and methods are available as supporting material on *Science* Online.
7. J. S. Raymond, in *Pacific Latin America in Prehistory: The Evolution of Archaic and Formative Cultures*, M. Blake, Ed. (Washington State Univ. Press, Pullman, 1999), pp. 149–159.
8. D. Lathrap, J. G. Marcos, J. A. Zeidler, *Archaeology* **30**, 2 (1977).
9. J. A. Zeidler, in *Archaeology of Formative Ecuador*, J. S. Raymond, R. Burger, Eds. (Dumbarton Oaks, Washington, DC, 2003), pp. 487–527.
10. D. M. Pearsall, K. Chandler-Ezell, J. A. Zeidler, *J. Archaeol. Sci.* **31**, 423 (2004).
11. D. M. Pearsall, in *Archaeology of Formative Ecuador*, J. S. Raymond, R. Burger, Eds. (Dumbarton Oaks, Washington, DC, 2003), pp. 213–257.
12. K. Chandler-Ezell, D. M. Pearsall, J. A. Zeidler, *Econ. Bot.* **60**, 103 (2006).
13. D. R. Piperno, A. J. Ranere, I. Holst, P. Hansell, *Nature* **407**, 894 (2000).
14. R. G. Cooke, A. J. Ranere, *World Archaeol.* **24**, 114 (1992).
15. R. Dickau, thesis, Temple University, Philadelphia, PA (2005).
16. D. R. Piperno, D. M. Pearsall, *The Origins of Agriculture in the Lowland Neotropics* (Academic Press, San Diego, CA, 1998).
17. L. Perry *et al.*, *Nature* **440**, 76 (2006).
18. M. J. Berman, A. K. Sievert, T. Whyte, *Lat. Am. Antiq.* **10**, 415 (1999).
19. M. J. Berman, D. M. Pearsall, *Lat. Am. Antiq.* **11**, 219 (2000).
20. W. R. DeBoer, *Am. Antiq.* **40**, 419 (1975).
21. K. Tarble, thesis, University of Chicago, Chicago, IL (2006).
22. L. Perry, *J. Archaeol. Sci.* **31**, 1069 (2004).
23. L. Perry, *Latin Am. Antiq.* **16**, 409 (2005).
24. C. E. Smith, in *Prehistory of the Tehuacan Valley*, D. S. Byers, Ed. (Texas Univ. Press, Austin, 1967), pp. 220–255.
25. O. L. Lentz, M. P. Beaudry-Corbett, M. L. R. del Aguila, L. Kaplan, *Lat. Am. Antiq.* **7**, 247 (1996).
26. B. Pickersgill, *Am. Antiq.* **34**, 54 (1969).
27. L. A. Newsom, E. S. Wing, *On Land and Sea: Native American Uses of Biological Resources in the West Indies* (Univ. of Alabama, Tuscaloosa, 2004).
28. C. S. Spencer, E. M. Redmond, M. Rinaldi, *Lat. Am. Antiq.* **5**, 119 (1994).
29. M. J. Berman, P. Grivetti, *World Archaeol.* **26**, 421 (1995).
30. A. J. Ranere, R. G. Cooke, in *Paths to Central American Prehistory*, F. W. Lange, Ed. (Univ. Press of Colorado, Niwot, 1996), pp. 49–77.

31. Comparative materials were supplied by the U.S. National Herbarium, E. Perry, J. Perry, and I. Shimada. B. Smith provided comments on the manuscript. Funding for archaeological excavations and starch grain studies was provided by the American Philosophical Society, the Consejo de Desarrollo Científico y Humanístico de la Universidad Central de Venezuela, the Escuela Superior Politécnica del Litoral, the Foundation for Exploration and Research on Cultural Origins, the Heinz Charitable Trust, Latin American Archaeology Program, NSF, the Office of the Provost at Ithaca College, the Programa de Antropología para el Ecuador, the Smithsonian National Museum of Natural History, the Smithsonian Tropical Research Institute, the Social Sciences and Humanities Council of Canada, Temple University, the University of Missouri Research Board, and Wenner-Gren.

Supporting Online Material

www.sciencemag.org/cgi/content/full/315/5814/986/DC1
Materials and Methods
SOM Text
Fig. S1
Tables S1 and S2
References

30 October 2006; accepted 21 December 2006
10.1126/science.1136914

Multipotent *Drosophila* Intestinal Stem Cells Specify Daughter Cell Fates by Differential Notch Signaling

Benjamin Ohlstein and Allan Spradling*

The adult *Drosophila* midgut contains multipotent intestinal stem cells (ISCs) scattered along its basement membrane that have been shown by lineage analysis to generate both enterocytes and enteroendocrine cells. ISCs containing high levels of cytoplasmic Delta-rich vesicles activate the canonical Notch pathway and down-regulate Delta within their daughters, a process that programs these daughters to become enterocytes. ISCs that express little vesiculate Delta or are genetically impaired in Notch signaling, specify their daughters to become enteroendocrine cells. Thus, ISCs control daughter cell fate by modulating Notch signaling over time. Our studies suggest that ISCs actively coordinate cell production with local tissue requirements by this mechanism.

Stem cells in adult tissues frequently reside in specific anatomical positions known as niches, whose microenvironment represses premature differentiation and controls proliferation (*1*, *2*). Several different signal transduction pathways, including BMP (bone morphogenetic protein), JAK/STAT (Janus kinase-signal transducer and activator of transcription), Wnt, and

Notch function in well-characterized niches such as those at the apex of the *Drosophila* ovariole (5), anchor cells (6), and the *Caenorhabditis elegans* gonad (7), or mammalian vertebrate hematopoietic stem cell niches (8, 9). Most of these stem cells are known to passively receive signals from surrounding stromal cells that inhibit differentiation, and to generate a single type of daughter cell (which may specialize further after subsequent divisions). Recently, intestinal stem cells (ISCs) that require Notch signaling for normal function were described in the *Drosophila* adult posterior midgut (Fig. 1A) (10–12). In contrast to previously studied *Drosophila* stem cells, ISCs generate two different cell types, enterocytes (ECs) and enteroendocrine (ee) cells, without intervening divisions and are not associated with specific anatomical sites containing candidate stromal partners (11).

To investigate the molecular regulation of ISC multipotency, we stained midguts with antibodies specific for the Notch ligand Delta. Under steady-state nutritional conditions (13), ISCs are dispersed singly or within small clusters (two or three diploid cells) ("cell nests," Fig. 1B), dispersed among the monolayer of polyploid ECs lining the gut. Each cell nest contains a single cell (or very rarely two cells) that expresses Delta (Fig. 1B), although the Delta levels in the positive cell vary (compare Fig. 1, C and D). Labeling is prominent in large punctate structures resembling endocytic vesicles (Fig. 1, C and D), similar to those observed in other cells with active Delta-Notch signaling (14–17).

The cell expressing Delta was shown to be the ISC by generating marked stem cell clones. While dissected guts of the appropriate genotype were heat-shocked to initiate a recombination mediated by the enzyme FLP that activates heritable *lacZ* expression in rare random dividing cells (11), ISCs can be identified in such clones as the unique *lacZ*-positive cell, and the ISC nucleus is known to be located closest to the basement membrane. Guts were isolated at various times after clone induction, stained for LacZ and Delta, and analyzed as three-dimensional (3D) optical sections (Fig. 1E). We observed that the ISC was always Delta-positive, whereas prospective ECs or ee cells lacked Delta. Thus, in the adult midgut, Delta expression serves as a highly specific stem cell marker.

All cells within the nests express Notch (11) (Fig. 1F). Consequently, to determine which cell actually receives Notch signals, we used a transgene containing tandem binding sites for the transcription factors Grainyhead and Suppressor of Hairless–Su(H)–that acts as a sensitive reporter for Notch activation (18). When guts from adults bearing this reporter were counterstained for Delta, we observed that the Notch reporter was highly expressed in the daughter cell (the enteroblast, EB) of ISCs with high Delta levels (Fig. 1G) but was at background levels in the ISC itself (Fig. 1G'). In rare cell nests with two Delta-positive cells, neither one strongly expressed the Notch reporter (Fig. 1, H and H'). The strong inverse relationship between Delta levels and Notch activity suggests that ISCs signal via Delta to activate Notch in their daughters (Fig. 1I).

We generated MARCM mosaic analysis with a repressible cell marker) clones (19) of seven different Notch pathway genes to test this hypothesis. The green fluorescent protein (GFP) marker gene and mutant gene produced in such experiments segregate to cells into just the ISC or just its daughter, yielding two possible outcomes (Fig. 2A). ISC clones of the null allele Dl^{rev10} (20) produced the results expected if Delta is an essential ligand to initiate Notch signaling. Many *Delta* mutant clones grew into tumors (Fig. 2B), indistinguishable from those generated previously by loss of *Notch* function (11), or into one EC and a tumor (Fig. 2C), because of transient perdurance of Delta protein. Perdurance probably also explains why, like *N* tumors (11), the *Dl* tumors are frequently mosaic for ee-like cells expressing Prospero and for ISC-like cells that lack Prospero (Fig. 2B). In many other *Dl* clones, a marked cell differentiated as a single EC (Fig. 2D), presumably because only the EB was mutated and it could still

Howard Hughes Medical Institute, Department of Embryology, Carnegie Institution of Washington, 3520 San Martin Drive, Baltimore, MD 21218, USA.

*To whom correspondence should be addressed. E-mail: spradling@gwemb.edu

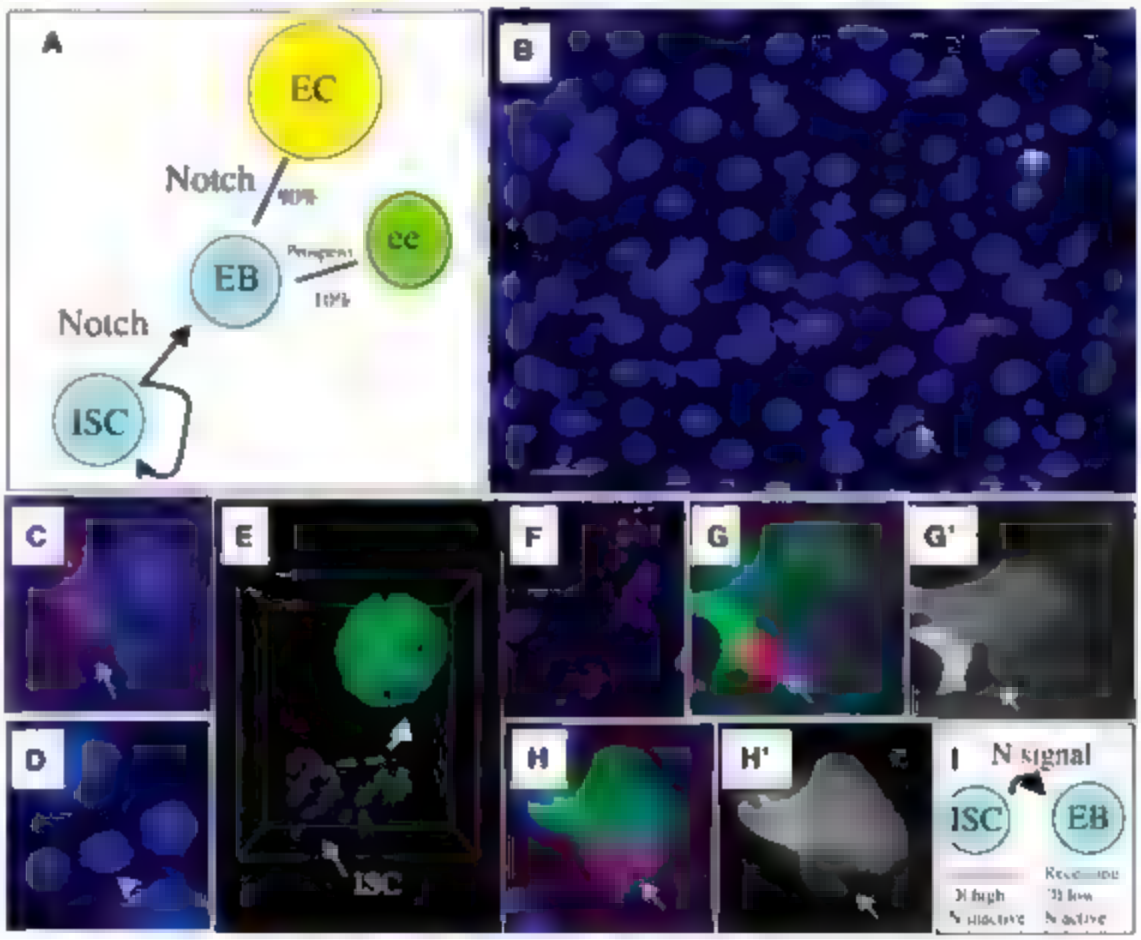

Fig. 1. ISCs usually divide asymmetrically with respect to Delta expression and Notch pathway activation. (**A**) Lineage analysis (11) shows that individual ISCs give rise to daughters (EB) that become enterocytes (EC) and less frequently enteroendocrine cells (ee). (**B**) Midgut cells express Delta (red) at high levels [arrow, also (**C**)] or low levels [arrowhead, also (**D**)] within one cell of each diploid cell nest. Here and in images in later figures, DNA is shown in blue. (**E**) 3D reconstruction of a 4-day ISC clone (green) showing that the Delta-expressing cell (red) is basal, the known location of ISCs (arrow). Dashed arrow indicates order of clone growth. (**F**) Notch (red) is expressed widely, except in mature ECs or ee cells. (**G**) Notch reception (green) is up-regulated in EBs but not in Delta-positive ISCs (arrow). (**G'**) Notch reception reporter channel (white) alone. (**H** and **H'**) A rare nest with two Delta-positive cells; colors as in (G). (**I**) Model. A Delta-rich ISC activates Notch signaling (arrow) in its daughter EB. Scale bar in (B), 20 μm.

receives Notch signal from the adjacent wild-type ISC (Fig. 2A). This implies that *Delta* is not needed outside the ISC for EC differentiation, consistent with the rapid down-regulation of Delta protein levels in ISC daughter cells. In contrast, clones mutant for a null allele of *Serrate* (Ser^{RX106}), encoding the other major Notch ligand, showed wild-type development (Fig. 2E). These experiments show that a Delta signal from the ISC is functionally required for daughter cells to exit the mitotic cell cycle and differentiate into ECs.

Other Notch pathway genes were removed in MARCM clones within ISCs to further analyze ISC signaling. *Neuralized* (*neu*) encodes an E3 ubiquitin ligase that is required in signaling cells for Delta endocytosis and activation (*19*). ISC clones of *neu* generated tumors mosaic for Prospero expression (Fig. 2F, arrow) or else single ECs (Fig. 2I, arrowheads), the expected result for a gene required in the ISC (Fig. 2A). Moreover, Delta protein in such tumors was predominantly adjacent to the plasma membrane (Fig. 2G), consistent with the known requirement for *neu* in Delta endocytosis (*19*, *20*). Loss of *Notch* (*N*) ISC clones, the direct or indirect target of the canonical Notch signaling pathway (*21*), also generated tumors mosaic for Prospero (Fig. 2J). The exceptions of no signaling consequences (about half of *N* clones) produced single ECs. As for *Notch* ISC clones, the *Notch* ISC clones that contained only tumors, indicating that these genes are required in the EB (Fig. 2L). Tumor cells lacking Prospero contained high levels of Delta (Fig. 2, J and K), which supports the idea that they are stem cell–like. Prospero-expressing tumor cells contained very little Delta (Fig. 2, G and L). Thus, ISC signaling does not direct EC daughters via the canonical Notch pathway.

The striking asymmetry in Delta content between ISCs and their pre-EC daughters must arise by asymmetric Delta segregation. To address this, we identified mitotic ISCs at various stages by staining with Armadillo and analyzed the distribution of Delta between the daughter cells. Similar amounts of Delta vesicles were observed in both cells of newly forming ISC and the cleavage furrow in telophase (Fig. 3A). However, in cell pairs that had just completed mitosis, as evidenced by the exclusion of Armadillo from daughter cell nuclei, Delta-rich vesicles persisted in the ISC near the former cleavage furrow, whereas they were distant from the furrow and weaker in the EB (Fig. 3B). These observations show that Delta asymmetry does not arise simply by differential segregation of Delta vesicles at cell division. Delta appears to be rapidly down-regulated in the EB after mitosis.

To investigate the mechanism of ISC multipotency, we first considered a role for mitotic spindle orientation. Mitotic chromosomes were stained with anti–phosphohistone H3 and centrosomes with anti–γ-tubulin (Fig. 3, C and D), and cells were analyzed in 3D reconstructions to determine the angle (θ) between the spindle and the basement membrane. These experiments revealed that ISCs divide nearly randomly with respect to the basement membrane, with values of θ ranging between 3° and 47° (mean = 29° ± 14°, $N = 50$). Using cytoplasmic markers, we found that the ISC (Fig. 3E) rarely contains a much greater surface area of contact with the basement membrane than does its daughter (Fig. 3, E and F), and consequently as a result of this divisional orientation. Division away from the basement membrane also explains why the nucleus of the ISC was previously observed to be more basally than other cell nuclei (*17*). No correlation between spindle orientation and daughter cell fate was discovered, however.

We next considered whether Notch signal reception might differ in EBs fated to become ECs and neuroblast/enteroblast cells. We generated marked ISC clones of two cells and stained them for Prospero and Delta (Fig. 4). The ISC in these clones could be determined by its basal location, as the daughter of its last mitosis. These data, in turn, could be used to infer whether two-cell clones (respectively) could be assigned on the basis of Prospero expression. ISCs that last produced pre-EC invariably expressed Delta in cytoplasmic vesicles, usually at high levels (Fig. 4A, $N = 100$). In striking contrast, ISCs that last produced a progenitor contained few or no cytoplasmic Delta vesicles (Fig. 4, B to D, $N = 50$). This was true for ISCs that had just switched from EC to EE production (Fig. 4D), as well as those that had just completed a second consecutive EC (Fig. 4C). In D. melanogaster, production of exactly two EE daughters appears to be rare, as we observed no counterexamples in these

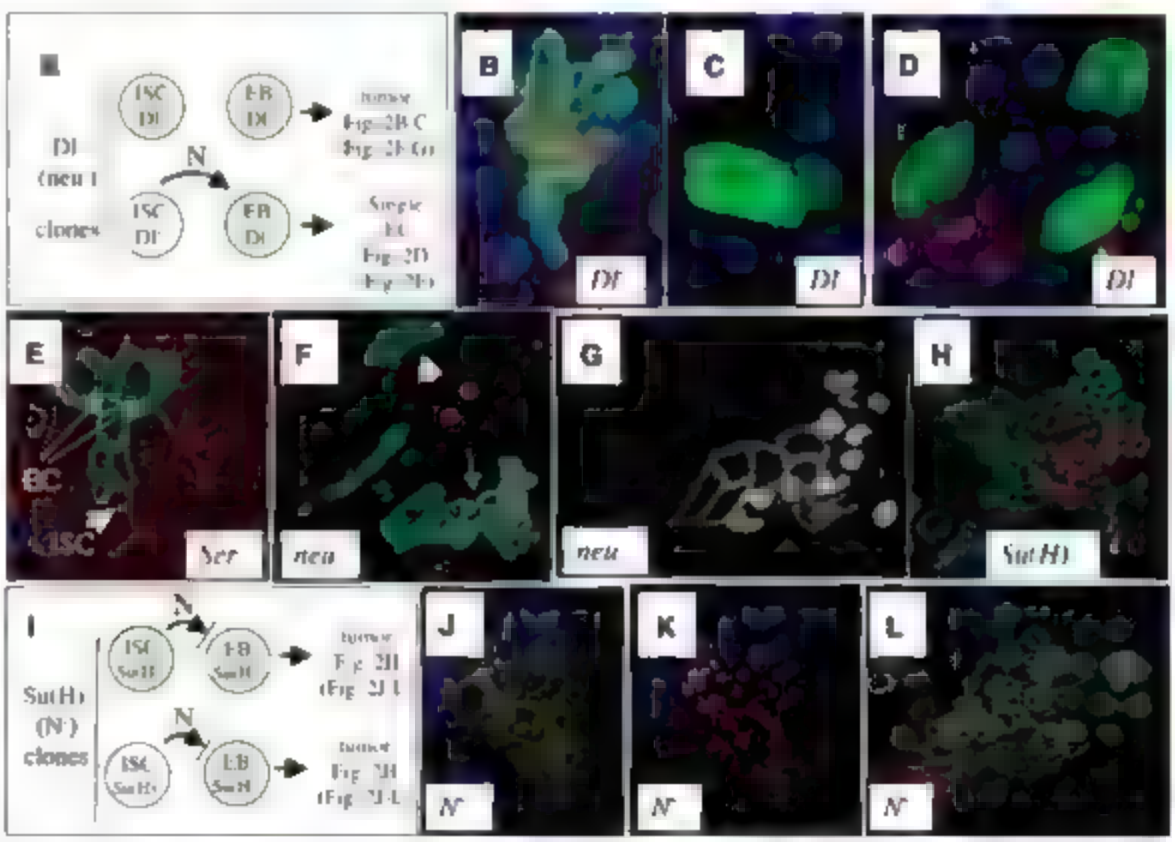

Fig. 2. Asymmetric Delta signaling from ISC to EB is functionally required for EC production and mitotic cell cycle exit. (**A**) Expected outcomes of ISC clones (green) lacking *Dl* (or *neu*). Notch signal (N) is shown by an arrow. Four-day ISC clones (green) of Dl^{rev10} generate (**B**) a tumor mosaic for Prospero (red), (**C**) a tumor plus a single EC, or (**D**) single ECs. (**E**) Four-day clone (green) of the $Serrate^{RX106}$ null allele showing normal ISC (arrowhead) and EC production (arrows). Armadillo (red) highlights cell boundaries. (**F**) Seven-day ISC clones (green) of neu^{3} form tumors (arrow) mosaic for Prospero expression (red, nuclear), or single mature ECs (arrowhead). Delta (red, cytoplasmic). (**G**) The red channel from (F), cells lacking Prospero contain plasma-membrane Delta. Cells expressing Prospero lack Delta. (**H**) Twelve-day ISC clone (green) of the $SuH^{\Delta 47}$ null allele forms a tumor mosaic for Prospero (nuclear, red). (**I**) Expected outcomes of ISC clones (green) lacking *SuHa* (or *N*). Impaired Notch signal reception in EB is denoted by a blocked arrow. (**J**) *Notch* clone (green) not expressing Prospero (nuclear red) expresses Delta (cytoplasmic, red) like ISCs. (**K**) Delta (red) and DNA (blue) from (J). (**L**) *Notch* clone (green) expressing Prospero (nuclear, red) lacks Delta (cytoplasmic, red).

experiments. However, ISCs that had recently completed an ee pair and had just returned to EC production contained multiple Delta vesicles (fig. 4E).

These results suggested a simple model for the determination of SC daughter cell fate. Daughters of ISCs with high Delta levels would receive a strong Notch signal and become ECs. Daughters of ISCs with low or no detectable cytoplasmic Delta vesicles would receive a much weaker Notch signal and become ee cells. If Notch signaling were disrupted entirely, as in Notch null mutant clones, after one or two divisions, only ISC-like daughters would be produced. Neither ee precursors nor ISC-like cells would cease division when Notch signaling is impaired. We tested this model by expressing an activated Notch receptor (N^{act}) in MARCM SC clones (fig. 4F). N^{act}-expressing cells would should contain high level of Notch signaling all because ECs (fig. 4F). In addition, none of these clones grew above two cells in size, which shows that Notch activation within the SC is sufficient to force its differentiation as an EC.

These experiments provide insight into several long-standing issues in stem cell biology. First, they illustrate that highly specific stem cell markers can be obtained, at least for a particular stem cell under particular conditions. Vertebrate ISCs cannot currently be identified with certainty (reviewed in (20)), but Notch signaling is similarly involved in secretory cell versus EC production. Consequently, it might be possible to identify vertebrate ISCs as a subpopulation of cells enriched in Notch signals within regions of the vertebrate gut that are known to contain ISCs. Second, our results suggest how stem cell activity may be coordinated with tissue requirements (fig. S1A). Local feedback signals from existing ee cells and other cells may influence an SC's Notch signaling capacity and hence the type of cell produced at any instant.

Drosophila neural stem cells and sensory organ precursors are predominantly specified by the asymmetric segregation of molecules that bias the subsequent transmission of Notch signals (reviewed in (21)). Differential Notch signaling requires the asymmetric endocytic trafficking of Delta and Notch after precursor cell division (reviewed in (15)). Recycling endosomes, an essential component of Notch signaling, tend to be concentrated in apical regions and have been reported to segregate differentially in *Drosophila* sensory organ precursor divisions (22). Our studies suggest that endocytic trafficking of Delta may also be involved in ISC function. We observed large Delta-rich vesicles accumulating near the apical membrane in the ISC shortly after mitosis at the division plane. Such a process might result in the inheritance of an endocytic vesicle compartment by the ISC but not its daughter, leading to differences in Delta stability between the two cells. Finally, our experiments suggest that *Drosophila* ISCs play a role different from that of stem cells in previously characterized niches. In the ovarian germline stem cell (GSC) niche (17), the GSC adheres to adjacent somatic cells at an anatomically fixed location and responds to local signals that block differentiation (fig. S3B). GSC daughters differentiate because they are moved outside this zone of maintenance. In contrast, the ISC plays an active role in signaling via Notch to induce either EC or ee differentiation. It remains to be determined whether external signals also influence

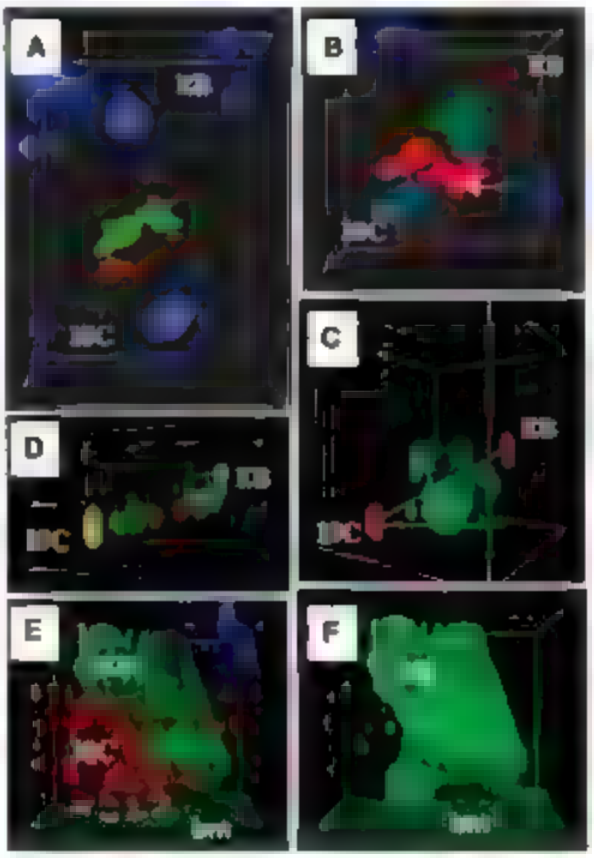

Fig. 3. Delta vesicles are distributed asymmetrically shortly after mitosis. (**A**) Equal distribution of Delta vesicles (red) during ISC anaphase. Cytokinesis furrow is shown by Anillin stain (green). (**B**) Down-regulation of Delta (red) in the newly formed EB and transient asymmetric positioning of vesicles within the ISC (arrow). Anillin (green) shows nuclei. (**C** and **D**) Mitotic ISCs in 3D reconstruction. Phosphohistone H3 (green) and γ-tubulin (red) staining define the division angle (α) relative to the basement membrane (blue and red axes). The ISC in (D) was also stained for α-tubulin (red). (**E** and **F**) An ISC-EB pair stained for Delta (red) and Notch activation reporter (green) reveals that ISCs have greater contact (dashed line) with the basement membrane (bm).

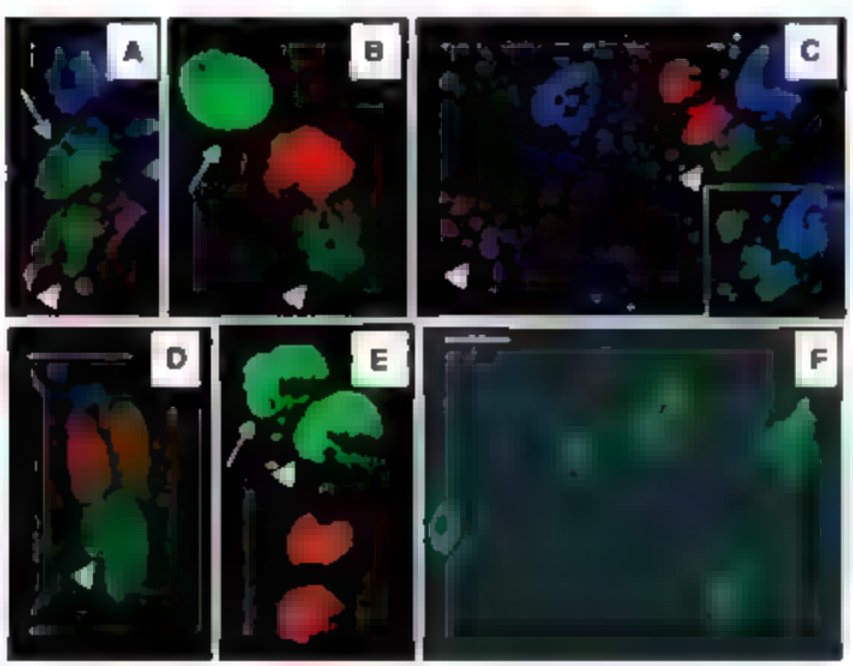

Fig. 4. (**A** to **E**) Delta expression levels in ISCs determine EC versus ee fate. Examples of two- to four-cell ISC clones (green) stained for Prospero (nuclear, red) and Delta (cytoplasmic, red) are shown. Arrowheads denote ISCs; arrows denote prospective ECs. (**A**) ISCs producing a prospective EC (Prospero absent) always express Delta. (**B**) ISCs that have just switched to ee cell (Prospero present) production express little or no Delta. (**C** and **D**) ISCs producing a second consecutive ee cell express little or no Delta. Inset: Clonal marker for (C). (**E**) ISCs that have just switched from ee to EC production express Delta. (**F**) ISC clones (green) expressing N^{act} generate one or two ECs, indicating that such ISCs are not maintained. Scale bar, 20 μm.

tant in maintaining ISCs in a manner analogous to CSCs. In any case, stem cells such as ISCs, which sense local cellular requirements and produce appropriate daughter cells in response, likely play a central role in the physiology, longevity, and pathology of the tissues they maintain.

References and Notes

1. T. Nystul, A. C. Spradling, *Curr. Opin. Genet. Dev.* **16**, 463 (2006).
2. D. T. Scadden, *Nature* **441**, 1075 (2006).
3. T. Xie, A. C. Spradling, *Cell* **94**, 251 (1998).
4. T. Xie, A. C. Spradling, *Science* **290**, 328 (2000).
5. X. Song, T. Xie, *Development* **130**, 3259 (2003).
6. N. Tulina, E. Matunis, *Science* **294**, 2546 (2001).
7. A. Kiger, D. L. Jones, C. Schulz, M. B. Rogers, M. T. Fuller, *Science* **294**, 2542 (2001).
8. S. L. Crittenden, K. A. Leonhard, D. T. Byrd, J. Kimble, *Mol. Biol. Cell* **17**, 3051 (2006).
9. E. M. Cairn *et al.*, *Nature* **425**, 841 (2003).
10. J. Zhang *et al.*, *Nature* **425**, 836 (2003).
11. B. Ohlstein, A. C. Spradling, *Nature* **439**, 470 (2006).
12. C. Michelli, M. Perrimon, *Nature* **439**, 475 (2006).
13. See supporting material on *Science* Online.
14. H. Jafar-Nejad *et al.*, *Dev. Cell* **9**, 351 (2005).
15. S. Bray, *Nat. Rev. Mol. Cell Biol.* **7**, 678 (2006).
16. M. Furnols, S. Bray, *Curr. Biol.* **11**, 60 (2001).
17. P. Heitzler, P. Simpson, *Cell* **64**, 1083 (1991).
18. E. Pavlopoulos *et al.*, *Dev. Cell* **1**, 807 (2001).
19. B. Le Borgne, S. Remaud, S. Hamel, F. Schweisguth, *PLoS Biol.* **3**, e96 (2005).
20. M. Bjerknes, H. Cheng, *Am. J. Physiol.* **289**, G381 (2005).
21. R. Roegiers, Y. N. Jan, *Curr. Opin. Cell Biol.* **16**, 195 (2004).
22. A. Gromley *et al.*, *Cell* **123**, 75 (2005).

23. We thank M. Buszczak and T. Nystul for comments on the manuscript and H. Ruhoula-Baker, K. Irvine, C. Field, S. DiNardo, and I. Rebay for gifts of materials.

Supporting Online Material

www.sciencemag.org/cgi/content/full/315/5814/988/DC1

Fig. S1
References

23 October 2006; accepted 8 January 2007
10.1126/science.1136606

Polymerizing Actin Fibers Position Integrins Primed to Probe for Adhesion Sites

Catherine G. Galbraith,[1] Kenneth M. Yamada,[1]* James A. Galbraith[2]

Migrating cells extend protrusions, probing the surrounding matrix in search of permissive sites to form adhesions. We found that actin fibers polymerizing along the leading edge directed local protrusions and drove synchronous sideways movement of β_1 integrin adhesion receptors. These movements lead to the clustering and positioning of conformationally activated, but unoccupied, β_1 integrins along the leading edge of fibroblast lamellae and growth cone filopodia. Thus, rapid actin-based movement of primed integrins along the leading edge suggests a "sticky fingers" mechanism to probe for new adhesion sites and to direct migration.

The first steps of mammalian cell migration are extension of the leading edge and attachment to the surrounding extracellular matrix (*1*). Extension is driven by actin polymerization (*2*), with the position (*3*), speed, and persistence (*4*) of the leading edge regulated by actin-binding proteins. However, extension is not uniform; adjacent regions of many broad, flat protrusions such as fibroblast lamellae and neuronal growth cones advance and retract independently, and which region moves forward is constantly redefined by transverse movement (*5*, *6*). Observations on protrusion dynamics led to the hypothesis that these protrusion variations are used to search for permissive sites to form new adhesions (*7*, *8*). However, no known direct relation between protrusion dynamics and the ability of adhesion receptors to probe the matrix has been identified.

We studied protrusion dynamics during the initial matrix exploration. Using high-contrast differential interference contrast (DIC) optics, we observed small ripple protrusions traversing the outermost edges of fibroblast lamellipodia, the leading 1 to 2 μm of the lamella (Fig. 1, A and B). The ripples did not move sideways at the same speed (0.10 ± 0.06 μm/s, n = 34) that actin network treadmilling (0.028 ± 0.013 μm/s, n = 51) (*9*) moved microspikes and filopodia precursors laterally (Fig. 1D) (*10*, *11*). Instead, the ripples moved at the same speed that actin polymerization elongates growth cone filopodia (*12*) and rockets *Listeria* bacteria (*13*). Although the frequency of ripples decreased in response to the actin-depolymerizing agent cytochalasin D (Fig. 1C), the associated actin dynamics are difficult to visualize with green fluorescent protein (GFP)–actin because of the density and rapid turnover (*9*). We therefore exploited the properties of photoactivatable GFP (PaGFP) (*14*) to establish the threshold of visible actin and to restrict visualization to ~40% of the expressed PaGFP-actin (*15*). Limiting activation revealed localized increases in actin density that moved sideways with the ripples (Fig. 1D and movie S1). The increases did not represent thickness variations or membrane lifting, because they persisted after normalization by the cotransfected monomeric red fluorescent protein (mRFP) signal, and the ripples remained within a single DIC optical section (*15*). The intensity increases are local actin polymerization at crests of ripples traversing the leading edge (82% colocalization, n = 198) (Fig. 1D and movie S1) (*15*).

Restricting the region of photoactivation revealed that activated PaGFP-actin localized at the tip of a nascent ripple and accumulated along the elongating ripple (Fig. 2A). In contrast to its

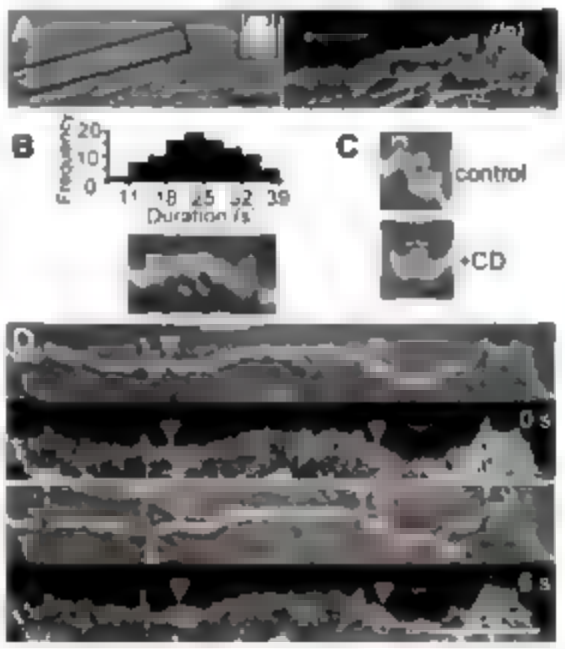

Fig. 1. Local increases in actin polymerization occur at small ripples traversing the leading edge of migratory fibroblasts. **(A)** DIC and PaGFP-actin images showing NIH3T3 fibroblast lamella (*l*) and lamellipodium (*lp*). Region of cell is shown in inset, and black box indicates region in (D). Scale bar, 5 μm. **(B)** Histogram of the ripple duration or wave period (n = 106, 21 cells) (*15*). Kymographs from DIC images show the duration of the transverse ripples (white bracket) and local forward protrusions (black bracket). Horizontal scale bar, 20 s; vertical, 0.5 μm. **(C)** Cytochalasin D (CD) decreases the frequency of the ripples. **(D)** At the tips of ripples, there are localized increases in PaGFP-actin fluorescent intensity (red arrowheads). The ripples move sideways faster than either the lateral movement of filopodia (vertical yellow arrowheads) or the rearward movement of actin (horizontal yellow arrowheads) due to lamella network treadmilling. Dashed lines mark initial positions of yellow arrowheads. Scale bar, 5 μm.

[1]National Institute of Dental and Craniofacial Research, National Institutes of Health, Bethesda, MD 20892, USA. [2]National Institute of Neurological Disorders and Stroke, National Institutes of Health, Bethesda, MD 20892, USA.

*To whom correspondence should be addressed. E-mail: kyamada@dir.nidcr.nih.gov

asymmetric accumulation of PaGFP-actin, photoactivation of PaGFP alone produced a symmetric signal that spread throughout the cell and was consistent with simple diffusion (fig. S1). We also found that the vasodilator-stimulated phosphoprotein (VASP), which protects barbed ends from capping (*6*), localized to actin elongating across the leading edge (Fig. 2B and movie S2). Thus, elongating VASP-tipped actin reshaped and redirected the larger regions of forward protrusion (movie S2). Thus, it seems that the transverse ripples represent local sites of preferential actin elongation along the edge of advancing protrusions.

To test if the localized increases in actin polymerization are involved in matrix probing, we compared them with the location of integrin adhesion receptors. Using a fluorescent, nonperturbing antibody, we observed clustering of β_1 integrins that was temporally and spatially synchronized with actin polymerization at the crests of ripples (Fig. 2, D to F, and movie S2). The β_1 integrins and actin remained colocalized during an 8-min monitoring period (correlation coefficient 0.50 ± 0.12, n = 27 five cells). In contrast, β_1 integrins did not colocalize with actin behind the leading edge (correlation coefficient 0.01 ± 0.16, n = 40 five cells) (Fig. 2, G and H, and movie S3) (*15*). Similar correlations were obtained for positive and negative controls, respectively (fig. S3). Thus, β_1 integrins move synchronously with polymerizing actin along the leading edge.

To test whether these β_1 integrins were capable of binding extracellular matrix, we examined their conformational state and found activated β_1 integrins colocalized to the tips of actin along the leading edge (correlation coefficient 0.63 ± 0.10, n = 14) (Fig. 3, A and B, figs. S2 to S5). To visualize activation and to determine where the transition to high-affinity state occurred, we developed a live-cell assay using a fluorescent antibody targeting high-affinity β_1 integrins (9EG7). We initially labeled all of the activated β_1 integrins on the cell surface so that any subsequent labeling would reveal newly activated β_1 integrins. These newly labeled integrins appeared only at the leading edge (Fig. 3C and movie S4).

The activated β_1 integrins were not localized to fibronectin but could bind fibronectin fragments (FN120kD), specifically, with the $\alpha_5\beta_1$ integrin heterodimer (Fig. 3D and fig. S2), which was consistent with an increased avidity for fibronectin at the leading edge (*16*, *17*). Although unligated high-affinity $\alpha_5\beta_1$ integrins, which can bind extracellular fibronectin, transiently localize to the edge of spreading cells (*18*), we did not find β_1 integrin localization (fig. S3) or increased fibronectin avidity at the leading edge of migrating cells (*17*–*19*). Moreover, the observed spatial correlation between high-affinity β_1 integrins and actin was not restricted to a single cell type, antibody, or extracellular matrix (Fig. 4 and fig. S3). Activated but unligated fibronectin adhesion receptors at the leading edge may thus have a direct role in sampling the extracellular matrix during migration.

We tested the functional relation between actin polymerization and activated β_1 integrins by altering actin dynamics (Fig. 4A and fig. S4). Decreasing the number of polymerizing actin ends by capping with cytochalasin D decreased the density of activated β_1 integrins, while increasing the number of polymerizing ends with the stabilizer jasplakinolide (*9*) increased the activated β_1 integrin density at the cell periphery. Moreover, increasing actin turnover without changing the number of barbed ends, with the myosin II adenosine triphosphatase (ATPase) inhibitor blebbistatin (*15*, *20*) did not change the activated β_1 integrin density. Consistent changes in activated β_1 integrin density were observed with siRNA (small interfering RNA) knockdown of the cofilin phosphatase slingshot and capping protein β_2 (fig. S4). Despite the changes in density, the correlation between activated β_1 integrins and polymerizing actin remained high (correlation coefficient 0.49 to 0.54 with no statistical difference (P > 0.05)

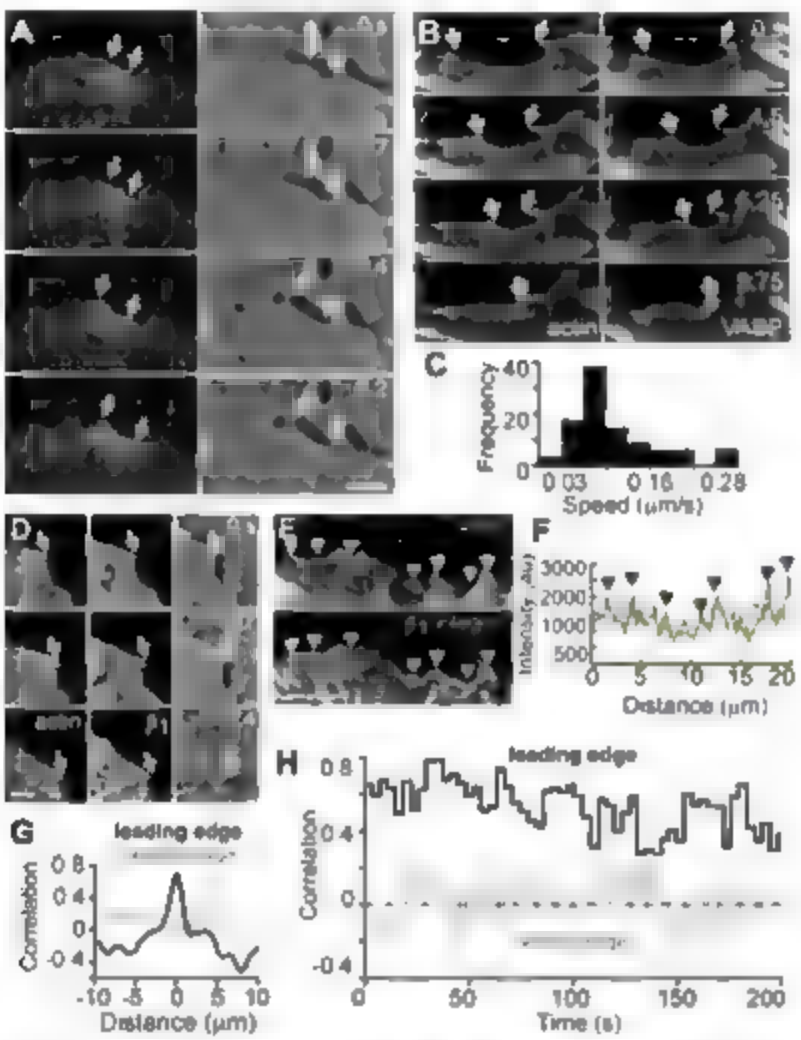

Fig. 2. β_1 Integrins move synchronously with actin polymerizing at the crests of ripples. (**A**) Activated PaGFP-actin (fluorescence) initially localizes to the tip of a nascent ripple (DIC) and accumulates along the entire ripple as it elongates. Arrows slanted toward direction of ripple movement. Scale bar, 1 μm. (**B**) VASP, which enhances actin polymerization (*4*), is localized at the tips of actin fibers elongating along the leading edge. Scale bar, 5 μm. (**C**) Histogram of ripple speed (n = 34, 27 cells). (**D**) A sequence from movie S3 shows enhanced green fluorescent protein (EGFP)–actin and β_1 integrin moving synchronously with the tip of an elongating ripple (arrows). Scale bar, 1 μm. (**E**) The first image of movie S3 shows EGFP-actin and β_1 integrins have corresponding increases in intensity. The yellow contour indicates the single-pixel-wide line used to obtain the intensity traces shown in (F). Scale bar, 5 μm. (**F**) Fluorescent intensity of EGFP-actin (red) and β_1 integrin (green) for image in (E); arrowheads correspond to those in (E). (**G**) Cross-correlation analysis shows a strong correlation between the intensity traces of EGFP-actin and β_1 integrin at the edge and essentially no correlation behind the edge. (**H**) A high correlation between EGFP-actin and β_1 integrins is maintained along a 20 μm length of the leading edge throughout the 8-min monitoring period (correlation coefficient 0.53 ± 0.13 at the leading edge, n = 54, and 0.01 ± 0.14 behind the lamellipodia in a region devoid of adhesive contacts, n = 54). (A to C) are NIH3T3 cells and (D to H) are human foreskin fibroblasts.

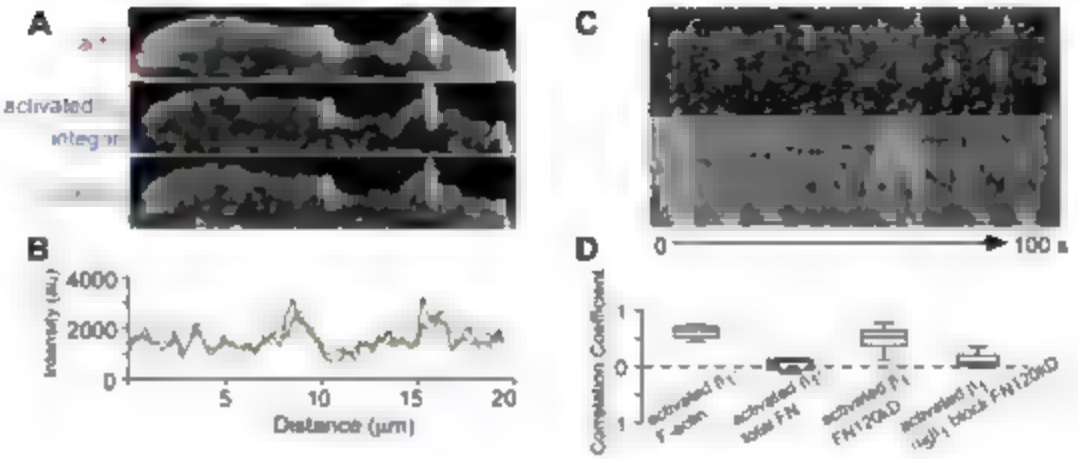

Fig. 3. Activated but unligated β_1 integrins are located at the tips of actin fibers at the leading edge. (**A**) Conformationally activated β_1 integrins are spatially concentrated at the tips of polymerizing actin at the leading edge of human foreskin fibroblasts. Scale bar, 5 μm. (**B**) Fluorescent intensity of F-actin (red), activated β_1 integrin (blue), and total (active + inactive) β_1 integrin (green) along the yellow line in (A). In this example, the correlation coefficient is 0.69 between total β_1 integrin and F-actin, and 0.75 between activated β_1 integrin and F-actin. The average correlation coefficients for multiple cells are shown in fig. S3 and Fig. 2D (n = 14). Total and active integrin distributions are compared in fig. S2D. Scale bar, 5 μm. (**C**) Sequential fluorescent (top) and DIC (bottom) images showing the activation of β_1 integrins on NIH3T3 cells. Different color arrowheads differentiate individual activation-specific antibody binding sites at the leading edge that subsequently move rearward. Vertical scale bar, 2 μm. (**D**) Boxplot shows activated β_1 integrins do not cross-correlate with endogenous fibronectin (n = 8) but do correlate with added FN120kD (n = 17) and can be blocked by inhibitory antibodies (n = 8) ($P < 0.001$).

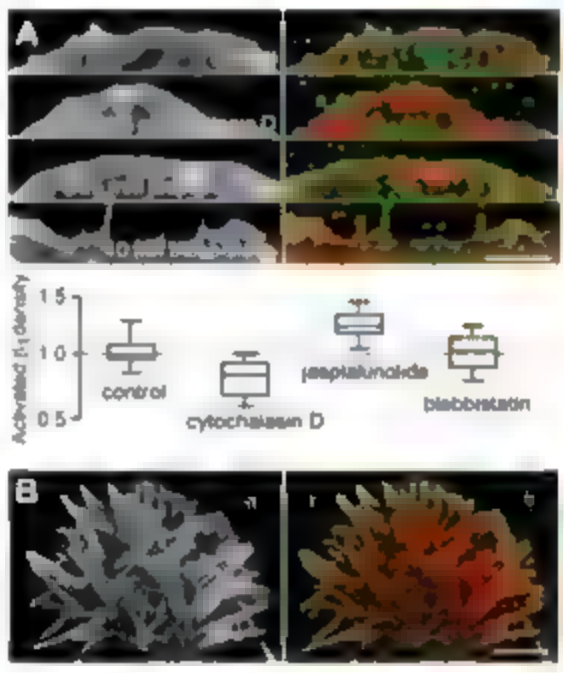

Fig. 4. Localization of activated β_1 integrins at the leading edge depends on availability of polymerizing actin ends. (**A**) NIH3T3 cells stained for activated β_1 integrins (green) and F-actin (red and grayscale) show a decrease in activated β_1 integrin density when actin is capped (cytochalasin D, n = 19) and an increase when actin is stabilized to increase the number of free ends (jasplakinolide, n = 22). Inhibiting myosin II ATPase (blebbistatin, n = 18) did not change the number of actin ends or the integrin concentration. Scale bar, 5 μm. Boxplot of activated β_1 integrin density normalized to control (n = 27). (**B**) Activated β_1 integrins are also localized to the tips of polymerizing growth cone filopodia (NG108 cells). Scale bar, 5 μm.

between cytochalasin D (n = 23), jasplakinolide (n = 27), blebbistatin (n = 34), and control (n = 25)] (*15*). The changes in activated β_1 integrin density thus correspond to the number of polymerizing actin ends.

To further test whether β_1 integrins interact with polymerizing actin, we demembranated cells with Triton X-100 to remove the cell membrane and membrane-associated proteins but leave behind the cytoskeleton and cytoskeletally associated proteins (*15*). Activated β_1 integrins quantitatively colocalized with the tips of polymerizing actin at the leading edge in the demembranated cells (fig. S5A). The leading edge localization of activated and total β_1 integrins was decreased by siRNA knockdown of talin 1, a direct physical linker between actin and β_1 integrins (*27*) that is associated with tips of actin fibers along the leading edge (*22*). Although the localization was not changed by knockdown of α-actinin 1, another direct linker (*24*) that is not similarly concentrated along the leading edge (fig. S5C), these data suggest that talin contributes to the linkage between β_1 integrins and polymerizing actin at the leading edge.

We also found activated β_1 integrins localized at the tips of growth cone filopodia (Fig. 4B). Growth cones guide migration by sampling the matrix for ligands and adhesiveness (*28*), and their actin-based filopodia are necessary for correct steering (*29*). The localization of activated β_1 integrins at filopodia tips suggests a role in growth cone path-finding. Additionally, we tested whether the activated adhesion receptors at the cell perimeter regulated migration force to match matrix stiffness by using an optical trap assay (*17*, *24*, *26*). We found connections formed between fibronectin and the adhesion receptors at ruffle protrusions were more likely to regulate migration force (85%, n = 13) than connections formed at other regions along the leading edge (25%, n = 12). This suggests that activated β_1 integrins are localized at the ends of actin fibers to probe for ligands, to guide migration direction, and to regulate migration force.

Polymerization of actin fibers directs the movement of a variety of protrusions ranging from rocketing *Listeria* (*27*) to elongating filopodia (*12*). Our data indicate that preferential localized polymerization and elongation of actin filaments or fibers along the leading edge steer local forward protrusions. The polymerization-directed and clustered β_1 integrins so spatially position integrins primed to probe the matrix at the very front of cell protrusions, creating "sticky fingers" along the leading edge. Transverse variations in actin polymerization along the advancing perimeter allow the primed integrin receptors to sample more of the extracellular matrix than simple forward and backward movement. This might allow cells with well-developed adhesive contacts to make small changes in migration direction without severing and reestablishing their matrix connections under the cell body. Thus the extended dynamic localizations in actin polymerization probe the matrix for adhesion sites by positioning primed adhesion receptors along the advancing cell perimeter during migration.

References and Notes

1. A. J. Ridley *et al.*, *Science* **302**, 1704 (2003).
2. T. D. Pollard, G. G. Borisy, *Cell* **112**, 453 (2003).
3. M. Ghosh *et al.*, *Science* **304**, 743 (2004).
4. J. E. Bear *et al.*, *Cell* **109**, 509 (2002).
5. M. Abercrombie, J. E. Heaysman, S. M. Pegrum, *Exp. Cell Res.* **59**, 393 (1970).
6. M. Machacek, G. Danuser, *Biophys. J.* **90**, 1439 (2006).
7. M. Abercrombie, J. E. Heaysman, S. M. Pegrum, *Exp. Cell Res.* **62**, 389 (1970).

8. G. Giannone *et al.*, *Cell* **116**, 431 (2004).
9. N. Watanabe, T. Hutchison, *Science* **295**, 1083 (2002).
10. G. Danuser, R. Oldenbourg, *Biophys. J.* **79**, 191 (2000).
11. T. M. Svitkina *et al.*, *J. Cell Biol.* **160**, 409 (2003).
12. A. Matlavarapu, T. Hutchison, *J. Cell Biol.* **146**, 1097 (1999).
13. J. A. Theriot, T. J. Mitchison, L. G. Tilney, D. A. Portnoy, *Nature* **357**, 257 (1992).
14. G. H. Patterson, J. Lippincott-Schwartz, *Science* **297**, 1873 (2002).
15. Materials and methods are available as supporting material on Science Online.
16. T. Nishizaka, Q. Shi, M. P. Sheetz, *Proc. Natl. Acad. Sci. U.S.A.* **97**, 692 (2000).
17. C. G. Galbraith, K. M. Yamada, M. P. Sheetz, *J. Cell Biol.* **159**, 695 (2002).
18. W. B. Kiosses, S. J. Shattil, N. Pampori, M. A. Schwartz, *Nat. Cell Biol.* **3**, 316 (2001).
19. D. P. Felsenfeld, P. L. Schwartzberg, A. Venegas, R. Tse, M. P. Sheetz, *Nat. Cell Biol.* **1**, 200 (1999).
20. M. A. Medeiros, D. T. Burnette, P. Forscher, *Nat. Cell Biol.* **8**, 215 (2006).
21. A. Horwitz, K. Duggan, C. Buck, M. C. Beckerle, K. Burridge, *Nature* **320**, 531 (1986).
22. J. A. DePasquale, C. S. Izzard, *J. Cell Biol.* **113**, 1351 (1991).
23. C. A. Otey, F. M. Pavalko, K. Burridge, *J. Cell Biol.* **111**, 721 (1990).
24. D. M. Suter, P. Forscher, *J. Cell Biol.* **155**, 427 (2001).
25. D. Bentley, A. Toroian-Raymond, *Nature* **323**, 712 (1986).
26. D. Choquet, D. P. Felsenfeld, M. P. Sheetz, *Cell* **88**, 39 (1997).
27. T. P. Loisel, R. Boujemaa, D. Pantaloni, M. F. Carlier, *Nature* **401**, 613 (1999).
28. We thank E. Smith and T. Reese for suggestions on the experiments and manuscript and M. Sheetz for use of optical trap data collected by C.G.G. while in his laboratory. For use of the laser scanning microscopes, we thank the National Institute of Neurological Disorders and Stroke (NINDS) Light Imaging Facility for the LSM 510 (VIS/MOS) and Carl Zeiss, Inc., for the LSM 5 LIVE and LSM 5 DUO. We also thank Z. Iwinski for confocal software; E. Shumsky, R. Engelmann, and S. Tille for assistance; G. Patterson and J. Lippincott-Schwartz for PaGFP and discussions; and M. Hoffman for assistance with reverse transcription-polymerase chain reaction studies. Reagents provided by R. Tsien (mRFP), J. Wehland (EGFP-VASP), and S. Yamada (human foreskin fibroblasts). Support provided by the intramural research program of NINDS and National Institute of Dental and Craniofacial Research, NIH.

Supporting Online Material
www.sciencemag.org/cgi/content/full/315/5814/992/DC1
Materials and Methods
Figs. S1 to S5
References
Movies S1 to S4

2 November 2006; accepted 5 January 2007
10.1126/science.1137904

Maplike Representation of Celestial *E*-Vector Orientations in the Brain of an Insect

Stanley Heinze and Uwe Homberg*

For many insects, the polarization pattern of the blue sky serves as a compass cue for spatial navigation. *E*-vector orientations are detected by photoreceptors in a dorsal rim area of the eye. Polarized-light signals from both eyes are finally integrated in the central complex, a brain area consisting of two subunits, the protocerebral bridge and the central body. Here we show that a topographic representation of zenithal *E*-vector orientations underlies the columnar organization of the protocerebral bridge in a locust. The maplike arrangement is highly suited to signal head orientation under the open sky.

Many animals, including birds, fishes, cephalopods, and insects, share the ability to perceive linearly polarized light (*1*, *2*). The plane of polarization (*E*-vector) varies systematically across the blue sky and depends on the Sun's position. For a variety of insects this pattern has been shown to guide spatial orientation (*2*). In locusts, polarotactic orientation depends on a specialized part of the compound eye, the dorsal rim area (*3*), and involves several central processing stages, including the central complex (*4*–*7*). The central complex (CC) is a group of neuropils spanning the midline of the insect brain. Substructures are the protocerebral bridge (PB) and the upper and lower divisions of the central body. An outstanding anatomical feature of the CC is its regular and highly sophisticated internal neuroarchitecture (*8*–*10*). In simplified terms, it consists of stacks of arrays, each composed of a linear arrangement of 16 columns with topographic interhemispheric connections between columns both within and between different arrays. Hypotheses on the functional roles of the CC range from a control center for motor coordination (*11*) to a recently demonstrated involvement in visual pattern learning and recognition (*12*). In the locust, several cell types of the CC are sensitive to the orientation of zenithal *E*-vectors (*5*), but the correspondence of cell morphology and *E*-vector tuning has remained obscure. In this study, we have used intracellular recordings combined with dye injections to analyze *E*-vector coding in CC neurons of the locust with columnar arborization domains.

Two major classes of polarization-sensitive (POL) neurons were encountered regularly when we recorded from CC neurons: (i) a particular type of tangential neuron of the PB and (ii) several types of columnar neurons. Tangential neurons of the PB, termed here TB1 neurons, have not been described previously in the locust or any other insect. A total number of 18 of these cells were analyzed. Their morphology was revealed by iontophoretic tracer injection, histological processing, and camera lucida reconstruction (*13*). TB1 neurons provide a connection between a posterior brain region, the posterior optic tubercle, and the PB (Fig. 1, A and B). Each TB1 neuron had two domains of varicose and, thus, putatively presynaptic arborizations confined to a single column in each hemisphere of the PB. When PB columns are numbered as L1 (lateralmost column in the left hemisphere of the PB) to L8 (most medial column in the left hemisphere) and, accordingly, from R1 to R8 in the right hemisphere of the bridge, TB1 neurons with varicose ramifications in columns R1 L8, R2 L7, R4 L5, R5 L4, R6 L3, and R7 L2 were encountered. Varicose processes were always eight columns apart, with processes positioned symmetrically in one of the four outer columns and contralaterally in one of the four inner columns (Fig. 1, B to D). The columns neighboring those with varicose processes were free of ramifications, and six to eight other columns were invaded with fine, smooth arborizations. Furthermore, all TB1 neurons had varicose arborizations in the posterior optic tubercle, a brain area connected to a small neuropil in the optic lobe, the accessory medulla (*14*).

The pattern of varicose arborizations in the PB corresponded to physiological properties of the TB1 neurons. For intracellular recordings, the animals were fixed in the recording setup and stimulated from the zenith with a rotating *E*-vector. Recordings were obtained from their main neurite in the PB. Each TB1 neuron showed polarization opponency, i.e., *E*-vector orientations leading to an increase in spiking activity (excitation) were oriented perpendicularly to *E*-vectors leading to a decrease in spiking activity (inhibition) (Fig. 1, C and D). The *E*-vector tuning (*E*-vector orientation resulting in maximum excitation, Φ_{max}) was determined for each neuron by circular statistics [Rayleigh test (*15*)]. *E*-vector tuning of TB1 neurons showed a linear relation to the position of their varicose ramifications in the PB (Fig. 1F). Thereby, a range of Φ_{max} tunings of 182° ± 71° extends through the eight columns of each hemisphere of the PB and, thus, corresponds to the whole range of possibly occurring *E*-vector orientations.

Because the *E*-vector map in the PB corresponds with the proposed output regions of the TB1 neurons, we asked whether candidate postsynaptic neurons show a similar representation of *E*-vector tuning. Columnar neurons have ar-

Animal Physiology, Department of Biology, Philipps University, 35032 Marburg, Germany.
*To whom correspondence should be addressed. E-mail: homberg@staff.uni-marburg.de

borizations in single columns of the PB and send axonal projections to an area outside the CC, the lateral accessory lobe (LAL). Several cell types have additional arborizations in distinct columns of the central body. Three types of these neurons are polarization-sensitive (Fig. 2). We evaluated the data from 19 recordings from these cell types, termed CPU1, CP1, and CP2 neurons. CPU1 neurons have smooth endings in single columns of the PB, in columns of the dorsalmost layer 1 of the upper division of the central body (CBU), and an axonal fiber with varicose endings in the LAL (Fig. 2A). Each neuron connects a single column of the PB with two neighboring columns of the CBU, following a wiring scheme described for *Drosophila* (9) (Fig. 2G). All CPU1 neurons (10 recordings) showed polarization opponency and background spiking activity of 20 to 40 Hz. Comparison of the innervated columns in the PB and Φ_{max} tuning again revealed a spatial representation of *E*-vector orientations across the PB, which covered a range of 228° ± 73° through the 8 PB columns in one brain hemisphere (Fig. 2I). The slope of the regression lines of TB1 and CPU1 neurons did not differ significantly ($P = 0.32$, analysis of covariance (*14*)), indicating that the tuning range through the 16 columns of the bridge matched for both cell types. However, the CPU1 map was shifted by 101° (equivalent to −79°) relative to the map of TB1 neurons (significantly different elevation of regression lines, $P < 0.00001$).

The remaining two types of columnar neurons, CP1 and CP2 neurons, also connected the PB with the LAL (Fig. 2, B, C, and H), but lacked arborizations in the central body. Within the LAL, projections were confined to either of two subcompartments, the medial olive (CP1) or the lateral triangle (CP2). Both types of neuron had smooth arborizations in the PB and varicose endings in the LAL. In all recordings ($n = 9$), CP1 and CP2 neurons showed polarization opponency, but had lower background activity (3 to 15 Hz) than CPU1 and TB1 neurons. As for CPU1 and TB1 neurons, regression analysis of pooled data from CP1 and CP2 neurons revealed a linear correlation between the innervated column in the PB and the *E*-vector tuning of the neurons (Fig. 2J). The linear regression for CP1 and CP2 covered a range of 206° ± 76° over one hemisphere (eight columns) of the PB and was not significantly different from the linear regressions for CPU1 neurons (slope: $P = 0.4777$, elevation: $P = 0.3525$). It was, however, phase shifted by 111° (equivalent to −69°) against the map of TB1 neurons.

The present study shows, independently for three different cell types, that a map of zenithal *E*-vector orientations underlies the columnar organization of the locust PB. This spatial representation adds a level of complexity to sensory processing in the insect brain, hitherto thought to be achieved only in vertebrates. In most neurons, a change in activity occurs over an *E*-vector orientation range of about 60°, implying considerable overlap for neighboring columns and the necessity of a population code for retrieving exact information from the firing rates of these cells (*7*).

Under the open sky, the activity in the POL neurons described here is directly related to the directional orientation of the locust's head, provided that additional mechanisms (color coding, intensity coding) allow the animal to distinguish the solar from the antisolar hemisphere of the sky. Color-coding properties suited to fulfill this requirement have been demonstrated recently for POL neurons at an input stage to the CX, the anterior optic tubercle (*18*). Neurons encoding head direction have been intensely studied in mammals (*19*, *20*). An important difference of the locust polarization analyzers in the CX is their global nature of signaling. The neurons fire according to zenithal *E*-vectors, which provide information about the Sun's azimuth and, therefore, these neurons behave like an internal 180° compass. In rats, in contrast, head-direction cells are recalibrated to visual landmarks in each new environment and are apparently not arranged topographically (*21*, *22*).

Although some progress has been made in analyzing the wiring principles from which computational maps arise in vertebrates (*23*, *24*), the simple brains of locusts offer the opportunity to address this question at the level of single identified neurons. Within the PB, the spatial maps of tangential and columnar neurons are out of phase by about 90°. If TB1 neurons are directly connected to the columnar neurons, a phase shift of 90° might most easily result from inhibitory connections of TB1 neurons to the dendritic

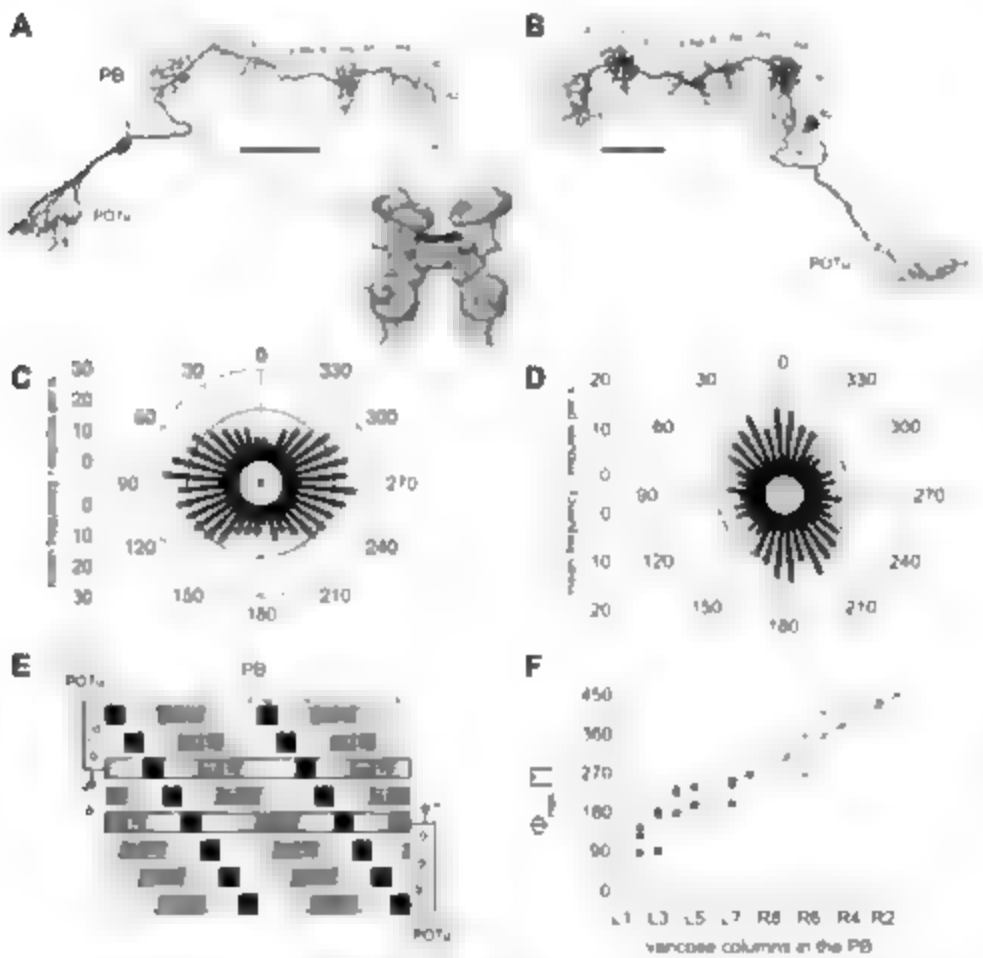

Fig. 1. Morphological and physiological properties of TB1 neurons. (**A** and **B**) Frontal reconstructions of two TB1 neurons, inset shows frontal view of the locust midbrain. Scale bars, 100 μm. (**C** and **D**) Circular plots of mean firing rate during *E*-vector rotations for the neuron in (A) [(C) and (B) (D); $n = 4$, bin width 10°, error bars, SD]. Solid lines indicate background activity. (**E**) Wiring scheme of the TB1 neuron system. Each line represents one TB1 neuron in the PB (black squares, columns with varicose arborizations; gray squares, columns with smooth arborizations; white squares, columns without arborizations). Asterisks indicate TB1 neurons shown in (A) and (B). (**F**) Correlation between location of varicose columns in the PB and *E*-vector tuning (Φ_{max}) of TB1 neurons ($n = 18$). Because each neuron has varicose arborizations in single columns in the right and left PB hemisphere, Φ_{max} values were plotted twice for the right hemisphere (open circles) and the left hemisphere (filled circles). Linear regression shows significant correlation ($r = 0.81$, SD = 35.8°, $P < 0.0001$, two-tailed *t* test, $y = 24.2x + 77.0$). Also shown are 95% confidence bands (*13*). AL, antennal lobe; CC, central complex; MB, mushroom body; PB, protocerebral bridge; POTu, posterior optic tubercle.

trees of columnar neurons. Double-labeling experiments showed that serotonin and a Dip-allatostatin related neuropeptide are present in TB1 neurons (fig. S5). For both substances, inhibitory effects have been demonstrated in other systems (75, 76). Whereas azimuthal space is linearly represented in the columns of the PB, the wiring of CPU1 neurons should result in a superposition of the two 180° representations of the PB in the CBL, but with a lateral shift of about 90° (fig. S3). The functional consequences of this shift are presently unknown. If the *E*-vector tunings of corresponding CPU1 neurons in each of the eight double columns of the CBL are merged, the azimuth representation would be reduced to only about 156° of frontal space.

On the basis of the data presented here and a recent paper by Liu *et al.* (*12*), a coherent functional role for the CC is emerging. In *Drosophila*, tangential neurons innervating specific layers of the central body are essential for recognizing features of visual objects (elevation in the panorama, contour orientation). Columnar neurons, like the CPU1 neurons, are ideal candidates to associate these visual features with information on their azimuthal direction (fig. S4). Liu *et al.* (*12*) already hypothesized that the width of the CBL represents azimuthal space. This is strongly supported by our data, but this representation may differ between cell types and CC substructures as pointed out above.

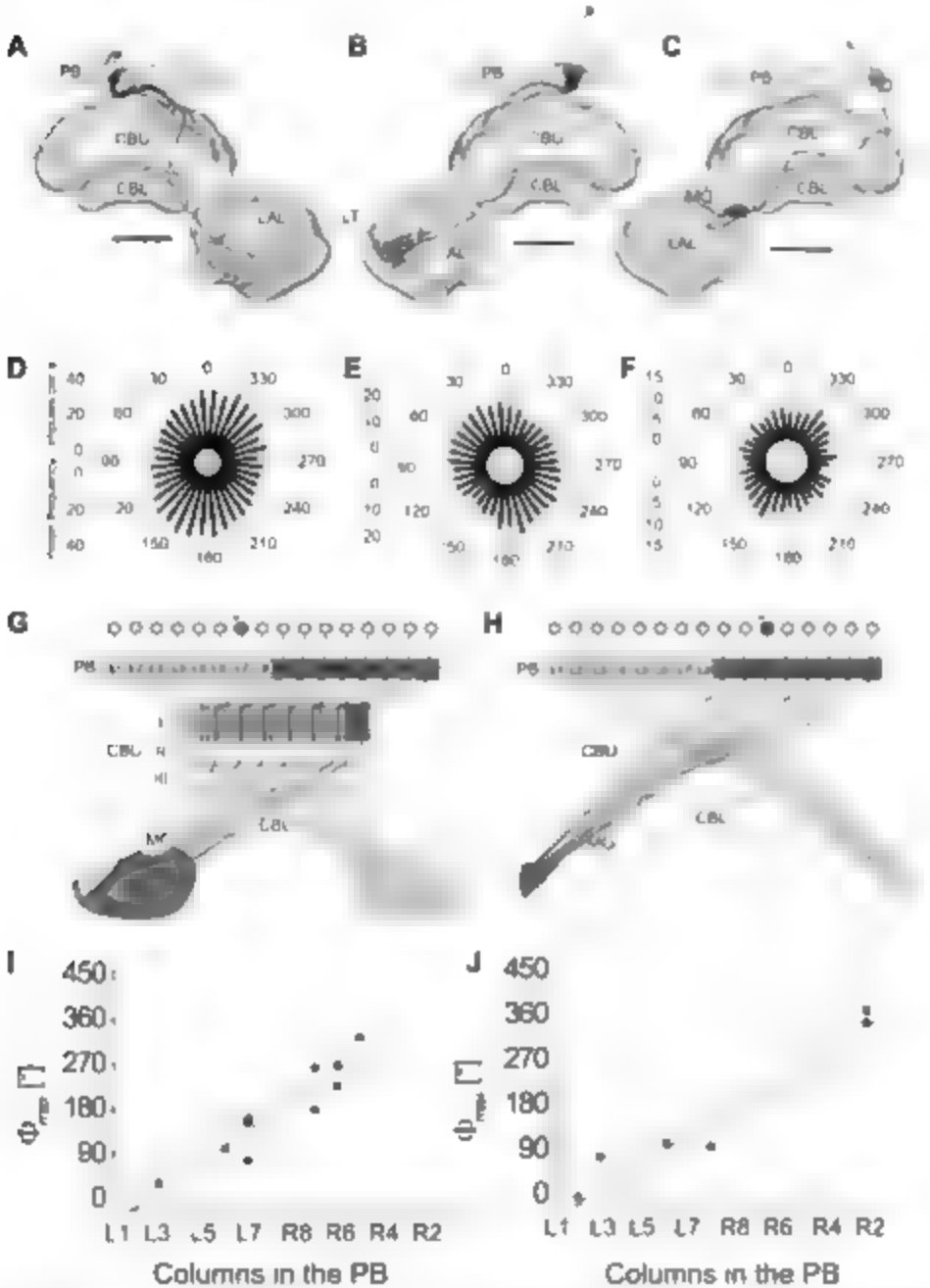

Fig. 2 Morphology and physiology of columnar neurons. (**A** to **C**) Camera lucida drawings of a CPU1 neuron (A), CP2 neuron (B), and CP1 neuron (C) projected onto three-dimensional reconstructions of the central complex. Scale bars, 100 μm. (**D** to **F**) Circular plots of mean firing rate during *E*-vector rotations for the neurons shown in (A) to (C) (n = 4, bin width 10°, error bars, SD). (**G** and **H**) Wiring schemes of the CPU1 neuron system and the CP2 neuron system. Asterisks indicate the CPU1 neuron shown in (A) (G) and the CP2 neuron shown in (B) (H). The CP1 neuron system (not shown) projects to the MO but is otherwise identical to the CP2 system. (**I** and **J**) Linear correlation between the location of the columnar arborization domain in the PB and the *E*-vector tuning (Φ_{max}) of columnar neurons. (I) CPU1 neurons (r = 0.93, SD = 36.5°, P = 0.0001, two-tailed t test, y = 30.4x − 76.2). Midline crossing occurs at 182°. (J) CP1 neurons (open circles) and CP2 neurons (filled circles) have been combined for statistical analysis (r = 0.97, SD = 38.0°, P < 0.0001, two-tailed t test, y = 27.4x − 61.8). Midline crossing occurs at 171°. Confidence bands are shown at 95%. CBL, CBU, lower and upper divisions of the central body; LAL, lateral accessory lobe; LT, lateral triangle; MO, median olive; PB, protocerebral bridge.

References and Notes

1. R. Wehner, *J. Exp. Biol.* **204**, 2589 (2001).
2. G. Horváth, D. Varjú, *Polarized Light in Animal Vision. Polarization Patterns in Nature* (Springer, Berlin, 2004).
3. M. Mappes, U. Homberg, *J. Comp. Physiol. A* **190**, 61 (2004).
4. M. Mappes, U. Homberg, *J. Comp. Physiol. A* **193**, 43 (2007).
5. M. Vitzthum, M. Müller, U. Homberg, *J. Neurocyt.* **32**, 1114 (2003).
6. U. Homberg, S. Hofer, K. Pfeiffer, S. Gebhardt, *J. Comp. Neurol.* **462**, 415 (2003).
7. K. Pfeiffer, M. Kinoshita, U. Homberg, *J. Neurophysiol.* **94**, 3903 (2005).
8. J. L. O. Williams, *J. Zool. London* **176**, 67 (1975).
9. U. Hanesch, K. F. Fischbach, M. Heisenberg, *Cell Tissue Res.* **257**, 343 (1989).
10. M. Müller, U. Homberg, A. Kühn, *Cell Tissue Res.* **288**, 159 (1997).
11. R. Strauss, *Curr. Opin. Neurobiol.* **12**, 633 (2002).
12. G. Liu *et al.*, *Nature* **439**, 551 (2006).
13. Material and methods are available as supporting material on *Science* Online.
14. U. Homberg, S. Würden, *J. Comp. Neurol.* **384**, 329 (1997).
15. E. Batschelet, *Circular Statistics in Biology* (Academic Press, London, 1981).
16. J. Zar, *Biostatistical Analysis* (Prentice-Hall, Englewood Cliffs, NJ, 1999).
17. E. I. Knudsen, S. du Lac, S. Esterly, *Annu. Rev. Neurosci.* **10**, 41 (1987).
18. K. Pfeiffer, M. Kinoshita, U. Homberg, *Proceedings of the 6th Meeting of the German Neuroscience Society* www.neuroanatomie.uni-goettingen.de/neurobio_archiv/2005/pdf/Proceedings-Goettingen-005.pdf, p. 248.
19. P. E. Sharp, H. T. Blair, D. Cho, *Trends Neurosci.* **24**, 289 (2001).
20. J. S. Taube, J. P. Bassett, *Cereb. Cortex* **13**, 1162 (2003).
21. F. Sargolini *et al.*, *Science* **312**, 758 (2006).
22. H. Mittelstaedt, *Biol. Cybern.* **83**, 261 (2000).
23. N. J. Chisum, D. Fitzpatrick, *Neural Netw.* **17**, 681 (2004).
24. E. Moser, W. H. Backhaus, D. Fitzpatrick, *Nat. Neurosci.* **7**, 87 (2004).
25. W. Bienau, A. Baumann, *Arch. Insect Biochem. Physiol.* **48**, 1 (2001).
26. E. M. Tan *et al.*, *Neuron* **51**, 157 (2006).

27. We thank S. Gebhardt, S. Gotthardt, K. Pfeiffer, and H. Vitzthum for contributing physiological data, K. Pfeiffer for help with data evaluation, A. Kurylas for providing three-dimensional reconstructions of brain structures, and E. Buchner for providing the antibody to synapsin. This work was supported by the Deutsche Forschungsgemeinschaft (grants HO 950/14-3 and HO 950/16-1).

Supporting Online Material

www.sciencemag.org/cgi/content/full/315/5814/995/DC1

Figs. S1 to S5

References

25 September 2006; accepted 4 January 2007

10.1126/science.1135593

The *Calyptogena magnifica* Chemoautotrophic Symbiont Genome

I. L. G. Newton,[1] T. Woyke,[2] T. A. Auchtung,[1] G. F. Dilly,[1] R. J. Dutton,[3] M. C. Fisher,[1] K. M. Fontanez,[1] E. Lau,[1] F. J. Stewart,[1] P. M. Richardson,[2] K. W. Barry,[2] E. Saunders,[2] J. C. Detter,[2] D. Wu,[4] J. A. Eisen,[5] C. M. Cavanaugh[1]*

Chemoautotrophic endosymbionts are the metabolic cornerstone of hydrothermal vent communities, providing invertebrate hosts with nearly all of their nutrition. The *Calyptogena magnifica* (Bivalvia: Vesicomyidae) symbiont, *Candidatus Ruthia magnifica*, is the first intracellular sulfur-oxidizing endosymbiont to have its genome sequenced, revealing a suite of metabolic capabilities. The genome encodes major chemoautotrophic pathways as well as pathways for biosynthesis of vitamins, cofactors, and all 20 amino acids required by the clam.

Metazoans at deep-sea hydrothermal vents thrive with the support of symbiotic chemoautotrophic bacteria (*1*). Analogous to photosynthetic chloroplasts, which evolved from cyanobacterial ancestors and use light energy to fix carbon for their plant and algal hosts, chemoautotrophic endosymbionts use the chemical energy of reduced sulfur emanating from vents to provide their hosts with carbon and a large array of additional necessary nutrients. In return, host invertebrates bridge the oxic-anoxic interface to provide symbiont bacteria with the inorganic substrates necessary for chemoautotrophy. The giant clam, *Calyptogena magnifica* Boss and Turner (Bivalvia: Vesicomyidae), was one of the first organisms described after the discovery of hydrothermal vents (*2*). It has a reduced gut and ciliary food groove and is nutritionally dependent on its γ-proteobacterial symbionts (here named *Candidatus Ruthia magnifica*) (*3*, *4*). We present the complete genome of *Ruthia magnifica* (Fig. 1). Despite having a relatively small genome (1.2 Mb), *R. magnifica* is predicted to encode all the metabolic pathways typical of free-living chemoautotrophs, including carbon fixation, sulfur oxidation, nitrogen assimilation, and amino acid and cofactor/vitamin biosynthesis (fig. S1 and table S1).

The following sections outline the reconstruction of *R. magnifica*'s chemoautotrophic metabolism and what this might mean for the biology of its host. Our analysis provides direct evidence that this symbiont fixes carbon via the Calvin cycle, the dominant form of carbon fixation in vent symbioses (*5*), by using energy derived from sulfur oxidation. The *R. magnifica* genome encodes enzymes specific to this cycle, including a form II ribulose 1,5-bisphosphate carboxylase-oxygenase (RuBisCO) and phosphoribulokinase (*6*). Interestingly, however, it appears that *R. magnifica* lacks homologs of sedoheptulose 1,7-bisphosphatase and fructose 1,6-bisphosphatase and may regenerate ribulose 1,5-bisphosphate via an unconventional route, one that was a reversible pyrophosphate-dependent phosphofructokinase [supporting online material (SOM) text].

Energy for carbon fixation in *R. magnifica* appears to result from sulfur oxidation via the *sox* (sulfur oxidation) and *dsr* (dissimilatory sulfite reductase) genes (fig. S1). The symbiont may oxidize its sulfur granules via *dsr* homologs when external sulfide is lacking, as occurs in both *Allochromatium vinosum* and *Chlorobium limicola* (*7*, *8*). Homologs encoding both a sulfide:quinone oxidoreductase and rhodanese are also present, and, with the *dsr* and *sox* proteins, these enzymes can oxidize sulfide or thiosulfate to sulfite (fig. S1). Sulfite can then be oxidized to sulfate by adenosine 5′-phosphosulfate (APS) reductase and adenosine triphosphate (ATP) sulfurylase before being exported from the cell via a sulfate transporter. Genomic evidence of the Calvin cycle and the sulfur oxidation pathways confirms the chemoautotrophic nature of this symbiosis. These data support prior reports showing RuBisCO and ATP sulfurylase activity in *C. magnifica* gill tissue (*4*, *9*), carbon dioxide uptake by the clam in response to sulfide or thiosulfate (*10*), and sulfide-binding, zinc-containing hemoprotein in the host blood stream (*11*).

Energy conservation via the creation of a charge across a membrane proceeds in *R. magnifica* through a reduced nicotinamide adenine dinucleotide (NADH) dehydrogenase, a sulfide:quinone oxidoreductase, and an *rnf* complex (*12*). The genome encodes a straightforward electron transport chain; thus, the reduced quinone in the symbiont membrane may transfer electrons to cytochrome *c* via a bc_1 complex, and a terminal cytochrome *c* oxidase could then transfer these electrons to oxygen (fig. S1).

Our analysis shows that *R. magnifica* has the potential to produce 20 amino acids, 10 vitamins or cofactors, and all necessary biosynthetic intermediates, supporting an essential role of symbiont metabolism in the nutrition of this symbiosis. Two nitrogen assimilation pathways, essential to provisioning of amino acids in the symbiosis, occur in *R. magnifica*. Nitrate and ammonia, which enter the cell via a nitrate or nitrite transporter and two ammonium permeases, are reduced via nitrate and nitrite reductase and assimilated via glutamine synthetase and glutamate synthase, respectively (fig. S1). Although nitrate is the dominant nitrogen form at vents (*13*), the symbiont may also assimilate ammonia via recycling of the host's amino acid waste. Unlike any other sequenced endosymbiont genome, *R. magnifica* encodes complete pathways for the biosynthesis of 20 amino acids, including 9 essential amino acids or their precursors (fig. S3). *R. magnifica* also has complete biosynthetic pathways for the majority of vitamins and cofactors (SOM text). The genome encodes a complete glycolysis pathway and the nonoxidative branch of the pentose phosphate pathway and, interestingly, also encodes a tricarboxylic acid (TCA) cycle lacking α-ketoglutarate dehydrogenase. The lack of this enzyme has been suggested to indicate obligate autotrophy in other bacteria (*14*). Carbon fixed via the Calvin cycle can enter the TCA cycle through phosphoenolpyruvate and here could follow biosynthetic routes either to fumarate or to α-ketoglutarate.

As with other intracellular species, genes not found in the *R. magnifica* genome reveal important details about the interaction between host and symbiont. Few substrate-specific transporters were found, suggesting that the symbionts are leaky or that the host actively digests symbiont cells. Indeed, *Ruthia*'s closest known relatives, the bathymodiolid mussel symbionts, are digested intracellularly by their host (*15*). Although the vesicomyids and the bathymodiolids are distantly related, putative degradative stages of symbionts also are observed within *C. magnifica* bacteriocytes (fig. S2b). The symbiont is also lacking the key cell division protein *ftsZ*, suggesting that, like *Chlamydia* spp., intracellular division may not proceed through usual pathways (SOM text).

Intracellular endosymbionts often follow distinctive evolutionary routes, including genome reduction, skewed base compositions, and elevated mutation rates (*16*). Given the apparent defects in DNA repair in *R. magnifica* (SOM text) and the likely evolutionary forces pushing this genome toward degradation, it is particularly informative that *Ruthia* retains genes encoding a full suite of chemoautotrophic processes. Indeed, *R. magnifica* has the largest genome of any intracellular symbiont sequenced to date and may represent an early intermediate in the evolution toward a plastid-like chemoautotrophic organelle. The broad array of metabolic pathways revealed through sequencing of the *R. magnifica* genome confirms and extends prior knowledge of host nutritional dependency.

[1]Harvard University, 16 Divinity Avenue, Biolabs 4080, Cambridge, MA 02138, USA. [2]Department of Energy Joint Genome Institute, 2800 Mitchell Drive, Walnut Creek, CA 94598, USA. [3]Harvard Medical School, Department of Microbiology and Molecular Genetics, 200 Longwood Avenue, Boston, MA 02115, USA. [4]Institute for Genomic Research, 9712 Medical Center Drive, Rockville, MD 20850, USA. [5]University of California, Davis Genome Center Genome and Biomedical Sciences Facility, Room 5311, 451 East Health Sciences Drive, Davis, CA 95616-8816, USA.

*To whom correspondence should be addressed. E-mail: cavanaug@fas.harvard.edu

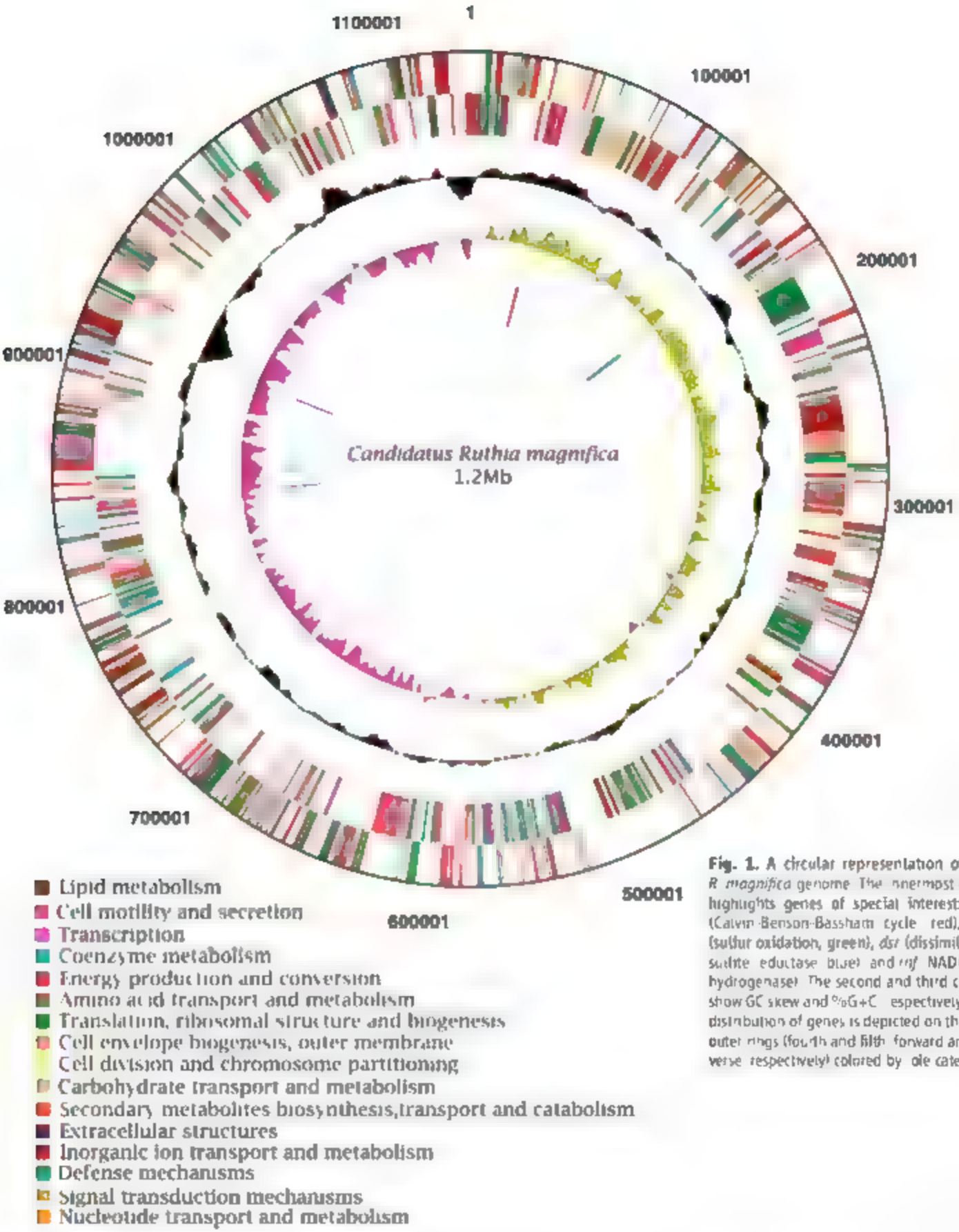

Fig. 1. A circular representation of the *R. magnifica* genome. The innermost circle highlights genes of special interest: *cbb* (Calvin-Benson-Bassham cycle, red), *sox* (sulfur oxidation, green), *dsr* (dissimilatory sulfite reductase, blue), and *nqr* (NADH dehydrogenase). The second and third circles show GC skew and %G+C, respectively. The distribution of genes is depicted on the two outer rings (fourth and fifth, forward and reverse, respectively) colored by role category.

References and Notes

1. C. M. Cavanaugh, Z. P. McGinnis, I. L. G. Newton, F. J. Stewart, in *The Prokaryotes* (Springer-Verlag, Berlin, 2004).
2. K. C. Boss, R. D. Turner, *Malacologia* 20, 161 (1980).
3. C. M. Cavanaugh, *Nature* 302, 58 (1983).
4. J. L. Robinson, thesis, Harvard University, Cambridge, MA (1997).
5. C. M. Cavanaugh, J. L. Robinson, in *Microbial Growth on C$_1$ Compounds*, M. E. Lidstrom, F. R. Tabita, Eds. (Kluwer Academic, Dordrecht, Netherlands, 1996), pp. 285–292.
6. J. M. Shively, G. van Keulen, W. G. Meijer, *Annu. Rev. Microbiol.* 52, 191 (1998).
7. C. Dahl *et al.*, *J. Bacteriol.* 187, 1392 (2005).
8. F. Verte *et al.*, *Biochemistry* 41, 2932 (2002).

9. C. R. Fisher *et al.*, *Deep-Sea Res.* **35**, 1811 (1988).
10. J. J. Childress, C. R. Fisher, J. A. Favuzzi, M. K. Sanders, *Physiol. Zool.* **64**, 1444 (1991).
11. F. Zal *et al.*, *Cah. Biol. Mar.* **41**, 413 (2000).
12. H. Kumagai, T. Fujiwara, H. Matsubara, K. Saeki, *Biochemistry* **36**, 5509 (1997).
13. K. S. Johnson, J. J. Childress, R. R. Hessler, C. M. Sakamoto-Arnold, C. L. Beehler, *Deep-Sea Res.* **35**, 1723 (1988).
14. A. P. Wood, J. P. Aurikko, D. P. Kelly, *FEMS Microbiol. Rev.* **28**, 335 (2004).
15. A. Fiala-Médioni, C. Métivier, A. Herry, M. Le Pennec, *Mar. Biol.* **92**, 65 (1986).
16. J. J. Vrijenhoek, *Mol. Ecol.* **10**, 393 (2001).
17. This research was funded by grants from the U.S. Department of Energy/Joint Genome Institute (JGI) Microbial Genomes Program (to C.M.C. and J.A.E.), a Merck Genome Related Research Award (to C.M.C.), and a Howard Hughes Medical Institute Predoctoral Fellowship (to I.L.G.M.). Sequencing was carried out at the JGI, and we thank D. Bruce and E. Rubin for project management, O. Fraenkel for review of metabolic pathways in *Rathke*, and P. Gogarten and K. Scott for their helpful comments on the manuscript. The *Candidatus R. magnifica* genome can be found in GenBank (CP000488).

Supporting Online Material

www.sciencemag.org/cgi/content/full/315/5814/998/DC1
Materials and Methods
SOM Text
Figs. S1 to S3
Table S1
References

5 December 2006; accepted 15 January 2007
10.1126/science.1138438

The Phosphothreonine Lyase Activity of a Bacterial Type III Effector Family

Hongtao Li,* Hao Xu,* Yan Zhou,* Jie Zhang, Chengze Long, Shuqin Li, She Chen, Jian-Min Zhou, Feng Shao†

Pathogenic bacteria use the type III secretion system to deliver effector proteins into host cells to modulate the host signaling pathways. In this study, the *Shigella* type III effector OspF was shown to inactivate mitogen-activated protein kinases (MAPKs) [extracellular signal–regulated kinases 1 and 2 (Erk1/2), c-Jun N-terminal kinase, and p38]. OspF irreversibly removed phosphate groups from the phosphothreonine but not from the phosphotyrosine residue in the activation loop of MAPKs. Mass spectrometry revealed a mass loss of 98 daltons in p-Erk2, due to the abstraction of the α proton concomitant with cleavage of the C-OP bond in the phosphothreonine residue. This unexpected enzymatic activity, termed phosphothreonine lyase, appeared specific for MAPKs and was shared by other OspF family members.

Gram-negative bacterial pathogens that use the type III secretion system (TTSS) to inject into host cells effector proteins (*1*) not interfere with host signal transduction pathways to promote pathogen infection. MAPK signaling plays an important role in activating host-innate immune responses in both plants and animals and is a frequent target of pathogenic effectors (*2*–*4*). Identification of host targets of TTSS effectors and elucidation of their biochemical functions are critical in understanding the mechanism and the evolution of bacterial pathogenesis (*3*, *5*, *6*).

The TTSS effector OspF is present in all the four known pathogenic species of *Shigella* (*7*–*9*), a causative agent of bacillary dysentery (*10*). OspF, together with SpvC and HopAI1, represents a family of TTSS effectors conserved in both plant and animal bacterial pathogens (*11*) (fig. S1). None of the OspF family effectors has an established biological or biochemical function. To define the biochemical function of OspF and the OspF family of effectors as well as to identify their potential in vivo targets, we examined effects of OspF on the host immune signaling pathways, including those of nuclear factor κB (NF-κB) and MAPKs.

Transient expression of OspF in human 293T cells efficiently blocked extracellular signal–regulated kinases 1 and 2 (Erk1/2) and c-Jun N-terminal kinase (JNK) signaling, whereas it did not alter NF-κB activation (Fig. 1A). OspF abrogated phosphorylation of endogenous Erk1/2, JNK, and p38 kinases (Fig. 1, B and C). These results suggest that OspF harbors a specific activity of down-regulating multiple MAPKs but not NF-κB signaling. When overexpressed in mammalian cells, each of the specific steps in the MAPK pathways blocked by OspF was critical to the canonical MAPK pathway that is activated by a phosphorylation cascade of Raf, MAPK kinase (MEK), and Erk kinases (*12*). OspF blocked Erk activation in 293T cells transfected with either RasV12, v-Raf (constitutive active Raf), or MEK1-ED (constitutive active MEK1) (Fig. 1D). Meanwhile, RasV12-induced MEK1 phosphorylation remained intact despite the disappearance of Erk1/2 phosphorylation in cells expressing OspF (Fig. 1E). Thus, inhibition of Erk phosphorylation by OspF is downstream of MEK1 along the classical Ras-Raf-MEK-Erk cascade.

Erk1/2 phosphorylation can be reconstituted in the cell-free extracts system by adding upstream signaling molecules (*3*). Addition of bacterially expressed and highly purified OspF (fig. S2A) in 293T cell extracts abolished both RasV12- and active B-Raf–induced Erk1/2 phosphorylation, whereas MEK1 phosphorylation was not affected (Fig. 2A). Thus, excludes the transcriptional regulation of MAPK pathway by OspF and also provides a system that recapitulates the inhibition of MAPK signaling by OspF in cells. To further test whether OspF directly targets the Raf-MEK1-Erk1/2 cascade biochemically, we reconstituted the phosphorylation cascade of B-Raf–MEK1–Erk2 by using purified kinases. Addition of OspF to this reaction largely abolished Erk2 phosphorylation (Fig. 2B). Furthermore, recombinant OspF could inhibit phosphorylation of glutathione *S*-transferase (GST)–Erk2 by MEK1-ED (Fig. 2C), suggesting that OspF directly targets Erks or MEKs. Recombinant Erk2 fused to maltose binding protein (MBP-Erk2), but not MBP alone, effectively precipitated OspF (fig. S2A). Flag-OspF also coprecipitated with endogenous Erk1/2 but not MEK1 from 293T cells (fig. S2B). Thus, OspF targets Erk and attenuates its phosphorylation status.

Given the direct association between OspF and Erk2 and that the basal amount of phospho-Erk1/2 (p-Erk1/2) was diminished by OspF addition in the cell-free reconstitution assay (Fig. 2A), we reasoned that OspF could harbor a phosphatase activity to reverse Erk phosphorylation. When in vitro phosphorylated GST-Erk2, JNK, and p38 were incubated with recombinant OspF, dephosphorylation indeed occurred (Fig. 2, D and E). Furthermore, OspF selectively removed phosphate groups from the threonine but not from the tyrosine residue in the pT-X-pY (*13*) motif in p-Erk2 (Fig. 2, D and E). Thus, OspF harbors an in vitro enzymatic activity of specifically removing phosphate groups from the phosphothreonine in the pT-X-pY motif in MAPKs, including Erk1/2, JNK, and p38.

OspF appears to function as a threonine-specific MAPK phosphatase. However, our analysis rules out the possibility of a classical protein phosphatase of OspF in nature [Supporting Online Material (SOM) text]. To reveal the chemical nature of OspF activity, we subjected MEK1-phosphorylated MBP-Erk2 (p-Erk2 control), as well as MBP-p-Erk2 further treated with OspF (p-Erk2-OspF), to tandem mass spectrometry analysis. More than 80% of the MBP-Erk2 sequence was covered by observed tandem peptides. All of the peptides from p-Erk2 control and p-Erk2-OspF were indistinguishable except for the peptide containing the TXY phosphomotif [VADPDHDHTGFL-pT-E-pY-VATR (*13*)]. The mass of the peptide from p-Erk2-OspF was 2204.9 dalton (Fig. 3A), 98 dalton less than that of the corresponding peptide from p-Erk2 control. The 98-dalton mass decrease occurred on the phosphothreonine residue in the pT-X-pY

National Institute of Biological Sciences, Beijing, 102206, China.

*These authors contributed equally to this work.
†To whom correspondence should be addressed. E-mail: shaofeng@nibs.ac.cn

mobility (Fig. 3B). Consistently, when a synthetic phosphopeptide containing the TXY phosphomotif in Erk2 (DHTGFL-pT-E-pY VATR) was modified by OspF and the resulting product analyzed by mass spectrometry, a mass decrease of 98 dalton on the phosphothreonine residue compared with the control peptide was also observed (Fig. 3C). Thus, upon OspF treatment, the phosphothreonine residue in the TXY motif in both p-Erk and the phosphopeptide substrate underwent a dehydration reaction (18 dalton of mass loss) in addition to the loss of a phosphate group (80 dalton). The reaction of p-Erk2 with OspF probably resulted in a C=C bond between Cβ and Cα in the side chain of the threonine residue (Fig. 3D), suggesting that OspF functions as a phosphothreonine lyase that cleaves the C-OP bond with the concomitant abstraction of the α proton in the phosphothreonine residue in p-Erk2. Furthermore, this chemical modification of p-Erk2 resulting from OspF phosphothreonine lyase activity led to a completely inactive kinase both in vitro and in cells (fig. S3). In addition, OspF "dephosphorylated" Erk2 could no longer be rephosphorylated by MEK ED (fig. S4). Thus, OspF functions as a phosphothreonine lyase, rather than a phosphatase, to irreversibly inactivate MAPKs.

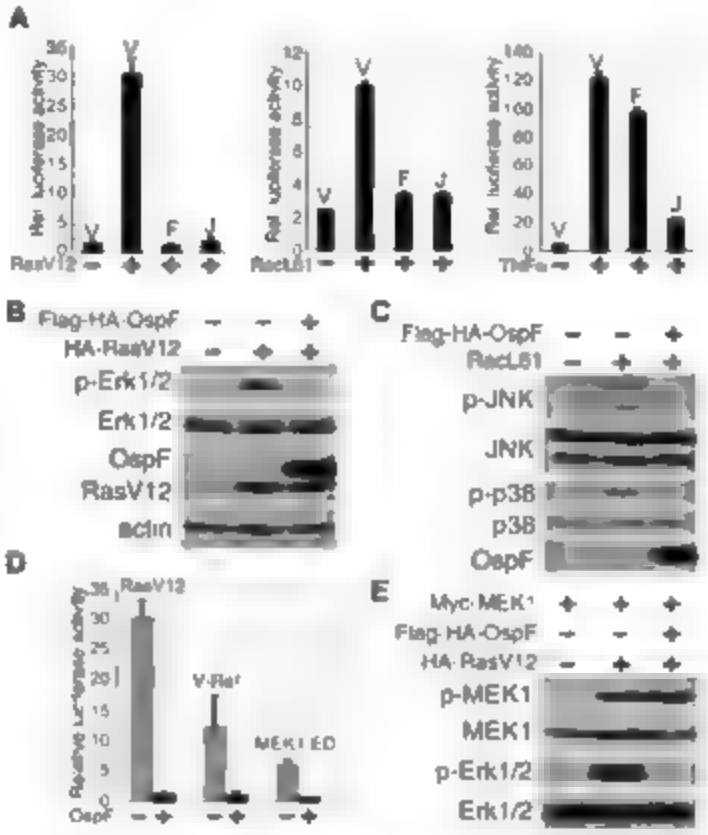

Fig. 1. Inhibition of multiple MAPK pathways downstream of MAPK kinase by OspF in 293T cells. (**A**) Luciferase assays of effects of OspF expression on Erk1/2, JNK, and NFκB pathways. Erk1/2 and NFκB activations were achieved by coexpression of constitutive active RasV12 and Rac1Q61, respectively, and NFκB was stimulated by tumor necrosis factor α treatment. V, F, and J denote vector, OspF, and YopJ, respectively. Error bars indicate standard deviation. (**B** and **C**) Phosphospecific immunoblotting assays of inhibition of MAPKs activation by OspF. p-Erk, p-JNK, and p-p38 antibodies recognize the dual phosphorylated TXY motif (pT-X-pY) in Erk1/2, JNK1/2, and p38, respectively. HA, hemagglutinin. (**D**) Luciferase assays of Ras-, Raf-, and MEK1-induced Erk activation in the presence of OspF. v-Raf and MEK1 ED are constitutive active variants of Raf and MEK1. Error bars indicate standard deviation. (**E**) Phosphospecific immunoblotting of activation of MEK1 and Erk1/2 in the presence of OspF.

To gain further understanding of the OspF phosphothreonine lyase activity, we mutated 10 residues conserved in all the OspF family members (fig. S5A). These mutants had similar expression and purification profiles to those of the wild-type protein, suggesting that they were folded correctly. Most of the mutants retained the Erk2 phosphothreonine lyase activity, whereas mutants of K^{102}→R^{102} (K102R), H^{104}→A^{104} (H104A), and K^{134}→A^{134} (K134A) were largely inactive (fig. S5, A and B). These mutants could still bind to Erk (fig. S2, A and C), suggesting a functional importance for K102, H104, and K134. A nonradioactive phosphatase assay was used to quantitatively measure the enzymatic activity of OspF. OspF efficiently removed phosphate groups from the Erk2 phosphopeptide with a Michaelis-Menton constant (K_m) of 95.8 ± 2.4 μM and a catalytic rate constant (k_{cat}) of 0.70 ± 0.04 s^{-1} (table S1). The K102R, H104A, and K134A mutants were almost completely inactive in the peptide assay (fig. S5C). Furthermore, these mutants were also deficient in down-regulating MAPK signaling when expressed in 293T cells (fig. S6). Thus, K102, H104, and K134 are probably essential for OspF phosphothreonine lyase activity toward MAPKs.

We then assessed the role of the phosphate on the tyrosine in pT-X-pY in the MAPK phosphothreonine lyase activity of OspF. When Erk2 (pT-X-pY) was tyrosine-dephosphorylated by protein tyrosine phosphatase (HePTP), subsequent dephosphorylation by OspF was assessed by measuring K_m. Consistent, kinetic analysis using the synthetic threonine monophosphorylated Erk2 peptide gave a higher K_m value compared with that of the dual phosphorylated Erk2 peptide (table S1). Thus, the phosphate on the tyrosine in the substrate probably contributes to substrate recognition by OspF. Further kinetics analysis using different peptide substrates showed that OspF was specific for the phosphothreonine in the classical MAPKs (with TXY motif), with the highest enzymatic activity toward p38 (table S1).

SpvC, a member of the OspF family of T3SS effectors from nontyphoid *Salmonella* strains, is required for full virulence and systemic infection

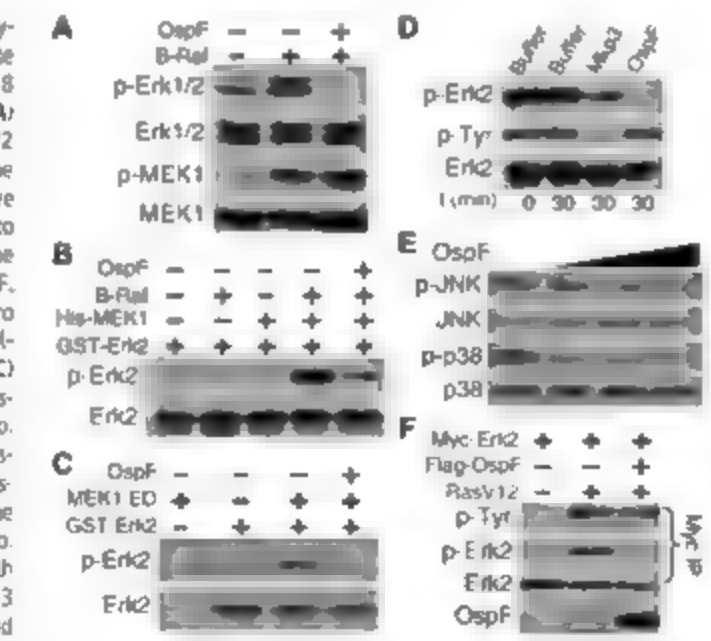

Fig. 2. Immunoblotting analyses of removal of phosphate groups from Erk, JNK, and p38 kinases by OspF in vitro. (**A**) Effects of OspF on Erk1/2 activation reconstituted in the cell-free extract system. Active B-Raf protein was added to activate Erk pathway in the presence or absence of OspF. (**B**) Effects of OspF on in vitro reconstituted Erk2 phosphorylation downstream of Raf. (**C**) Effects of OspF on Erk2 phosphorylation by MEK1 in vitro. (**D**) Selective removal of phosphate groups from the phosphothreonine residue in the pT-X-pY motif in Erk2 in vitro. GST-p-Erk2 was treated with OspF or MAPK phosphatase 3 (MKP3), followed by p-Erk and a phosphotyrosine-specific antibody (p-Tyr) immunoblotting. (**E**) Removal of the phosphate groups from p-JNK and p-p38 by OspF in vitro. (**F**) Phosphotyrosine immunoblotting of Myc-Erk2 modified by OspF in 293T cells.

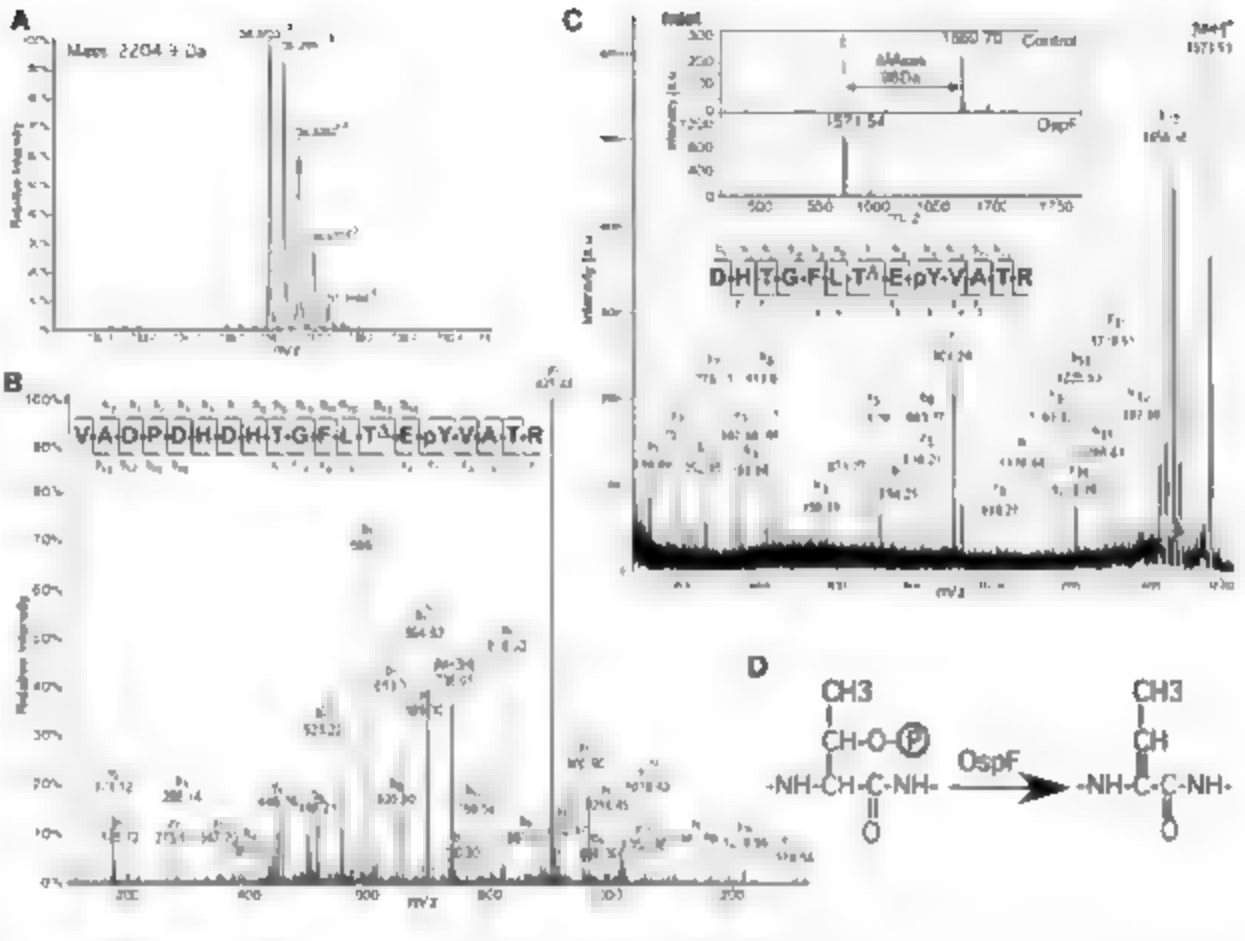

Fig. 3. The phosphothreonine lyase activity of OspF. (**A**) The mass spectrometry analysis of the molecular mass of the tryptic peptide (VADPDHDHTGFL-pT-E-pY-VATR) from OspF-treated p-Erk2. Different peaks correspond to the isotopic peaks of the peptide. (**B**) Electrospray ionization (ESI) tandem mass spectrometry (MS/MS) spectrum of the tryptic peptide shown in (A). b and y ions are marked in the spectrum. The amino acid sequence of the peptide is shown at top left, and T^ marks the OspF-modified phosphothreonine residue. The fragmentation patterns that generate the observed b and y ions are illustrated along the peptide sequence. (**C**) MS/MS spectrum of the OspF-modified synthetic Erk2 phosphopeptide (DHTGFL-pT-E-pY-VATR). Notations are the same as described in (B). Inset shows the molecular mass of the Erk2 phosphopeptide before (control) and after (OspF) treatment. a.u., arbitrary units. (**D**) Diagram of the chemical alteration of the phosphothreonine residue in Erk2 by OspF. OspF cleaves the C-OP bond with the concomitant abstraction of the α proton, which results in a C=C bond between the Cα and the Cβ in the phosphothreonine residue in Erk2.

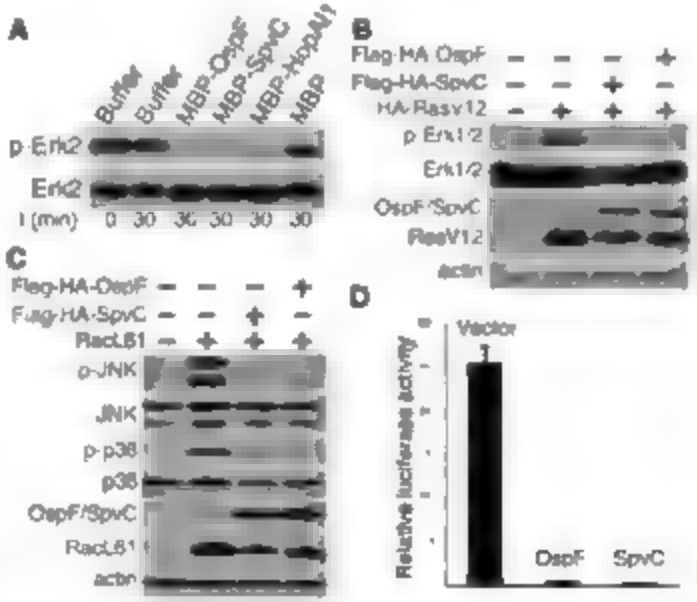

Fig. 4. The phosphothreonine lyase activity of other OspF family members. (**A**) Immunoblotting assays of removing phosphate groups from p-Erk2 by indicated OspF family members in vitro. *t*, time. (**B** and **C**) Phospho-Erk immunoblotting assays of down-regulation of Erk (B), JNK, and p38 (C) pathways by SpvC transfection in 293T cells. The assay was performed and the results are presented similarly as shown in Fig. 1, B and C, respectively. (**D**) Luciferase assays of effects of SpvC on Erk signaling activated by RasV12 in 293T cells. Error bars indicate standard deviation.

(*14*, *15*). Recombinant SpvC efficiently removed phosphate groups from GST p-Erk2 (Fig. 4A). SpvC catalyzed the same enzymatic conversions of the Erk2 phosphopeptide with kinetics comparable to that observed for OspF (k_{cat} = 1.94 ± 0.05 s^{-1} and K_m = 28.5 ± 0.5 μM). Similarly to OspF overexpression of SpvC in mammalian cells abrogated phosphorylation and activation of Erk1/2, JNK, and p38 kinases (Fig. 4, B to D). In addition, HopAI1, a type III effector from plant pathogen *Pseudomonas syringae* (*11*), possessed the same in vitro catalytic activity as described for OspF and SpvC, using either p-Erk2 (Fig. 4A) or the Erk2 phosphopeptide as the artificial substrate (k_{cat} = 0.70 ± 0.02 s^{-1} and K_m = 132.1 ± 8.1 μM). Thus, the entire OspF family of T3SS effectors has an in vitro phosphothreonine lyase activity.

To examine whether the type III–secreted OspF indeed targeted the host MAPKs, we generated an OspF-deletion strain of *Shigella flexneri* 2a and performed an infection assay (*16*). In contrast to a recent report that analyzed p-Erk1/2 at 3 hours postinvasion (*17*), we analyzed p-p38 at 30 min postinvasion, because OspF was 8 times more active toward the p38 phosphopeptide compared with the Erk2 phosphopeptide (table S1). In addition, several studies have suggested that OspF is only transcribed for 2 hours after bacteria invasion (*18*, *19*). A higher amount of p-p38 was observed in HeLa cells infected with the OspF-deletion strain of *Shigella* compared with the amount in cells infected with the wild-type strain (fig. S8A). Furthermore, reintroducing wild-type OspF, but not the H104A mutant, into the OspF-deletion strain lowered the amount of p-p38 in infected HeLa cells (fig. S8B). Thus, MAPK is a potential target

of the phosphothreonine lyase activity of OspF during *Shigella* infection.

Phosphothreonine lyase activity has not been described previously. The closest enzyme might be the threonine synthase (EC 4.2.3.-) in bacteria and plants, which uses a pyridoxal phosphate cofactor. This enzyme converts O-phospho-L-homoserine into threonine through an intermediate that has a C=C bond between the Cβ and the Cγ. However, OspF did not show any sequence identity with any phospholyase, including threonine synthase, and required no cofactors. Thus, suggests that the OspF family phosphothreonine lyase has designed an unusual mechanism for enzyme catalysis. Together, OspF, SpvC, and HopAI1 define a family of conserved pathogenic effectors with a unique phosphothreonine lyase activity that probably targets the host MAPKs in pathogenesis.

References and Notes

1. J. E. Galan, A. Collmer, *Science* **284**, 1322 (1999).
2. F. M. Ausubel, *Nat. Immunol.* **6**, 973 (2005).
3. S. Mukherjee *et al.*, *Science* **312**, 1211 (2006).
4. J. M. Park, F. R. Greten, Z.-W. Li, M. Karin, *Science* **297**, 2048 (2002); published online 29 August 2002 (10.1126/science.1073163).
5. F. Shao *et al.*, *Science* **301**, 1230 (2003).
6. F. Shao, P. M. Merritt, Z. Bao, R. W. Innes, J. E. Dixon, *Cell* **109**, 575 (2002).
7. O. J. Philpott, S. E. Girardin, P. J. Sansonetti, *Curr. Opin. Immunol.* **13**, 410 (2001).
8. S. E. Girardin *et al.*, *EMBO Rep.* **2**, 736 (2001).
9. H. Kohler, S. P. Rodrigues, B. A. McCormick, *Infect. Immun.* **70**, 1150 (2002).
10. M. Ogawa, C. Sasakawa, *Cell. Microbiol.* **8**, 177 (2006).
11. X. Li *et al.*, *Proc. Natl. Acad. Sci. U.S.A.* **102**, 12990 (2005).
12. C. Dong, R. J. Davis, R. A. Flavell, *Annu. Rev. Immunol.* **20**, 55 (2002).
13. Single-letter abbreviations for the amino acid residues are as follows: A, Ala; C, Cys; D, Asp; E, Glu; F, Phe; G, Gly; H, His; I, Ile; K, Lys; L, Leu; M, Met; N, Asn; P, Pro; Q, Gln; R, Arg; S, Ser; T, Thr; V, Val; W, Trp; X, any amino acid; and Y, Tyr.
14. P. A. Going, T. J. Doyle, *Infect. Immun.* **61**, 504 (1993).
15. S. J. Libby *et al.*, *Infect. Immun.* **65**, 1786 (1997).
16. Materials and methods are available as supporting material on *Science* Online.
17. D. V. Zurawski, C. Mitsuhata, K. L. Mumy, B. A. McCormick, A. T. Maurelli, *Infect. Immun.* **74**, 5964 (2006).
18. T. Le Gall *et al.*, *Microbiology* **151**, 951 (2005).
19. C. D. Kane, R. Schuch, W. A. Day Jr., A. T. Maurelli, *J. Bacteriol.* **184**, 4409 (2002).

20. We thank J. Dixon for critical reading of this manuscript, K. Guan, J. Dixon, M. Cobb, M. Solomon, A. Lin, T. Mustelin, M. Donnenberg, and M. Ahn for providing reagents; W. Luo for providing technical suggestions about bacteria recombination; and members of the Shao lab for helpful discussions and technical assistance. This work was supported by Chinese Ministry of Science and Technology "863" grants 2005AA210950 (F.S.) and 2005AA210080 (J.-M.Z.).

Supporting Online Material

www.sciencemag.org/cgi/content/full/315/5814/1000/DC1
Materials and Methods
SOM Text
Figs. S1 to S9
Table S1
References

18 December 2006; accepted 12 January 2007
10.1126/science.1138960

Archaeal Type III RuBisCOs Function in a Pathway for AMP Metabolism

Takaaki Sato, Haruyuki Atomi, Tadayuki Imanaka*

The type III ribulose-1,5-bisphosphate carboxylase-oxygenase (RuBisCO) present in the archaeon *Thermococcus kodakaraensis* was found to participate in adenosine 5′-monophosphate (AMP) metabolism, a role that is distinct from that of classical RuBisCOs of the Calvin-Benson-Bassham cycle. Genes annotated as thymidine phosphorylase (*deoA*) and eukaryal translation initiation factor 2B (*e2b2*) were found to encode AMP phosphorylase and ribose-1,5-bisphosphate isomerase, respectively. These enzymes supplied the RuBisCO substrate ribulose-1,5-bisphosphate from AMP and phosphate. Archaea with type III RuBisCOs all harbor both DeoA and the corresponding E2b2 homologs. In this pathway, adenine was released from AMP and the phosphoribose moiety entered central carbon metabolism.

Ribulose-1,5-bisphosphate carboxylase-oxygenase (RuBisCO) is presumed to be the most abundant enzyme on our planet (*1*) and is widely known as the key CO_2-fixing enzyme of the Calvin-Benson-Bassham (CBB) cycle, which is present in all plants, algae, cyanobacteria, and many other autotrophic bacteria (*2*, *3*). Besides the classical type I and II RuBisCOs of the CBB cycle, two groups of proteins that are structurally related to the type I and II enzymes have been identified and designated as type III (*4*, *5*) and type IV RuBisCOs (*6*, *7*). Type IV RuBisCOs, also called the RuBisCO-like proteins, lack several residues necessary for conventional RuBisCO catalysis. Thus, type IV RuBisCO from *Bacillus subtilis* instead exhibits 2,3-diketo-5-methylthiopentyl-1-phosphate enolase activity and operates in the methionine (Met) salvage pathway in *B. subtilis* (*7*).

Department of Synthetic Chemistry and Biological Chemistry, Graduate School of Engineering, Kyoto University, Katsura, Nishikyo-ku, Kyoto 615-8510, Japan.

*To whom correspondence should be addressed. E-mail: imanaka@sbchem.kyoto-u.ac.jp

The type III RuBisCOs are found only in the Archaea, and they harbor all of the residues necessary for ribulose-1,5-bisphosphate (RuBP) carboxylase-oxygenase activity. Proteins from *Thermococcus kodakaraensis* (*4*, *8*–*10*), *Methanocaldococcus jannaschii*, *Archaeoglobus fulgidus*, and other archaea (*5*, *11*) exhibit RuBisCO activity. However, a functional CBB pathway has not been identified in Archaea, and archaeal genome sequences do not support the presence of a CBB pathway. In particular, homologs of phosphoribulokinase, another key enzyme of the CBB pathway that supplies RuBP for RuBisCO, cannot be found on the archaeal genomes. Hence, we first investigated whether archaeal RuBisCOs were involved in Met salvage, similar to type IV RuBisCOs.

Many organisms use Met as a precursor for polyamine elongation with concomitant generation of methylthioadenosine (MTA). The Met salvage pathway is present in some bacteria and eukaryotes and recycles MTA to Met (fig. S1) (*12*–*14*). Homologs of enzymes involved in the conversion of Met to MTA are present on the *T. kodakaraensis* genome (*15*). Although homologs of several steps in the Met salvage pathway, including three YkrS homologs, are present, YkrX and YkrZ homologs cannot be identified on the *T. kodakaraensis* genome.

The absence of a complete Met salvage pathway in *T. kodakaraensis* was confirmed by examining a mutant that lacks the ability to synthesize Met de novo. Two adjacent genes presumed to encode the components of Met synthase, *metE1* (TK1446) and *metE2* (TK1447), were disrupted (*16*). The resulting strain, Δ*metE21*-1, displayed the expected genotype (Δ*pyrF* Δ*metE21*::*pyrF*) and could grow only in the presence of exogenous Met. The Δ*metE21*-1 strain could not grow when Met was substituted with various concentrations of MTA. We then disrupted the *T. kodakaraensis* (*Tk*) RuBisCO gene (*Tk-rbc*) itself and subsequently isolated the gene-disruption mutant (Δ*rbc*-1AA), which indicated that *Tk-rbc* is not essential for growth. We did, however, consistently observe a slight decrease in the cell yield of Δ*rbc*-1AA as compared to the host strain when cells were grown in nutrient-rich medium.

We then shifted our attention to the three YkrS homologs present on the *T. kodakaraensis* genome and considered various possibilities for the roles of these homologs. The three homologs, *Tk*-E2b1 (45% identical with YkrS from *B. subtilis*), *Tk*-E2B2 (32% identical), and *Tk*-Ged2 (27% identical), are members of the eukaryotic translation initiation factor 2B (eIF2B) α/β/δ family (*17*–*19*). However, the functions of the eIF2B homologs in the Archaea are not known. The *B. subtilis* YkrS is a member of this family and it catalyzes the isomerization of methylthioribose-1-phosphate (MTR-1-P) to methylthioribulose-1-phosphate (MTRu-1-P) (*7*). We noticed structural similarities between MTR-1-P and ribose-1,5-bisphosphate (R15P) and between MTRu-1-P and RuBP, indicating that these archaeal E2B (aIF2B) proteins might be involved in the generation of RuBP. The

isomerization of R1SP to RuBP also corresponds to the reaction proposed to be responsible for RuBP synthesis in methanogenic Archaea (*20*).

A phylogenetic tree was constructed with 49 aIF2B homologs from 27 archaeal genomes. The homologs composed several subgroups, and we found that one branch (shaded in Fig. 1) included homologs only from organisms harboring type III RuBisCOs, with the only exception being AAG20059 from *Halobacterium* sp. NRC 1. The based distribution did not correlate at all with the phylogenetic relationships of the organisms themselves. The correlation prompted us to examine experimentally whether there was a functional relationship between this subgroup of aIF2B homologs, which includes *Tk*-E2b2 and type III RuBisCO.

The *Tk-e2b2* and *Tk-e2b1* genes were expressed in *Escherichia coli* and heat-treated. An initial examination of RuBP synthesis activity from R1SP was performed using an R1SP solution enzymatically prepared with glucose 1,6-bisphosphate (G16P$_2$), ribose 5-phosphate (R5P), and phosphoglucomutase. Extracts containing *Tk*-E2b1 displayed only negligible levels of activity that were equivalent to those found in extracts from *E. coli* harboring a mock plasmid pET21a(+) (0.001 to 0.002 μmol min^{-1} mg^{-1}). In contrast, although expression levels were substantially lower than those of *Tk*-E2b1 extracts containing *Tk*-E2b2 displayed levels of RuBP-synthesizing activity that were over 10 times higher than those of *Tk*-E2b1. Purified *Tk*-E2b2 generated RuBP from the R1SP solution with activity levels of 0.4 μmol min^{-1} mg^{-1}. High-performance liquid chromatography analyses confirmed that only R1SP and not G$_1$6P or R5P was the substrate for RuBP synthesis (fig. S2).

In order to identify a protein that supplies R1SP we searched for genes that were specifically present in archaeal strains harboring type III RuBisCO. This led to the identification of a putative thymidine phosphorylase gene (*deoA*). The only exception was *Methanococcus maripaludis* which harbors a *deoA* gene but not

Fig. 1. Phylogenetic tree of archaeal proteins annotated as members of the aIF2B family. aIF2B family proteins present in the 27 complete archaeal genome sequences were aligned with the ClustalW program available at the DNA Data Bank of Japan, and a phylogenetic tree was constructed with the maximum-likelihood method by means of PHYML (*26*, *27*). The shaded branch harbors the aIF2B homologs from archaeal strains that possess a type III RuBisCO. *A. pernix*, *Aeropyrum pernix* K1; *A. fulgidus*, *Archaeoglobus fulgidus* VC 16; *H. marismortui*, *Haloarcula marismortui* ATCC 43049; *M. jannaschii*, *Methanocaldococcus jannaschii* DSM2661; *M. burtonii*, *Methanococcoides burtonii* DSM6242; *M. maripaludis*, *Methanococcus maripaludis* S2; *M. kandleri*, *Methanopyrus kandleri* AV19; *M. acetivorans*, *Methanosarcina acetivorans* C2A; *M. barkeri*, *Methanosarcina barkeri* str. Fusaro; *M. mazei*, *Methanosarcina mazei* Go1 OCM88; *M. hungatei*, *Methanospirillum hungatei* JF-1; *M. stadtmanae*, *Methanosphaera stadtmanae* DSMZ3091; *M. thermautotrophicus*, *Methanothermobacter thermautotrophicus* ΔH; *N. pharaonis*, *Natronomonas pharaonis* DSM2160; *P. torridus*, *Picrophilus torridus* DSM9790; *P. aerophilum*, *Pyrobaculum aerophilum* IM2; *P. abyssi*, *Pyrococcus abyssi* GE5; *P. furiosus*, *Pyrococcus furiosus* DSM3638; *P. horikoshii*, *Pyrococcus horikoshii* OT3; *S. solfataricus*, *Sulfolobus solfataricus* P2; *S. tokodaii*, *Sulfolobus tokodaii* 7; *S. acidocaldarius*, *Sulfolobus acidocaldarius* DSM639; *T. kodakaraensis*, *Thermococcus kodakaraensis* KOD1; *T. acidophilum*, *Thermoplasma acidophilum* DSM1728; *T. volcanium*, *Thermoplasma volcanium* GSS1

a RuBisCO (Table 1). DeoA is known to release the thymine base from thymidine while phosphorylating the 1′-carbon of the ribose moiety (27). If DeoA could phosphorylate nucleoside monophosphates, this would generate R1P. We expressed the *Tk-deoA* gene (TK0352) in *E. coli*, purified the protein, and found that it produced high levels of R1P in the presence of phosphate and adenosine 5′-monophosphate (AMP) (Table 2). *Tk*-DeoA displayed a specific activity of 22.3 μmol min^{-1} mg^{-1} for the reaction AMP + Pi → R1P + adenine. The stoichiometric ratio of the concentration of AMP consumed ([AMP consumed]) and [adenine produced] was confirmed as 1:1 (fig. S3). The equilibrium constant K ([R1P][adenine]/[AMP][Pi]) was $6.02 \times 10^{-3} \pm 0.46 \times 10^{-3}$ at 85°C. Using *Tk*-DeoA, we were able to synthesize large amounts of R1P and to test the R1P isomerase activity of *Tk*-E2b2 in the presence of abundant substrate. We observed that 1.80 ± 0.07 mol of 3-phosphoglycerate (3-PGA) were produced for every mole of R1P consumed when *Tk*-E2b2 and *Tk*-RuBisCO were coupled at 85°C, strongly supporting a stoichiometric ratio of [R1P consumed]:[3-PGA produced] = 1:2. *Tk*-E2b2 exhibited a specific activity of 32.3 μmol min^{-1} mg^{-1} for the reaction R1P ⇌ Ru1P (Table 2).

Table 1. Distribution of RuBisCO, aIF2B, DeoA, and ADP-dependent sugar kinase homologs on archaeal genomes. Shaded boxes indicate the presence of a homolog on the genome.

Organism	Type III RuBisCO	aIF2B homolog*	DeoA homolog	ADP-dependent sugar kinase
Aeropyrum pernix				
Archaeoglobus fulgidus				
Haloarcula marismortui				
Halobacterium sp. NRC-1				
Methanocaldococcus jannaschii				
Methanococcoides burtonii				
Methanococcus maripaludis				
Methanosarcina acetivorans				
Methanosarcina barkeri				
Methanosarcina mazei				
Methanosphaera stadtmanae				
Methanospirillum hungatei				
Methanothermobacter thermautotrophicus				
Methanopyrus kandleri				
Nanoarchaeum equitans				
Natronomonas pharaonis				
Picrophilus torridus				
Pyrobaculum aerophilum				
Pyrococcus abyssi				
Pyrococcus furiosus				
Pyrococcus horikoshii				
Sulfolobus acidocaldarius				
Sulfolobus solfataricus				
Sulfolobus tokodaii				
Thermococcus kodakaraensis				
Thermoplasma acidophilum				
Thermoplasma volcanium				

*Homologs included in the shaded branch of Fig. 1.

Table 2. Specific activities of *Tk*-DeoA and *Tk*-E2b2. Synthesis of 3-PGA was not observed in the absence of protein or substrate.

Protein	Substrate	Specific activity (μmol min^{-1} mg of protein)
Tk-DeoA	AMP	22.3 ± 0.2
	GMP	0.01
	CMP	0.14 ± 0.01
	UMP	0.06 ± 0.01
	TMP	0.01
Tk-E2b2	R1P*	32.3 ± 0.4

*Produced with *Tk*-DeoA.

The protein proposed to catalyze the isomerization between R1P and Ru1P in *M. jannaschii* is the product of MJ0601, but the recombinant protein does not seem to be active in vitro (20). Likewise, the MJ0601 homolog in *T. kodakaraensis* (*Tk-deoB*, TK0834) was expressed in *E. coli* and, again, activity was not detected. This indicates that, at least in *T. kodakaraensis*, *Tk*-E2b2 is the enzyme primarily responsible for Ru1P synthesis from R1P.

Our results showed that in *T. kodakaraensis*, a putative thymidine phosphorylase is actually an AMP phosphorylase, whereas an aIF2B homolog is actually a R1P isomerase. Because the Archaea possessing a type III RuBisCO are all anaerobes, it is most likely that only the carboxylase activity of RuBisCO, and not the oxygenase activity, is biologically relevant in these strains. Thus, *Tk*-DeoA, *Tk*-E2b2, and the RuBisCO convert AMP, phosphate, CO_2, and H_2O, respectively, to adenine and two molecules of 3-PGA (Fig. 2). This pathway hence salvages the adenine base of AMP and diverts the ribose moiety into central-carbon metabolism.

Many of the Archaea that possess this pathway are organisms that use adenosine 5′-diphosphate (ADP)–dependent (AMP-forming) sugar kinases for glycolysis (22, 23). These enzymes would produce a larger intracellular pool of AMP as compared with organisms possessing classical ATP-dependent kinases. Because the product of the pathway, 3-PGA, can be used for ATP generation, the pathway may enable anaerobic Archaea to use AMP when energy levels are low and/or intracellular AMP is in excess. In *I. fulgidus*, which does not harbor ADP-dependent sugar kinases, the pathway may be involved in the conversion of the AMP generated by adenosylphosphosulfate reductase (24) during sulfate reduction. Another possibility is that AMP is produced from 5-phosphoribosyl-1-pyrophosphate (PRPP) by adenine phosphoribosyltransferase, whose homolog is present in *T. kodakaraensis*. This reaction would recycle the adenine molecule released by *Tk*-DeoA and also complete a cyclic pathway composed of (i) pentose synthesis, (ii) conversion of PRPP to 3-PGA, and (iii)

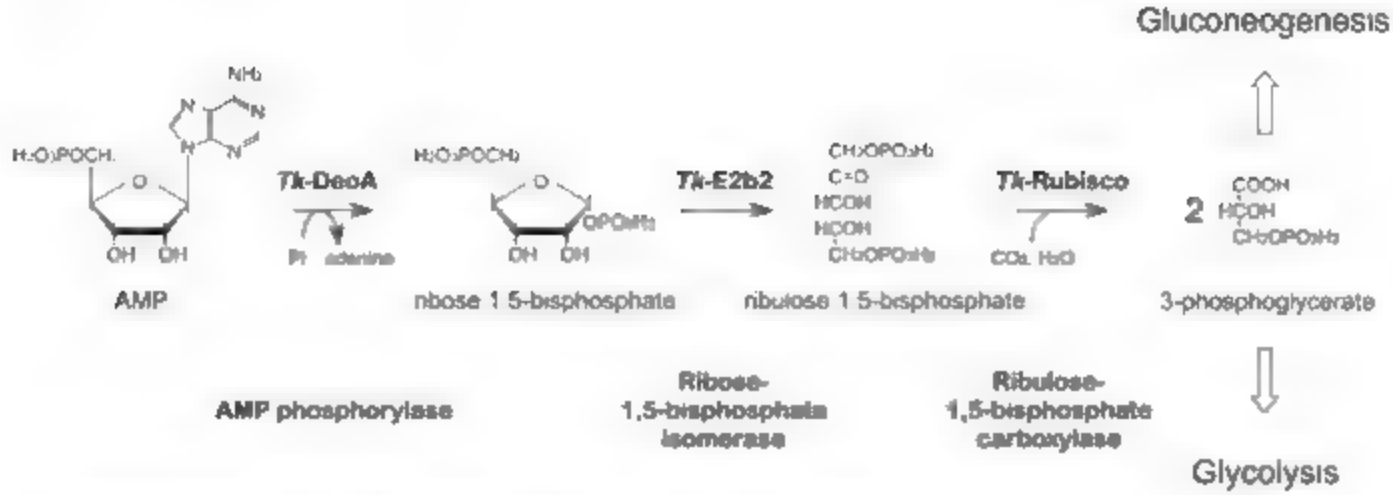

Fig. 2. A metabolic pathway composed of homologs of DeoA, aIF2B, and type III RuBisCOs.

conversion of 3-PGA to fructose 6-phosphate (gluconeogenesis). If the non-oxidative branch of the pentose phosphate pathway were to be responsible for pentose synthesis, the cyclic pathway would constitute a CO_2 fixation pathway (fig. S4). Although their genome sequences are not available, there are several autotrophic strains in the Crenarchaeota that exhibit RuBisCO activity despite lacking phosphoribulokinase activity (*25*).

Type III RuBisCOs seem to have a function distinct from that of the classical RuBisCOs in the CBB pathway of *Bacteria* and *Eucarya*. When considering that the organisms harboring type III RuBisCOs represent relatively deep and short lineages in evolution, it may well be that the carboxylase activity of RuBisCO originally evolved to function in this pathway.

References and Notes

1. R. J. Ellis, *Trends Biochem. Sci.* **4**, 241 (1979).
2. G. M. F. Watson, F. R. Tabita, *FEMS Microbiol. Lett.* **146**, 13 (1997).
3. J. M. Shively, G. van Keulen, W. G. Meijer, *Annu. Rev. Microbiol.* **52**, 191 (1998).
4. S. Ezaki, N. Maeda, T. Kishimoto, H. Atomi, T. Imanaka, *J. Biol. Chem.* **274**, 5078 (1999).
5. G. M. F. Watson, J.-P. Yu, F. R. Tabita, *J. Bacteriol.* **181**, 1569 (1999).
6. T. E. Hanson, F. R. Tabita, *Proc. Natl. Acad. Sci. U.S.A.* **98**, 4397 (2001).
7. H. Ashida *et al.*, *Science* **302**, 286 (2003).
8. N. Maeda *et al.*, *J. Mol. Biol.* **293**, 57 (1999).
9. K. Okano *et al.*, *Structure* **9**, 473 (2001).
10. N. Maeda, T. Kanai, H. Atomi, T. Imanaka, *J. Biol. Chem.* **277**, 31656 (2002).
11. M. W. Finn, F. R. Tabita, *J. Bacteriol.* **185**, 3049 (2003).
12. J. W. Way, R. H. Abeles, *J. Biol. Chem.* **270**, 1347 (1995).
13. A. Setkowska, A. Danchin, *BMC Microbiol.* **2**, 8 (2002).
14. A. Setkowska *et al.*, *BMC Microbiol.* **4**, 9 (2004).
15. T. Fukui *et al.*, *Genome Res.* **15**, 352 (2005).
16. Materials and methods are available as supporting material on Science Online.
17. P. Gebauer, M. W. Hentze, *Nat. Rev. Mol. Cell Biol.* **5**, 827 (2004).
18. E. D. Kapp, J. R. Lorsch, *Annu. Rev. Biochem.* **73**, 657 (2004).
19. C. G. Proud, *Semin. Cell Dev. Biol.* **16**, 3 (2005).
20. M. W. Finn, F. R. Tabita, *J. Bacteriol.* **186**, 6360 (2004).
21. M. R. Walter *et al.*, *J. Biol. Chem.* **265**, 14016 (1990).
22. S. W. M. Kengen, J. E. Tuininga, F. A. M. de Bok, A. J. M. Stams, W. M. de Vos, *J. Biol. Chem.* **270**, 30453 (1995).
23. B. Siebers, P. Schönheit, *Curr. Opin. Microbiol.* **8**, 695 (2005).
24. A. Schäfer, G. Fritz, P. M. H. Kroneck, O. Ermler, *Biochemistry* **45**, 2960 (2006).
25. M. Hügler, H. Huber, K. O. Stetter, G. Fuchs, *Arch. Microbiol.* **179**, 160 (2003).
26. S. Guandon, O. Gascuel, *Syst. Biol.* **52**, 696 (2003).
27. S. Guandon, F. Lethiec, P. Duroux, O. Gascuel, *Nucleic Acids Res.* **33**, W557 (2005).

28. This study was supported by a grant-in-aid for scientific research (no. 14103031 to T.I.), a grant-in-aid for scientific research on priority areas "Applied Genomics" (no. 18018026 to H.A.), and a grant for the Japan Society for the Promotion of Science fellows (no. 1500*649 to T.S.) from the Ministry of Education, Culture, Sports, Science and Technology of Japan.

Supporting Online Material

www.sciencemag.org/cgi/content/full/315/5814/1003/DC1
Materials and Methods
Figs. S1 to S4
References

6 October 2006; accepted 8 January 2007
10.1126/science.1135999

Cadherin-11 in Synovial Lining Formation and Pathology in Arthritis

David M. Lee,[1] Hans P. Kiener,[1] Sandeep K. Agarwal,[1*] Erika H. Noss,[1*] Gerald F. M. Watts,[1*] Osamu Chisaka,[2] Masatoshi Takeichi,[3] Michael B. Brenner[1]†

The normal synovium forms a membrane at the edges of joints and provides lubrication and nutrients for the cartilage. In rheumatoid arthritis, the synovium is the site of inflammation and it participates in an organized tissue response that damages cartilage and bone. We identified cadherin-11 as essential for the development of the synovium. Cadherin-11–deficient mice have a hypoplastic synovial lining, display a disorganized synovial reaction to inflammation, and are resistant to inflammatory arthritis. Cadherin-11 therapeutics prevent and reduce arthritis in mouse models. Thus, synovial cadherin-11 determines the behavior of synoval cells in their proinflammatory and destructive tissue response in inflammatory arthritis.

Cadherin adhesion molecules are a family of integral membrane proteins that contain five immunoglobulin (Ig)–like extracellular (cadherin) domains, ligated as an extended chain by interdomain calcium binding (reviewed in (*1*, *2*)). Cadherins mediate cellular adhesion by binding a cadherin of the same type on an adjacent cell via interactions of the extracellular N-terminal first cadherin domains. During embryonic development, cadherins provide the basis for cell sorting, aggregation, and tissue morphogenesis (*1*, *3*). Postnatally, cadherins provide cell-to-cell adhesion within tissues, contributing to the maintenance of tissue integrity and architecture (*3*, *4*). Knowing these activities of cadherin proteins, we hypothesized that a mesenchymal cadherin may function to provide cell adhesion to organize the synovial membrane.

[1]Department of Medicine and Division of Rheumatology, Immunology and Allergy, Brigham and Women's Hospital, Harvard Medical School, 1 Jimmy Fund Way, Boston, MA 02115, USA. [2]Department of Cell and Developmental Biology, Graduate School of Biostudies, Kyoto University, Sakyo-ku, Yoshida-honmachi, Kyoto 606-8501, Japan. [3]RIKEN Center for Developmental Biology, Minatojima-Minamimachi, Chuo-ku, Kobe 650-0047, Japan.

*These authors contributed equally to this work.
†To whom correspondence should be addressed. E-mail: mbrenner@rics.bwh.harvard.edu

The synovium consists of a lining layer containing fibroblasts and macrophages that overlies a sublining layer of loose connective tissue. Using immunohistochemical staining, we found that the cadherin-11 in the lining layer of synoviocytes in healthy mice expresses cadherin-11 (Fig. 1, A and B). In a strain of mice that develops spontaneous autoimmune arthritis (K/BxN) (5, 6), marked cadherin-11 expression was seen on cells with fibroblast morphology in the synovial lining and in the synovial pannus, a pathological outgrowth of synovial tissue derived from fibroblast-like synoviocytes (FLS) (Fig. 1, C and D). Particularly intense staining for cadherin-11 was also noted in FLS within the pannus adjacent to bone and cartilage.

To define which synovial cellular lineages express cadherin-11, we used multicolor cytofluorometric staining of freshly disaggregated joint tissues, using a newly generated monoclonal antibody (mAb) to cadherin-11 anti-cadherin-11 (fig. S1) and CD45 (anti-CD45) (a marker of bone marrow–derived cells). Consistent with its expression on the FLS lineage in humans (7), we observed that cadherin-11 identifies a synovial population distinct from that identified by CD45 (Fig. 1, E and F). These findings were confirmed biochemically by fluorescence-activated cell sorting (FACS) isolation of CD45- or cadherin-11–expressing subpopulations. Western blotting of these subpopulations demonstrated restriction of cadherin-11 expression on the CD45- subpopulation (Fig. 1G). Previous studies have demonstrated that fibroblasts of the synovium express CD55 (8). In our analyses, CD55 expression was seen on about half of cadherin-11+ cells in arthritic joints (fig. S2). Cadherin-11 expression on cultured FLS, with the use of cell surface biotinylation and immunoprecipitation with anti-cadherin-11, revealed the anticipated protein species of molecular weight 140,000 from wild-type FLS but not from FLS derived from cadherin-11–deficient mice (Fig. 1H and fig. S3) (9). In addition, because cadherins associate with cytoplasmic β-catenin, we performed multicolor immunofluorescence microscopy and found colocalization of cadherin-11 with β-catenin in adherens junctions, specifically at sites of cell-to-cell contact between FLS (Fig. 1K to M). By means of a cell-to-substrate adhesion assay (10), the ability of FLS derived from either wild-type or cadherin-11–deficient mice was assessed for binding to recombinant cadherin-11 Fc. Wild-type FLS demonstrated robust adhesion to cadherin-11 Fc, whereas cadherin-11–deficient FLS failed to adhere (Fig. 1N and fig. S4). These studies demonstrate cadherin-11 expression in murine synovial fibroblasts, the localization of cadherin-11 to adherens junctions, and the role of cadherin-11 in homophilic adhesion by synovial fibroblasts.

The functional contribution of cadherin-11 to synovial fibroblast organization in synovial tissues was next explored. When compared to wild-type synovium, cadherin-11–deficient synovium

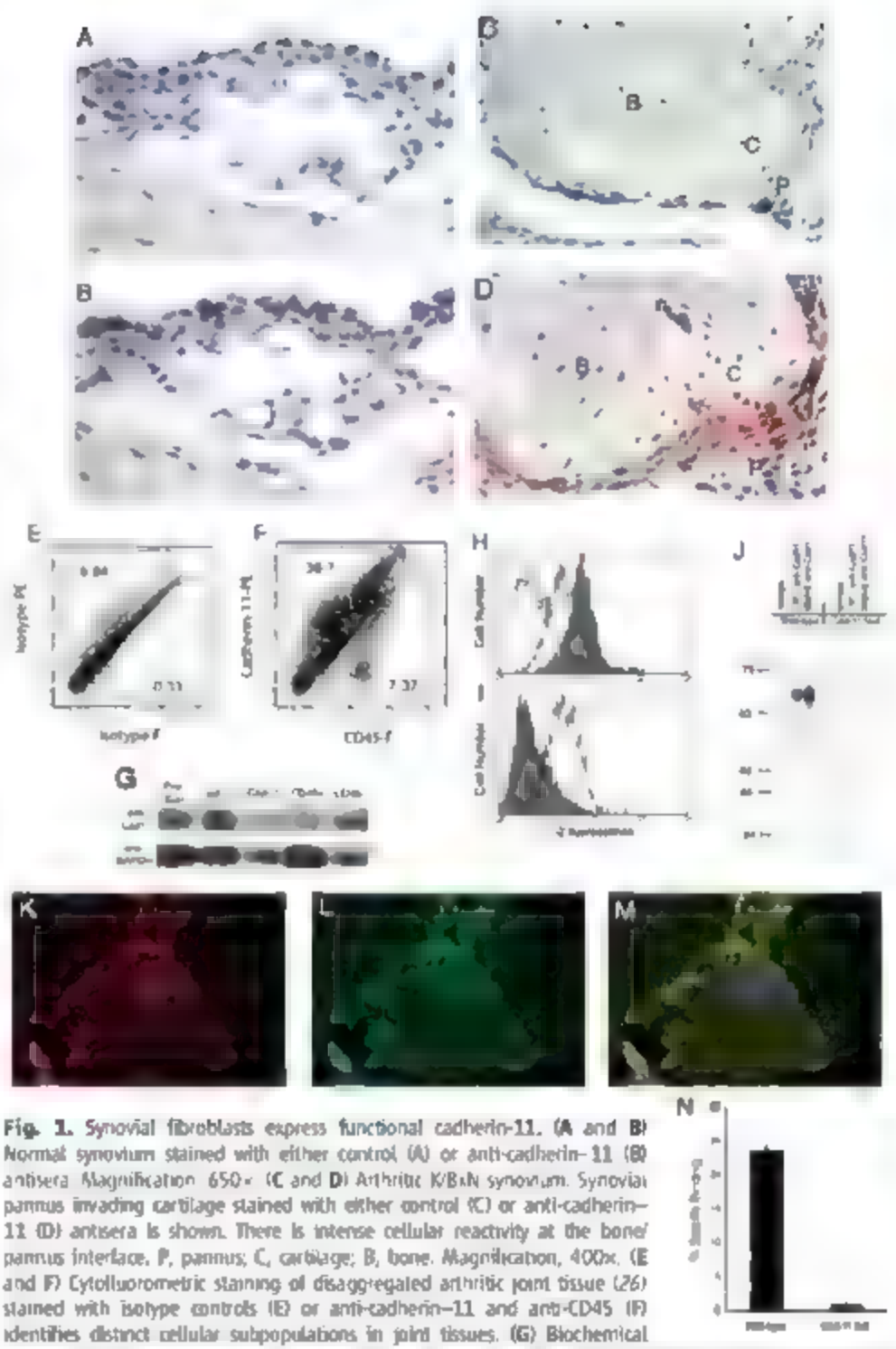

Fig. 1. Synovial fibroblasts express functional cadherin-11. (**A** and **B**) Normal synovium stained with either control (A) or anti-cadherin–11 (B) antisera. Magnification, 650×. (**C** and **D**) Arthritic K/BxN synovium. Synovial pannus invading cartilage stained with either control (C) or anti-cadherin–11 (D) antisera is shown. There is intense cellular reactivity at the bone/pannus interface. P, pannus; C, cartilage; B, bone. Magnification, 400×. (**E** and **F**) Cytofluorometric staining of disaggregated arthritic joint tissue (*26*) stained with isotype controls (E) or anti-cadherin–11 and anti-CD45 (F) identifies distinct cellular subpopulations in joint tissues. (**G**) Biochemical analysis of FACS-sorted synovial subpopulations. Dispersed arthritic joint tissues were labeled with either anti-CD45 or anti-cadherin–11 and sorted by means of FACS. Lysates of these subpopulations and presorted cells were analyzed by Western blot for cadherin-11 and glyceraldehyde-3-phosphate dehydrogenase (GAPDH) expression. There is an absence of detectable cadherin-11 expression in CD45-expressing cells. (**H** and **I**) Cytofluorometric staining of cultured FLS. FLS derived from wild-type (WT) (H) and cadherin-11–null (I) mice and passaged five times were stained with an anti-cadherin–11 mAb (gray fill), isotype control (dashed line), and an antibody to major histocompatibility complex class I (solid line). (**J**) Immunoprecipitation of cadherin-11 from cultured FLS. WT and cadherin-11–null FLS were surface biotinylated, lysed, and immunoprecipitated with isotype control Ig (IgG1) or anti-cadherin–11 (15F7 and 5B2H5). (**K** to **M**) FLS express cadherin-11 in adherens junctions. WT FLS were fixed and stained with anti-cadherin–11 (K) and anti–β-catenin (L) (*11*). The colocalization of cadherin-11 and β-catenin ((M), merged image) at sites of cellular interface is in a pattern consistent with that of adherens junctions. Magnification, 1000×. (**N**) Cadherin-11 mediates homophilic adhesion in FLS. WT and cadherin-11–null FLS were allowed to adhere to substrate cadherin-11–Fc in a cell-to-substrate adhesion assay (*10*). The homophilic adhesion of WT FLS to cadherin-11–Fc is absent in cadherin-11–null FLS. Error bars indicate SEM.

demonstrated marked hypoplasia of the synovial lining, with decreased synovial lining compaction and reduced membrane folds (Fig. 2, A to C). A primary function of FLS is the elaboration of extracellular matrix (ECM). Using Masson's trichrome stain to highlight ECM, we found that the dense ECM of the synovial lining, apparent in wild-type mice, was markedly attenuated in cadherin-11 null mice (Fig. 2, D and E). Thus, we conclude that cadherin-11 is necessary for cellular organization, compaction, and matrix elaboration of the synovial lining in vivo.

To further confirm the role of cadherin-11 in synovial tissue organization, we used a three-dimensional (3D) synovial micromass organ culture system in vitro (fig. S3A) (*11*). Single-cell suspensions of wild-type and cadherin-11 null FLS were dispersed in a surrogate ECM, and synoviocyte capacity for lining layer formation was assessed. Wild-type FLS establish a condensed lining-like structure at the matrix-media interface with marked similarity to that seen in the synovial lining at the synovial fluid interface in vivo (Fig. 2F). In contrast, cadherin-11 null FLS micromass cultures failed to develop lining condensation or compaction (Fig. 2G). Thus, this in vitro model of synovial tissue function confirms that lining layer compaction is an inherent feature of synovial fibroblast behavior that relies on cadherin-11.

We next examined the role of cadherin-11 in synovial fibroblast behavior in the K/BxN serum transfer model of autoimmune inflammatory arthritis. In this model, passive transfer of arthritogenic autoantibodies elicits a distal symmetric erosive polyarthritis with pathology mediated by immune complex formation, complement activation, myeloid lineage cell activation, and elaboration of cytokines interleukin-1 and tumor necrosis factor (TNF) (*5*, *6*, *12*–*15*). Administration of arthritogenic K/BxN serum revealed a measurable resistance to clinical arthritis in cadherin-11 null mice (Fig. 3, A and B). Indeed, pooled data for the clinical index from these mice demonstrated an average 50% reduction of clinical arthritic activity in cadherin-11 null mice. This reduction suggests that cadherin-11 expressed on fibroblasts can substantially influence the severity of pathology in arthritis.

As in rheumatoid arthritis, murine models of inflammatory arthritis display hyperplasia and outgrowth of synovial tissue composed of synovial fibroblasts (pannus tissue). The pannus attaches to and migrates over bone and cartilage surfaces, locally invading and destroying these structures (*16*). Examination of inflamed joint tissue architecture from wild-type and cadherin-11 null mice demonstrated that the typical condensed hyperplastic synovial lining architecture in inflammatory arthritis is largely absent in cadherin-11 deficient mice (Fig. 3, C and D). Rather, the synovial architecture in cadherin-11 deficient mice was chaotic and loosely organized.

The 3D micromass organ culture provides a means of analyzing selected factors that modulate synovial fibroblast function in a simplified model of the complex synovial microenvironment. Wild-type and cadherin-11 null synovial micromass organ cultures were stimulated with TNF, a potent inflammatory cytokine implicated in rheumatoid arthritis. In contrast to the dramatic ultrastructural changes in wild-type cultures, which are characterized by surface lining cellular accumulation and condensation, only modest changes were apparent in cadherin-11 deficient synovial micromass organ cultures (Fig. 3, E and F).

The results thus far suggested that cadherin-11 might be a potentially useful therapeutic target. To examine this, we used a cadherin-11 Fc fusion protein and an anti-cadherin-11 mAb. Similar to the cadherin-11 null phenotype, administration of either reagent ameliorated K/BxN serum transfer arthritis activity in wild-type mice (Fig. 3, G and H). To examine a role for cadherin-11 in ongoing inflammatory arthritis, we assessed its ability to reduce established disease. Because the K/BxN serum transfer model of arthritis is rapid and self-limited, we used a variation of this model, administering arthritogenic serum weekly to drive persistent synovitis (Fig. 3I). After allowing at least 2 weeks of active arthritis, we administered anti-cadherin-11 or isotype control treatments for a period of 10 days and examined arthritis clinical responses (Fig. 3, I and J). Similar to our observations in preventing acute arthritis, we find that anti-cadherin-11 displays moderate amelioration of established arthritis. These observations provide evidence that cadherin-11 contributes to the regulation of arthritic tissue responses in both acute and chronic synovitis.

The ability of FLS to migrate and invade through ECM is a potentially important feature of tissue remodeling that forms the hyperplastic lining and accompanies erosion into cartilage. Cadherins and especially mesenchymal cadherins, like cadherin-11, are known to influence cell migration and invasion (*17*). To gain further insight into the cadherin-11 regulation of FLS function, we performed migration and invasion assays through ECM-coated transwells. Although cadherin-11 null FLS display similar basal migratory activity to that of wild-type cells, their inducible migratory capacity was attenuated (Fig. 4A). Examination of platelet-derived growth factor (PDGF)–stimulated ECM invasive capacity revealed a dramatic deficit in cadherin-11 null FLS, which displayed only ~25% of the invasive activity of wild-type cells (Fig. 4B). These observations prompted us to examine cartilage and bone erosion in the inflammatory arthritis model in vivo. Indeed, synovial tissue attachment to, migration over, and

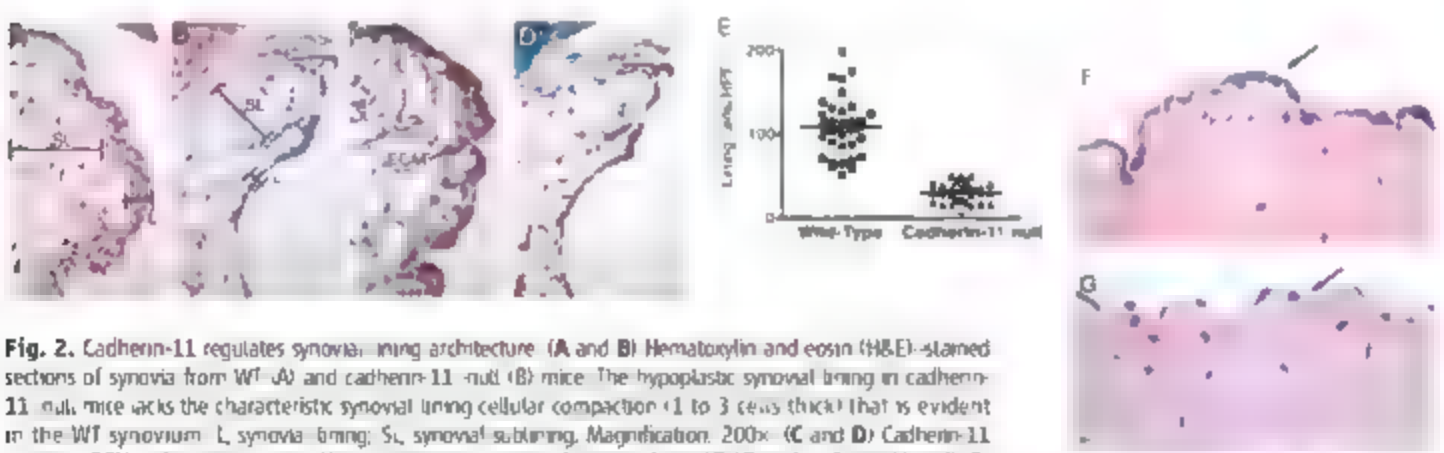

Fig. 2. Cadherin-11 regulates synovial lining architecture. (**A** and **B**) Hematoxylin and eosin (H&E)–stained sections of synovia from WT (A) and cadherin-11 null (B) mice. The hypoplastic synovial lining in cadherin-11 null mice lacks the characteristic synovial lining cellular compaction (1 to 3 cells thick) that is evident in the WT synovium. L, synovial lining; SL, synovial sublining. Magnification, 200×. (**C** and **D**) Cadherin-11 regulates ECM architecture in vivo. Masson's trichrome stains of synovia from WT (C) and cadherin-11 null (D) mice are shown. The hypoplastic synovial cellular lining (red) and markedly attenuated condensed ECM (blue) in cadherin-11 null mice as compared to those of the WT synovium are shown. Magnification, 200×. (**E**) Synovial lining cell density. Lining layer cells per high power field (HPF) (100 μm^2) were enumerated in WT (squares) and cadherin-11 null (triangles) mice. Individual results, mean, and SEM are provided. $n = 11$ mice per group. $P < 0.0001$. (**F** and **G**) Micromass organ culture lining compaction. WT (F) and cadherin-11 null (G) FLS were placed in micromass organ culture for 21 days (*11*) and were fixed, sectioned, and stained with H&E. The cellular condensation and lining formation behavior evident in WT FLS (arrow in F) and markedly attenuated in cadherin-11 null FLS (arrow in G) are shown. Magnification, 400×. Data are representative of five independent experiments.

invasion into cartilage were markedly diminished in cadherin-11–deficient mice. Wild-type synovial pannus caused full-thickness cartilage erosion, whereas cadherin-11 null synovial pannus stopped at the cartilage edge (Fig. 4, C and D, black arrowheads). Quantification by histomorphometric methods confirmed an 80% reduction in cartilage erosion in cadherin-11 deficient mice. By comparison, bone erosions, which are primarily dependent on osteoclast function (*18*, *20*), were evident to a similar degree in both wild-type and cadherin-11 null mice (Fig. 4E).

These studies suggest that, in healthy mice, cadherin-11 directs the establishment and maintenance of the normal synovial lining by conferring on FLS an ability to form cell-to-cell adhesion and compaction, as well as a capacity to produce ECM (Fig. 2). In the context of inflammatory arthritis, in which the synovium undergoes organized pathologic changes, mesenchymal lineage FLS contribute to these dramatic changes in the synovial lining (*7*, *9*). In cadherin-11 deficient mice, the synovial lining and synovial pannus tissue appeared architecturally aberrant and chaotic (Fig. 3, C and D), underscoring the role of cadherin-11 in fibroblast participation in the organized pathological synovial lining hyperplasia and pannus tissue destruction of cartilage in inflammatory arthritis.

The data suggest that cadherin-11 influences both the degree of inflammation (Fig. 3, A and B and G and H) and the organized pathologic response of the synovial tissue in response to arthritogenic K/BxN serum transfer (Fig. 4, C and E). In rheumatoid arthritis, the FLS population demonstrates a metabolically active, secretory state (*21*). Stimulation of FLS can induce secretion of a number of proinflammatory mediators that have been postulated to amplify and perpetuate synovial inflammation. Our findings suggest that cadherin-11 influences FLS participation in the synovial inflammatory reaction, in addition to its role in tissue remodeling and cartilage invasion. These insights identify previously unappreciated mechanisms governing the behavior of the joint lining and reveal the central role of a synovial cadherin in determining the behavior of the resident synovial mesenchy-

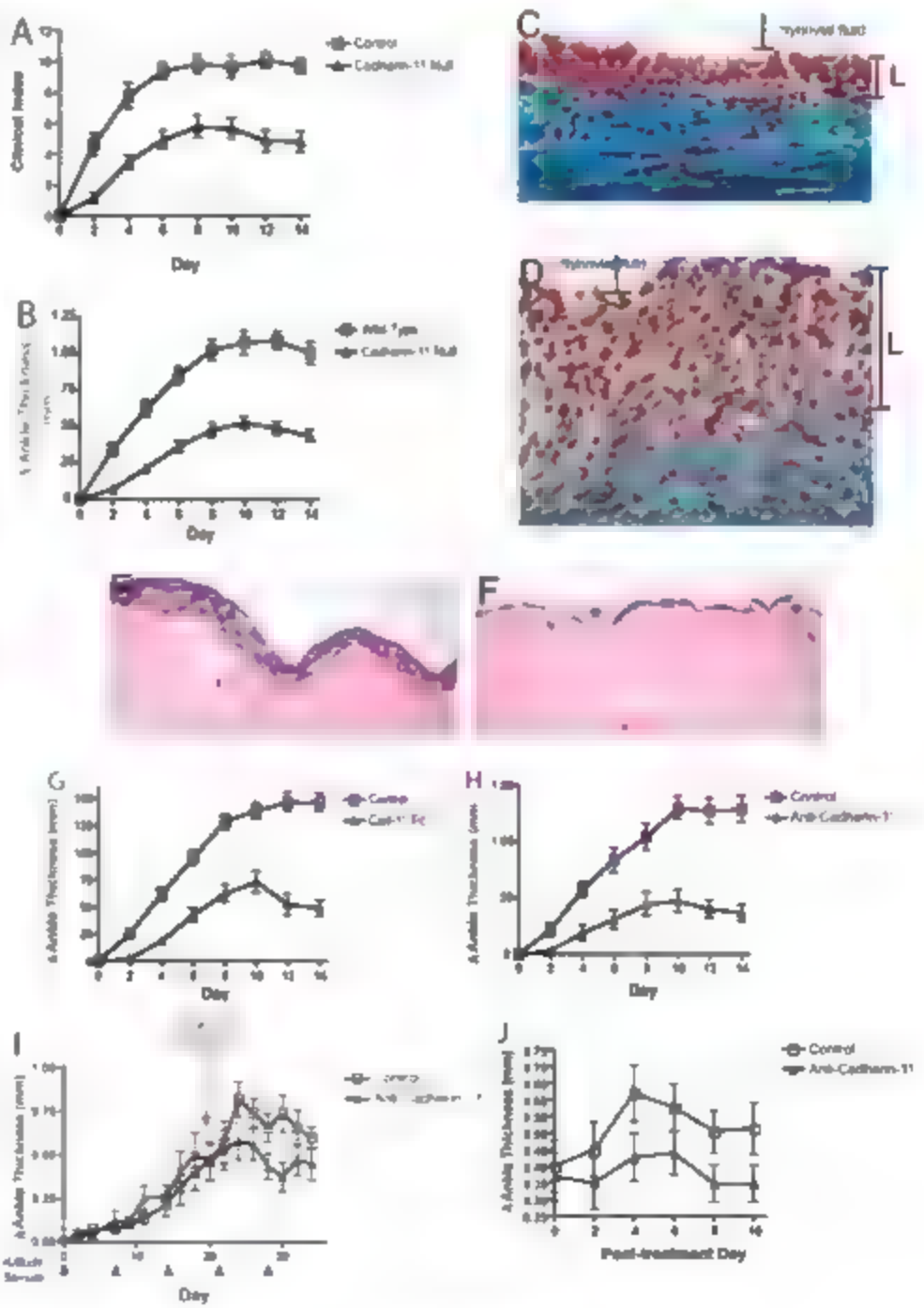

Fig. 3. Cadherin-11 modulates synovial tissue response in arthritis. (**A** and **B**) Cadherin-11–null mice are resistant to inflammatory arthritis. WT and cadherin-11 -null mice were injected with arthritogenic K/BxN serum, and clinical index (A) and changes (Δ) in ankle thickness (B) were recorded over 2 weeks (*6*). Pooled results from 24 (WT) or 26 (cadherin-11 -null) mice from four independent experiments ($P < 0.0005$) are shown. (**C** and **D**) Synovial architecture in inflammatory arthritis. Masson's trichrome–stained ankle sections from arthritic WT (C) and cadherin-11 -null (D) mice demonstrate synovial lining hyperplasia (red) and dense ECM deposition (blue) in WT mice. In contrast, cadherin-11 -null inflamed tissues demonstrate chaotic cellular organization within a minimal ECM. Synovial effusion in joint space is labeled. Magnification, 400×. (**E** and **F**) FLS lining architecture in vitro. WT (E) or cadherin-11 -null (F) FLS micromass organ cultures (*12*) were exposed to TNF (10 ng/ml) for 21 days. The high degree of lining condensation and lining layer formation evident in WT FLS (E) is markedly aberrant in cadherin-11 -null FLS (F). Magnification, 400×. Data are representative of three independent experiments. (**G** to **J**) Cadherin-11 biotherapeutics ameliorate inflammatory arthritis. WT C57BL/6 mice were injected with arthritogenic K/BxN serum [blue triangles in (I)] and co-injected [(G) and (H)] with control Ig (open squares) and with either cadherin-11–Fc [(G), solid triangles] or anti-cadherin–11 [(H), solid triangles] administered with a loading dose (0.5 mg) followed by maintenance dosing (0.1 mg) every 48 hours. Pooled results from 18 (cadherin-11–Fc) and 10 (anti-cadherin–11) mice are shown from four and two independent experiments, respectively. $P < 0.003$. For treatment studies [(I) and (J)], control Ig (open squares) or anti-cadherin–11 [(H), solid triangles] were administered for 10 days after allowing at least 2 weeks of arthritic activity. Results representative of two independent experiments (I) ($n = 5$ mice per group) and pooled treatment results (J) ($n = 10$ mice per group; $P = 0.0027$) are shown. Error bars in (A), (B), and [(G) to (J)] indicate SEM.

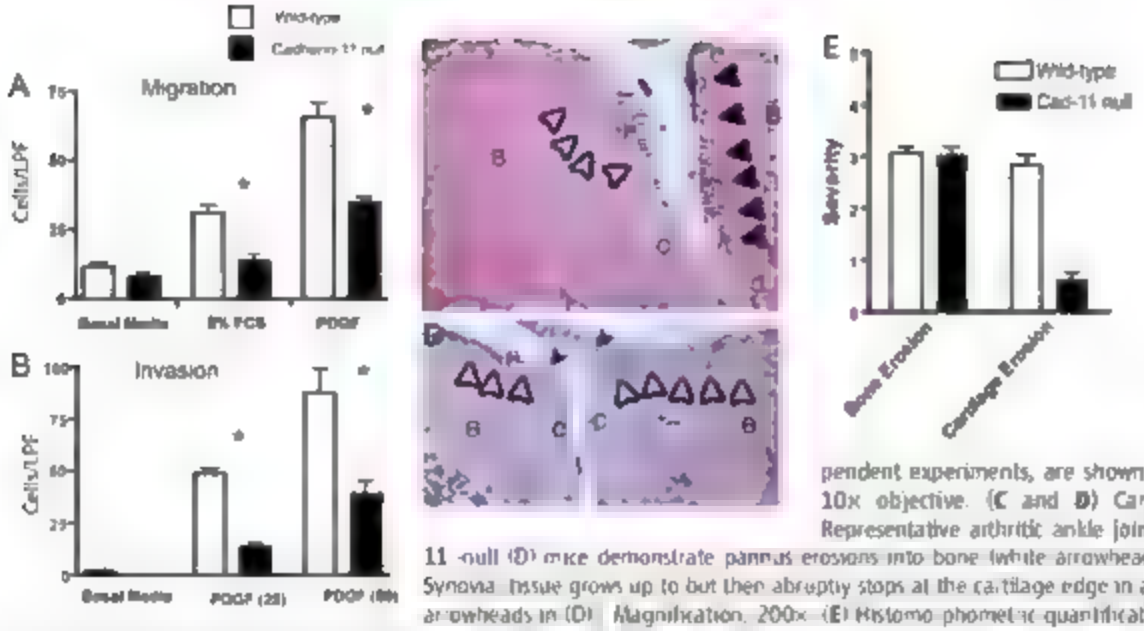

Fig. 4. Cadherin-11 regulates FLS invasive activity and cartilage erosion. (**A** and **B**) FLS migratory and invasive activity. FLS migratory activity was assessed in fibronectin-coated 8 μM transwell chambers (17) in the presence of basal media or stimulatory fetal calf serum (FCS) (5%) or PDGF. Invasive activity of WT (white bars) or cadherin-11–null (black bars) FLS was quantified in Matrigel ECM-coated transwells (17) in either basal media or PDGF (25 or 50 ng/ml). Mean ± SEM of quadruplicate counts from triplicate wells, representative of two independent experiments, are shown. *, $P < 0.01$. LPF, low power field, 10× objective. (**C** and **D**) Cartilage and bone erosions in vivo. Representative arthritic ankle joint tissues from WT (C) and cadherin-11 –null (D) mice demonstrate pannus erosions into bone (white arrowheads) and cartilage (black arrowheads). Synovial tissue grows up to but then abruptly stops at the cartilage edge in arthritic cadherin-11–null mice (black arrowheads in (D). Magnification, 200×. (**E**) Histomorphometric quantification of bone and cartilage erosions in ankle tissues from WT and cadherin-11 –null mice (27). There is a decrease in cartilage erosions in cadherin-11–null mice. Results are pooled data from 24 (WT) and 26 (cadherin-11 –null) mice from four independent experiments. $P < 0.0001$. Error bars represent SEM.

mal cells in the dynamic and orchestrated tissue response in inflammatory arthritis.

References and Notes

1. B. M. Gumbiner, *Cell* **84**, 345 (1996).
2. M. Takeichi, *Curr. Opin. Cell Biol.* **7**, 619 (1995).
3. M. J. Hamilton, J. I. Gordon, *J. Cell Biol.* **129**, 489 (1995).
4. M. Wheelock, K. R. Johnson, *Annu. Rev. Cell Dev. Biol.* **19**, 207 (2003).
5. V. Knudsen *et al.*, *Cell* **87**, 811 (1996).
6. D. M. Jee *et al.*, *Science* **297**, 1689 (2002).
7. K. valencia *et al.*, *J. Exp. Med.* **200**, 1673 (2004).
8. M. E. Medof, E. I. Walter, J. L. Rutgers, D. M. Knowles, V. Nussenzweig, *J. Exp. Med.* **165**, 848 (1987).
9. K. Horikawa, G. Radice, M. Takeichi, O. Chisaka, *Dev. Biol.* **215**, 182 (1999).
10. J. M. Higgins *et al.*, *J. Cell Biol.* **140**, 197 (1998).
11. H. P. Kiener, D. M. Lee, S. K. Agarwal, M. B. Brenner, *Am. J. Pathol.* **168**, 1486 (2006).
12. ., Matsumoto *et al.*, *Nat. Immunol.* **3**, 360 (2002).
13. ., Matsumoto, A. Staub, C. Benoist, D. Mathis, *Science* **288**, 1732 (1999).
14. H. Ji *et al.*, *Immunity* **16**, 157 (2002).
15. H. Ji *et al.*, *J. Exp. Med.* **196**, 77 (2002).
16. D. M. Lee, H. P. Kiener, M. B. Brenner, in *Kelley's Textbook of Rheumatology*, E. D. Harris Jr. *et al.*, Eds. (Saunders, St. Louis, ed. 7, 2004).
17. M. F. Kiernan, R. S. Prudoff, K. R. Johnson, M. J. Wheelock, *J. Cell Biol.* **142**, 631 (1999).
18. K. Yoshida *et al.*, *J. Clin. Invest.* **110**, 1419 (2002).
19. A. R. Pettit *et al.*, *Am. J. Pathol.* **159**, 1689 (2001).
20. V. Y. Kong *et al.*, *Nature* **402**, 304 (1999).
21. H. R. Schumacher, R. C. Kalunian, *Arthritis Rheum.* **15**, 465 (1972).
22. J. P. Kulka, D. Becking, M. W. Ropes, W. Bauer, *Arch. Pathol.* **59**, 129 (1955).
23. B. Henderson, E. R. Pettipher, *Semin. Arthritis Rheum.* **15**, 1 (1985).
24. M. A. Athanasou, J. Quinn, *Ann. Rheum. Dis.* **50**, 331 (1991).
25. C. Holbwell, C. J. Morris, M. Farr, K. W. Walton, *Virchows Arch. A Pathol. Anat. Histopathol.* **400**, 345 (1983).
26. Materials and methods are available as supporting material on Science Online.
27. M. Chen *et al.*, *J. Exp. Med.* **203**, 837 (2006).

28. This work was funded by NIH grants K08 AR2214 (D.M.L.) and RO1 AR48114 (M.B.B.), the Cogan Family Foundation (D.M.L.), the Arthritis Foundation Investigator Award (D.M.L.) and Fellowship Award (H.P.K. and E.H.N.), the Riva Foundation (M.B.B.), and an Abbott Scholar Award in Rheumatology Research (S.K.A.). M.B.B. and D.M.L. have equity holdings in Synovex Incorporated, which develops therapeutics for rheumatoid arthritis, and D.M.L. is a paid consultant to Resolvyx, Repligen, Medimmune, UCB Pharma, and MEDAcorp. The authors acknowledge the expert histotechnical assistance of I. Bowman.

Supporting Online Material

www.sciencemag.org/cgi/content/full/1137306/DC1
Materials and Methods
Figs. S1 to S3

8 November 2006; accepted 22 December 2006
Published online 25 January 2007;
10.1126/science.1137306
Include this information when citing this paper.

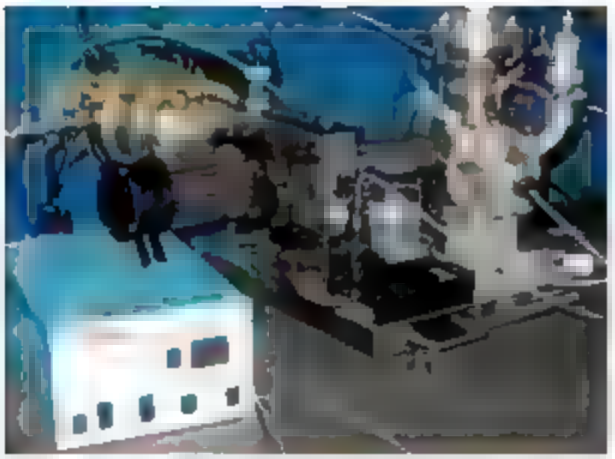

Spectrometer

Model 248/310 spectrometer is a tool for scientists developing new pulsed and tunable x-ray laser sources. It can detect laser harmonics over the 4 eV to 1.2 keV energy range. It bridges the gap between diffraction grating instruments and dedicated x-ray instruments. Model 248/310G is suitable for work in the 10^{-6} torr vacuum range. An ultra high vacuum version is available for work in the 10^{-10} torr vacuum range. An assortment of diffraction gratings is available to match the experimental region of interest. The 248/310 complements the McPherson line of vacuum-capable spectrometers suitable for lower energies and longer wavelengths. It features clean stainless steel construction and compact design that works well with a variety of laboratory discharge light sources and detectors.

McPherson For information 800-255-1055 www.McPhersonInc.com

Specialty Amino Acid Derivatives

Activotec offers a wide selection of amino acid derivatives. The comprehensive product line covers the full range of standard protected amino acids and hundreds of unusual amino acids as well as Boc, Fmoc, and Cbz-N-protected amino acids. The line includes activated amino acids, such as acid chloride, N-hydroxysuccinimide and pentafluorophenyl ester, as well as a wide variety of amino esters and amides.

Activotec For information +44-208-546-0869 www.activotec.com

Thermostable DNA Ligase

Ampligase Thermostable DNA Ligase for ligation-dependent mutation screening applications is derived from a thermophilic bacterium. It is stable and active at higher temperatures that T4 DNA Ligase. With a half-life of 48 hours at 65°C and more than 1 hour at 95°C, Ampligase Ligase permits extremely high hybridization stringency and ligation specificity.

Epicentre Biotechnologies For information 800-284-8474 www.EpiBio.com/Ampligase.asp

Laser Scanning Multiphoton Microscope

The LSM 5 MP is a laser scanning microscope configured for multiphoton microscopy that offers an excellent price/performance ratio. Efficient coatings on the optics ensure minimal power losses of the directly coupled femtosecond lasers. Leading-edge filter technology provides efficient suppression of the exciting light with simultaneous sensitive detection. Objective lenses adapted to the needs of multiphoton microscopy and featuring optical correction in the near infrared (IR) spectral range allow the optimum use of different IR excitation wavelengths, also in ranges of more than 1000 nm. Because these wavelengths enable even greater depths of tissue penetration thanks to lower absorption and scatter, their use in multiphoton microscopy is particularly beneficial. The W Plan-Apochromat objective lens with 20× magnification at a numerical aperture of 1.0 and a working distance of 2 mm is suitable for electrophysiology combined with multiphoton microscopy. It allows the imaging of larger areas of the specimen with excellent resolution and light collecting efficiency.

Carl Zeiss For information 914-681-7627 www.zeiss.com

X-ray Diffractometer

The MiniFlex II benchtop x-ray diffractometer offers compact design, portability, and simple installation. With dimensions slightly larger than a personal computer, the MiniFlex II incorporates technology usually reserved for larger, more expensive systems. A variable incident beam slit and diffracted beam monochromator make it suitable for a wide range of applications, including phase identification, quantitative analysis, crystallinity measurement, and structural characterization. The system includes all data analysis and other software in a complete turnkey package.

Rigaku For information 281-362-2300 www.Rigaku.com

Enzyme Labeling Kits

The HOOK HRP Plus Labeling Kit allows researchers to directly label enzymes with horseradish peroxidase (HRP). This kit makes use of an amine-reactive activated HRP that offers >90% coupling efficiency, which is superior to the commonly used glutaraldehyde coupling chemistry. There is a higher abundance of amines, compared to free sulfhydryls, allowing for a greater degree of labeling.

G Biosciences/Genotech For information 800-628-7730 www.GBiosciences.com

Incubators

The ProCulture 150UV incubators offer performance, ease of use, and fail-safe reliability even in demanding cell culture applications. The ultraviolet (UV) sterilization source reduces decontamination time to 30 min, enabling the system to be ready for operation with minimal interruption. Microprocessor control and monitoring of temperature, humidity, and carbon dioxide concentration ensure that optimal conditions for cell growth are maintained. A rear-wall plenum airflow distribution feature ensures that conditions in the entire chamber are stable and uniform. High relative humidity maintains optimum osmotic pressure in the cells, which is particularly suitable for long-term cultures.

SP Industries For information 800-523-2327 www.SPindustries.com

Newly offered instrumentation, apparatus, and laboratory materials of interest to researchers in all disciplines in academic, industrial, and government organizations are featured in this space. Emphasis is given to purpose, chief characteristics, and availability of products and materials. Endorsement by *Science* or AAAS of any products or materials mentioned is not implied. Additional information may be obtained from the manufacturer or supplier by visiting www.science.labvelocity.com on the Web, where you can request that the information be sent to you by e-mail, fax, mail, or telephone.

POSITIONS OPEN

FACULTY POSITION
Department of Biochemistry and Molecular Biology

The Department of Biochemistry and Molecular Biology, School of Medicine, Southern Illinois University Carbondale (SIUC), invites applications for a tenure-track position as an **ASSISTANT PROFESSOR** to start July 1, 2007. Modest teaching responsibilities in departmental and medical school curriculums may include biochemistry, molecular biology, and/or medical biochemistry. The position entails a cross appointment at the Simmons Cooper Cancer Institute. We seek a candidate with an earned M.D. or Ph.D. in life sciences or related area with experience in cancer research with an emphasis on understanding the molecular basis of cell cycle control, cellular development, signal transduction, or transcriptional regulation. Two or more years of postdoctoral experience preferred. Promise of a strong and externally funded research program required. Salary based on education, experience, and established School of Medicine guidelines. Please send curriculum vitae with a statement of research objectives and the names of three references to **Dr. Joseph C. Schmit, Chair, Department of Biochemistry and Molecular Biology, School of Medicine, Neckers Building, Mail Code 4413, Southern Illinois University Carbondale, 1345 Lincoln Drive, Carbondale, IL 62901, e-mail: jschmit@siumed.edu.** Applications review will begin April 1, 2007 and continue until the position is filled. *SIUC is an Equal Opportunity/Affirmative Action Employer that strives to enhance its ability to develop a diverse faculty and staff and to increase its potential to serve a diverse student population. All applications are welcomed and encouraged and will receive consideration. This is a security-sensitive position. Before any offer of employment is made, the University will conduct a pre-employment investigation which includes a criminal background check.*

ASSISTANT PROFESSOR
Division of Research
Department of Pathology
Louisiana State University School Health Sciences Center–Shreveport

The Division of Research within the Department of Pathology at Louisiana State University Health Sciences Center–Shreveport is seeking applicants for a tenure-track appointment at the Assistant Professor level. This position is open to individuals possessing [illegible] degrees. The successful candidate should have [illegible] in one or more of the following areas: molecular cell biology of [illegible], molecular mechanisms of cell adhesion and signaling, and/or vascular cell pathology. Applicants with expertise in the above areas [illegible]. The successful candidate will participate in graduate and medical education, clinical responsibilities, primarily defined by his/her research and training. Applicants should submit a curriculum vitae, list of at least three references, and a brief description of research interests and direction by March 30, 2007 to: **Kevin McCarthy, Ph.D., Professor, Department of Pathology, Louisiana State University Medical Center in Shreveport, P.O. Box 33932, Shreveport, LA 71130.** [illegible]. *Louisiana State University Medical Center is an Affirmative Action Employer.*

The College of Life Science at Fujian Normal University, China, invites applications for tenure-track faculty positions at **ASSOCIATE PROFESSOR** and **PROFESSOR** level. Individuals experienced in the area of developmental biology, cell biology, neurobiology, and microbiology are encouraged to apply. The positions offer an attractive startup package and excellent laboratory space. Candidates should have a Ph.D., suitable postdoctoral research experience, and an ability to develop innovative research programs.

For further information visit website: **http://life.fjnu.edu.cn/** or contact: **Prof. Yanding Zhang, Dean of the College (e-mail: life@fjnu.edu.cn).**

POSITIONS OPEN

TENURE TRACK
ASSOCIATE PROFESSOR or PROFESSOR
ASSOCIATE DEAN for BIOMEDICAL SCIENCES

Oklahoma State University (OSU) Center for Health Sciences, College of Osteopathic Medicine is a nationally ranked medical school with a long standing teaching tradition. We are seeking a dynamic individual who will serve as the Associate Dean for Biomedical Sciences, enjoying an excellent full-time career opportunity for the faculty of the College and OSU Medical Center in downtown Tulsa, Oklahoma.

Position provides oversight of planning, development, delivery, and evaluation of the biomedical sciences programs in the Center for Health Sciences. Supervises the planning, coordination, delivery and evaluation of biomedical courses. Recommends program for the development and enrichment of unit personnel. Consults with departmental Chairs to assign personnel to instructional services and related activities. Evaluates personnel performance and recommends personnel actions pertaining to acquisition, promotion and/or tenure, retention, and dismissal. Facilitates regularly scheduled meetings between Senior Associate Dean and Biomedical Department Chairs. Works closely with Associate Dean for Graduate Studies to develop and grow the graduate programs in biomedical sciences. Works closely with the Associate Dean for Clinical Education and Associate Dean for Graduate Medical Education in maintaining an integrated curriculum from OMS One to OGME Five, including research. Serves as a member of the Curriculum Committee and the Academic Deans Council. Requires a Ph.D. or D.O. degree and five years of related experience in postbaccalaureate [illegible] programs, [illegible] skills, record of scholarship [illegible] and publications. Prefer postdoctoral training, experience teaching biomedical sciences medical and graduate courses. Interested candidates must apply online at website: **https://jobs.okstate.edu,** job number 02809.

The Department of Surgery at the University of Pennsylvania's School of Medicine seeks candidates for an **ASSISTANT PROFESSOR** position in the nontenure research track. The successful applicant will have experience in the field of endocrine and oncologic surgery research with a focus on basic cell biology. Responsibilities include research investigation of the molecular mechanism of cancer, including cell surface receptors and their functions, cancer cell migration and invasion pathways, and identification of molecular biomarkers to improve prognostic [illegible] and diagnostics. Responsibilities also include mentorship and supervision of research and support staff in the surgical oncology laboratory. Applicants must have an M.D. or Ph.D. or M.D./Ph.D. degree.

The successful candidate will be expected to develop an independent but related research program in support of divisional research efforts. Past grant writing, including experience in cancer research, is essential, and a background in molecular imaging approaches in cancer applications is preferable.

Please submit curriculum vitae, a letter of interest, and references to:

Douglas L. Fraker, M.D.
Associate Professor and Chief, Division of Endocrine and Oncologic Surgery
c/o Peter Atherton
University of Pennsylvania School of Medicine
3400 Spruce Street, 4029 Maloney
Philadelphia, PA 19104

The University of Pennsylvania is an Equal Opportunity/Affirmative Action employer. Women and minority candidates are strongly encouraged to apply.

WWW.NIH.GOV
Positions NIH
THE NATIONAL INSTITUTES OF HEALTH

Senior Scientist, Vaccine Research Center
National Institute of Allergy and Infectious Diseases
National Institutes of Health (NIH)

The National Institute of Allergy and Infectious Diseases (NIAID) Vaccine Research Center (VRC) is seeking a Senior Scientist to provide technical research activities in emerging and novel vaccine delivery methods and serve as the lead of the Laboratory of Animal Medicine. The VRC is a major research component of the NIH and the Department of Health and Human Services (DHHS).

Doctoral level research and management experience is required of the position. The VRC is seeking candidates with a Ph.D. in virology, immunology or a related scientific field, and a Doctorate of Veterinary Medicine. The position requires a broad spectrum of scientific research activities and business management skills. Research projects include laboratory and clinical research activities. Must manage, develop, manage and oversee extramural research contracts for the VRC. Financial oversight and contract administration. Develop and plan studies and analyze data from animal studies evaluating the development of vaccine candidates. Board certification in either Veterinary Pathology or Laboratory Animal Medicine and experience in financial oversight of a large program is preferred.

The ideal candidate will have experience in research in non-human primate studies and good laboratory practices (GLP) for toxicity studies, and will have a record of independent research and peer-reviewed publications.

The Senior Scientist selected will receive a competitive salary and access to state-of-the-art resources to support laboratory research and a dedicated research budget to cover such costs as supplies and travel. Salary will be based on the individual's qualifications and experience in the range of $150,000 - $180,000.

Interested candidates may contact **Dr. John Mascola via E-mail: VRC_Positions@mail.nih.gov** for additional information about the position. To apply, the applicant must submit a curriculum vitae, bibliography (list of titles of articles), a detailed statement of research interests (not to exceed 3 pages), and the names of 3 selected publications to: **National Institute of Allergy and Infectious Diseases, Vaccine Research Center, c/o Intramural Administrative Management Branch, Attn: Ms. Marie Hirsch, Building 40, Room 1118, 40 Convent Drive, Bethesda, MD 20892-3013 or email hirschm@niaid.nih.gov by April 12th, 2007.**

Postdoctoral opening

A POSTDOCTORAL position is available in the Laboratory of Molecular Microbiology (LMM) National Institutes of Allergy and Infectious Diseases (NIAID), at the National Institutes of Health (NIH) within the Department of Health and Human Services (DHHS) to investigate retroviral budding and release. This program will focus on the interactions between viral and cellular proteins involved in the budding and release of HIV-1. The ideal candidate should have a Ph.D. degree and a strong background in molecular biology, biochemistry, virology, or cell biology. Interested individuals should submit a CV and names of three references to:

Fadila Bouamr Ph.D.
Laboratory of Molecular Microbiology, NIAID/NIH, Bldg. 4, Room 337, 4 Center Drive, Bethesda, Maryland, 20892-0460; e-mail: bouamrf@mail.nih.gov

Advancing Science by

Seeking Your Input

NIH Center for Scientific Review

2007

Peer Review

Open House Workshops

Learn more at http://www.csr.nih.gov/Openhouse

THE CHINESE UNIVERSITY OF HONG KONG

Applications are invited for

School of Chinese Medicine
(1) Associate Professor/ Assistant Professor
(Ref: 07013-0005#2) (Closing date: March 5, 2007)

Applicants should have: (a) a PhD degree (or its science preferably in Chinese medicine or related areas, (b) established scholarship with a track record of high-quality publications and award of competitive research grants, preferably (c) teaching and clinical experience in Chinese medicine and (d) qualification for practice in Hong Kong. Duties include: (a) teaching, (b) research, (c) supervision of graduate theses, (d) participating research projects, (e) consultancy work or even holding (f) specialty clinic and (g) serving in administration in the School and service share development. Appointment will normally be made on contract for up to three years initially, leading to longer-term appointment or subsequent ones later subject to mutual agreement.

Department of Anatomy
(2) Research Associate Professor/ Research Assistant Professor
(Ref: 07023-0005#2) (Closing date: March 12, 2007)

Applicants should have: (a) a PhD or an MD degree, (b) several years relevant research experience, (c) a good publication record in international refereed journals, desirably with high impact factors, and preferably (d) sound knowledge of the state-of-art techniques in biomedical research. The appointee will: (a) participate in research on bone science, cancer and immunology, (b) supervise graduate students, (c) undertaking teaching responsibilities within these fields, and (d) teach anatomy courses. Appointment will normally be made on contract basis for two years, renewable subject to mutual agreement.

Salary and Fringe Benefits

Salary will be highly competitive, commensurate with qualifications and experience. The University offers a comprehensive fringe benefit package, including medical care, plus a contract-end gratuity for appointments of two years or longer. Housing benefits for eligible appointees.

Further information about the University and the general terms of service for appointments is available at http://www.cuhk.edu.hk/policy/hkstaff/. The terms mentioned herein are for reference only and are subject to revision by the University.

Application Procedure

Please send full resume, copies of academic credentials, a publication list and/or about up to six selected published papers together with names, addresses, fax and e-mail addresses of three referees (whom will be approached only with consent has been given for their providing references (unless otherwise specified), to the Personnel Office, The Chinese University of Hong Kong, Shatin, N.T., Hong Kong (Fax: (852) 2603 6852) by the closing date. The Personal Information Collection Statement will be provided upon request. Please quote the reference number and mark "Application - Confidential" on cover.

Oklahoma State University
Division of Agricultural Sciences and Natural Resources

Professor and Stillington Chair Agricultural Biosciences

Applications and nominations are invited for the position of Professor and Stillington Chair Agricultural Biosciences at Oklahoma State University. This position will provide research leadership for a new Oklahoma State University Institute for Agricultural Biosciences at the Noble Foundation to be located on the campus of the Samuel Roberts Noble Foundation in Ardmore, OK. The major research programs of the new Institute will be forage improvement for livestock, fundamental research in plant biology, and bioenergy alternative fuels.

Applicants must hold a doctorate in agricultural, chemical, biological, science germane to the research emphases of the Institute and possess extensive research qualifications commensurate with an appointment at the full professor rank. More information and guidelines for application are at **http://jobs.dasnr.okstate.edu**.

Formal review of applications will begin **April 2, 2007** and will continue until a suitable candidate is identified.

Contact: **Clarence Watson, Chair, Search and Screening Committee, 139 Agricultural Hall, OSU, Stillwater, OK, 74078-6019. Phone: 405-744-5398. Email: c.watson@okstate.edu.**

OSU and DASNR are Affirmative Action/Equal Opportunity Employers committed to multicultural diversity. Women and members of other under-represented groups are strongly encouraged to apply.

The Department of Oceanography at Texas A&M University reopens the search for an experienced and visionary **department head** with exceptional communication skills and a background in academic leadership. Candidates must have a track record of scholarship that is fitting for appointment as a tenured full professor of Oceanography.

The department (**http://oceanography.tamu.edu**) was established in 1949 and has a rich history of fundamental and applied ocean research. The department consists of a combined faculty and staff of 69 with 71 graduate students. It resides in the College of Geosciences (**http://geosciences.tamu.edu**) which also includes the departments of Atmospheric Sciences, Geography, Geology and Geophysics, and several related units: the Sea Grant Program, the Geochemical and Environmental Research Group, and the Integrated Ocean Drilling Program. The department also maintains close ties with a branch campus at Texas A&M University-Galveston.

The department head is responsible for leadership of the department including strategic planning, academic administration, graduate student recruitment, development activities, connections with the broader national and international community, and effective use of the department's financial, administrative, and human resources. The new head will oversee the hiring of a significant number of positions that will complement a 28 faculty hiring effort that the College of Geosciences began in 2004 in four target areas: Climate Change; Oceans, Atmospheres and Human Health; Environmental and Hydrological Geosciences; and Ocean Drilling and Sustainable Earth Sciences (ODASES).

Candidates are asked to submit a detailed curriculum vitae, statements of research interests, of educational philosophy, and of administrative philosophy, and three letters of reference to: **Dr. John R. Giardino, Search Committee Chair, Office of Graduate Studies, Texas A&M University, College Station, Texas 77843-1113, rickg@tamu.edu.** Screening of applicants will begin mid-February 2007; however, applications and nominations will continue to be accepted until the position is filled.

Texas A&M University is an Affirmative Action/Equal Opportunity Employer. The University is dedicated to the goal of building a culturally diverse and pluralistic community committed to teaching and working in a multicultural environment. We strongly encourage applications from women, underrepresented ethnic groups, and individuals with disabilities.

Top 100 Hospital expanding in Central Texas

Endowed Chair in Pediatric Research
Scott & White Health System
Texas A&M System Health Science Center College of Medicine

The Children's Hospital at Scott & White and The Texas A&M System Health Science Center College of Medicine are seeking a nationally recognized research scientist as the first holder of the Josephine Ballard Endowed Chair in pediatric research. Applicants should be accomplished investigators (Ph.D., M.D. or M.D./Ph.D.) at the associate or professor level with current federal grants and a proven track record in basic, clinical, and/or translational research. The successful candidate will join an expanding faculty within a large academic healthcare system. The chair holder will play a critical role in directing and expanding research activities in pediatric diseases, in close collaboration with investigators in local, national and international experts in cell biology, genomics and proteomics.

The Children's Hospital at Scott & White serves a large clinical base throughout Central Texas. There are outstanding clinical practice and laboratory facilities on campus that perform state of the art molecular and cellular biology techniques. flow cytometry, proteomics and genomics as well as biostatistical support services. Animal laboratory facilities include areas to perform medical and surgical procedures. Laboratory space and an appropriate start-up package for the chair holder will be provided. The Scott & White Healthcare system is one of the largest multi-specialty integrated delivery systems in the nation. Scott & White is the primary clinical and hospital teaching campus for the College of Medicine. Academic appointments at the associate and professor level through the College of Medicine are commensurate with qualifications and experience.

Interested candidates should send a copy of their curriculum vitae, letter addressing their qualifications and a list of 3 individuals who can provide references to: **Don P. Wilson, M.D., Chair, Search Committee for Josephine Ballard Centennial Chair in Pediatric Research, Chairman, Department of Pediatrics, 2401 South 31st Street, Temple, Texas 76508, 254-724-4383, fax: 254-724-1938, email: dwilson@swmail.sw.org.**

Scott & White is an equal opportunity employer. For more information regarding Scott & White and The Texas A&M System Health Science Center College of Medicine, please log onto: www.tamu.edu and www.sw.org

The Children's Hospital

Scott & White Memorial Hospital and Scott, Sherwood and Brindley Foundation

COLUMBIA UNIVERSITY

Center for Neuroscience Initiatives
Executive Director

Columbia University is recognized as a global leader in the basic and clinical neurosciences. The Center for Neuroscience Initiatives (CNI) is an organizing arm for the development, implementation, and coordination of new neuroscience related initiatives at Columbia University. CNI will focus on launching new programs and centers that will accelerate the translation of fundamental discoveries into new insights and potential therapies for neurological and psychiatric disorders. Important objectives of CNI will be to integrate preclinical and clinical neuroscience, and to bridge the gap between molecular neurobiology and cognitive neuroscience.

We are seeking an Executive Director to play a leading role in the development and ongoing implementation of scientific, business, and operational plans to support of CNI. Reporting to the co-directors of CNI, the incumbent will be responsible for the day to day management of the center, programmatic, scientific and financial activities, which will include the development and support of the work of the center, new faculty recruitment, coordination of program grants, communications, public relations, and fund raising. He/She manages administrative activities for the center. Provides strategic oversight for center initiatives including new programs, grants, core facilities, meetings, and communications. Oversees and manages all internal and external meetings. Researches and develops ideas for new translational programs. Develops a strong internal and external network for collaboration and support of neuroscience activities, and coordinates internal and external communications to publicize and disseminate these activities. Prepares monthly updates on CNI activities to the co-directors. Participates in external meetings and professional activities where relevant to CNI goals.

Bachelor's degree required with ten years of experience in program management for a private/corporate foundation, public charity, government organization, academic institution, or corporation. Master's degree or equivalent may substitute for part of the experience. High intellectual capacity abroads applied to learning new areas of science and technology and related fields. Demonstrated project management skills, including project design, launch execution, oversight, and effective budget management. Strong oral and written communication skills that take into account the audience and equally effective listening skills. Desire to be part of an evolving center and to contribute to its growth and reputation. Demonstrated ability to work with scientists in a staff role.

Ph.D. or M.D. in scientific/medical area related to neuroscience and/or graduate level degree M.P.H., M.B.A., J.D. preferred.

Submit resume and cover letter online through the Columbia University job site (http://jobs.columbia.edu/applicant/Central?quickFind=104703).

Contact David Leyden at dgl2102@columbia.edu with any questions.

Columbia University takes affirmative action toward equal employment opportunity.

ASSISTANT or ASSOCIATE PROFESSOR
Stem Cell Biology
UNIVERSITY OF PENNSYLVANIA

The Department of Animal Biology and the newly established Institute for Stem Cells and Regenerative Medicine at the University of Pennsylvania are soliciting applications for two TENURE-TRACK faculty positions at the ASSISTANT or ASSOCIATE PROFESSOR level. Animal Biology has a strong commitment to basic biomedical research and is located at the heart of Penn's Philadelphia campus in an interactive scientific environment. Candidates with research interests in the broad areas of basic science and translational research in stem cell biology are encouraged to apply. Applicants must have a PhD, MD, VMD/DVM, or equivalent degree along with postdoctoral training, and should be prepared to establish an independent extramurally funded research program. Applicants are expected to interact with multiple existing Research Centers at Penn, such as the Center for Animal Transgenesis and Germ Cell Research, and to teach in the Department and in University-wide graduate programs.

Candidates should submit by **April 2, 2007** a PDF file with a curriculum vitae, a statement of research interests, and arrange for electronic submission of three reference letters to **Dr. O. Jacenko at stemcellsearch@vet.upenn.edu. University of Pennsylvania School of Veterinary Medicine, 3800 Spruce Street, Philadelphia, PA 19104-6046; FAX: 215-573-5189.**

The University of Pennsylvania is an Equal Opportunity/Affirmative Action Employer. Minorities/Females/Individuals with Disabilities/Veterans encouraged to apply.

DUKE UNIVERSITY
Center on Global Change
Two Postdoctoral Positions

(1) Regional Biogeosciences and Environmental Sciences: Duke University's Center on Global Change and Nicholas School of the Environment & Earth Sciences seek an earth scientist in biogeosciences, ecology, hydrology, modeling, or remote sensing to analyze the interactions of climate change with terrestrial ecosystems in the southeastern U.S. The candidate will contribute to Dept. of Energy efforts (**http://www.nicer.duke.edu**) to study and synthesize climate change effects in the region. Approaches may include remote sensing of ecosystem change, field experiments, and/or regional modeling. The scientist will have access to field facilities at Duke, including the Forest FACE experiment of elevated CO_2 and N fertilization (**http://face.env.duke.edu**). For more information see **http://www.nicholas.duke.edu/cgc/** and **http://www.biology.duke.edu/jackson**

(2) Climate Change, Biofuels and Agriculture: Postdoctoral position in Duke's Center on Global Change and Nicholas School of the Environment and Earth Sciences. We seek a scientist with experience in biogeosciences, plant ecology, agriculture, hydrology, modeling of remote sensing to analyze interactions of climate change with agricultural systems in the U.S. An applicant could also combine economic modeling and forecasting for the agricultural market sector; such efforts might include synthesizing climate change effects on crop production, and interactions between alternative fuel market growth and food and feed production capacity.

Send a CV, statement of interests, and 3 recommendation letters to: **Rob Jackson, Director - Center on Global Change, Nicholas School, Box 90658, Duke Univ., Durham, NC 27708-0658.** Applications received by **March 25, 2007** will be assured consideration.

Duke is an Equal Opportunity Employer; minority applicants are particularly encouraged to apply.

YALE UNIVERSITY
School of Forestry & Environmental Studies
School of Architecture
Junior Faculty Position in Sustainable Design and Development

Yale University's School of Forestry & Environmental Studies and School of Architecture seek applicants for an unprecedented joint tenure level Assistant Professorship in Sustainable Design and Development, with an emphasis on the urban environment. More specifically, we seek individuals who have expertise, or the potential to establish this expertise, in the management and design of urban environmental systems and urban ecological infrastructures with a focus on the neighborhood and community scale rather than the building and site scale. Candidates should not only demonstrate an interest in minimizing adverse environmental impacts of urban development but also in enhancing beneficial human connections to natural systems in urban areas. The successful candidate will be expected to advise, supervise and instruct both environmental studies and architecture students, offering lecture, seminar and/or project-based courses in areas such as sustainable design and development, urban design, urban ecology, landscape ecology and design, and restoration of urban environmental systems. This person will be expected to assume a leadership role in the recently established School of Forestry & Environmental Studies and School of Architecture joint Master's Degree program. We prefer a candidate with advanced training in any of the following fields: sustainable design and development, urban design, landscape ecology and design, urban ecology, architecture, or allied fields.

Applicants should send a curriculum vitae, statement of research, teaching and or professional practice interests, two representative examples of research or professional publications and/or design work, and a list of three references to: **Professor Stephen R. Kellert, Yale University, School of Forestry & Environmental Studies, 205 Prospect Street, New Haven, CT 06511, USA AND Professor James Axley, Yale University, School of Architecture, 180 York Street, New Haven, CT 06511, USA.** The deadline for applications is **April 1, 2007.**

Yale University is an Affirmative Action/Equal Opportunity Employer. Men and women of diverse racial/ethnic backgrounds and cultures are encouraged to apply.

Three Tenure Track Associate or Assistant Professor Positions for Biomedical Engineering, Tohoku University, Sendai, Japan

http://www.ttsc.cress.tohoku.ac.jp

Tohoku University is seeking young scientists who are eligible to be independently engaged in research of biomedical engineering, for example artificial organs, biomaterials, biomechanics, medical imaging, medical informatics, medical robotics, nanomedicine, tissue engineering and/or related areas. We encourage women and foreigners to apply.

The successful applicants are expected to be enrolled in a "Program of Frontiers of Advanced Interdisciplinary Area" that is sponsored by Ministry of Education, Science, Culture, Sports and Technology, Japan. This program covers the period of 2006 through Mar. 31, 2011, and offers annual salaries for three tenure track researchers and three additional researchers (postdoctoral fellows or technicians). Financial supports for equipment and reagents are also awarded. During or at the end of the program, the researchers will be able to obtain tenured positions after evaluation by the committee.

Interested applicants should send curriculum vitae, a publication list, PDF files of major papers (less than 5), a summary of research activities as well as future research plans in about 1,000 words, a list of scientific grants awarded previously, and three recommendation letters or names and contact information of three references to: **Masaaki Sato, Professor (satow@bme.mech.tohoku.ac.jp), Department of Biomechanics and Robotics, Graduate School of Engineering, Tohoku University, 6-6-01, Aza-Aoba, Aramaki, Aoba-ku, Sendai 980-8579, Japan.**

Deadline for application is **March 30, 2007**. A committee consisting of mpty as well as extramural members will select successful applicants through paper-review and interview.

DIRECTOR
Bigelow Laboratory for Ocean Sciences

Bigelow Laboratory for Ocean Sciences, West Boothbay Harbor, Maine seeks an imaginative, accomplished and entrepreneurial scientist with exceptional leadership and communication skills for the position of Director.

Bigelow Laboratory is an independent, non-profit organization renowned for its major contributions to oceanography through cutting-edge research on processes affecting the productivity of the oceans, coastal seas and estuaries. Founded by visionary scientists Drs. Charles and Clarice Yentsch in 1974, Bigelow Laboratory is distinguished by a spirit of scientific freedom, a tradition of open interdisciplinary team-building, and mentorship. It is a unique community of scientists, staff, trustees and global neighbors with a common dedication to ocean sciences. Present interdisciplinary research strengths include phytoplankton ecology and evolution, optical oceanography, marine microbiology, and the ecology of higher trophic levels, with expansion into trophodynamics and ecological chemistry. Facilities include the Provasoli-Guillard National Center for Culture of Marine Phytoplankton, the MacIsaac Facility for Individual Particle Analysis and the Center for Transmission and Scanning Electron Microscopy. For more information, please visit: **http://www.bigelow.org**

The Director will help Bigelow Laboratory realize a shared vision for future excellence including planned expansion to a new facility. He/she will lead staff and operations, ensuring continuing recruitment, retention and development of top-quality staff. The Director will work effectively with the Board of Trustees, and will encourage creativity and innovation at all levels. She/he will help shape the agenda for future ocean sciences research at the state, national and international levels, communicate the importance of oceanographic research to policymakers and the general public, and diversify Bigelow Laboratory's funding from public and private sources, building on its long-standing success in acquiring competitive external funding.

Salary will be competitive and commensurate with experience and qualifications; a complete benefits package is available. Nominations and applications including curriculum vitae, evidence of leadership, relevant scientific organizations, scientific achievement, and professional goals should be sent to: **Director Search Committee, Bigelow Laboratory, PO Box 475, W. Boothbay Harbor, ME 04575, USA or Bigelowdirector@bigelow.org, +1 207-633-9615.** Review of applications will begin by **April 1, 2007**.

An Affirmative Action/Equal Opportunity Employer

CASE
SCHOOL OF MEDICINE

Postdoctoral Position in HIV Molecular Biology
Department of Molecular Biology and Microbiology

A POSTDOCTORAL SCHOLAR RESEARCH ASSOCIATE POSITION is available in the group headed by **Dr. Jonathan Karn**, Chairman of the Department of Molecular Biology and Microbiology at the Case Western Reserve University School of Medicine. The Department has strong ties to the Case Center for AIDS Research, and is currently undergoing a period of rapid expansion.

The work of Dr. Karn's group focuses on the control of HIV transcription. Ongoing projects concern biochemical and genetic studies of the mechanisms of action of Tat, HIV's transcription transactivator, and regulation of promoter clearance by transcription factors. For a recent publication see **Kim et al.** *EMBO J.* 25, 3596-3604, 2006. Further details may be viewed at **http://www.case.edu/med/microbio/karn.htm**.

The position of **POSTDOCTORAL SCHOLAR/RESEARCH ASSOCIATE** is open to candidates with less than 5 years postdoctoral experience. Salary and benefits in keeping with NIH scales, and relocation expenses will be provided. Exceptionally qualified and more senior applicants will be considered for an Instructor position. **Experience in the biochemistry of transcription, molecular virology and/or gene expression in mammalian cells is essential.** For further information on the position and for detailed instructions on how to apply, please visit: **http://www.case.edu/med/microbio/karnpostdoc.htm**. Interested applicants are asked to visit the website, complete a brief online application and provide a letter of application, curriculum vitae, brief statement of research goals and accomplishments, and names and contact information of three professional references. Please respond by **March 31, 2007**. Applications will be considered upon receipt.

In employment as in education, Case Western Reserve University is committed to Equal Opportunity and World Class Diversity.

Automation Chemist/ Instrument Specialist

The Merck Catalysis Center in the Chemistry Department at Princeton University is engaged in supporting academic research in the area of catalytic reaction development as part of a fast-paced discovery environment.

Job responsibilities for this position include, but are not limited to, operating, modifying computer-based procedures for the control of automated high-throughput equipment, preparation of catalyst/ligand libraries and the maintenance of laboratory instrumentation. Examples of laboratory equipment include liquid and solid dispensing robots, parallel reactor systems, and analytical instrumentation (HPLC, SFC, GC, LC/MS, etc.). Additionally, there is the opportunity for a motivated candidate to conduct publishable independent research in collaboration with the Catalysis Center.

The job candidate will have a Ph.D. (or M.S. degree with extensive experience) in chemistry and with practical experience in working with HTS instrumentation. The candidate should have proficiency in the operation and maintenance of automated HTS instrumentation, analytical instruments (SFC, HPLC, GC, LC/MS), and glove boxes, etc. It would be desirable to have a strong background in analytical characterization, specifically in development of chiral HPLC/LC/MS/GC/SFC methods as well as computer programming skills. The ability to work in a team environment is required with effective interpersonal skills to communicate clearly and interact with academic collaborators (faculty, graduate students, and postdoctoral associates).

Applicants should send their CV, a brief statement of research interests, and three letters of reference to: **Ms. Caroline Phillips, Department of Chemistry, Princeton University, Princeton, NJ 08544-1009**. For information about applying to Princeton and how to self-identify please link to **http://web.princeton.edu/sites/dof/ApplicantsInfo.htm**

Princeton University is an Equal Opportunity/Affirmative Action Employer.

SIXTY FACULTY POSITIONS
Université Claude Bernard Lyon 1, Lyon, France

Universite Claude Bernard University Lyon 1 is offering 60 tenure-track positions (associate and full professors) in the following fields: mathematics, physics, chemistry, computer science, mechanical engineering, electronics, biochemistry, biology, pharmaceutical and medical sciences (including virology). Applications are invited to consult our web site **www.univ-lyon1.fr** and to click on "portail de mobilite". They will find a short description of the different positions offered in terms of teaching and research activities and the Lyon 1 addresses of the department heads to contact for detailed information. Appointees will be selected through national and local scientific committees. Indications on the selection procedure and the salary ranges can be found on our web site. The appointed faculty members are expected to establish a successful research program and secure extramural funding. They will be involved in undergraduate and graduate student education and research. The university is one of the largest in France with more than 30 000 students involved in all the domains of science including life science and engineering. It can boast of a very strong and efficient research activity that takes place in more than 90 laboratories carrying out cutting edge research focusing on three main domains: health, material, and environmental sciences. Lyon, in the heart of France's second most important region is the third largest city with 1.2 million people famous for its industrial network, higher education and gastronomy.

More information about Lyon can be found in the Higher Education and Research Researcher's Guide **http://www.lyoncampus.org/pagesguide-etab3.htm**

Applications should be sent before **March 30, 2007** for positions opened in September 2007. Applications should be sent by e-mail only to **Prof. J.F. Mornex**, Vice President in charge of research **mornex.cevu@adm.univ-lyon1.fr**

BOSTON UNIVERSITY

The **Department of Pharmacology & Experimental Therapeutics** at Boston University School of Medicine (**http://www.bumc.bu.edu/busm/pm**) has open faculty positions at the **Assistant, Associate** or **Full Professor** levels. Individuals with an interest in translational neuroscience or with research programs bridging disciplines such as cancer, cardiovascular or infectious disease biology are especially encouraged to apply. The Department has strengths in a broad range of research areas including learning and memory, neuropeptides, substance abuse, neurodegenerative diseases, neuroinflammation, anxiety, and epilepsy. The Department administers an active university-wide pharmacological sciences training program that is supported by an NIGMS T32 and awards a combined PhD in Pharmacology Biomedical Neuroscience or Pharmacology-Cell and Molecular Biology.

Interested individuals should send a C.V., statement of research directions and up to three publications to: **David H. Farb, Ph.D., Chairman, Department of Pharmacology & Experimental Therapeutics, Boston University School of Medicine, 715 Albany Street, L-603, Boston, MA 02118**

An Equal Opportunity/ Affirmative Action Employer

Grant for Postdoctoral Positions in Sweden

The grant will enable researchers with Swedish or non-Swedish doctorates (PhDs or equivalent) to work at Swedish higher education institutions or research establishments. The programme will span two years. Research areas: Natural Sciences, Engineering Sciences, Humanities, Social Sciences and Educational Sciences.

Application documents will be posted on the website at the end of February. The last application date is 29 March 2007.

www.vr.se

Vetenskapsrådet

KU MEDICAL CENTER
The University of Kansas

FACULTY POSITIONS IN MAGNETOENCEPHALOGRAPHY

The Hoglund Brain Imaging Center and the Department of Neurology at the University of Kansas Medical Center seek two faculty to join an established magnetoencephalography (MEG) based research and clinical neuroscience program. Specific research areas of interest include but are not limited to speech, language and hearing, motor control, brain injury, and signal processing. Clinical activity includes integrated multi-modality imaging in epilepsy and brain tumor pre-surgical planning.

Research (2 positions): (a) a senior faculty (Professor or Associate Professor) who will lead the research MEG program and continue his/her funded research program. (b) a junior faculty (Assistant Professor) who will focus on his/her own computational or applied MEG research.

Clinical (1 position): a clinical epileptologist (Professor or Associate) who will direct a Comprehensive Epilepsy service and lead the clinical MEG program.

The faculty members will be expected to develop independent research or clinical programs and to collaborate with existing university researchers. Research candidates should have a doctoral degree in neuroscience or related discipline. Clinical candidates should have an M.D. with specialist training in epilepsy. Experience and research funding in MEG or EEG is highly desirable. Facilities include whole head and fetal MEG systems and 3T (human) and 9.4T (animal) MRI in a dedicated research building. Further details of the HBIC program are at **www.kumc.edu/hoglund**. Competitive salary and start-up packages are available.

Interested individuals should send a statement of research interest and resume to:

William M. Brooks, Ph.D.
Director, Hoglund Brain Imaging Center
wbrooks@kumc.edu

uOttawa

L'Université canadienne
Canada's university

FACULTY OF MEDICINE

Department of Cellular and Molecular Medicine

The Faculty of Medicine at the University of Ottawa is presently undergoing a significant strategic expansion of research within its basic science departments with a specific focus on molecular, cellular and systems approaches to understanding fundamental questions of cellular function and growth and development. In the context of this overall strategy, the Department of Cellular and Molecular Medicine is presently inviting applications for tenure stream Faculty positions from outstanding candidates at all career stages. Strong candidates using innovative approaches to study important biological problems are invited to apply, although in this application cycle priority will be given to applicants with research interests in **Molecular and Cellular Biology** to complement and extend existing research strengths in

Regulation of Growth Control

Developmental Genetics

Molecular Physiology

Regenerative Medicine

Successful applicants will be provided with generous and comprehensive start-up packages and will be housed within a new 100,000 sq. ft. state of the art expansion of the Faculty of Medicine's Health Sciences complex. Canada Research Chairs will also be available to exceptional candidates. Successful applicants will possess a Ph.D. and are expected to develop vigorous independent research programs and to contribute to the teaching mission of the Department. The University of Ottawa is a bilingual institution, thus proficiency in both English and French is an asset.

As Canada's National Capital, Ottawa is a vibrant and attractive city with a high standard of living.

More information on the Department can be obtained at
http://www.uottawa.ca/academic/med/cellmed/

Interested individuals are requested to submit a curriculum vitae, a list of at least three references and a statement of research interests to:

Chair
Search Committee
Department of Cellular and Molecular Medicine
Faculty of Medicine
University of Ottawa
451 Smyth Road
Ottawa, Ontario
Canada K1H 8M5
mhincke@uottawa.ca

Electronic submissions are encouraged and applications will be accepted until
April 30, 2007

www.uOttawa.ca

According to government policy, all qualified candidates are invited to apply; however, preference will be given to Canadian citizens and permanent residents. The University of Ottawa is an equal opportunity employer.

The University of Ottawa, at the heart of Canada's capital, is one of our country's leading research universities. We are a cosmopolitan community of over 40,000 students, faculty and staff who live, work and study in both English and French. We are proud to be Canada's university.

MICHIGAN STATE UNIVERSITY

Tenure Track Position in Nutrition
Department of Food Science and Human Nutrition

http://www.fshn.msu.edu/nutrition.pdf

Chair
Nutrition Search Committee Department of Food Science and Human Nutrition Michigan State University, East Lansing, MI 48824-1224. Fax: 517-353-8963

MSU IS AN AFFIRMATIVE ACTION, EQUAL OPPORTUNITY EMPLOYER

CARDIOLOGIST
TRANSLATIONAL RESEARCH SCIENTIST

Please e-mail your curriculum vitae, a description of your research programs, career goals and the names of three references to: michael.simons@dartmouth.edu. Dr. Michael Simons, Director, Angiogenesis Research Center, Dartmouth Medical School, Lebanon, NH 03756.

DARTMOUTH-HITCHCOCK
MEDICAL CENTER
www.dhmc.org

A Tenure Track Associate Professor Position for Medical/Dental Engineering
Tohoku University
Graduate School of Dentistry
Sendai, Japan
http://www.ddh.tohoku.ac.jp

Tohoku University Graduate School of Dentistry is seeking a young scientist who is eligible to be independently engaged to research of medical dental engineering, including medical dental tissue engineering system cell engineering, medical dental biomaterials, nanomaterials bioimaging, bioinformatics, medical dental robotics, biomechanics nanomedicine nanodentistry and of related areas. We encourage women and foreigners to apply.

The successful applicant is expected to be enrolled as a "Program of Frontiers of Advanced Interdisciplinary Area" that is sponsored by Ministry of Education, Science, Culture, Sports and Technology, Japan. This program covers the period of 2007 through March 31, 2011, and covers annual salary for the tenure track associate professor and one additional researcher (postdoctoral fellow or technician). Financial supports for equipment and reagents are also awarded. During or at the end of the program, the researcher will be able to obtain tenured position after evaluation by the committee.

Interested applicants should send curriculum vitae, a publication list, PDF files of major papers (less than 3), a summary of previous activities as well as future research plans in about 1,000 words, a list of scientific grants awarded previously, and three recommendation letters (or names and contact information of three references) to **Tohoku University Graduate School of Dentistry, Personnel Section, Address: 4-1 Seiryo-machi, Aoba-ku, Sendai, 980-8575 Japan. E-mail: den-jim@bureau.tohoku.ac.jp; Fax: +81 (Japan) 22 717 8279**

Deadline for application is **April 16, 2007**. A committee consisting of intra- as well as extramural members will select a successful applicant through paper-review and interview.

MERCK & CO., INC
Our work is someone's hope. Join us.

Director — Structural Biology

Where patients come first MERCK

Discovery of Great Drugs demands continuous discovery of Great People.

Merck is an equal opportunity employer. M/F/D/V. proudly embracing diversity in all of its manifestations.

advancing health through research

Faculty Positions in Clinical Research

The University of Massachusetts Medical School and its clinical partner, UMass Memorial Health Care, have declared the expansion of clinical and translational research as a major institutional priority. The new Department of Clinical and Translational Science will play a leading role in the expansion of the clinical research enterprise in the University of Massachusetts Medical School and UMass Memorial Health Care and will be housed in the 258,000 sq. ft. Advanced Education and Clinical Practice Center, currently under construction.

The University of Massachusetts Medical School is one of the fastest growing medical schools in the country, attracting more than $174 million in research funding annually. The University of Massachusetts Medical School has built a reputation as a world-class research institution, consistently producing noteworthy advances in clinical, epidemiological and basic research. University of Massachusetts Medical School faculty member **Craig Mello, PhD**, a graduate of Yale and Andrew Fire, PhD from Stanford University, shared the 2006 Nobel Prize in Physiology or Medicine for the discovery of RNA interference.

In the first phase of development of the Department of Clinical and Translational Science, three senior-level or tenure-track faculty will be recruited to head up the Centers and Divisions of the Department. We seek leaders to build strong research and education programs and core support facilities in Epidemiology and Biostatistics, Bioinformatics and Community Research, which will be new Departments of Clinical and Translational Science. These Divisions will support the mission of the Department of Clinical and Translational Science to promote the development of a broad agenda in clinical, epidemiological, and translational research in order to positively impact the health of communities and populations, and to serve as a national model for others.

The Directors will develop Divisions that perform nationally recognized research, education and service programs, provide support for interdisciplinary research and education programs that link basic, clinical and translational research within the Medical School, the Graduate School of Biomedical Sciences, the Graduate School of Nursing, the UMass Memorial Health Care system, and the wider Central Massachusetts community.

Division of Epidemiology and Biostatistics: In addition to their own research, faculty in this Division will support research programs of investigators from clinical and basic science departments in developing innovative methods for epidemiologic and statistical analyses of cohort studies, observational studies, outcomes research and health services research. This Division's faculty will play a major role in teaching epidemiology and biostatistics in graduate research training programs including an MS degree in clinical research and a recently initiated PhD Program in Clinical and Population Health Research.

Division of Bioinformatics: Beyond their own research, faculty in the Division of Bioinformatics will support research programs of investigators from clinical and basic science departments. We are particularly interested in bioinformatics research focused on genetic variation, proteomics, metabonomics and bioinformatics in populations enrolled in observational studies, randomized trials and large disease registries. Faculty in this Division will play a major role in teaching bioinformatics in the graduate PhD and clinical research training programs.

Division of Community Research: Faculty and staff in this Division will work to ensure that clinical and translational research processes throughout the institution is integrated into the community. Responsibilities include promoting community and healthcare provider participation in clinical and translational research, and leading efforts to increase levels and diversity of subject participation in research. The faculty in this Division will participate in developing recruitment and training clinical investigators in community-based participatory research. A strong track record of peer-reviewed community-based research will be required.

Applicants for these Division Director positions must have an MD and/or PhD degree, postdoctoral experience or equivalent training and an outstanding record of research achievements. Candidates must be committed to excellence in graduate education and a track record of independent external funding for their research. Applicants must have shown leadership experience as well as the ability to work as part of an interdisciplinary team.

Applicants should send a CV, statement of research interest, and names and addresses of three references to **John L. Sullivan, MD, Chair, Department of Clinical and Translational Science, Vice Chancellor for Research, Office of Research, S1-859, University of Massachusetts Medical School, 55 Lake Avenue North, Worcester, MA 01655-0002**. Documents may be submitted electronically at **DCTS@umassmed.edu**

The University of Massachusetts is an Affirmative Action Equal Opportunity Employer

Basic Scientist Faculty Position

Neonatal Pulmonary Biology/Vascular Biology

[redacted]

be provided to facilitate program development. Please submit resumes an[redacted]

G. Ganesh Konduri, MD • Chief of Neonatology
Department of Pediatrics
Medical College of Wisconsin
8701 Watertown Plank Road • CCC410
Milwaukee, WI 53226
[redacted]
gkonduri@mcw.edu

Children's Hospital and Health System® | Medical College of Wisconsin

Children's Specialty Group®

E E-AA M F T

University of Massachusetts Lowell

UMASS Lowell

Careers with Mass Appeal

Assistant Professor Clinical Toxicologist

Department of Clinical Laboratory and Nutritional Sciences

The University of Massachusetts Lowell is conducting a search for a Clinical Toxicologist for a tenure track faculty position to assess the impact of nanomanufacturing and related emerging technologies on human health and the environment. Knowledge and experience with liquid chromatography/tandem mass spectroscopy (LC/MS/MS) is required to determine and quantitate novel biomarkers in body fluids and tissues to evaluate the toxicity associated with occupational and environmental exposure to the processes and products of nanomanufacturing using green chemistry principles. The successful candidate will be in the Department of Clinical Laboratory and Nutritional Sciences and the successful applicant will work in close collaboration with other faculty in the School of Health and Environment as well as with NSF Nanoscale Science and Engineering Center for High Rate Nanomanufacturing and the Lowell Center of Excellence in Nanomanufacturing at the University. The successful candidate will be required to carry out a vigorous research program to establish extramural funding, graduate courses in Clinical Biochemistry, Clinical Toxicology and related subjects.

This position is available at the Assistant Professor level, but more senior appointments will be considered for candidates with an outstanding record of research and teaching.

For additional information on this opening, please visit http://www.uml.edu/Employment/

Applications will be received until position is filled. The position will start on September, 2007. Applicants are requested to send curriculum vitae, statements of teaching and research interests, and a list of three references to:

Search Committee Chair, Professor Eugene Rogers Ph.D., MT (ASCP),
Department of Clinical Laboratory and Nutritional Sciences,
University of Massachusetts Lowell, 3 Solomont Way, Suite 4,
Lowell, MA 01854 USA

Job Reference #FC 02016002

Email cover letter and resume to clintoxicology@uml.edu

Please include reference number in subject line of email.

University of Massachusetts Lowell is an Equal Opportunity/Affirmative Action, Title IX, IRV and ADA 1990 Employer.

中国科学院上海巴斯德研究所
INSTITUT PASTEUR OF SHANGHAI
CHINESE ACADEMY OF SCIENCES

PI Recruitment

The Institut Pasteur of Shanghai (IPS), Chinese Academy of Sciences is seeking outstanding young Principal Investigators with previous experiences in HIV, hepatitis B and C, and emerging viruses causing acute respiratory infection to reinforce its world-class research projects in innovation and discoveries of methods to prevent and treat viral diseases, including the development of vaccines and treatments. The mission of IPS, CAS is to promote and facilitate basic research on virus entry and release, virus assembly in host cells and interaction between viral proteins and host factors. The scope of the research covers the understanding of the natural history and mechanisms of viral infection and pathogenesis and the host immune response.

Candidates shall have a Ph.D. in basic virology and immunology, viral pathogenesis, anti-viral vaccine development or viral immunology with outstanding accomplishments in internationally well-known institutions, and a good track record of publications in high-level international journals. Candidates may be eligible for the "100 Talent" program from the Chinese Academy of Sciences.

Candidates should be able to develop new projects based on national key projects and conduct good research work in the field. IPS, CAS offers a large panel of core facilities and excellent working conditions in a highly collaborative environment and in strong connection with the Chinese Academy of Sciences and Pasteur Institute networks. Candidates should be able to work full time in the Institute. The successful applicants will also demonstrate a commitment to post-graduate level teaching and training program.

The initial appointment is for a period of three years, renewable upon evaluation. Competitive salary will be commensurate with experiences and qualifications. Applicants should submit electronically a full CV (in English) that includes history of training, employment, awards, achievements, a publication list, two-page summary of research interest in the proposed fields of research, three letters of recommendation and dates of availability preferably by **March 30, 2007** for first batch of review to: **Ms. Caroline Wu, Institut Pasteur of Shanghai, CAS, 225 South Chongqing Road, Shanghai, 200025, China; Tel: 86-21-6384-2921 Fax: 86-21-6384-7571, E-mail: wwu@sibs.ac.cn**. Personal data collected will be used for recruitment purposes only. Please contact the following website for further information: **www.shanghaipasteur.ac.cn**

Postdoctoral Fellowships
Dartmouth College
Life Sciences

The Department of Biological Sciences at Dartmouth College, with funding from the Howard Hughes Medical Institute, seeks applications for two **HHMI Postdoctoral Fellowships in the Life Sciences**. The HHMI Fellowships are two-year, non-tenure track positions with NIH NRSA scale salaries and comprehensive Dartmouth health benefits; they are designed to provide further training to beginning postdoctoral fellows in the arts of teaching and research. Each fellow will pursue a life science-related research project in the laboratory of a Dartmouth faculty member from an appropriate department in the Arts and Sciences, Medical School, or Engineering School. Collaborative projects that involve more than one laboratory at Dartmouth will also be considered. In addition, during each of the two academic years that span their fellowship, each fellow will be paired with a senior faculty member with whom they will co-teach an undergraduate course in biology, thus receiving substantial training under the guidance of an experienced faculty mentor. The goal of the HHMI Fellowships is to ensure that the fellows develop strong research and teaching credentials.

Applicants should prepare a cover letter, in which they indicate up to three laboratories with which they would like to be affiliated (contact with these laboratories prior to application submission is encouraged but not required; see **http://www.dartmouth.edu/~biology/HHMIpostdoc.html** for more information), a curriculum vitae, and a statement of career goals and teaching interests. These materials, plus three letters of recommendation from individuals qualified to comment on the applicant's credentials, should be sent to **HHMI-Fellowship@mac.dartmouth.edu**. Materials may also be submitted by **FAX (603-646-1347)** or **U. S. mail (HHMI Fellowship Search Committee, Department of Biological Sciences, 6044 Gilman, Dartmouth College, Hanover, New Hampshire 03755)**. Consideration of applications will begin on **16 April 2007** and continue until the positions are filled. Fellowships will run for two years and could begin as early as 1 September 2007.

Dartmouth College is an Equal Opportunity/Affirmative Action Employer

OTOLARYNGOLOGIST

The Section of Otolaryngology - Head and Neck Surgery at Dartmouth-Hitchcock Medical Center seeks a board certified or board eligible Otolaryngologist for a full-time faculty position. The candidate should possess an interest in an academic career and in the education of medical students and residents. This position will combine a general otolaryngology with a subspecialty practice in otology or pediatric otolaryngology. Fellowship training in otology/ neurotology or pediatric otolaryngology is desirable. Research interests will be encouraged. Academic rank will be commensurate with qualifications and experience.

Interested applicants are encouraged to send letters of inquiry and CV to:

Daniel Morrison, MD, Chairman
Section of Otolaryngology - Head & Neck Surgery
Dartmouth-Hitchcock Medical Center
One Medical Center Drive
Lebanon, NH 03756
Telephone: 603-650-8123

DARTMOUTH-HITCHCOCK
MEDICAL CENTER

Dartmouth-Hitchcock Medical Center is an affirmative action/equal opportunity employer and is especially interested in identifying female and minority candidates.

www.DHMC.org

Max-Planck-Institut für Züchtungsforschung

Max Planck Institute for Plant Breeding Research

International Max Planck Research School:
"The molecular bases of plant development and environmental interactions"

10 Ph. D. Studentships

The Max Planck Institute for Plant Breeding Research together with the University of Cologne, the Institute of Biorganic Chemistry Poznan, Poland; the Institute for Plant Sciences, Gif-sur-Yvette, France; and the Biological Research Centre (Szeged, Hungary) invite applications for Ph.D. fellowships as part of the International Max Planck Research School (IMPRS) in Cologne (Germany).

The IMPRS is intended for highly motivated students with a strong training in molecular sciences. The constellation of participating institutions provides excellent conditions and expertise in plant genetics and biochemistry, structural biology, biochemistry, cell biology and molecular microbiology. The training includes regular seminars, supervision of a thesis committee of the research school, soft skill courses, practical courses on e.g. reverse genetics, non-invasive imaging, 3-D structural analysis of proteins, bioinformatics, and novel mass spectrometry based protein biochemistry at the participating institutions. The program is taught in English and open to students from all countries holding a Master's degree or a [illegible].

For detailed information about the application process and the Ph.D. program please visit the IMPRS homepage at www.mpiz-koeln.mpg.de/english/student information/index.html. Deadline for applications is March 30, 2007.

The Max Planck Society is an equal opportunity employer. We highly encourage female scientists to apply for the program. The fellowship application should be mailed to:

Max Planck Institute
for Plant Breeding Research
IMPRS - Molecular Basis of Plant Development
Scientific Coordinator
Carl-von-Linné Weg 10
50829 Cologne, Germany

VANDERBILT UNIVERSITY
SCHOOL OF MEDICINE

Faculty Position
in
Drug Disposition and Metabolism

The Division of Clinical Pharmacology at Vanderbilt University School of Medicine is recruiting a tenured or tenure-track faculty member in the field of **Drug Disposition and Metabolism**. Areas such as drug pharmacokinetics and pharmacodynamics, drug transporters, receptors, and mechanisms of drug metabolism are of high interest. Vanderbilt has a superb environment related to Pharmacology and Clinical Pharmacology and possesses outstanding cores to support this research.

Candidates with an M.D. and or Ph.D. should send curriculum vitae, statement of research interests, and at least three supporting letters from mentors or colleagues to:

Dr. Jason Morrow, Chief
Division of Clinical Pharmacology
Departments of Medicine and Pharmacology
536 RRB, Vanderbilt University School of Medicine
Nashville TN 37232-6602
Tel: 615.322.4785
Fax: 615.343.9659
Email: jason.morrow@vanderbilt.edu

Vanderbilt University School of Medicine is an Equal Opportunity/ Affirmative Action Employer

John B. Pierce Laboratory/ Yale School of Medicine/ Yale University

The John B. Pierce Laboratory, an endowed research institute affiliated with Yale University, seeks to expand its research program in body energy balance by adding two outstanding scientists with active research programs in metabolism and or environmental physiology.

METABOLISM/ENVIRONMENTAL PHYSIOLOGY

The Laboratory takes a systems approach to physiology, integrating physiology with molecular biology, biochemistry, neuroscience, behavior and epidemiology. Programmatic interests include, but are not limited to, thermoregulatory, metabolic, and cardiovascular responses by humans and or animals to environmental stimuli. Joint appointments are anticipated in the Department of Epidemiology and Public Health, Yale University School of Medicine.

Candidates should show evidence of ability to obtain external funding. Rank of appointment is open.

The Laboratory offers competitive salary, benefits, and start-up, as well as an outstanding work environment. Applicants should submit hard and electronic copies of CV, description of research interests, set of representative publications, and names of at least three references to:

Chair, Metabolism/Environmental Physiology Search
The John B. Pierce Laboratory, Inc.
290 Congress Avenue
New Haven, CT 06519
Electronic copies: metsearch@jbpierce.org

Review of applications will begin on **March 1, 2007** and continue until the positions are filled.

EOE/AA

www.jbpierce.org

West Virginia University
ROBERT C. BYRD HEALTH SCIENCES CENTER

Associate Professor or Professor Center for Respiratory Biology and Lung Disease

As part of a major growth initiative supported by a new **Strategic Research Plan (SRP), West Virginia University Health Sciences Center** invites applications from outstanding scientists to join the Center for **Respiratory Biology and Lung Diseases**. The Center is one of six interdisciplinary research centers being established in accordance with the SRP (*Science*: Sept. 8, vol. 313, p. 1461 2006). Preference will be given to faculty with established research programs and credentials for appointment as Associate Professor or Professor (tenure-track) in either **a basic science or clinical department in the School of Medicine**. The goal of the Center is to develop an interdisciplinary group of collaborating basic and clinical scientists focused on translational research in respiratory biology and lung disease. We are seeking investigators that explore cellular, molecular or genetic mechanisms of asthma, COPD or inflammatory lung injury resulting from viral, bacterial or environmental exposures. Respiratory complications due to childhood or adult obesity and associated vascular disorders are also a high priority.

Appointee must have transferable NIH-RO1 funding and a desire to participate in either graduate and/or health professional education. The Health Sciences Center has seven interdisciplinary Ph.D. programs and a joint M.D./Ph.D. Scholars Program in the biomedical sciences which include graduate faculty from multiple departments. Appointee will receive a generous start-up package, competitive salary, laboratory space and be named a **Wyeth Research Scholar**.

Qualifications: A Ph.D., M.D., or M.D./Ph.D. with significant research accomplishments. Applications should include curriculum vitae, cover letter with a brief description of research interests and the names and addresses (including e-mail) of three references. E-mailed applications with attachments are preferred and should be addressed to Sandy Ammons **sammons@hsc.wvu.edu**. Mailed correspondence should be addressed to **Richard D. Dey, Ph.D., Search Committee Chair and Director, Center for Respiratory Biology and Lung Disease, PO Box 9130, West Virginia University Health Sciences Center, Morgantown, WV 26506-9130 (rdey@hsc.wvu.edu)**. Review of applications will continue until positions are filled.

West Virginia University is a comprehensive, public Carnegie-designated Research institution, with approximately 23,000 undergraduates plus 5,500 graduate and professional students. The Health Sciences Center located on the university campus includes the Schools of Medicine, Pharmacy, Dentistry and Nursing, each having both health professional as well as graduate training programs. Two new research buildings which collectively provide 200,000 sq ft of additional research space are under construction at Health Sciences to accommodate our research growth agenda. Morgantown has 55,000 residents and is rated as one of the best small towns in the U.S. with affordable housing, excellent schools, a picturesque countryside and many outdoor activities.

West Virginia University is an Affirmative Action/Equal Opportunity Employer

West Virginia University
ROBERT C. BYRD HEALTH SCIENCES CENTER

School of Pharmacy

Professor or Associate Professor

In accordance with the **WVU Health Sciences Center (HSC) Strategic Research Plan (SRP)** (*Science*: Sept. 8, vol. 313, p. 1461 2006), we are seeking an outstanding scientist to be appointed as a Wyeth Research Scholar. The SRP is designed to expand research in specific thematic areas through the building of **Interdisciplinary Research Centers** for neuroscience, cancer cell biology, cardiovascular sciences, respiratory biology and lung diseases, immunopathology and microbial pathogenesis, as well as diabetes and obesity. Appointee will be a member of a Research Center and have a primary **faculty appointment in the School of Pharmacy**. Candidates should have experience in health professional education and graduate research training. Candidates with biomedical research interests in either cardiovascular diseases, diabetes and obesity, or lung diseases are preferred for the title of Wyeth Research Scholar. Appointee must have a transferable NIH-RO1 funded research program.

Qualifications: Ph.D. or M.D. with significant research experience. Submit (e-mail preferred) curriculum vitae with contact information for three references to: **Dr. Patrick Callery, Search Committee Chair, WVU School of Pharmacy, PO Box 9530, Morgantown, WV 26506; pcallery@hsc.wvu.edu**

Associate Dean for Research and Graduate Studies

The School of Pharmacy is seeking an outstanding investigator as Associate Dean. The incumbent will be expected to maintain an active independent research program and develop collaborative research efforts among the **Departments of Basic Pharmaceutical Sciences; Clinical Pharmacy; and Pharmaceutical Systems and Policy** within the School of Pharmacy. The Associate Dean must also advance the goals of the **WVU Health Sciences Center (HSC) Strategic Research Plan (SRP)** (*Science*: Sept. 8, vol. 313, p. 1461 2006) and its newly formed six Interdisciplinary Research Centers. The position will be filled at either the **Professor or Associate Professor** rank with expectations of the appointee to devote approximately 50% effort to administrative duties and 50% effort toward research. Preference will be given to candidates with both pharmacy education and Ph.D. research training. Appointee must have a transferable NIH funded research program. The Associate Dean must have established a strong interdisciplinary, translational and clinical research relevant to a School of Pharmacy, a record of leadership experience and excellent interpersonal skills.

Qualifications: Ph.D. with significant research experience. Submit curriculum vitae and contact information (including e-mail) for three references to: **Suresh Mudhavan, Ph.D., Search Committee Chair, West Virginia University School of Pharmacy, PO Box 9510, Morgantown, WV 26506 smudhavan@hsc.wvu.edu**

Douglas Glover Endowed Chair for Clinical Pharmacology Research

In accordance with the WVU Health Sciences **Strategic Research Plan (SRP)**, the School of Pharmacy is seeking an outstanding scientist, educator and leader to serve as the **Douglas Glover Chair for Clinical Pharmacology Research**. The Health Sciences research growth agenda includes the building of six thematic **Interdisciplinary Research Centers**. Excellent opportunities exist in each thematic area for collaborations with faculty involved in drug discovery and therapeutics as well as health outcomes research. Appointee must direct a transferable NIH-R01 funded research program and have credentials for appointment at the Associate Professor or Professor level. The appointed investigator will be expected to establish a major research program related to basic clinical pharmacology. Patient care facilities at Health Sciences include a 460 bed University Hospital, an adjacent 70 bed Psychiatric Hospital, the Mary Babb Randolph (MBR) Cancer Center and a recent 90 bed addition to the Hospital.

Qualifications: Ph.D. or M.D. with significant research experience. Submit (e-mail preferred) curriculum vitae and contact information for three references to: **Dr. Patrick Callery, Search Committee Chair, WVU School of Pharmacy, PO Box 9530, Morgantown, WV 26506; pcallery@hsc.wvu.edu**

The Health Sciences Center – General Information: West Virginia University is a public, comprehensive, Carnegie-designated research institution, with approximately 23,000 undergraduates plus 5,500 graduate and professional students. The Health Sciences Center located on the University campus includes the Schools of Medicine, Pharmacy, Dentistry and Nursing, each with both health professional and graduate training programs. Two new research buildings which collectively provide 200,000 sq ft of additional research space are under construction at Health Sciences to accommodate our research growth agenda. Core facilities exist for proteomics, flow cytometry, confocal microscopy, gene chip analysis, cellular imaging, molecular modeling, transgenic biology, functional brain imaging (fMRI & PET/CT) and pharmacogenomics. Morgantown has 55,000 residents and is rated as one of the best small towns in the U.S., with affordable housing, excellent schools, a picturesque countryside and many outdoor activities. Appointees will receive research space, a competitive salary and start-up funds. Search processes will continue until all positions are filled.

West Virginia University is an Affirmative Action/Equal Opportunity Employer

Vice Provost for Research and Economic Development

The State University of New York System Administration, located in Albany, New York invites nominations and applications for the position of Vice Provost for Research and Economic Development. The Vice Provost will work with faculty, deans, vice presidents for research, provosts and university presidents from throughout the 64-campus SUNY system to lead and promote SUNY's research and economic development agenda.

The State University of New York is the largest comprehensive university system in the United States, with 10 doctoral degree granting institutions including two research universities that are members of AAU.

This is a newly-created position within the SUNY Provost's office. The Vice Provost will be part of the senior administrative team making decisions and recommendations affecting the academic and research strength of the component campuses. The first major challenge will be the allocation of a large expected increment of salary and start-up funding that will continue the university's program of "cluster hiring" in areas likely to win large grant support. In addition, the Vice Provost, working with the Provost, will have the challenge of working with campus administrators to recruit and retain strong graduate students in order to enable the SUNY system both to meet its overall research goals and to recruit and retain the strongest research faculty on the individual campuses.

The Vice Provost will serve as the Provost's liaison to the Research Foundation, a private nonprofit educational corporation that administers externally funded contracts and grants for and on behalf of the State University of New York. The sponsored program grants and gifts awards were in excess of $750 million in the 2005-06 fiscal year.

The Vice Provost will provide energetic leadership in defining, and promoting synergistic research opportunities among SUNY campuses, and will provide vision, energy and leadership for a research and economic development agenda linking SUNY with the entire State of New York.

As a senior member of the academic affairs team, it is expected that the Vice Provost will have an earned doctorate or equivalent degree and have had experience as a faculty member in a research university setting. The individual should have held the position of full professor with teaching and research accomplishments suitable for a tenured position at one of our campuses.

The search is being co-chaired by Provost Satish Tripathi (University at Buffalo) and Provost Robert McGrath (Stony Brook University). Apply online at **www.suny.edu/SUPEmployment** or email resume and letter of application clearly identifying your interest by job title to: **VPResearch@sysadm.suny.edu** or mail it to **Vice Provost for Research and Economic Development Search Committee, State University of New York System Administration, Room T-801, State University Plaza, Albany, New York 12246.** The anticipated start date is May 1, 2007.

The State University of New York is an EEO/AA employer. Women, minority persons, disabled workers and/or Vietnam Era Veterans or other protected veterans are encouraged to apply.

Director
Dell Pediatric Research Institute
The University of Texas at Austin

The University of Texas invites applications and nominations for the position of Director of the Dell Pediatric Research Institute (DPRI). The successful candidate will play a pivotal role in creating this major new biomedical research institute. DPRI will be the first of several institutes planned for a new Health Research Campus at UT Austin located approximately three miles from the main UT Austin campus near downtown Austin within a 711 acre, new urban village. The DPRI will be housed in a new 150,000 ft² building with capacity for 28 senior faculty and their research programs. The DPRI Director will be expected to play a major role in recruiting these faculty; generous compensation and start-up packages will be available. We expect strong interactions between DPRI scientists and those on the UT Austin main campus.

We are seeking a dynamic leader with demonstrated experience in administration and communication, ability to lead a major biomedical research unit, and ability to interact well with both private supporters and public education leaders in the state. Additionally, he or she must have an earned Ph.D. or M.D. with a demonstrated record of accomplishment in biomedical research. The Director will report to the Executive Vice President and Provost and the Executive Vice Chancellor for Health Affairs through the Dean of the College of Natural Sciences.

The University of Texas at Austin is the flagship university of the UT System's 15 academic and health institutions. Among the top research universities in the US, UT Austin is home to almost 50,000 students, 2,700 faculty and 17,000 staff members, the largest graduate program in the nation, and one of the largest total student enrollments. The University received more than $300 million in grants and contracts, had more than 96 patents awarded last year, and has recently completed a successful seven-year capital campaign resulting in gifts totaling nearly $1.55 billion.

Please submit a letter of nomination or interest and for the latter, a statement of experience and curriculum vitae to: **Dr. Mary Ann Rankin, College of Natural Sciences G2500, 1 University Station, The University of Texas, Austin, Texas 78712**. For additional information please see **http://cns.utexas.edu/dpri**.

The University of Texas is an Equal Opportunity Employer. Qualified women and minorities are encouraged to apply.

West Virginia University
ROBERT C. BYRD HEALTH SCIENCES CENTER

Associate Professor or Professor Center for Immunopathology and Microbial Pathogenesis

As part of a major research growth initiative supported by a new **Strategic Research Plan (SRP), West Virginia University Health Sciences Center** is recruiting an outstanding scientist to join the Center for Immunopathology and Microbial Pathogenesis. The Center is one of six interdisciplinary research centers being established in accordance with the **SRP** (*Science*, Sept. 8, vol. 313, p. 1461, 2006). A major goal of this interdisciplinary center is to foster collaborations between basic and clinical investigators at Health Sciences. We are especially interested in scientists with established research programs who have credentials for appointment at the Associate Professor or Professor rank **in the School of Medicine.** Appointee must have transferable NIH-R01 funding and a desire to participate in either graduate and/or health professional education. Health Sciences has seven interdisciplinary Ph.D. programs and a joint M.D/Ph.D. Scholars Program in the biomedical sciences.

The successful candidate will receive a generous startup package, competitive salary and excellent laboratory space. We seek investigators across broad areas of immunology, inflammatory disease or immunopathology who are utilizing molecular biology and/or molecular genetic approaches in their research. Collaborative efforts with other basic scientists as well as physician-scientists at the Health Sciences Center who are investigating inflammatory bowel diseases, viral mediated chronic respiratory diseases, pathogenesis mediated by biofilms, or inflammatory mediated vascular injury are being encouraged. The candidate's tenure-track faculty appointment will be in a basic science or clinical department. For this specific position, appointment would likely be in the Department of Microbiology, Immunology and Cell Biology or the Department of Biochemistry.

Qualifications: A Ph.D., M.D. or M.D./Ph.D. with significant research accomplishments. Applications should include curriculum vitae, a brief description of research interests and contact information (including e-mail) for three references sent to: **Christopher Cuff, Ph.D., Search Committee Chair, Center for Immunopathology & Microbial Pathogenesis, PO Box 9177, West Virginia University Health Sciences Center, Morgantown, WV 26506-9106.** Review of applications will continue until the position is filled.

West Virginia University is a comprehensive, public Carnegie-designated Research institution, with approximately 23,000 undergraduates plus 5,500 graduate and professional students. The Health Sciences Center located on the university campus includes the Schools of Medicine, Pharmacy, Dentistry and Nursing; each having both health professional as well as graduate training programs. Two new research buildings which collectively provide 200,000 sq ft of additional research space are under construction at Health Sciences to accommodate our research growth agenda. Morgantown has 55,000 residents and is rated as one of the best small towns in the U.S., with affordable housing, excellent schools, a picturesque countryside and many outdoor activities.

West Virginia University is an Affirmative Action/Equal Opportunity Employer.

Director of the Stroke Program

The University of Kentucky - Lexington, KY

The University of Kentucky invites applications and nominations for the position of Director of the Stroke Program. The Stroke Program is housed in the Sanders-Brown Center on Aging of the UK College of Medicine. In 1987, the Sanders-Brown Center on Aging was designated by the Kentucky Council on Higher Education as a University Center of Excellence in Stroke. To implement this designation, the Sanders-Brown Center received an allotment of funds to establish the Stroke Program as a multi-disciplinary enterprise focused on stroke prevention, treatment, rehabilitation, and research. Within the University of Kentucky, the Stroke Program has become the fulcrum of vigorous research activity in the clinical, behavioral, and basic sciences relating to circulatory disease of the brain.

The position of Director is supported by endowment funds combined with recurrent state-based funding, staff support, and extensive office/laboratory space in the Sanders-Brown Center on Aging. The Director will be expected to implement a vision for continued growth and development of the Stroke Program to further enhance the national prominence of the University of Kentucky in this field. Candidates for the position should have an M.D., Ph.D., or M.D./Ph.D. degree. Academic neurologists or neurosurgeons with necessary experience and board certifications to qualify at the Professor level will be given preference. We seek an individual with a sustained record of NIH funding and a national/international reputation for his or her investigative accomplishments in stroke. Although all areas of investigative research pertinent to stroke will be considered, we are particularly interested in (1) CNS plasticity, recovery, rehabilitation, neuroimaging, and (2) molecular biology, genetics, and cell signaling as applied to neural injury/stroke.

Application materials should include a letter, curriculum vitae, and the names, addresses, and email addresses of three or more references. Submission of materials via email attachment is strongly encouraged. Applications will be reviewed as they are received until the position is filled. Nominations, inquiries, and expressions of interest should be forwarded in confidence to:

Rebecca Copeland, Dean's Office/College of Medicine
MN150 UKMC, 800 Rose Street, Lexington, KY 40536-0298
Phone: 859-257-3861; Fax: 859-323-2039; Email: rbcope0@uky.edu

UK
UNIVERSITY OF KENTUCKY
College of Medicine

Upon offer of employment, successful applicants must pass a pre-employment drug screen and undergo a national background check as required by University of Kentucky Human Resources.

The University of Kentucky is an equal opportunity employer and encourages applications from minorities and women.

■ SCHOOL OF BIOMEDICAL SCIENCES, THE UNIVERSITY OF QUEENSLAND, BRISBANE, AUSTRALIA

Professor and Chair of General Physiology

The role: Actively participate in the school's teaching program at both undergraduate and postgraduate levels; play an important academic leadership role with the school and the wider University community.

The person: The school is particularly interested in encouraging applicants with research programs using molecular and genomic/proteomic approaches to investigate physiologically significant problems; applicants must have a PhD or a medical degree and be competitive within the Australian research funding schemes; opportunities exist for joint appointments with Institutes and other schools; the University is seeking to make appointments as soon as possible and preferably before the end of 2007.

Remuneration: AUD$147,277 p.a. (Professor), including 17% superannuation contributions. Full-time continuing appointment.

Contact: Obtain the position description and selection criteria online or contact Professor David Adams, telephone +61-7-3365-2905 or email dadams@uq.edu.au.

Applications close: 12 March 2007. **Reference No:** 1017190.

Professor of Regenerative Biology

The role: Actively participate in the school's teaching program at both undergraduate and postgraduate levels; play an important academic leadership role with the school and the wider University community.

The person: The school is particularly interested in encouraging applicants with research programs involving genetic interactions, genomic regulatory networks, developmental variation and disease, organ regeneration and tissue repair; applicants must have a PhD or a medical degree and be competitive within the Australian research funding schemes; opportunities exist for joint appointments with institutes and other schools; the University is seeking to make appointments as soon as possible and preferably before the end of 2007.

Remuneration: AUD$147,277 p.a. (Professor), including 17% superannuation contributions. Full-time continuing appointment.

Contact: Obtain the position description and selection criteria online. To discuss the role contact either Professor David Adams, telephone +61-7-3365-2905 or email dadams@uq.edu.au; or Professor Brian Key telephone +61-7-3365-2955 or email brian.key@uq.edu.au.

Applications close: 12 March 2007. **Reference No:** 3015648.

Lecturer / Senior Lecturers in Developmental Biology (2 positions)

The role: Actively participate in the school's teaching program at both undergraduate and postgraduate levels.

The person: The school is particularly interested in encouraging applicants with research programs involving genetic interactions, genomic regulatory networks, developmental variation and disease, organ regeneration and tissue repair; applicants must have a PhD or a medical degree and be competitive within the Australian research funding schemes; opportunities exist for joint appointments with Institutes and other schools; the University is seeking to make appointments as soon as possible and preferably before the end of 2007.

Remuneration: AUD$77,514 – $92,048 p.a. (Lecturer B) or AUD$94,855 – $109,488 p.a. (Senior Lecturer C), including 17% superannuation contributions. Full-time continuing appointments.

Contact: Obtain the position descriptions and selection criteria online. To discuss the roles contact either Professor David Adams, telephone +61-7-3365-2905 or email dadams@uq.edu.au; or Professor Brian Key, telephone +61-73365-2955 or email brian.key@uq.edu.au.

Applications close: 12 March 2007. **Reference No:** 1030926/1039763.

How to apply:
■ visit **www.jobsatUQ.net** to obtain a copy of the position description and selection criteria.

CRICOS Provider Number 00025B

POSITIONS OPEN

NC STATE UNIVERSITY

ASSISTANT PROFESSOR of PLANT PATHOLOGY

The Department of Plant Pathology at North Carolina State University, Raleigh, North Carolina, invites applications for a tenure-track, 12-month position in plant pathology. This position is primarily research at the Assistant Professor level. The individual must have a Ph.D. with training in epidemiology, ecology, plant pathology, or a closely related field. The successful candidate will build a program that will provide leadership in advancing the understanding of plant disease epidemiology at the population or ecosystem level. The incumbent is expected to develop analytical or simulation modeling methods that will further our understanding of the spatio-temporal trends in epidemic development in agricultural or natural ecosystems. The individual will have the opportunity to collaborate with strong ongoing programs in epidemiology, disease forecasting, and population biology. The successful candidate is expected to participate in the graduate program by developing and teaching a course in advanced epidemiology, mentoring graduate students, and participating in other academic programs within the Department of Plant Pathology. The candidate filling this position will have a competitive startup package including technical support. Applications will only be received electronically, and the position will remain open until a suitable candidate is identified. For priority consideration, applicants must submit North Carolina State's online application form and attach to that application curriculum vitae including a list of relevant publications, transcripts, a description of research and teaching interests and goals, the names and contact information for three professional references, and a cover letter by March 31, 2007. To submit the required application materials, candidates should visit **website: http://jobs.ncsu.edu/applicants/Central?quickFind=74948** and follow the instructions there. For additional information concerning this position contact **James Moyer, e-mail: james_moyer@ncsu.edu, Head, Department of Plant Pathology, North Carolina State University.** *Affirmative Action/Equal Employment Opportunity. North Carolina State welcomes all persons without regard to sexual orientation. Persons with disabilities who need accommodations in the application process should contact:* ***Marci Walker, Department of Plant Pathology, via telephone: 919-515-6498, or via e-mail: marci_walker@ncsu.edu.***

POSTDOCTORAL ELECTROPHYSIOLOGIST

A Postdoctoral position is open for an in vitro Electrophysiologist in an interdisciplinary group at the NanoScience Technology Center, University of Central Florida (UCF), in Orlando. Our group is interested in the development of high-throughput drug screening/toxin detection methods based on intracellular/extracellular recordings from neurons. Job responsibilities include whole-cell patch clamp recordings from neurons, dual-electrode recordings from connected neurons, characterizing drug effects on currents and action potentials, extracellular recordings.

Requirements: Doctoral degree in neuroscience or related field, a solid background in whole-cell patch-clamp. Cell culture, extracellular recording, and mathematical modeling experience is a plus.

Review of applications will start February 19, 2007. Candidates should submit curriculum vitae including summary of past accomplishments, research experience, publications and three reference letters to: **Ms. Raji Natarajan at 12424 Research Parkway Suite 400, Orlando, FL 32826, e-mail: mataraj@mail.ucf.edu.** Electronic applications are encouraged. *UCF is an Affirmative Action Employer. Women and minorities are encouraged to apply. UCF makes all application materials, including transcripts, and all search materials available for public review upon request, in accordance with Florida statute.*

POSITIONS OPEN

UNIVERSITY of CALIFORNIA, BERKELEY
Functional Genomics Laboratory
Associate Specialist/Specialist
Salary: Range $46,872 to $92,772
Closing date: March 12, 2007

Description: The University of California, Berkeley Functional Genomics Laboratory (FGL) (**website: http://microarrays.berkeley.edu/**) is seeking a highly motivated individual to oversee and manage the operations of this campus-supported, multi-user core facility. The FGL specializes in gene expression and other genomics-level analyses using state-of-the-art DNA microarray technologies. Duties will include the planning and coordination of the unit's original research together with the FGL Director; consulting on and coordinating client projects; and day-to-day management of the unit's activities, including supervision of the FGL's more junior employees and training of FGL client scientists. The successful applicant will manage the use of the unit's DNA microarray instrumentation, which presently includes an Affymetrix GeneChip System, Agilent microarray system, and robotics for custom spotted array fabrication. Duties will also include designing, performing, and analyzing DNA microarray-based experiments, interfacing with FGL administrative staff, and working directly with FGL scientists and FGL clients on projects involving DNA microarray experimentation, genetics, and statistics and bioinformatics.

Qualifications: Minimum of five years of experience in molecular biology and genomics technologies, including hands-on experience with Affymetrix GeneChip processing, spotted array technology platforms, and robotics technologies. Ability to work independently and supervise and manage multiple projects simultaneously. Attention to detail, effective organizational skills, and effective communication skills (both written and oral). Applicants must have a M.S. or M.A. degree in the biological sciences or related area; Ph.D. is desirable but not essential.

To apply, candidates should send a cover letter summarizing his/her background and accomplishments; curriculum vitae, including a list of publications; and the names of three people who can be contacted for letters of recommendation to:

Functional Genomics Laboratory, c/o Helen Wills Neuroscience Institute
Attn: Associate Specialist/Specialist Recruitment-FGL
132 Barker Hall #3190
University of California
Berkeley, CA 94720-3190

Resumes must be postmarked no later than March 12, 2007. *The University of California is an Equal Opportunity/Affirmative Action Employer. All qualified applicants including minorities and women are encouraged to apply.*

The Duke University Center for Computational Immunology (**website: http://www.dukci.org**) seeks applicants for a **POSTDOCTORAL FELLOWSHIP** to work on the development of an ontology and knowledgebase for immunobiology and its formal representation for automated reasoning. The successful candidate will have a recent Ph.D. in immunology or biology and experience with a variety of molecular and cell biology experimental techniques. Experience with ontology development, text mining and information retrieval, knowledge representation, or automated reasoning is an added strength, but we are prepared to provide training in those areas. Please submit an application package consisting of a letter of interest containing contact information and *citizenship status*, curriculum vitae and a one-page statement of research interests. Please arrange to have three letters of reference sent. The application package and reference letters should be submitted electronically, as PDF files, to **e-mail: harrison.daniels@duke.edu.** The position will remain open until filled. *Duke University is an Equal Opportunity Employer. Women and members of minority groups under-represented in the sciences are encouraged to apply.*

POSITIONS OPEN

USDA ars Agricultural Research Service

SUPERVISORY RESEARCH MICROBIOLOGIST/ ANIMAL SCIENTIST / VETERINARY MEDICAL OFFICER
USDA/Agricultural Research Service
National Animal Disease Center
Ames, Iowa

The Pre-Harvest Food Safety and Enteric Diseases Research Unit conducts basic and applied research on the microbiological safety of foods of animal origin and selected bacterial enteric diseases of livestock. The unit is seeking an experienced Supervisory Research Microbiologist, Animal Scientist, or Veterinary Medical Officer to perform individual research as well as provide leadership and management to the research unit. The successful candidate will plan, conduct, and report independent research on microbial ecology of commensal intestinal populations that affect the health of the animal host, contribute to the persistence of antimicrobial resistance, or impact colonization by food borne pathogens.

A Bachelor's degree in microbiology, animal science, or Doctor of veterinary medicine is required to meet the basic requirements. Knowledge of microbiology, molecular biology, epidemiology, or veterinary medicine to assess microbial ecology and its impact on bacterial colonization and pathogenicity is highly desirable. For information on this position contact **Dr. Kurt Zuelke at e-mail: kzuelke@nadc.ars.usda.gov.**

Candidates must be U.S. citizens. Salary commensurate with experience. Range from $89,115 to $136,273. Comprehensive benefits package includes paid annual and sick leave, life insurance, health insurance, and a federal retirement plan. Vacancy announcements and application information can be obtained from the ARS **website:http://www.afm.ars.usda.gov/divisions/hrd/.** For questions regarding application procedures call **Lynnette Richey, telephone: 815-663-7278.** Applications in response to this ad must be postmarked by May 1, 2007, and reference vacancy announcement number ARS-X7W-0116. Approved by Latania Maise on January 29, 2007. *The USDA/ARS is an Equal Opportunity Provider and Employer.*

The University of Southern California/Norris Comprehensive Cancer Center of the Keck School of Medicine at the University of Southern California (USC) seeks applicants for faculty positions at the **ASSISTANT, ASSOCIATE,** and **FULL PROFESSOR** level in the following areas of cancer-related research: signal transduction, cell cycle regulation, apoptosis, autophagy, and animal models of cancer. Other areas of innovative cancer-related research will also be considered. Successful applicants will likely be investigators with funded research programs. Send a current curriculum vitae, research plan, and three letters of reference to: **Dr. Michael Stallcup, c/o Isabel Lora, University of Southern California/Norris Comprehensive Cancer Center, 1441 Eastlake Avenue, Room 8302K, MC-9181, Los Angeles, CA 90089-9181.** *USC is an Equal Opportunity Employer.*

RESEARCH POSITION
Columbia University
College of Physicians and Surgeons

POSTDOCTORAL scientist to study molecular genetics of kidney diseases in humans. Requires training in cell or molecular biology at Ph.D./M.D. level. Prior training in human genetics or statistical genetics a plus. Please send curriculum vitae and names of three references to: **Dr. Ali Gharavi, Columbia University, Department of Medicine, P.O. Box 84, 630 W. 168th Street, New York, NY 10032 or e-mail: ag2239@columbia.edu.**

Columbia University is an Equal Opportunity/Affirmative Action Employer.

POSITIONS OPEN

The Department of Anatomy and Neurobiology at the Virginia Commonwealth University's School of Medicine seeks an exceptional individual to participate in the Department's complex teaching missions in medical and dental gross anatomy, histology, embryology, and neuroscience. Applicants should have a Ph.D., M.D., or D.D.S. with both postdoctoral research experience and a demonstrated track record in teaching the anatomical sciences. The ideal candidate will also have research experience that complements one of the Department's major areas of scientific inquiry focusing on traumatic brain injury and repair. This position is offered at the collateral level at the rank of **ASSISTANT PROFESSOR** (F20640), with an excellent starting salary and full University benefits. Interested candidates should send their curriculum vitae, a letter of intent including career goals and the names, addresses, telephone numbers, fax numbers, and e-mail addresses of three references. Electronic submissions to **e-mail: anatrecruit@vcu.edu** are preferred. For mailing contact: **Dr. John Bigbee, Chair, Faculty Search Committee, Virginia Commonwealth University, Department of Anatomy and Neurobiology, P.O. Box 980709, Richmond, VA 23298-0709.** Deadline for receipt of applications is March 20, 2007. *Virginia Commonwealth University is an Equal Opportunity/Affirmative Action Employer. Women, minorities, and persons with disabilities are encouraged to apply.*

AVIAN RESEARCH ECOLOGIST
U.S. Geological Survey's Patuxent Wildlife Research Center

The U.S. Geological Survey's Patuxent Wildlife Research Center in Laurel, Maryland, **website: http://www.pwrc.usgs.gov/** seeks a full-time, GS-12/13, Research Ecologist with experience conducting research in avian biology, ecology, and conservation. As lead investigator the Ecologist designs, conducts, analyzes, and prepares reports on studies that respond to regional and national conservation goals, primarily in support of Department of Interior agencies missions. Applications must be completed online at **website: http://www.usgs.gov/ohr/oars/.** The Delegated Examining Unit announcement *(open to all qualified U.S. citizens)* will be vacancy announcement number ER-2007-0096; the MP announcement (open to current and former Federal employees) will be vacancy announcement number ER-2007-0107. Announcements will open on February 20, 2007, and close at midnight EST on March 19, 2007. Details on the position and application provided on the website.

ASSOCIATE RESEARCH SCIENTIST

Division of Vascular Surgery at Columbia University's College of Physicians and Surgeons seeks Associate Research Scientist to study human vascular diseases. Prior training and experiences in vascular biology, gene therapy, and stem cell technology required. Four years of research experience required. Strong skills in communication, grant application, and manuscript preparation desired.

Please contact **Drs. K. C. Kent** and **B. Liu** at **e-mail: bol2001@med.cornell.edu.**

Columbia University is an Affirmative Action/Equal Opportunity Employer.

POSTDOCTORAL POSITION is available to study drug-protein interactions in HIV-1 reverse transcriptase. Candidates should have a Ph.D. in chemistry or biochemistry and have experience in molecular biology, enzyme kinetics, and protein structure analyses. Interested applicants should send curriculum vitae and names of three references to: **Dr. Nicolas Sluis-Cremer, Division of Infectious Diseases, University of Pittsburgh School of Medicine, S817 Scaife Hall, 3550 Terrace Street, Pittsburgh, PA 15261. E-mail: cremern@dom.pitt.edu.**

The University of Pittsburgh is an Equal Opportunity Employer.

POSITIONS OPEN

NEUROSCIENCE POSTDOCTORAL FELLOWS. Two NIH-funded Postdoctoral Fellow positions available to study the molecular mechanisms by which nicotinic receptor activation promotes addiction and alters the etiology of Alzheimer's disease, Parkinson's disease, neuroinflammation, schizophrenia, and autism. Significant experience using molecular, protein, cell culture, transgenic, and imaging techniques and knowledge of neuroscience is desirable. The Laboratory is part of the interdisciplinary Neuroscience Signature Program and located in the newly constructed Biomedical Research Tower with state-of-the-art facilities for proteomics, genomics, and neuroimaging. Please send curriculum vitae and names of references to: **Rene Anand, Department of Pharmacology, Ohio State University, 5072 Graves Hall, 333 W. 10th Avenue, Columbus, OH 43210** by e-mail to **e-mail: anand.20@osu.edu.** *Ohio State University is an Equal Opportunity Employer.*

Several **POSTDOCTORAL POSITIONS** are available immediately to study vascular wall remodeling and/or angiogenesis. Experience with balloon injury model of restenosis and/or angiogenesis is highly desirable.

Salaries are highly competitive and opportunities to become Instructor/Assistant Professor exist in the laboratory. Highly motivated candidates with a Ph.D. and/or M.D. degree and with demonstrated experience in molecular biology, signaling, or angiogenesis should send their curriculum vitae and three letters of references to: **Prof. G. N. Rao, Department of Physiology, University of Tennessee Health Science Center, 894 Union Avenue, Memphis, TN 38163 U.S.A. E-mail: grao@physio1.utmem.edu.**

The University of Tennessee is an Equal Employment Opportunity/Affirmative Action/Title VI/Title IX/Section 504/ADA/ADEA Employer.

ANNOUNCEMENTS

INDO-U.S. SCIENCE AND TECHNOLOGY FORUM
Fulbright House, 12 Hailey Road, New Delhi-110 001, India
Website: http://www.indousstf.org
SECOND CALL FOR PROPOSAL 2007

The Indo-U.S. Science and Technology Forum (IUSSTF), established under an agreement between the Governments of India and the United States of America, is an autonomous, not-for-profit society that promotes and catalyzes the Indo-U.S. bilateral collaborations in science, technology, engineering, and biomedical research through substantive interaction among government, academia, and industry.

The IUSSTF seeks to support innovative programs aimed to stimulate interactions that have a strong potential for generating follow-on activities and building long-term Indo-U.S. S&T relationships. The IUSSTF promotes program that nurtures contacts between the young and midcareer scientists and technologists and fosters active public-private partnership in R&D.

The IUSSTF solicits proposals thrice a year (submission deadline: February, June, October) jointly submitted by the U.S. and Indian Principal Investigators from academia, government-funded institutions/laboratories, and private R&D entities for: (1.) Knowledge R&D networked and public-private networked Indo-U.S. centers, (2.) Bilateral workshop, conference, symposium, (3.) Training schools, (4.) Travel grants (i.) To avail already awarded fellowship and sabbatical positions in U.S./India, (ii.) For selected U.S. participants to attend international conferences / events in India, (iii.) For specific exploratory/planning visits aimed at large scale collaborations.

Detailed format available at **website: http://www.indousstf.org.**

For further details and electronic submission, contact: **Arabinda Mitra, e-mail: amitra@indousstf.org** and **Michael Cheetham, e-mail: mcheetham@si.edu.**

Submission deadline: 15 June 2007. Award announcement: mid September 2007.

POSITIONS OPEN

DIRECTOR, SCIENCE, and TECHNOLOGY DIVISION
Enjoy Challenging Work and Make Important Contributions to the Nation

The Institute for Defense Analyses (IDA) is a not-for-profit corporation that operates three Federally Funded Research Centers (FFRDCs), two serving the Department of Defense (DoD) and one serving the Office of Science and Technology Policy in the Executive Office of the President. The IDA Centers provide objective analyses of national security issues, particularly those requiring scientific and technical expertise, and conduct related research on other national challenges. The scientists and engineers in the Science and Technology Division, one of seven research divisions within the Alexandria-based Studies and Analyses Center, conduct technology assessments critical to research and development programs, to acquisition decisions, as well as to technology planning, technology readiness, and counter-proliferation efforts; perform technical characterizations and evaluations of devices and systems to assess the limits of performance available in their operational environments and the mission capability they provide; and investigate and model scientific phenomena.

The Director leads the Division in providing high-quality analyses and advice to its sponsors in the Office of the Secretary of Defense, the Joint Staff, the Combatant Commands, and defense agencies such as DARPA and the Missile Defense Agency. The Division also provides studies to other federal agencies that conduct research and/or develop advanced systems to support national security missions. The Director manages an 80 staff-years level of effort and supervises a highly trained staff, 85 percent have PhDs. The Director reports directly to the President of IDA.

The individual we seek must be familiar with the national security research community and be able to interact effectively with senior leadership and staff in sponsoring offices. In addition, he/she must be able to work with the managers of leading research institutions both within and outside the federal government. He/she needs a working knowledge of federal decision-making processes related to advanced technology developments. Experience working on technology issues in government and/or industry is desirable. The successful candidate will be well-educated, with a Ph.D. in the sciences or engineering. He/she must have management experience and a proven ability to build and oversee the execution of a program of diverse scientific and technical studies. A national reputation in a scientific or technical field is a plus. The Director leads and works with an intellectually vibrant staff and should have a genuine intellectual curiosity in a variety of technical subjects.

IDA offers a competitive salary, an excellent benefits package and a superior professional working environment. IDA is located in a modern office facility, directly off an interstate, minutes from the Pentagon. To the right individual, IDA offers the opportunity to have a major impact on key national programs while working on fascinating technical issues. The selected individual will be subject to a security investigation and must meet the requirements for access to classified information. *U. S. citizenship is required.*

Please send responses or inquiries to: **Institute for Defense Analyses, 4850 Mark Center Drive, Attn: Employment Office (Science and Technology Division-Director), Alexandria, VA 22311-1882. E-mail: resumes@ida.org, fax: 240-282-8314.** *The Institute for Defense Analyses is proud to be an Equal Opportunity Employer.*

MARKETPLACE